Reduced order models for nonlinear dynamic analysis of rotating structures : Application to turbomachinery blades

Mikel Balmaseda Aguirre

N°d'ordre NNT : 2019LYSEI067

THESE de DOCTORAT DE L'UNIVERSITE DE LYON
opérée au sein de
L'Institut National des Sciences Appliquées de Lyon

Ecole Doctorale N° 162
Mécanique, Énergétique, Génie civil, Acoustique

Spécialité/ discipline de doctorat :
GÉNIE MÉCANIQUE

Soutenue publiquement le 19/09/2019, par :

Mikel Balmaseda Aguirre

Reduced Order Models for Nonlinear Dynamic Analysis of Rotating Structures: Application to Turbomachinery Blades

---

Devant le jury composé de :

G. CHEVALLIER	Professeur, Université de Franche-Comté	Président
J.-F. DEÜ	Professeur, CNAM	Rapporteur
C. TOUZÉ	Professeur, ENSTA Paris	Rapporteur
T. BERRUTI	Professeure, Politecnico di Torino	Examinatrice
E. CAPIEZ-LERNOUT	MCF, Université Paris-Est Marne-la Vallée	Examinatrice
G. JACQUET-RICHARDET	Professeur, INSA de Lyon	Directeur de thèse
D.-M. TRAN	Maître de Recherche, HDR, ONERA	Co-Directeur de thèse
A. PLACZEK	Ingénieur de Recherche, ONERA	Encadrant
M. MBAYE	Ingénieur R&T Vibration, Safran Tech	Invité

LaMCoS – UMR CNRS 5259 – INSA Lyon
Bât. Sophie Germain, 27bis Avenue Jean Capelle,
F69621 Villeurbanne Cedex, France

Département FEDORA – INSA Lyon - Ecoles Doctorales – Quinquennal 2016-2020

SIGLE	ECOLE DOCTORALE	NOM ET COORDONNEES DU RESPONSABLE
CHIMIE	**CHIMIE DE LYON** **http://www.edchimie-lyon.fr** Sec. : Renée EL MELHEM Bât. Blaise PASCAL, 3e étage **secretariat@edchimie-lyon.fr** INSA : R. GOURDON	M. Stéphane DANIELE Institut de recherches sur la catalyse et l'environnement de Lyon IRCELYON-UMR 5256 Équipe CDFA 2 Avenue Albert EINSTEIN 69 626 Villeurbanne CEDEX **directeur@edchimie-lyon.fr**
E.E.A.	**ÉLECTRONIQUE, ÉLECTROTECHNIQUE, AUTOMATIQUE** **http://edeea.ec-lyon.fr** Sec. : M.C. HAVGOUDOUKIAN **ecole-doctorale.eea@ec-lyon.fr**	M. Gérard SCORLETTI École Centrale de Lyon 36 Avenue Guy DE COLLONGUE 69 134 Écully Tél : 04.72.18.60.97 Fax 04.78.43.37.17 **gerard.scorletti@ec-lyon.fr**
E2M2	**ÉVOLUTION, ÉCOSYSTÈME, MICROBIOLOGIE, MODÉLISATION** **http://e2m2.universite-lyon.fr** Sec. : Sylvie ROBERJOT Bât. Atrium, UCB Lyon 1 Tél : 04.72.44.83.62 INSA : H. CHARLES **secretariat.e2m2@univ-lyon1.fr**	M. Philippe NORMAND UMR 5557 Lab. d'Ecologie Microbienne Université Claude Bernard Lyon 1 Bâtiment Mendel 43, boulevard du 11 Novembre 1918 69 622 Villeurbanne CEDEX **philippe.normand@univ-lyon1.fr**
EDISS	**INTERDISCIPLINAIRE SCIENCES-SANTÉ** **http://www.ediss-lyon.fr** Sec. : Sylvie ROBERJOT Bât. Atrium, UCB Lyon 1 Tél : 04.72.44.83.62 INSA : M. LAGARDE **secretariat.ediss@univ-lyon1.fr**	Mme Emmanuelle CANET-SOULAS INSERM U1060, CarMeN lab, Univ. Lyon 1 Bâtiment IMBL 11 Avenue Jean CAPELLE INSA de Lyon 69 621 Villeurbanne Tél : 04.72.68.49.09 Fax : 04.72.68.49.16 **emmanuelle.canet@univ-lyon1.fr**
INFOMATHS	**INFORMATIQUE ET MATHÉMATIQUES** **http://edinfomaths.universite-lyon.fr** Sec. : Renée EL MELHEM Bât. Blaise PASCAL, 3e étage Tél : 04.72.43.80.46 **infomaths@univ-lyon1.fr**	M. Luca ZAMBONI Bât. Braconnier 43 Boulevard du 11 novembre 1918 69 622 Villeurbanne CEDEX Tél : 04.26.23.45.52 **zamboni@maths.univ-lyon1.fr**
Matériaux	**MATÉRIAUX DE LYON** **http://ed34.universite-lyon.fr** Sec. : Stéphanie CAUVIN Tél : 04.72.43.71.70 Bât. Direction **ed.materiaux@insa-lyon.fr**	M. Jean-Yves BUFFIÈRE INSA de Lyon MATEIS - Bât. Saint-Exupéry 7 Avenue Jean CAPELLE 69 621 Villeurbanne CEDEX Tél : 04.72.43.71.70 Fax : 04.72.43.85.28 **jean-yves.buffiere@insa-lyon.fr**
MEGA	**MÉCANIQUE, ÉNERGÉTIQUE, GÉNIE CIVIL, ACOUSTIQUE** **http://edmega.universite-lyon.fr** Sec. : Stéphanie CAUVIN Tél : 04.72.43.71.70 Bât. Direction **mega@insa-lyon.fr**	M. Jocelyn BONJOUR INSA de Lyon Laboratoire CETHIL Bâtiment Sadi-Carnot 9, rue de la Physique 69 621 Villeurbanne CEDEX **jocelyn.bonjour@insa-lyon.fr**
ScSo	**ScSo*** **http://ed483.univ-lyon2.fr** Sec. : Véronique GUICHARD INSA : J.Y. TOUSSAINT Tél : 04.78.69.72.76 **veronique.cervantes@univ-lyon2.fr**	M. Christian MONTES Université Lyon 2 86 Rue Pasteur 69 365 Lyon CEDEX 07 **christian.montes@univ-lyon2.fr**

*ScSo : Histoire, Géographie, Aménagement, Urbanisme, Archéologie, Science politique, Sociologie, Anthropologie

Abstract

In the present work reduced order models (ROMs) that are independent from the full order finite element models (FOMs) considering geometrical non linearities are developed and applied to the dynamic study of rotating structures. The structure is considered to present nonlinear vibrations around the pre-stressed equilibrium induced by rotation enhancing the classical linearised approach. The reduced nonlinear forces are represented by a polynomial expansion obtained by the Stiffness Evaluation Procedure (STEP) and then corrected by means of an original procedure by means of a Proper Orthogonal Decomposition (POD) that filters the full order nonlinear forces before projection. The latter model is named STEP with Correction (StepC). Different types of reduced basis are presented and tested. Some of these bases are parametrised with respect to the rotating velocity reducing considerably the construction of the ROM. The results obtained with the StepC ROM are in good agreement with the solutions of the FOM and are capable of reproducing the coupled motion of the structure. Furthermore they are more accurate than the classsical Linearised ROM solutions and than the STEP ROM without correction. The proposed StepC ROM provides the best compromise between accuracy and time consumption of the ROM.

Keywords: ROMs, Rotating structures, Nonlinear dynamics, Geometrical nonlinearities, STEP, POD based correction, Contact Nonlinearities.

Résumé

Dans le présent travail, des modèles d'ordre réduits (ROMs) indépendant des modèles éléments finis d'haute fidélité (FOMs) ont été développés pour l'étude de la dynamique non linéaire des structures en rotation. Les vibrations de la structure autour de l'équilibre précontraint induit par la rotation sont considérées comme non linéaires, améliorant l'approche linéarisée classique. Les forces généralisées non linéaires sont approximées par un polynôme d'ordre trois obtenu avec la procédure Stiffness Evaluation Procedure (STEP). Ici, une approche originale est proposée pour corriger les forces non linéaires à l'aide d'une base de forces non linéaires obtenue avec une décomposition orthogonale aux valeurs propres (POD). Ce modèle est nommé STEP avec Correction (StepC). Différents types de base réduite sont présentés et testés. Certaines de ces bases sont paramétrées en fonction de la vitesse de rotation, ce qui réduit considérablement le temps de construction du modèle réduit. Les résultats obtenus avec le modèle StepC ROM sont en bon accord avec le FOM et sont capables de reproduire le couplage en déplacement entre les dégrés de liberté de la structure. De plus, elles sont plus précises que les solutions ROM linéarisées classiques et que le modèle STEP ROM sans correction. Le modèle StepC ROM proposé offre le meilleur compromis entre précision et temps de construction du ROM.

Mots-clé: Modèles d'ordre réduit, Structures tournantes, Dynamique non linéaire, non linéarités géométriques, STEP, Correction POD, non linéarités de contact frottant.

Remerciements

This PhD manuscript resumes three years of research that are fruit of many professional and personal intense moments. I would like to address my thanks and gratefulness to all of those that have specially contributed to this research.

Tout d'abord je tiens à remercier M. le Professeur Georges Jacquet-Richardet pour la direction de ces travaux de thèse, ses conseils et disponibilité en lui remerciant très spécialement pour son engagement durant la fin de rédaction de ce manuscrit. Ses précieuses indications m'ont permis d'élargir la vision de mon travail et du besoin de prouver l'utilité pratique de mes recherches.

Je tiens à remercier également Duc-Minh Tran, co-directeur de thèse et principal encadrant à l'ONERA pour son soutien. Sans ses innumérables investissement, conseils, directives et infinis échanges techniques cette thèse n'aurait sans doute vu le jour.

Merci également à Antoine Placzek encadrant à l'ONERA pour ses conseils, revues critiques et intérêt sur la poursuite de ces travaux. Un gran merci également pour sa disponibilité et soutien. J'espère qu'un jour nous serons capable de mettre en œuvre un couplage aéroelastique de ces modèles.

I would like to thank Pr. Jean-François Deü and Pr. Cyril Touzé for reviewing this manuscript and for their patience, fruitful advises and comments. I appreciate that Pr. Gaël Chevallier, Pr. Teresa Berruti, Dr. Évangeline Capiez-Lernout and Dr. Moustapha Mbaye found time to participate as members of the PhD defense board. I am grateful to the jury members for their interest and numerous questions.

Je tiens à remercier également à tous les collègues et doctorants de l'ONERA qui ont contribué aux bons moments ensemble et qui ont également contribué d'une ou d'une autre forme au bon déroulement de cette thèse.

Me gustaría enviar un enorme abrazo a mi familia y especialmente a mis padres Angel y Cristina, por su cariño, ayuda y apoyo en todas las decisiones que he tomado. Last but not least, me gustaría agradecer infinitamente a mi querida mujer, Anna, por su paciencia y comprensión durante estos tres años de tesis, por su apoyo incondicional y por traer a este mundo a nuestro querido hijo Daniel cuya sonrisa me alegra la vida todos los días.

Bihotz bihotzez eskerrik asko denoi.

Contents

List of Figures

List of Tables

Nomenclature

α_f	Loading factor.
$\mathbb{C}_p\left(\mathbf{u}_p(\mathbf{p},\, t), t\right)$	Right Cauchy-Green tensor.
$\mathbb{D}$	Fourth order tensor associated with the Hook's law of elasticity.
μ	Friction contact coefficient.
Ω	Rotating velocity.
ω_e	Excitation frequency.
Ω_N	Nominal rotating velocity of the blade.
ρ	Density.
$\mathbf{a} \cdot \mathbf{b}$	Scalar product between $\mathbf{a}$ and $\mathbf{b}$ vectors.
ξ	Damping coefficient.
A^p_{ij}	Quadratic nonlinear polynomial coefficients.
B^p_{ijk}	Cubic nonlinear polynomial coefficients.
g_n	Normal gap.
r	Number of modes that form the reduced bases.
r_b	Number of constraint modes.
r_c	Number of fixed interface modes.
r_f	Number of modes that form the nonlinear forces basis.
$V(0)$	Volume of the initial configuration.
$V(t)$	Volume of the deformed configuration.
$\mathbf{E}_p(\mathbf{u}_p(\mathbf{p},\, t),\, t)$	Green-Lagrange symmetric strain tensor.
$\mathbf{J}(\, \mathbf{u}_p(\mathbf{p},\, t))$	Jacobian of the transformation.

$\mathbf{K}_c(\Omega)$ Centrifugal softening stiffness matrix.

$\mathbf{K}_g(\mathbf{u}_s)$ Geometrically nonlinear stiffness matrix.

$\mathbf{K}_{nl}(\mathbf{u}_s)$ Nonlinear part of the tangent matrix.

$\tilde{\cdot}$ Representation of $\cdot$ in the reduced space.

Φ_c Fixed interface linear normal modes basis.

Φ_f Nonlinear forces filtering basis.

Φ_{CB} Craig-Bampton reduction basis.

Φ_{LNM} Linear Normal Modes reduction basis.

Ψ_c Constraint modes.

$\mathbf{A}$ Nonlinear forces snapshot matrix.

$\mathbf{B}$ Nonlinear forces filtering projection basis.

$\mathbf{C}$ Structural viscous damping matrix.

$\mathbf{I}$ Identity matrix.

$\mathbf{K}_e$ Elastic stiffness matrix.

$\mathbf{M}$ Mass matrix.

$\mathbf{Q}$ Reduction basis.

$\mathbf{K}(\Omega)$ Global stiffness matrix, $\mathbf{K}(\Omega) = \mathbf{K}_e + \mathbf{K}_{nl}(\mathbf{u}_s) + \mathbf{K}_c(\Omega)$.

FOM: Full Order Model.

Linear ROM: Classical linearised vibrations ROM.

LNM: Linear Normal Modes.

MAC: Modal Assurance Criterion.

POD: Proper Orthogonal Decomposition.

STEP ROM: ROM formed by the STEP polynomial method.

StepC ROM: ROM with POD based correction, proposed ROM.

$\tau_p(\mathbf{u}_p(\mathbf{p}, t), t)$ First Piola-Kirchoff stress tensor.

$\mathbf{f}_c(\mathbf{u}, \dot{\mathbf{u}})$ Contact forces vector.

$\mathbf{u}_p(\mathbf{p}, t)$ Current displacements refereed to the initial configuration.

$\mathbf{X}_p(\mathbf{u(p,}\ t\mathbf{),}\ t\mathbf{)}$ Gradient of the transformation.

$\mathbf{x(p,}\ t\mathbf{)}$ Displacements in the deformed configuration at time t.

$\sigma_x(\mathbf{u}_x\mathbf{(x,}\ t\mathbf{)})$ Cauchy stress tensor.

$\mathbf{f}_e(\mathrm{t})$ External forces vector.

$\mathbf{f}_{ei}(\Omega)$ Centrifugal forces vector.

$\mathbf{g}_{nl}(\mathbf{u})$ Purely nonlinear internal forces vector.

$\mathbf{g}(\mathbf{u}_p)$ Nonlinear internal forces vector.

$\mathbf{S}_p(\mathbf{u}_p\mathbf{(p,}\ t\mathbf{)})$ Second Piola-Kirchoff stress tensor.

$\sum$ Singular values.

$\mathbf{a}_x$ Acceleration vector.

$\mathbf{p}$ Initial configuration.

$\mathbf{q}_i$ Modal coordinates.

$\mathbf{q}$ Generalised coordinates.

$\mathbf{u}_b$ Boundary interface degrees of freedom.

$\mathbf{u}_p$ Physical absolute displacements vector, $\mathbf{u}_p = \mathbf{u}+\mathbf{u}_s$.

$\mathbf{u}_s$ Vector of the static displacements induced by rotation.

$\mathbf{U}$ Left-singular vectors.

$\mathbf{u}$ Vibrations vector around the pre-stressed displacements state.

$\mathbf{V}$ Right-singular vectors.

Introduction

Rotating structures in industry such as fan or compressor blades, helicopter blades or wind turbine blades among others are submitted to large displacement nonlinearities during their life cycle. The latter is specially true in the actual context where the design tendency is to create more flexible and larger slender structures leading to an amplification of the nonlinear effects due to larger displacements. These effects create a dependency of the structure's behaviour with respect to its displacement state. Furthermore, additional friction contact nonlinearities should be considered when studying the interaction between the disk and blades root or between blades and rubbing systems. These interactions impact the behaviour of the structure as they lead to an energy dissipation as well as to possible effects such as wear or induced vibrations.

The finite element method (FEM) is commonly used to solve the discretised weak form of the physical problem. During the design phase, by means of the FEM, the nonlinear behaviour of the structure is accurately reproduced with models consisting on a large number of degrees of freedom. These models are called full order models (FOMs) or high fidelity models as they are capable of providing precise results for the studied nonlinear problems. However, the computational cost for design, optimisation or control processes, where multiple computations are carried out, can easily become "unassumable" for industrial standards, with a computational time per solution within the order of some days up to some months. Thus, the development of nonlinear reduced order models, that provide the best compromise between accuracy and time performances, are of major interest for the designers.

In the framework of geometrically nonlinear rotating structures, the weak form of the problem is presented by [Desceliers, 2001, Schotte, 2001, Sternchüss, 2009]. From the strong form of the problem, expression of the continuous weak form is developed with respect to the rotating frame of reference, by implementing the kinematic relationships. The finite element method provides a discretisation of the continuous problem adapted to numerical analysis. The FEM model is constituted with different matrices that represent the behaviour of the structure. The vibrations of the structure around the nonlinear equilibrium state induced by rotation are usually supposed to be linear. These formulations provide the theoretical basis to develop the equations of the sys-

tem as a function of the vibrations around the pre-stress equilibrium state when the vibrations are considered as nonlinear. The expression of the tangent matrix, around a pre-stressed displacement state, is given by the sum of a linear stiffness matrix and a series of nonlinear matrices. When the structure rotates, the effect of rotation induces a pre-stress state that is modelled by the so called geometrical stiffness, which corresponds to one of the components that form the nonlinear part of the tangent matrix.

Considering contact type nonlinearities [Wriggers and Nackenhorst, 2006, Yastrebov, 2011] studied the weak form of the continuum problem as well as its numerical implementation by regularising the associated variational inequality. The contact surfaces phenomenology, discretisation (node-node, node-segment, segment-segment), projection types between the master and slave surfaces as well as the numerical representation of stick-slip phenomena, among others, are modelled and implemented for different numerical applications in most finite element softwares.

In the framework of geometrically nonlinear reduced order models [Muravyov and Rizzi, 2003] provided a third order polynomial formulation to represent the nonlinear forces within the structure called the Stiffness Evaluation Procedure (STEP). The polynomial coefficients represent the nonlinear stiffness of the structure and are identified during an OFFline stage used to construct the reduced order model (ROM). This stage is computationally expensive as several FOM static computations are carried out to determine the nonlinear forces for a series of imposed displacements that are obtained as a combination of the modes in the reduced basis. This procedure makes the ROM independent from the FOM during the ONline stage, increasing its time performances. However, the validation of this model is carried out only for structures that exhibit stretching of the middle surface (i.e simply supported plate structures with a vertical loading applied at the centre of the plate).

The accuracy and representativity of different classical reduced basis is investigated in [Lülf, 2013] where a method to construct accurate and parametrisable ROMs, capable of reproducing the dynamic solution of a geometrically nonlinear structure is presented. One of the conclusions arisen from the study of different classical reduced order basis is that not all are capable of accurately reducing any type of nonlinearity. However, in terms of representativity, the reduced basis should be chosen, first with respect to the type of excitation and then with respect to the studied nonlinear configuration. During the transient solution, when a chosen criteria is fulfilled, the reduced basis is updated with the current displacements of the structure and also with new terms adapted for the new value of the external parameter by interpolating the reduced basis into a tangent space.

Parametrised projection based reduced order models, valid for a range of rotating velocity with application to bladed disk mistuning, are presented in [Kurstak et al., 2018]. This parametrisation is inspired from the work of [Hong et al., 2011] that parametrised the nonlinear forces of a structure. The parametrised reduced basis is obtained by computing the full order model at three rotating velocities. The developed parametrised but linear ROM is tested for two existing mistuning methods. This ROM is valid for different loading excitations and rotating velocities providing accurate results with respect to the reference full order model solution.

The generalised coordinates of the classical reduced basis such as the linear normal modes (LNM) or the proper orthogonal decomposition (POD) are not capable of representing the physical displacements at some given degrees of freedom of the structure. When the friction contact is implemented, the ROM should be capable of keeping the contact degrees of freedom associated to the contact interface in order to implement an appropriate nonlinear model. The component mode synthesis techniques are capable of providing reduced order models by reducing the dimension of the inner degrees of freedom while keeping the degrees of freedom at the contact boundary. Thus, the fixed interface techniques [Craig and Bampton, 1968] and free interface techniques [Rubin, 1975] are widely developed in literature.

The works that are described previously have permitted the development of the theoretical continuum framework to model the dynamic behaviour of rotating structures with large displacements and to implement numerical simulations of contact problems. Furthermore, the development of autonomous reduced order models, that are independent from the FOM, has increased the ONline stage performances. The parametrisation of the reduced basis with respect to the rotating velocity has enlarged the application of the linearised reduced order models for a range of rotating velocities. In addition, component mode synthesis techniques provide a tool capable of reducing the dimension of the problem while keeping in the generalised coordinates the interface degrees of freedom. Nevertheless, these reduced order models are not capable to deal with the dynamics of rotating structures with large displacements and friction contact nonlinearities. These nonlinear effects have been separately studied without assessing the influence that could have one on another. With respect to the reduced order models, that study the contact problem, either they consider that the structure has a purely linear behaviour or either they evaluate the nonlinear contact forces by means of FOM computations leading to non autonomous reduced order models that depend on the size of the FOM. Finally, the vibrations around the pre-stressed equilibrium state induced by rotation are considered as linear.

This is what justifies this study, which consist in the development of nonlinear reduced order models independent from the FOM (autonomous) for the study of the dynamics of rotating structures with large displacements nonlinearities and with friction contact nonlinearities.

Four main contributions are presented in this work: i) the displacements around the pre-stressed equilibrium are considered as nonlinear. Thus, the identification of the nonlinear stiffness coefficients of the STEP method is adapted in order to study the geometrically nonlinear vibrations. ii) The nonlinear forces within the structure are corrected by means of a nonlinear forces POD basis (before the projection is performed) in order to remove the spurious artefacts observed in the ROMs without correction. iii) The nonlinear ROM is parametrised with respect to the rotating velocity of the structure and is constructed in order to be valid for a given range of rotating velocities. iv) The geometrical nonlinearity is combined with the friction contact nonlinearity by means of a Craig-Bampton reduced basis that is capable of keeping some of the physical degrees of freedom as generalised displacements.

In the present work the finite element software Code_Aster [EDF, 1989] and the programming languages Python [van Rossum, 1995] and Fortran were used. Code_Aster is capable of executing Python code providing an integrated environment for the FOM and the ROM. The reduced order model is fully implemented in Python/Fortran which leads to very flexible programming. Code_Aster is capable of providing the necessary informations to perform the OFFline construction of the ROMs and to perform the FOM solutions used as reference.

Context of the study

Mechanical and aerodynamic effects in turbomachinery blades

Turbomachinery blades are submitted to different loadings induced by aerodynamic or by mechanical sources. In order to design these structures, aeroelastic computations are needed. Aeroelasticity studies the vibrations of a structure induced by fluid-solid interactions.

From a mechanical point of view, turbomachinery blades are traditionally designed as stiff as possible in order to resist extreme conditions. Nevertheless, the blades are submitted to a very hight number of working vibrations cycles that could lead to fatigue failure. Thus, the study of fatigue is critical for these components. The trend to increase turboengines diameter (Fig. 1) to improve aerodynamic performances increases the risk of occurrence of geometrically

nonlinear behaviour of the structure leading to nonlinear vibrations. The assessment of this nonlinear behaviour is vital in the design process because it influences the maximum amplitudes of the structure as well as frequency at which the structure presents a peak of displacements (resonance) which may differ from the natural frequency of the structure. Besides these geometrical nonlinearities, the disk-blade contact interactions induces vibrations to the system and the wear between both surfaces can lead to an accelerated deterioration of the properties of the engine. Furthermore, the reduction in tip clearance can lead to contact conditions between the blade and the stator. In order to reduce the clearance gap some techniques imply contact between the blade tip and an abrasive material.

An accurate evaluation of the nonlinear behaviour of the structure leads to an improved stress analysis. Thus, the structure's design could be adapted in order to optimize its weight while being capable of resisting the amplitudes in the surroundings of the nonlinear resonance frequency.

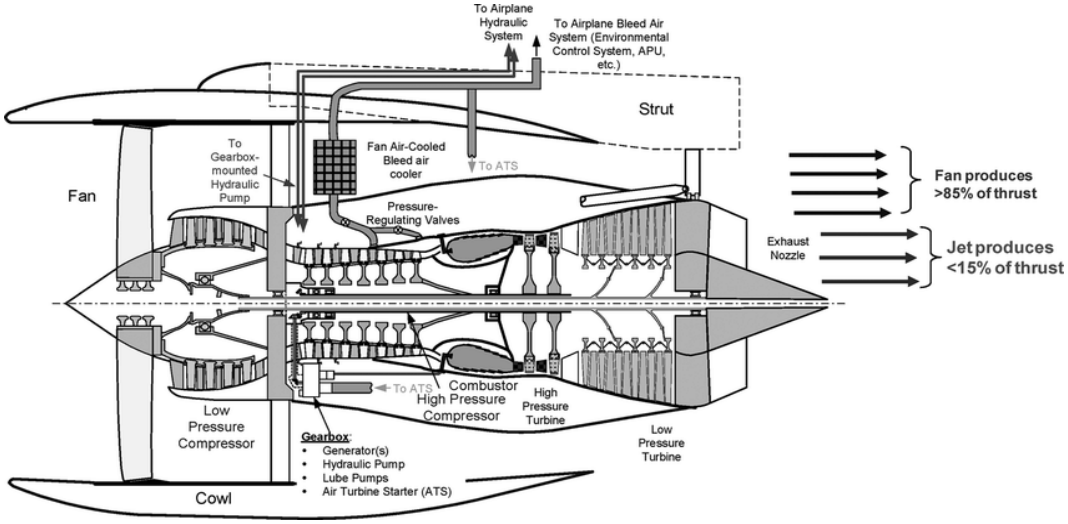

Figure 1: Scheme of a turboengine [Luongo et al., 2009].

As shown in Fig. 2 the fluid flow between the blades is particularly complex due to: the geometry of these elements, the relative movements between the rotor and the stator as well as the extreme conditions in terms of temperature and pressure. Furthermore, the fluid is accelerated from subsonic to transonic regimes. The resulting blade-wall pressure, that might present sonic shocks, induces unsteady loadings on the blades. The latter loadings are coupled with the vibrations of the blade and require aeroelastic analysis to be accurately predicted. Due to the high Reynolds number involved, complex aerodynamic computations are carried out to properly capture the turbulent effects. Additionally, the complex flow is influenced by the tip clearance flow and the environmental effects such as multistage.

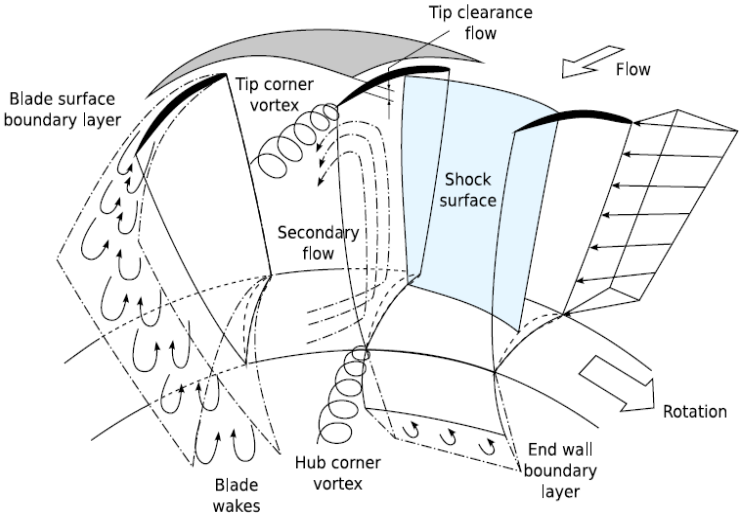

Figure 2: Main aerodynamic phenomena in turbomachinery blades [McNally, 1977].

The study of unsteady aerodynamics is out of the scope of this thesis and therefore the aerodynamic loading is represented as an harmonic external excitation at the tip of the studied structures.

The Campbell diagram

The Campbell diagram is a graphical representation of the natural frequencies of the structure with respect to the rotating velocity. The Campbell diagram also represents the engine order lines that correspond to the excitation at multiples of the rotating velocity of the shaft. In the surroundings of the intersections between the engine orders and the natural frequency lines of the structure (see Fig. 3), the risk of resonant responses is increased. When the structure is operating at these intersections, the rotating velocity induces external loadings at resonance leading generally to large displacements of the structure with a potential risk of failure. The operating regime of the engines are placed out of these intersection areas, however, in the acceleration/deceleration phases the structure is submitted to an amplified regime for some cycles. The natural frequencies that are studied in the Campbell diagram correspond to the linearised natural frequencies. For very nonlinear structures, the nonlinear shift of the resonant peak would lead to large displacements regions out of the Campbell intersections.

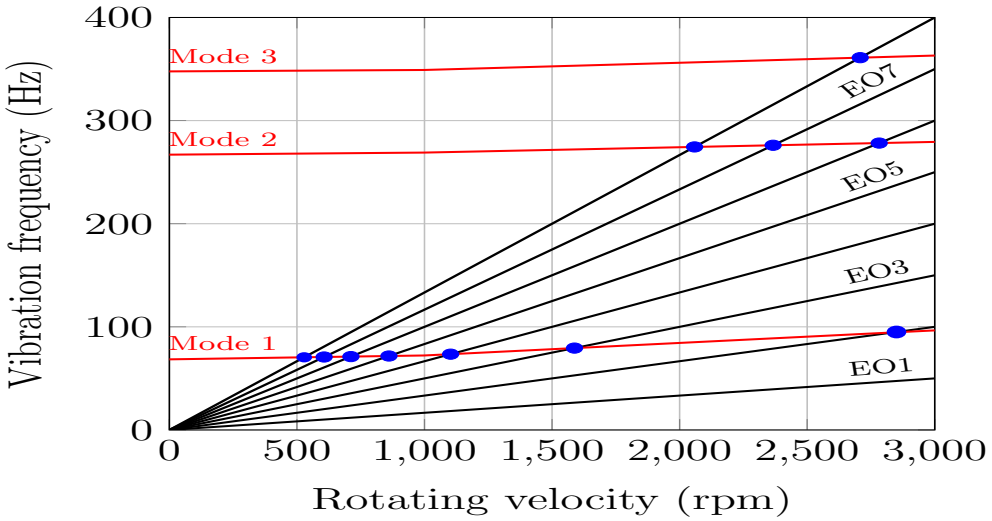

Figure 3: Example of a Campbell diagram.

Interest of constructing ROMs

One of the tools widely used to determine the response level of a structure with respect to the excitation frequency is the forced response. By computing the force response at a given excitation intensity, the response of the structure is obtained. Furthermore, the construction of the forced response permits to identify the resonant frequencies of the structure and the maximum level of the response. Thus, the maximum stress state is computed in order to identify the resistant properties of the studied structure and design it in order to fulfil the resistant constraints. The finite element softwares developed now a days are capable of providing accurate results for complex structures with multiple nonlinearities (geometrical, contact, ...). However, for nonlinear evaluations, the computational time can be very large. For example, in the fan blade structure presented in Chapter 3, to compute one single point of the curve in Fig. 4 with the finite element model, 90 CPU hours are needed, which corresponds to 3 days and 18 hours of computation. From an industrial point of view, such computational time is unacceptable, thus, the need for accurate ROMs that provide an approximate solution but with an optimised computational time (of the order of 20s) is a powerful tool for the designer.

If the ROM is capable of providing accurate results, the designer can construct a forced response in some minutes versus some weeks of computation with the finite element model. In nonlinear dynamics, in the neighbourhood of the nonlinear resonance, for a given excitation frequency the solution presents more than one solution. The latter leads to supplementary computations in order to evaluate the branches of the backbone curve (Fig. 2.2c).

Then, considering the geometrically nonlinear behaviour of the structure in

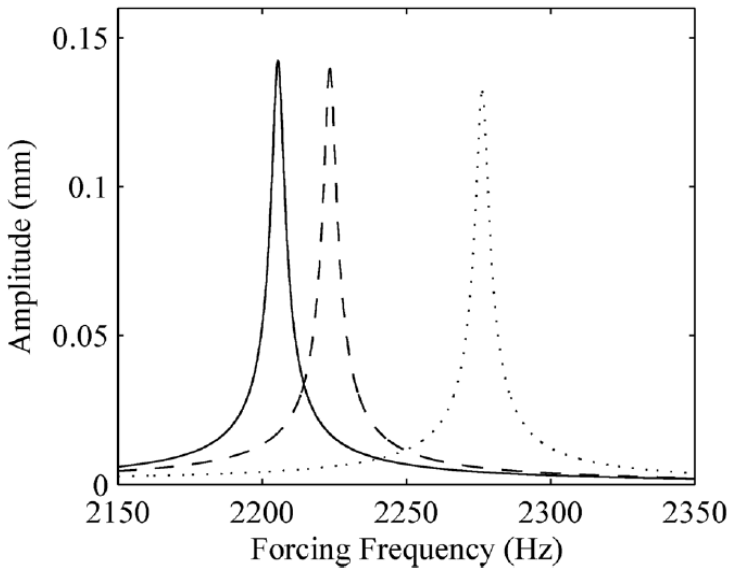

Figure 4: Forced response curves of a linear ROM showing the effects rotational speed has on system responses under $\omega_{ext} = \omega_1$ (Ω) (EO1) for 0 RPM (-), 10,000 RPM (–), and 20,000 RPM ($\cdots$) rotational speed values [Kurstak et al., 2018].

the ROM would permit to improve the prediction of the structure's behaviour and thus optimise its dimensions with a reduced computational cost.

Outlook of the manuscript

The remainder of this manuscript is structured as follows:

In Chapter 1 the strong from of the problem, that represents the dynamic behaviour of the structure for the studied nonlinearities, is transformed into the continuum weak form suitable for discretisation by means of the finite element method. The discretised equation of motion for the dynamic analysis of rotating structures is adapted to be a function of the nonlinear vibrations of the structure. The concept of the reference solution also called full order model (FOM) is introduced.

In Chapter 2, the reduced order techniques are introduced. The concept of reduced basis is defined and some of the classical projection based methods are presented. The geometrical and contact nonlinearities are studied in order to introduce them into the ROM. In this section, an original POD based correction is proposed to correct the spurious artefacts that arise when considering the classical Stiffness Evaluation Procedure for complex slender structures, when combined with the classical reduced basis. The proposed POD based correction consists in filtering the FOM forces before projection. Besides, the

solution methods that are implemented to study the time response of the structure are presented.

Chapter 3 includes all the studied numerical applications. Three different structures are studied in order to asses the accuracy of different ROMs. First a thick cantilever beam is studied in order to highlight the necessity of the POD based correction to represent the nonlinear coupling between motions. Second, a thin cantilever structure is considered to asses the best procedure to construct the proposed Stiffness Evaluation Procedure with POD nonlinear forces Correction (StepC ROM). Then, the model is evaluated for two excitation cases (static and dynamic) for rotating and non rotating states. In addition, a simple contact case is studied to verify that the ROM is capable of considering the effect of the nonlinear coupling between contact and geometrical nonlinearities. The third structure is a complex structure representing a fan blade. The reduced basis are parametrised in order to reduce the construction time of the ROM and to be capable of providing rapid results for a variety of rotating velocities. The structure is studied at the first bending mode. In addition, the forced response of the structure is also evaluated in the surrounding of the first mode. For all the studied cases and structures, the proposed StepC ROM provides more accurate solutions than the classical Linearised ROM and than the STEP ROM.

Chapter 1

Equations of motion of nonlinear rotating structures

THIS FIRST CHAPTER provides the theoretical bases to solve the dynamics of rotating structures with large displacement and friction contact nonlinearities which is the physical problem for which reduced order models (ROMs) are developed and studied in the following chapters. First, the "integral" or "weak form" of the physical problem, suitable for discretisation, is obtained from its "differential" or "strong form". Then, by means of the Finite Element Method (FEM) the continuum formulation is discretised and the Full Order Model (FOM) of the structure is defined. The motion of the structure is represented as the sum of a static displacement induced by the rotation and a nonlinear vibration around the static state. The FOM defined in this chapter will provide the reference solution of the reduced order models (ROMs) developed later.

Contents

1.1 Introduction

Rotation of structures induces an inertial static loading state whose influence on the aerodynamic performances of these structures is not negligible when the rotating velocity is high. This is amplified for slender structures such as, blades in turbomachinery, specially for the blades of wind generators, helicopter blades, and fan and booster stages where long wide-chord blades are found. The design tendency to reduce the mass and the rotating velocity and to augment the length of these structures increases the nonlinear effects associated to large displacements. Furthermore, in the dynamic case, the aerodynamic interactions with the blades can induce large displacements on these components, i.e. the forced response in aeroelasticity.

Hereinafter the classical hypothesis that the vibrations around the quasi-static equilibrium state induced by rotation [Henry, 1981, Sternchüss, 2009] are linear is enhanced to consider large displacement vibrations. The latter statement is specially true for low rotating velocities. For high and very high rotating regimes, the classical hypothesis remains valid as the behaviour of the structure is stiffened. However, even for small vibrations, considering a geometrically nonlinear behaviour of the structure permits to identify the shift in the natural frequency that is observed in geometrically nonlinear dynamics (see section 2.4.1) and the level of vibration is accurately represented.

The length-extension and the de-twisting effect of the inertial load may lead to contact between the tip of the rotating structures and the stator [Burton et al., 1976, Padova et al., 2007, Legrand et al., 2008, Batailly et al., 2014]. Furthermore, some of the energy dissipation devices such as *under-platform* dampers [Sanliturk et al., 2001, Petrov and Ewins, 2007, Firrone et al., 2011, Gastaldi et al., 2017], *shroud* dampers [D'Ambrosio et al., 2005, Jiazhe et al., 2018] or *lacing wire* dampers [Hager et al., 1968, Drozdowski et al., 2016] need to consider the nature of contact. The study of different contact models is developed in [Sayed, 2011, Petrov and Ewins, 2006] and a review of the vibration behaviour of bladed disks is carried out in [Krack et al., 2017]. The contact mechanics formulations and their numerical implementations are developed in [Laursen, 2002, Wriggers and Zavarise, 2004, Yastrebov, 2011, Konyukhov and Schweizerhof, 2012].

The remainder of this chapter is structured as follows: First, the strong form of the dynamics of a rotating structure with large displacements and contact nonlinearities is presented. Second, the continuum weak form of a rotating structure with large displacements non linearities is developed inspired by [Sternchüss, 2009]. Third, the continuum weak form for the contact problem that takes the form of a variational inequality and some classical contact laws are presented based on the work of [Yastrebov, 2011]. Then, the variational

inequality is solved by the penalty optimisation technique. Fourth, the discrete formulation of the mechanical problem is obtained. Fifth, the latter formulation is adapted as a function of the vibrations around the static-equilibrium induced by rotation and the Full Order Model (FOM) is introduced. Finally, some concluding remarks are drawn to justify the modelling hypotheses considered in the following chapters.

1.2 Continuum formulation of rotating structures with large displacements and contact non linearities

1.2.1 Strong form of the problem

Considering the solid presented in Fig. 1.1, submitted to surface and volumetric external forces, imposed displacement and contact boundary conditions, the strong form, or differential form, of the mechanical dynamic problem with respect to the current configuration is defined as follows,

$$
\begin{aligned}
-\rho \mathbf{a}_x + \operatorname{div} \sigma_{\mathbf{x}} + \mathbf{f}_{v_x} &= \mathbf{0} \quad \text{in} \quad V(t)\,, && (1.1)\\
\sigma_{\mathbf{x}} \mathbf{n} &= \sigma_0 \quad \text{at} \quad \Gamma_f\,, && (1.2)\\
\mathbf{u}_p &= \mathbf{u}_{p_0} \quad \text{at} \quad \Gamma_u\,, && (1.3)\\
g_n \geq 0,\ 0 \geq \sigma_n,\ \sigma_n g_n = 0,\ \sigma_t &= \mathbf{0} \quad \text{at} \quad \Gamma_c\,, && (1.4)
\end{aligned}
$$

where ρ is the material density, $\mathbf{a}_x$ represents the acceleration of the body, σ is the *Cauchy stress* tensor and $\mathbf{f}_{v_x}$ is the vector of volume forces in the current deformed configuration V(t).

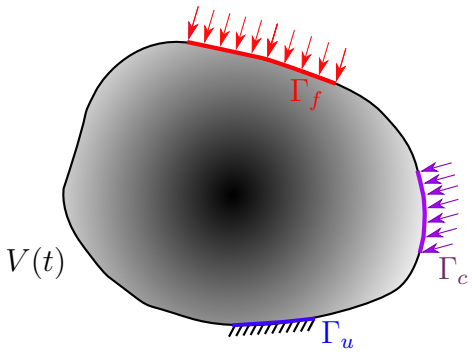

Figure 1.1: Scheme of the studied solid and its boundary conditions.

The boundary conditions are defined in Eqn. (1.2) to (1.4) where σ_0 is a prescribed force (Neumann boundary condition) applied at Γ_f, $\mathbf{u}_{p_0}$ represents an imposed displacement (Dirichlet boundary condition) at the boundary Γ_u

and Eqn. (1.4) presents the Hertz-Signorini-Moreau frictionless contact conditions as presented in [Wriggers and Nackenhorst, 2006] where σ_n and σ_t are the normal and tangential stresses respectively and g_n is the normal gap. In subsection 1.2.4 the weak form of the variational inequality for contact problem with friction is introduced. For the latter problem, some classical friction laws are presented. Furthermore, the variational inequality is solved using the *penalty* method and the Coulomb's law of friction. In litterature other techniques are found such as, the *Lagrange multipliers* method, the *augmented Lagrangian* method [Powell, 1969, Hestenes, 1969], the *perturbed Lagrangian* method or the *barrier* method.

1.2.2 Transformation gradient and material behaviour

The displacements of the solid in the deformed configuration at time t, defined as $\mathbf{x}(\mathbf{p},\, t)$, are the mapping that transforms the initial volume, $V(0)$, into the deformed configuration volume, $V(t)$, between times 0 and t as shown in Fig. 1.2.

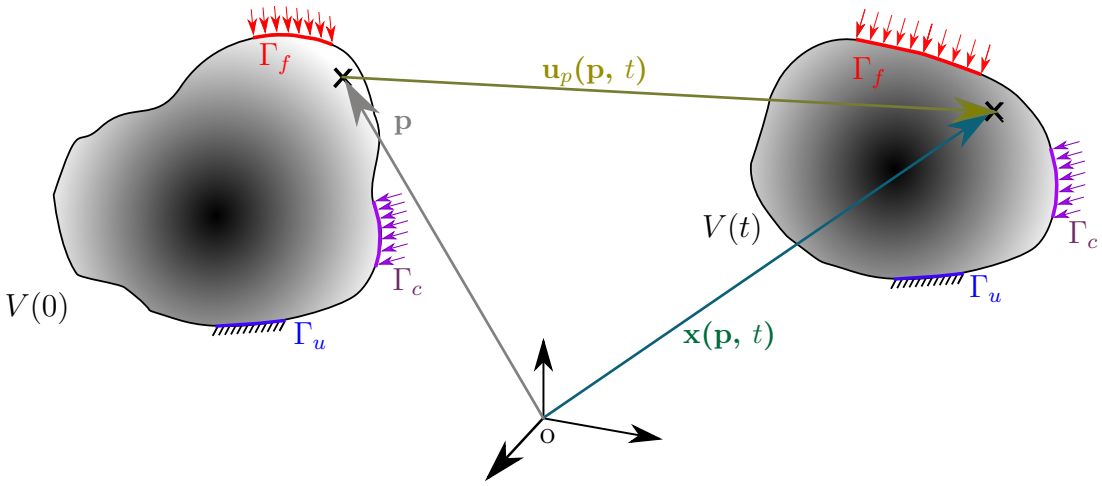

Figure 1.2: Transformation of the studied solid between the initial $V(0)$ and the current $V(t)$ configurations.

Thus, the gradient of the transformation, $\mathbf{X}$, is defined as,

$$\mathbf{X}_p(\mathbf{u}_p(\mathbf{p},\, t),\, t) = \frac{\partial \mathbf{x}}{\partial \mathbf{p}}\,(\mathbf{p}, t)\ . \tag{1.5}$$

If the current displacements are defined with respect to the initial configuration as,

$$\mathbf{u}_p(\mathbf{p},\, t) = \mathbf{x}(\mathbf{p},\, t) - \mathbf{p} \tag{1.6}$$

the gradient of the transformation becomes,

$$\mathbf{X}_p(\mathbf{u}_p(\mathbf{p},\, t),\, t) = \mathbf{I} + \frac{\partial \mathbf{u}_p}{\partial \mathbf{p}}\,(\mathbf{p}, t)\ . \tag{1.7}$$

The right *Cauchy-Green* tensor is defined as,

$$\begin{aligned}\mathbb{C}_p\left(\mathbf{u}_p(\mathbf{p},\, t),t\right) &= \mathbf{X}_p(\mathbf{u}_p(\mathbf{p},\, t),\, t)^T\mathbf{X}_p(\mathbf{u}_p(\mathbf{p},\, t),\, t)\\ &= \mathbf{I} + \frac{\partial \mathbf{u}_p}{\partial \mathbf{p}}(\mathbf{p},t) + \left(\frac{\partial \mathbf{u}_p}{\partial \mathbf{p}}(\mathbf{p},t)\right)^T + \left(\frac{\partial \mathbf{u}_p}{\partial \mathbf{p}}(\mathbf{p},t)\right)^T \frac{\partial \mathbf{u}_p}{\partial \mathbf{p}}(\mathbf{p},t)\ .\end{aligned} \tag{1.8}$$

Then, the *Green-Lagrange* symmetric strain tensor which assuming large displacements with small strains configuration is obtained as,

$$\mathbf{E}_p(\mathbf{u}_p(\mathbf{p},\, t),\, t) = \frac{1}{2}\left(\mathbb{C}_p\left(\mathbf{u}_p(\mathbf{p},\, t),t\right) - \mathbf{I}\right)\ , \tag{1.9}$$

and in terms of the displacements with respect to the initial configuration,

$$\mathbf{E}_p(\mathbf{u}_p(\mathbf{p},\, t),\, t) = \underbrace{\frac{1}{2}\left(\frac{\partial \mathbf{u}_p}{\partial \mathbf{p}}(\mathbf{p},t) + \left(\frac{\partial \mathbf{u}_p}{\partial \mathbf{p}}(\mathbf{p},t)\right)^T\right)}_{\text{Linear part}} + \underbrace{\frac{1}{2}\left(\left(\frac{\partial \mathbf{u}_p}{\partial \mathbf{p}}(\mathbf{p},t)\right)^T \frac{\partial \mathbf{u}_p}{\partial \mathbf{p}}(\mathbf{p},t)\right)}_{\text{Nonlinear part}}\ . \tag{1.10}$$

The *Green-Lagrange* strain tensor is formed by a linear part (called *Cauchy's infinitesimal strain tensor*) and a nonlinear part. In the study of the mechanical vibrations, it is commonly considered that the initial volume of the structure is similar to the current configuration volume, $V(0) \approx V(t)$. The hypothesis is largely implemented in the turbomachinery field. Thus, hereinafter, a small strain with large displacements formulation is considered.

The viscous behaviour of the structure is introduced by means of a damping matrix, $\mathbf{C}$ (defined in Eqn. (1.75)) once the continuum problem is discretised.

By using the *Principle of virtual work* the weak form of the problem is obtained. A *virtual work* is the work done by a *real force* acting through a *virtual displacement*, $\delta\mathbf{u}_x(\mathbf{x})$, where a virtual displacement is defined as any displacement that satisfies the boundary conditions of the problem and belongs to the Sobolev space, $\mathcal{H}^1(V)$ and $\delta\mathbf{u}_x(\mathbf{x}) = 0$ at Γ_u. Thus, in practice, the expression in Eqn. (1.1) is multiplied by the virtual displacement, $\delta\mathbf{u}_x(\mathbf{x})$, and integrated through the volume V(t). Then the equivalence between the virtual displacements referred to the initial configuration, $\delta\mathbf{u}_p(\mathbf{p})\in \mathcal{H}^1(V(0))$, and between the virtual displacements referred to the current configuration, $\delta\mathbf{u}_x(\mathbf{x}(\mathbf{p},\, t))\in \mathcal{H}^1(V(t))$ is,

$$\delta\mathbf{u}_p(\mathbf{p}) = \delta\mathbf{u}_x(\mathbf{x}) = \delta\mathbf{u}_x(\mathbf{x}(\mathbf{p},\, t))\ , \tag{1.11}$$

this equation is used in the following to compute the integrals of the current configuration with respect to the initial configuration.

Hereunder, the weak form related to each of the considered nonlinearities is developed separately. First, the weak form that considers the rotation of the structure with large displacements nonlinearity is developped. Then, the weak

variational inequality of the contact between two elastic bodies is introduced. Both nonlinearities are merged to formulate the weak form of the problem and to define the Full Order Model (FOM) equation of movement in the discrete domain, Eqn. (1.74).

1.2.3 Continuum weak form of a rotating structure with large displacement nonlinearities

Weak form in the current configuration

Let $\xi(V(t))$ be a subspace of the Sobolev space $\mathcal{H}^1(V)$ representing the space of *kinematically admissible* displacements for any configuration V. The weak form of the problem in the current configuration is:

Find $\boldsymbol{u}_x \in \xi(V(t))$ *such that* $\forall \delta\boldsymbol{u}_x(\boldsymbol{x}) \in \xi(V(t))$, *the equilibrium of the virtual work is satisfied,* $\delta W_a(\boldsymbol{u}_x, \delta\boldsymbol{u}_x) = \delta W_i(\boldsymbol{u}_x, \delta\boldsymbol{u}_x) + \delta W_e(\boldsymbol{u}_x, \delta\boldsymbol{u}_x)$.

The virtual work associated to the acceleration, $\mathbf{a}_x(\mathbf{x},\, t)$, is,

$$\delta W_a(\mathbf{u}_x, \delta\mathbf{u}_x) = \int_{V(t)} \rho_x(\mathbf{x})\mathbf{a}_x(\mathbf{x},\, t) \cdot \delta\mathbf{u}_x(\mathbf{x})\mathrm{d}V(t)\ , \tag{1.12}$$

with $\rho_x(\mathbf{x})$ as the density at $V(t)$ configuration.

The virtual work of the internal forces is,

$$\delta W_i(\mathbf{u}_x, \delta\mathbf{u}_x) = -\int_{V(t)} \sigma_x(\mathbf{u}_x(\mathbf{x},\, t)) : \varepsilon_x(\delta\mathbf{u}_x(\mathbf{x}))\,\mathrm{d}V(t)\ , \tag{1.13}$$

where $\sigma_x(\mathbf{u}_x(\mathbf{x},\, t))$ is the *Cauchy stress* tensor and $\varepsilon_x(\delta\mathbf{u}_x(\mathbf{x}))$ is the *strain* at the deformed configuration.

The virtual work of the external forces is,

$$\delta W_e(\mathbf{u}_x, \delta\mathbf{u}_x) = \textstyle\int_{V(t)} \mathbf{f}_{v_x}(\mathbf{x},\, t) \cdot \delta\mathbf{u}_x(\mathbf{x})\mathrm{d}V(t) + \int_{\partial V(t)} \mathbf{f}_{s_x}(\mathbf{x},\, t) \cdot \delta\mathbf{u}_x(\mathbf{x})\mathrm{d}S(t)\ , \tag{1.14}$$

where $\mathbf{f}_{v_x}(\mathbf{x},\, t)$ is the volumetric external forces and $\mathbf{f}_{s_x}(\mathbf{x},\, t)$ if the external surface forces. Note that the contact nonlinearity corresponds to a surface force. In order to simplify the formulation of the studied phenomena, the continuum formulation of the contact type nonlinearity is developed in section 1.2.4.

Weak form in the undeformed initial configuration

As the current configuration $V(t)$is "a priori" unknown, the integrals in Eqn. (1.12) to (1.14) are difficult to evaluate. Thus, it is suitable to asses the

problem with respect to the known initial configuration, $V(0)$. Furthermore, the latter configuration is discretised with the finite element method (FEM). Thus, the weak form of the problem in terms of the undeformed initial configuration:

Find $\boldsymbol{u}_p(\boldsymbol{p},\ t) \in \xi\left(V(0)\right)$ *such that* $\forall \delta\boldsymbol{u}_p(\boldsymbol{p}) \in \xi\left(V(0)\right)$*, the work done by the virtual displacements is in equilibrium,* $\delta W_a\left(\boldsymbol{u}_p, \delta\boldsymbol{u}_p\right) = \delta W_i\left(\boldsymbol{u}_p, \delta\boldsymbol{u}_p\right) + \delta W_e\left(\boldsymbol{u}_p, \delta\boldsymbol{u}_p\right)$.

Transforming the acceleration term due to rotation

The velocity of the structure with respect to the fixed reference frame in terms of the current configuration [Desceliers, 2001] is,

$$\mathbf{v}_x(\mathbf{x},\ t) = \frac{\partial \mathbf{x}}{\partial t} + \Omega(\mathrm{t})\mathbf{x}\ , \tag{1.15}$$

or with respect to the initial configuration,

$$\mathbf{v}_p(\mathbf{p},\ t) = \underbrace{\frac{\partial \mathbf{u}_p}{\partial t}\left(\mathbf{p}, t\right)}_{\text{Elastic motion}} + \underbrace{\boldsymbol{\Omega}(\mathrm{t})\left(\mathbf{p} + \mathbf{u}_p(\mathbf{p},\ t)\right)}_{\text{Rigid body motion of rotation}} \tag{1.16}$$

Thus, the velocity of the structure results from the sum of an elastic motion and a rigid body motion of rotation. The vector $\boldsymbol{\omega}(t)$ with components $\omega_x(t), \omega_y(t), \omega_z(t)$, represents the rotation relative to a basis $(\mathbf{e}_x, \mathbf{e}_y, \mathbf{e}_z)$. The matrix product $\boldsymbol{\Omega}(\mathrm{t})\cdot$ is equivalent to the cross product $\boldsymbol{\omega}(t)\wedge$ where $\Omega(\mathrm{t})$ is defined as the skew-symmetric matrix,

$$\boldsymbol{\Omega}(\mathrm{t}) = \begin{bmatrix} 0 & -\omega_z(t) & \omega_y(t) \\ \omega_z(t) & 0 & -\omega_x(t) \\ -\omega_y(t) & \omega_x(t) & 0 \end{bmatrix}\ . \tag{1.17}$$

Deriving Eqn. (1.15) and (1.16) with respect to time, the expressions of the acceleration for the fixed frame of reference are obtained. With respect to the current configuration,

$$\mathbf{a}_x(\mathbf{x},\ t) = \frac{\partial \mathbf{v}_x}{\partial t}\left(\mathbf{x}, t\right) + \frac{\mathrm{d}\boldsymbol{\Omega}(\mathrm{t})}{\mathrm{d}t}\mathbf{x} + 2\boldsymbol{\Omega}(\mathrm{t})\frac{\partial \mathbf{x}}{\partial t}\left(\mathbf{x}, t\right) + \boldsymbol{\Omega}(\mathrm{t})^2\mathbf{x}\ , \tag{1.18}$$

and with respect to the initial configuration,

$$\begin{aligned} \mathbf{a}_p(\mathbf{p},\ t) = & \underbrace{\frac{\partial^2 \mathbf{u}_p}{\partial t^2}\left(\mathbf{p}, t\right)}_{\text{Acc. in the rotating frame}} + \underbrace{\frac{\mathrm{d}\boldsymbol{\Omega}(\mathrm{t})}{\mathrm{d}t}\left(\mathbf{p} + \mathbf{u}_p(\mathbf{p},\ t)\right)}_{\text{Euler acc.}} + \underbrace{2\boldsymbol{\Omega}(\mathrm{t})\frac{\partial \mathbf{u}_p}{\partial t}\left(\mathbf{p}, t\right)}_{\text{Coriolis acc.}} \\ & + \underbrace{\boldsymbol{\Omega}(\mathrm{t})^2\left(\mathbf{p} + \mathbf{u}_p(\mathbf{p},\ t)\right)}_{\text{Centrifugal acc.}}\ . \end{aligned} \tag{1.19}$$

Since the density in both frames is related to the Jacobian, $\rho_p(\mathbf{p}) = \mathbf{J}(\mathbf{u}_p(\mathbf{p}, t))\rho_x(\mathbf{x})$, the virtual work related to the acceleration is,

$$\begin{aligned}\delta W_a(\mathbf{u}_p, \delta\mathbf{u}_p) &= \int_{V(0)} \rho_p(\mathbf{p})\mathbf{a}_p(\mathbf{p},t)\cdot\delta\mathbf{u}_p(\mathbf{p})\mathrm{d}V(0)\\ &= \int_{V(0)} \rho_p(\mathbf{p})\frac{\partial^2\mathbf{u}_p}{\partial t^2}(\mathbf{p},t)\cdot\delta\mathbf{u}_p(\mathbf{p})\mathrm{d}V(0)\\ &+ \int_{V(0)} 2\rho_p(\mathbf{p})\mathbf{\Omega}(\mathrm{t})\frac{\partial\mathbf{u}_p}{\partial t}(\mathbf{p},t)\cdot\delta\mathbf{u}_p(\mathbf{p})\mathrm{d}V(0)\\ &+ \int_{V(0)} \rho_p(\mathbf{p})\left(\mathbf{\Omega}(\mathrm{t})^2 + \frac{\mathrm{d}\mathbf{\Omega}(\mathrm{t})}{\mathrm{d}t}\right)\mathbf{p}\cdot\delta\mathbf{u}_p(\mathbf{p})\mathrm{d}V(0)\\ &+ \int_{V(0)} \rho_p(\mathbf{p})\left(\mathbf{\Omega}(\mathrm{t})^2 + \frac{\mathrm{d}\mathbf{\Omega}(\mathrm{t})}{\mathrm{d}t}\right)\mathbf{u}_p(\mathbf{p},t)\cdot\delta\mathbf{u}_p(\mathbf{p})\mathrm{d}V(0)\,.\end{aligned} \tag{1.20}$$

Transforming the internal forces term

Considering that $\mathrm{d}V(t) = \mathbf{J}(\mathbf{u}_p(\mathbf{p}, t), t)\mathrm{d}V(0)$ and introducing the expression of the derivative of $\delta\mathbf{u}_x(\mathbf{x})$ with respect to $\mathbf{x}$, $\frac{\partial\delta\mathbf{u}_x(\mathbf{x})}{\partial\mathbf{x}}$, into Eqn. (1.13) the virtual work of the internal forces is integrated with respect to the initial configuration,

$$\begin{aligned}\delta W_i(\mathbf{u}_p, \delta\mathbf{u}_p) = -\int_{V(0)} &\left(\sigma_x(\mathbf{u}_x(\mathbf{x}, t), t)\mathbf{X}_p(\mathbf{u}_p(\mathbf{p}, t), t)^{-T}\right)\\ &: \frac{\partial\delta\mathbf{u}_p}{\partial\mathbf{p}}(\mathbf{p})\,\mathbf{J}(\mathbf{u}_p(\mathbf{p}, t), t)\mathrm{d}V(0)\,.\end{aligned} \tag{1.21}$$

Note that in the expression above, the non-symmetric *first Piola-Kirchhoff* tensor, or Boussinesq stress tensor, $\tau_p(\mathbf{u}_p(\mathbf{p}, t))$, is implicitly represented,

$$\tau_p(\mathbf{u}_p(\mathbf{p}, t)) = \mathbf{J}(\mathbf{u}_p(\mathbf{p}, t))\sigma_x(\mathbf{u}_x(\mathbf{x}, t))\mathbf{X}_p(\mathbf{u}_p(\mathbf{p}, t))^{-T}\,. \tag{1.22}$$

Then, the virtual work of the internal forces is rewritten as,

$$\delta W_i(\mathbf{u}_p, \delta\mathbf{u}_p) = -\int_{V(0)} \tau_p(\mathbf{u}_p(\mathbf{p}, t), t) : \frac{\partial\delta\mathbf{u}_p}{\partial\mathbf{p}}(\mathbf{p})\,\mathrm{d}V(0)\,, \tag{1.23}$$

however, the non-symmetry of the *first Piola-Kirchhoff* tensor is not suitable for the weak form of the problem. Thus, the symmetric *second Piola-Kirchhoff* tensor is defined as,

$$\mathbf{S}_p(\mathbf{u}_p(\mathbf{p}, t)) = \mathbf{J}(\mathbf{u}_p(\mathbf{p}, t))\mathbf{X}_p(\mathbf{u}_p(\mathbf{p}, t))^{-1}\sigma_x(\mathbf{u}_x(\mathbf{x}, t))\mathbf{X}_p(\mathbf{u}_p(\mathbf{p}, t))^{-T}\,. \tag{1.24}$$

The *second Piola-Kirchhoff* tensor does not have a physical meaning. It corresponds to a suitable stress measure which is energetically conjugate with

the *Green-Lagrange* strain tensor.

Thus, for an homogeneous, isotropic, non-dissipative and linearly elastic material the displacements (or strains) and the stress tensor are related through the constitutive equation,

$$\mathbf{S}_p(\mathbf{u}_p(\mathbf{p},\, t),\, t) = \mathbb{D}\,(\mathbf{p}) : \mathbf{E}_p(\mathbf{u}_p(\mathbf{p},\, t),\, t)\ , \tag{1.25}$$

where $\mathbb{D}\,(\mathbf{p})$ is the fourth-order tensor associated with Hook's law of elasticity. Then, by substituting the expression of the *second Piola-Kirchhoff* tensor and introducing the constitutive equation of the material into the virtual work associated to the internal forces,

$$\begin{aligned}\delta W_i\,(\mathbf{u}_p, \delta\mathbf{u}_p) &= -\int_{V(0)} \mathbf{S}_p(\mathbf{u}_p(\mathbf{p},\, t),\, t) : \left(\mathbf{X}_p(\mathbf{u}_p(\mathbf{p},\, t),\, t)^T \frac{\partial \delta\mathbf{u}_p}{\partial \mathbf{p}}\,(\mathbf{p})\right) \mathrm{d}V(0) \\ &= -\int_{V(0)} \underbrace{\mathbb{D}\,(\mathbf{p}) : \mathbf{E}_p(\mathbf{u}_p(\mathbf{p},\, t),\, t) : \left(\mathbf{X}_p(\mathbf{u}_p(\mathbf{p},\, t),\, t)^T}_{(*)}\ \frac{\partial \delta\mathbf{u}_p}{\partial \mathbf{p}}\,(\mathbf{p})\right) \mathrm{d}V(0)\ .\end{aligned} \tag{1.26}$$

Then, from the expression in * the following development is obtained,

$$\begin{aligned}\mathbf{X}_p(\mathbf{u}_p(\mathbf{p},\, t),\, t)\mathbf{S}_p(\mathbf{u}_p(\mathbf{p},\, t),\, t) = \mathbb{D}\,(\mathbf{p}) &: \frac{\partial \mathbf{u}_p}{\partial \mathbf{p}}\,(\mathbf{p}, t) \\ &+ \frac{1}{2}\mathbb{D}\,(\mathbf{p}) : \left(\left(\frac{\partial \mathbf{u}_p}{\partial \mathbf{p}}\,(\mathbf{p}, t)\right)^T \frac{\partial \mathbf{u}_p}{\partial \mathbf{p}}\,(\mathbf{p}, t)\right) \\ &+ \frac{\partial \mathbf{u}_p}{\partial \mathbf{p}}\,(\mathbf{p}, t)\, \mathbf{S}_p(\mathbf{u}_p(\mathbf{p},\, t),\, t)\ ,\end{aligned} \tag{1.27}$$

and the virtual work related to the internal forces is rewritten as,

$$\begin{aligned}\delta W_i\,(\mathbf{u}_p, \delta\mathbf{u}_p) = &-\int_{V(0)} \frac{\partial \delta\mathbf{u}_p}{\partial \mathbf{p}}\,(\mathbf{p}) : \mathbb{D}\,(\mathbf{p}) : \frac{\partial \mathbf{u}_p}{\partial \mathbf{p}}\,(\mathbf{p}, t)\, \mathrm{d}V(0) \\ &-\int_{V(0)} \frac{\partial \delta\mathbf{u}_p}{\partial \mathbf{p}}\,(\mathbf{p}) : \frac{\partial \mathbf{u}_p}{\partial \mathbf{p}}\,(\mathbf{p}, t)\, \mathbf{S}_p(\mathbf{u}_p(\mathbf{p},\, t),\, t)\mathrm{d}V(0) \\ &-\int_{V(0)} \frac{1}{2}\frac{\partial \delta\mathbf{u}_p}{\partial \mathbf{p}}\,(\mathbf{p}) : \mathbb{D}\,(\mathbf{p}) : \left(\frac{\partial \mathbf{u}_p}{\partial \mathbf{p}}\,(\mathbf{p}, t)\, \frac{\partial \mathbf{u}_p}{\partial \mathbf{p}}\,(\mathbf{p}, t)^T\right) \mathrm{d}V(0)\ .\end{aligned} \tag{1.28}$$

Transforming the external forces term

The virtual work of the exterior forces with respect to the initial configuration is obtained by means of the *Jacobian*, $\mathbf{J}(\mathbf{u}_p(\mathbf{p},\, t),\, t)$, thus,

$$\mathbf{f}_{v_p}(\mathbf{p},\, t) = \mathbf{J}(\mathbf{u}_p(\mathbf{p},\, t),\, t)\mathbf{f}_{v_x}(\mathbf{x},\, t)\ , \tag{1.29}$$

$$\mathbf{f}_{s_p}(\mathbf{p},\, t) = \mathbf{J}(\mathbf{u}_p(\mathbf{p},\, t),\, t)||\mathbf{X}_p(\mathbf{u}_p(\mathbf{p},\, t),\, t)^{-T}\mathbf{n}_p(\mathbf{p},\, t)||\mathbf{f}_{s_x}(\mathbf{x},\, t) \tag{1.30}$$

where $\mathbf{n}_p(\mathbf{p},\, t)$ is the outward-pointing vector normal to the elementary surface $\mathrm{d}S(0)$. Then, the virtual work of the exterior forces with respect to the initial configuration $V(0)$ is,

$$\delta W_e\,(\mathbf{u}_p, \delta\mathbf{u}_p) = \int_{V(0)} \mathbf{f}_{v_p}(\mathbf{p},\, t)\delta\mathbf{u}_p(\mathbf{p})\mathrm{d}V(0) + \int_{\partial V(0)} \mathbf{f}_{s_p}(\mathbf{p},\, t)\delta\mathbf{u}_p(\mathbf{p})\mathrm{d}S(0)\ . \tag{1.31}$$

Bilinear and linear forms of the continuum problem

The bilinear and linear forms function of $\mathbf{u}_p$ and $\delta\mathbf{u}_p$ presented hereunder are the continuum forms that are discretised in section 1.3.1 with a Ritz-Galerkin procedure.

1. Bilinear form of *mass*:

$$\mathcal{M}(\mathbf{u}_p,\, \delta\mathbf{u}_p) = \int_{V(0)} \rho_p\,(\mathbf{p})\, \mathbf{u}_p(\mathbf{p},\, t) \cdot \delta\mathbf{u}_p(\mathbf{p}) \mathrm{d}V(0)\ . \tag{1.32}$$

2. Bilinear form of *gyroscopic effects*:

$$\mathcal{D}_g(\mathbf{u}_p,\, \delta\mathbf{u}_p) = 2\int_{V(0)} \rho_p\,(\mathbf{p})\, \mathbf{\Omega}(t)\mathbf{u}_p(\mathbf{p},\, t) \cdot \delta\mathbf{u}_p(\mathbf{p}) \mathrm{d}V(0)\ . \tag{1.33}$$

3. Bilinear form of *centrifugal acceleration*:

$$\mathcal{K}_a(\mathbf{u}_p,\, \delta\mathbf{u}_p) = \int_{V(0)} \rho_p\,(\mathbf{p})\, \frac{\mathrm{d}\mathbf{\Omega}(t)}{\mathrm{d}t}\mathbf{u}_p(\mathbf{p},\, t) \cdot \delta\mathbf{u}_p(\mathbf{p}) \mathrm{d}V(0)\ . \tag{1.34}$$

4. Bilinear form of *centrifugal softening*:

$$\mathcal{K}_c(\mathbf{u}_p,\, \delta\mathbf{u}_p) = \int_{V(0)} \rho_p\,(\mathbf{p})\, \mathbf{\Omega}(t)^2\mathbf{u}_p(\mathbf{p},\, t) \cdot \delta\mathbf{u}_p(\mathbf{p}) \mathrm{d}V(0)\ . \tag{1.35}$$

5. Linear form of *non-follower exterior inertial load*:

$$\mathcal{F}_{ei}(\delta\mathbf{u}_p) = -\int_{V(0)} \rho_p\,(\mathbf{p})\, \left(\mathbf{\Omega}(t)^2 + \frac{\mathrm{d}\mathbf{\Omega}(t)}{\mathrm{d}t}\right)\mathbf{p} \cdot \delta\mathbf{u}_p(\mathbf{p}) \mathrm{d}V(0)\ . \tag{1.36}$$

   Note that for a rotating frame of reference the exterior inertial load is present in the second member of the virtual work equilibrium equation.

6. Linear form of the *nonlinear internal efforts*:

$$\mathcal{G}(\mathbf{u}_p,\, \delta\mathbf{u}_p) = \textstyle\int_{V(0)} (\mathbf{X}_p(\mathbf{u}_p(\mathbf{p},\, t),\, t)\mathbf{S}_p(\mathbf{u}_p(\mathbf{p},\, t),\, t)) : \frac{\partial\delta\mathbf{u}_p}{\partial\mathbf{p}}\,(\mathbf{p})\, \mathrm{d}V(0)\ . \tag{1.37}$$

7. Linear form of the *external forces*:

$$\begin{aligned} \mathcal{F}_e(\delta\mathbf{u}_p) = &-\int_{V(0)} \rho_p\,(\mathbf{p})\, \mathbf{f}_{v_p}(\mathbf{p},\, t) \cdot \delta\mathbf{u}_p(\mathbf{p}) \mathrm{d}V(0) \\ &-\int_{\partial V(0)} \mathbf{f}_{s_p}(\mathbf{p},\, t) \cdot \delta\mathbf{u}_p(\mathbf{p}) \mathrm{d}S(0)\ . \end{aligned} \tag{1.38}$$

Reformulating the weak form in the initial configuration

The weak form of the problem in the initial configuration is nonlinear. Thus, an equivalent formulation is obtained searching the zeros of a residual function,

$$\begin{aligned}\mathcal{R}(\mathbf{u}_p,\, \delta\mathbf{u}_p) = \mathcal{M}(\frac{\partial^2\mathbf{u}_p}{\partial t^2},\, \delta\mathbf{u}_p) + \mathcal{D}_g(\frac{\partial\mathbf{u}_p}{\partial t},\, \delta\mathbf{u}_p) + \mathcal{K}_a(\mathbf{u}_p,\, \delta\mathbf{u}_p) \\ + \mathcal{K}_c(\mathbf{u}_p,\, \delta\mathbf{u}_p) + \mathcal{G}(\mathbf{u}_p,\, \delta\mathbf{u}_p) - \mathcal{F}_e(\delta\mathbf{u}_p) - \mathcal{F}_{ei}(\delta\mathbf{u}_p)\ .\end{aligned} \tag{1.39}$$

Then, the continuum weak form of the problem in the initial configuration is formulated as follows:

Find $\boldsymbol{u}_p(\boldsymbol{p},\, t) \in \xi V(0)$ *such that* $\forall \delta\boldsymbol{u}_p(\boldsymbol{p}) \in \xi V(0)$*, and that the equilibrium of virtual work is reached,* $\mathcal{R}(\boldsymbol{u}_p,\, \delta\boldsymbol{u}_p) = 0$.

1.2.4 Continuum weak form of the contact problem

The existence and uniqueness of the frictional contact between two elastic bodies is, in many aspects, an open problem, specially in dynamics. The Signorini problem is the first unilateral problem in elasticity, studied by [Fichera, 1964, Lions and Stampacchia, 1967]. The analogous dynamic weak form of the contact problems is studied in [Duvaut and Lions, 1972] where the conditions for existence and uniqueness are stated for linear elastic materials an for visco-elastic materials with frictionless contact. The finite element problem with unilateral contact for friction and frictionless problems considering small and large deformations for incompressible and elasto-plastic materials are studied in [Kikuchi and Oden, 1988]. A model for the dynamic, adhesive, frictionless contact between a visco-elastic body and a deformable foundation is presented in [Chau et al., 2003].

The weak form of the problem with contact type nonlinearities is obtained by the principle of virtual displacements. The contact acts as a surface force satisfying the Hertz-Signorini-Moreau conditions that imposes the non-penetration and non-adhesion of the contact boundary, Eqn. (1.4). The virtual work of the internal efforts, δW_i, and the virtual work associated to the acceleration term, δW_a, are developed in the previous section. The virtual work related to contact is developed in the following. The latter is evaluated to study the contact interaction between two elastic solids.

Considering two elastic solids, a master solid S_1 and a slave solid S_2, the virtual work of the contact forces, $\delta W_c\,(\mathbf{u}_p,\, \delta\mathbf{u}_p)$, in the active contact regions ($\overline{\Gamma}_c^1 \in \Gamma_c^1$ and $\overline{\Gamma}_c^2 \in \Gamma_c^2$) is presented as,

$$\delta W_c\,(\mathbf{u}_p,\, \delta\mathbf{u}_p) = \int_{\overline{\Gamma}_c^1} \mathbf{n}\cdot\sigma^1\cdot\delta\mathbf{w}\mathrm{d}\overline{\Gamma}_c^1 + \int_{\overline{\Gamma}_c^2} \mathbf{v}\cdot\sigma^2\cdot\delta\mathbf{r}\mathrm{d}\overline{\Gamma}_c^2 = \int_{\overline{\Gamma}_c^1} \mathbf{n}\cdot\sigma^1\cdot\delta(\mathbf{w}-\mathbf{r})\mathrm{d}\overline{\Gamma}_c^1\ , \tag{1.40}$$

where $\mathbf{n}$ and $\mathbf{v}$ are respectively the unit vectors normal to the active contact surfaces $\overline{\Gamma}_c^1$ and $\overline{\Gamma}_c^2$, each of them pointing towards the outside of their respective solids and σ^b is the stress state of the b body. If $\delta\mathbf{r}$ is the virtual displacement of an independent point $\mathbf{r}(\mathrm{t})\in S_2$, $\delta\mathbf{w}$ is the virtual displacement of the projection of $\mathbf{r}(\mathrm{t})$ in the master surface S_1 represented by the point $\mathbf{w}(\mathrm{t})\in S_1$. The 3^{rd} Newton's law implies that $\mathbf{n}\sigma \mathrm{d}\overline{\Gamma}_c^1 = -\mathbf{v}\sigma \mathrm{d}\overline{\Gamma}_c^2$, thus, the virtual displacements in the contact region are defined with respect to one of the contact surfaces by means of the virtual difference, $\delta(\mathbf{w}-\mathbf{r})$, related to the active contact surface, $\overline{\Gamma}_c^1$.

Depending on the emitter type and position (focus from which imaginary rays are emitted to perform the projection) the expression of the *projection function* that projects the points of the slave surface over the master surface varies. This affects the representation of the virtual difference, $\delta(\mathbf{w}-\mathbf{r})$. A detailed study of this problem is developed in [Yastrebov, 2011] and its references. Here, a normal projection is considered. Thus, the relation between a point $\mathbf{r}(\mathrm{t})\in S_2$ and its projection $\mathbf{w}(\mathrm{t})\in S_1$ is defined as $\mathbf{r} = \mathbf{w} + g_n\mathbf{n}$ considering that g_n is the normal gap between solids. Hence, the expression of the virtual difference is rewritten as follows,

$$\delta(\mathbf{w}-\mathbf{r}) = \delta g_n\mathbf{n} + g_n\overline{\delta}\mathbf{n} + \tfrac{\partial \mathbf{w}^T}{\partial \underset{\sim}{\xi}}\delta\underset{\sim}{\xi} = \delta g_n\mathbf{n} + g_n\underbrace{\left(\delta\mathbf{n} + \frac{\partial \mathbf{n}^T}{\partial \underset{\sim}{\xi}}\delta\underset{\sim}{\xi}\right)}_{\overline{\delta}\mathbf{n},\text{ full variation of }\mathbf{n}} + \tfrac{\partial \mathbf{w}^T}{\partial \underset{\sim}{\xi}}\delta\underset{\sim}{\xi}\,, \quad (1.41)$$

where $\delta\underset{\sim}{\xi}$ is a perturbation of the local coordinate of projection of the point $\mathbf{r}$ on the surface $\overline{\Gamma}_c^1$. Figure 1.3 shows the scheme of a 2D contact between two elastic solids and the graphical representation of some of the concepts introduced above.

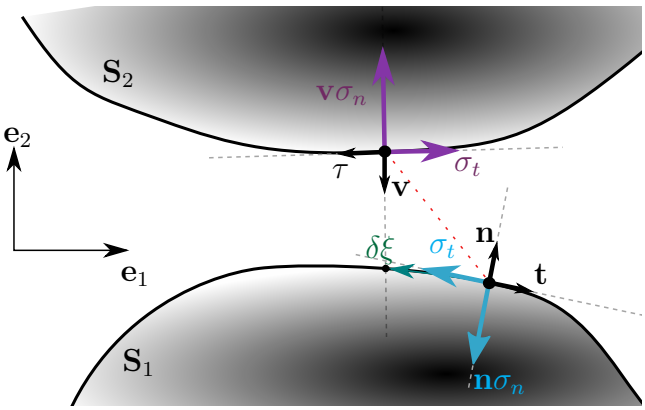

Figure 1.3: Scheme of the contact between two solids.

Then, the stress is splitted into its normal and tangential components,

$$\mathbf{n}\sigma = \mathbf{n}\sigma_n + \sigma_t = \mathbf{n}\sigma_n + \underset{\sim}{\sigma}_t^T \overline{\frac{\partial \mathbf{w}}{\partial \underset{\sim}{\xi}}} \,, \tag{1.42}$$

where $\overline{\frac{\partial \mathbf{w}}{\partial \underset{\sim}{\xi}}}$ is the contravariant surface basis, σ_n is the normal stress and σ_t is the tangential stress.

The virtual work associated to the contact is rewritten by introducing Eqn. (1.41) and (1.42) into the virtual work of the contact forces defined in Eqn. (1.40), thus,

$$\delta W_c\left(\mathbf{u}_p, \delta\mathbf{u}_p\right) = \int_{\overline{\Gamma}_c^1} \mathbf{n}\cdot\sigma\cdot\delta(\mathbf{w}-\mathbf{r})\mathrm{d}\overline{\Gamma}_c^1 = -\int_{\overline{\Gamma}_c^1} \left(\sigma_n \delta g_n + \underset{\sim}{\sigma}_t^T \delta\underset{\sim}{\xi}\right) \mathrm{d}\overline{\Gamma}_c^1 \,. \tag{1.43}$$

Due to the non penetration condition, the variation of the normal gap, δg_n is always positive. Moreover, the contact pressure is non-positive by definition, $\sigma_n \leq 0$, leading to $\delta g_n \sigma_n \leq 0$. The frictional term is always positive as the work of frictional forces has the same sign as the virtual work of internal forces. The energy dissipated due to friction is not recovered.

Hence, the weak form of the problem is represented by a variational inequality and is formulated as follows:

Find $\boldsymbol{u}_p(\boldsymbol{p},\ t) \in \xi\left(V(0)\right)$ *such that* $\forall \delta\boldsymbol{u}_p(\boldsymbol{p}) \in \xi\left(V(0)\right)$*, the work done by the virtual displacements is in equilibrium,* $\delta W_a\left(\boldsymbol{u}_p, \delta\boldsymbol{u}_p\right) \geq \delta W_i\left(\boldsymbol{u}_p, \delta\boldsymbol{u}_p\right) + \delta W_c\left(\boldsymbol{u}_p, \delta\boldsymbol{u}_p\right) + \delta W_e\left(\boldsymbol{u}_p, \delta\boldsymbol{u}_p\right)$ *and that the condition* $\left(\boldsymbol{r}+\delta\boldsymbol{r}-\boldsymbol{w}-\delta\boldsymbol{w}\right)\boldsymbol{n} \geq -g_{n_0}$ *is fulfilled in the contact boundary,* Γ_c*, where* g_{n_0} *is the initial gap.*

Note that in this formulation, the relation between the normal and tangential forces is not defined. Thus, the proposed weak form of the problem is valid for any frictional law. In the following, some of the classical friction laws that are found in literature are presented.

Contact laws

Depending on the behaviour of the contact boundary of the structure, two friction models are differentiated. When all the contact surfaces behave identically, the friction law is defined as *Macroslip* [Menq, 1985]. For the latter, the totality of the contact surface is either in a locked state or in a motion state. These models are largely used to study the nonlinear behaviour of dry friction due to their simplicity. Hence, the contact can be modelled by a single point. The friction laws that consider partial blocking/sliding behaviour are defined as *Microslip* [Mindlin, 1949, Menq et al., 1986]. The latter contact laws improve the accuracy of the friction contact representation, however, their

implementation is more complex than for the macroslip type of friction laws. A node-node or surface-surface discretisations are suitable for these type of contact laws.

Coulomb's law

The Coulomb's law represents a relation between the normal and tangential forces by means of a fiction coefficient, μ, that represents the roughness of the contact surface. The value of μ varies between stick and slip states,

$$\begin{cases} F_t < \mu_s F_n & \text{if} \quad \dot{x}_t = 0 \quad \text{Stick} \\ F_t = \mu_d F_n & \text{if} \quad \dot{x}_t \neq 0 \quad \text{Slip} \end{cases} , \tag{1.44}$$

which is a particular case of Tresca's law of friction where the normal force F_n is imposed. In Coulomb's law, the tangential force F_n is obtained once the normal force is determined.

Masing macroslip model

The Masing model [Menq and Yang, 1998, Al Sayed et al., 2011] is a regularisation of the Coulomb's law. During the stick state, a tangential force linearly proportional to the displacement of the structure appears until the slip conditions are fulfilled. This represents the elastic deformation of the rough surfaces in contact. Once the applied effort overcomes the maximum tangential effort that the contact surface can resist stick state is switched to the slip state.

$$f_{nl} = \begin{cases} \mu F_n + k_d(x - x_{lim}) & \text{if} \quad x < x_{lim} \quad \text{Stick} \\ \mu F_n sgn(\dot{x}_t) & \text{if} \quad x > x_{lim} \quad \text{Slip} \end{cases} . \tag{1.45}$$

Dahl's model

The Dahl model [Dahl, 1968, Bastien et al., 2007] is a generalisation of the Coulomb's law where the elastic restitution forces are analytically described for the dissipating point. Here the behaviour of the contact is modelled by a local law. A similar approximation could be used with a Bouc-Wen hysteresis relation model [Ismail et al., 2009]. The Dahl's model is defined as,

$$\frac{\partial F_t}{\partial x} = \sigma_d \left| 1 - \frac{F_t}{\mu F_n} sgn(\dot{x}) \right|^i sgn\left(1 - \frac{F_t}{\mu F_n} sgn(\dot{x}) \right) , \tag{1.46}$$

where σ_d and i are parameters of the model that need to be identified.

Iwan type model

The Iwan's model [Iwan, 1966] is a microslip contact model that represents the behaviour of the contact surface by combining bilinear macroslip contact

elements along a contact line. This approximation is suitable for numerical analysis and permits the representation of an inhomogeneous behaviour of the stick/slip states. The macroslip elements are combined either in parallel, as shown in Fig. 1.4, or in a row. The hysteresis behaviour of friction joints exhibiting planar motion is studied using the Iwan model in [Sanliturk and Ewins, 1996].

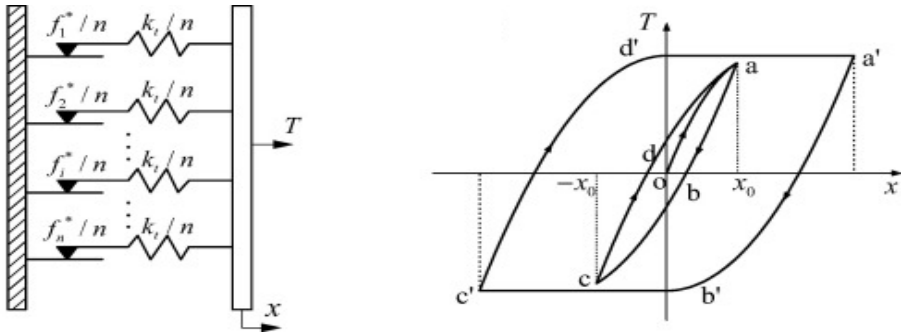

Figure 1.4: Parallel Iwan model with its hysteresis loop [Li et al., 2019].

The numerical study of large displacements (large sliding) contact is often formulated as a variational equality when the contact boundary is known. The variational inequality is then transformed in a variational equality by means of the *penalty* method, the *Lagrange multipliers* method or the *augmented Lagrangian* method. Other regularisation methods are presented in [Wriggers and Nackenhorst, 2006, Kikuchi and Oden, 1988]. In the following the contact problem is addressed by means of the penalty method, knowing that, the chosen contact resolution method does not impact the construction and resolution steps of the proposed reduced order models.

Penalty method

If the active contact regions $\overline{\Gamma}_c^1 \in \Gamma_c^1$ and $\overline{\Gamma}_c^2 \in \Gamma_c^2$ are known. The variational inequality becomes the following equality,

$$\delta W_a\left(\mathbf{u}_p, \delta\mathbf{u}_p\right) = \delta W_i\left(\mathbf{u}_p, \delta\mathbf{u}_p\right) + \delta W_c\left(\mathbf{u}_p, \delta\mathbf{u}_p\right) + \delta W_e\left(\mathbf{u}_p, \delta\mathbf{u}_p\right) \ , \qquad (1.47)$$

with $g\left(\mathbf{u}_p, \delta\mathbf{u}_p\right) \geq 0$ as the boundary constraint in the active contact regions. The latter represents a standard minimization problem with inequality boundary conditions.

For the friction contact case, the virtual work of contact is divided into three different contributions, the normal virtual work due to the interpenetration between solids that occurs in the active contact region, $\overline{\Gamma}_c^1$, the tangent virtual work due to the sticky region, $\overline{\Gamma}_c^{1^\bullet} \in \overline{\Gamma}_c^1$, and the tangent virtual work due to the slippery region, $\overline{\Gamma}_c^{1^*} \in \overline{\Gamma}_c^1$.

Normal contribution

The non-penetration condition is defined as,

$$g \geq 0,\ \sigma_n \leq 0,\ g\sigma_n = 0\ . \tag{1.48}$$

The penalty method is activated for negative gaps, $g < 0$, between the slave and the master surfaces. For those cases, a contact pressure is activated in the active boundary as shown in Fig. 1.5. Considering that the latter pressure is a function of the gap, the normal penalty function, $\epsilon_n(\langle -g \rangle)$, is defined as a *non-positive* continuous strictly monotonically decreasing function where, $\varepsilon_n > 0$, is the normal linear penalty factor,

$$\sigma_n(g) = \epsilon_n(\langle -g \rangle) = \left\{ \begin{array}{lll} 0 & \text{if} \quad g > 0 \quad \text{thus} \quad g\sigma_n = 0 \\ \epsilon_n(-g) & \text{if} \quad g \leq 0 \quad \text{thus} \quad g\sigma_n \neq 0 \end{array} \right\} \leq 0\ , \tag{1.49}$$

where $\langle \cdot \rangle$ are the Macaulay brackets. Note that when the penetration is activated, not all the conditions stated in Eqn. (1.48) are validated. This implies that small penetrations happen between the two solids. Hence, the allowed interpenetration is proportional to the normal penalty factor, ε_n.

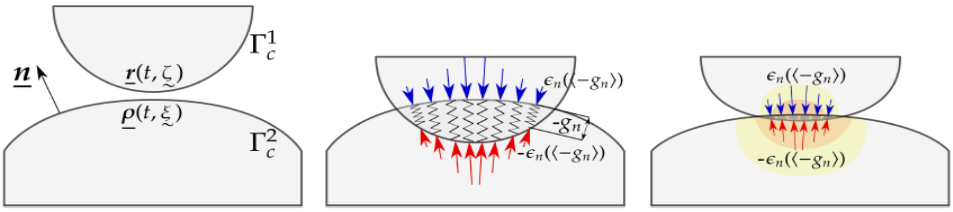

Figure 1.5: Spring penalty method interpretation [Yastrebov, 2011].

On the one hand, small values of ε_n imply a large interpenetration between the solids, which is not physically acceptable. On the other hand, very large ε_n imply small interpenetration closer to the observed physics, however, this can lead to numerical instabilities.

Thus, the normal contribution to the contact virtual displacements considering a normal projection is written as,

$$\delta W_{c_n} = -\int_{\overline{\Gamma}_c^1} \epsilon_n\left(\langle -g_n \rangle\right) \delta g_n \mathrm{d}\overline{\Gamma}_c^1 = \int_{\overline{\Gamma}_c^1} \varepsilon_n\left(-g_n\right) \delta g_n \mathrm{d}\overline{\Gamma}_c^1\ , \tag{1.50}$$

and the classical Coulomb friction law is formulated as,

$$\underbrace{||\sigma_t|| \leq \mu|\sigma_n|}_{\text{Stick condition}},\ \underbrace{\sigma_t - \mu|\sigma_n|\mathbf{s} = 0}_{\text{Slip condition}},\ \underbrace{||\mathbf{s}||\,||\sigma_t - \mu|\sigma_n|\mathbf{s}|| = 0}_{\text{Complimentary condition}}\ , \tag{1.51}$$

where $\mathbf{s}$ denotes the tangent velocity direction unitary vector.

Following the same procedure as for the normal effort, the tangent tension is activated when a tangential sliding, $\mathbf{g}_t$, appears. If a tangential penalisation function, positive and monotonically increasing, $\epsilon_t\left(||\mathbf{g}_t||\right)$, is considered, the tangential stress is,

$$\sigma_t = \begin{cases} \epsilon_t\left(||\mathbf{g}_t||\right)\mathbf{s} & \text{if} \quad \epsilon_t\left(||\mathbf{g}_t||\right) < \mu|\sigma_n| \quad \text{Stick} \\ \mu|\sigma_n|\mathbf{s} & \text{if} \quad \epsilon_t\left(||\mathbf{g}_t||\right) \geq \mu|\sigma_n| \quad \text{Slip} \end{cases} . \tag{1.52}$$

Tangential stick state

The virtual work of the forces in the region where the contact surface is sticked, $\overline{\Gamma}_c^{1\bullet}$, is,

$$\begin{aligned} \delta W_{c_{stick}} &= -\int_{\overline{\Gamma}_c^{1\bullet}} \sigma_t \cdot \delta\mathbf{g}_t \mathrm{d}\overline{\Gamma}_c^1 = -\int_{\overline{\Gamma}_c^{1\bullet}} \epsilon_t\left(||\mathbf{g}_t||\right)\mathbf{s} \cdot \delta\mathbf{g}_t \mathrm{d}\overline{\Gamma}_c^1 \\ &= -\int_{\overline{\Gamma}_c^{1\bullet}} \varepsilon_t \Delta\mathbf{g}_t^{\bullet} \cdot \delta\mathbf{g}_t \mathrm{d}\overline{\Gamma}_c^1 \\ &= -\int_{\overline{\Gamma}_c^{1\bullet}} \varepsilon_t \underbrace{\underbrace{\left(\Delta\underset{\sim}{\xi}^{\bullet}\right)^T \overbrace{\overline{\frac{\partial\mathbf{w}}{\partial\underset{\sim}{\xi}}}}^{=\mathbf{I}} \cdot \frac{\partial\mathbf{w}^T}{\partial\underset{\sim}{\xi}}\delta\underset{\sim}{\xi}}_{\Delta\mathbf{g}_t^{\bullet} \qquad \delta\mathbf{g}_t}}_{\text{Change to local coordinates}} \mathrm{d}\overline{\Gamma}_c^1 \\ &= -\int_{\overline{\Gamma}_c^{1\bullet}} \varepsilon_t \Delta\underset{\sim}{\xi}^{\bullet T} \delta\underset{\sim}{\xi} \mathrm{d}\overline{\Gamma}_c^1 , \end{aligned} \tag{1.53}$$

where $\Delta\mathbf{g}_t^{\bullet}$ is the difference between the actual point and the theoretical stick point, $\Delta\underset{\sim}{\xi}^{\bullet}$ is the cumulative "slip-in-stick" magnitude over the time solutions that represents the cumulative elastic deformations in the contact surface coordinates, $\Delta\underset{\sim}{\xi}$ is the perturbation of the local coordinate of projection o the point and ε_t is the tangential penalty factor.

Tangential slip state

The tangential stress in the slip direction is obtained from Eqn. (1.51),

$$\sigma_t^* = \mu|g_n|\mathbf{s} = \mu|g_n|\frac{\dot{\mathbf{g}}_t}{||\dot{\mathbf{g}}_t||} = \mu|g_n|\underset{\sim}{s}^T\overline{\frac{\partial\mathbf{w}}{\partial\underset{\sim}{\xi}}} . \tag{1.54}$$

Then, the virtual work of the forces in the region where the contact surface is in the slip state, $\overline{\Gamma}_c^{1^*}$, is,

$$\begin{aligned} \delta W_{c_{slip}} &= -\int_{\overline{\Gamma}_c^{1^*}} \sigma_t^* \cdot \delta\mathbf{g}_t \mathrm{d}\overline{\Gamma}_c^1 = -\int_{\overline{\Gamma}_c^{1^*}} \mu|\sigma_n|\mathbf{s} \cdot \delta\mathbf{g}_t \mathrm{d}\overline{\Gamma}_c^1 \\ &= -\int_{\overline{\Gamma}_c^{1^*}} \mu|\sigma_n|\underset{\sim}{s}^T\delta\underset{\sim}{\xi}\mathrm{d}\overline{\Gamma}_c^1 = \int_{\overline{\Gamma}_c^{1^*}} \mu\varepsilon_n\left\langle -g_n\right\rangle \underset{\sim}{s}^T\delta\underset{\sim}{\xi}\mathrm{d}\overline{\Gamma}_c^1 \\ &= -\int_{\overline{\Gamma}_c^{1^*}} \mu\varepsilon_n\left(-g_n\right)\underset{\sim}{s}^T\delta\underset{\sim}{\xi}\mathrm{d}\overline{\Gamma}_c^1 , \end{aligned} \tag{1.55}$$

where μ is the friction coefficient, ε_n is the normal penalisation factor and g_n is the normal gap.

Weak form of the friction contact problem with the penalty method

From Eqn. (1.50), (1.53) and (1.55) the contact contribution to the weak form of the virtual work is obtained by means of the penalty method,

$$\begin{aligned} \delta W_c^{Penalty}\left(\mathbf{u}_p, \delta\mathbf{u}_p\right) &= \delta W_{c_n} + \delta W_{stick} + \delta W_{slip} \\ &= \int_{\overline{\Gamma}_c^{1\bullet}} \left(\varepsilon_n\left(-g_n\right)\delta g_n - \epsilon_t \Delta\underset{\sim}{\xi}^{\bullet^T}\delta\underset{\sim}{\xi}\right) \mathrm{d}\overline{\Gamma}_c^1 \\ &+ \int_{\overline{\Gamma}_c^{1*}} \varepsilon_n\left(-g_n\right)\left(\delta g_n - \mu\underset{\sim}{s}^T\delta\underset{\sim}{\xi}\right) \mathrm{d}\overline{\Gamma}_c^1 \,. \end{aligned} \tag{1.56}$$

Thus, the weak form of the problem with friction contact nonlinearities is formulated as:

Find $\boldsymbol{u}_p(\boldsymbol{p},\ t) \in \xi\left(V(0)\right)$ *such that* $\forall\delta\boldsymbol{u}_p(\boldsymbol{p}) \in \xi\left(V(0)\right)$*, and that the work done by the virtual displacements is in equilibrium,* $\delta W_a\left(\boldsymbol{u}_p, \delta\boldsymbol{u}_p\right) = \delta W_i\left(\boldsymbol{u}_p, \delta\boldsymbol{u}_p\right) + \delta W_c^{Penalty}\left(\boldsymbol{u}_p, \delta\boldsymbol{u}_p\right) + \delta W_e\left(\boldsymbol{u}_p, \delta\boldsymbol{u}_p\right)$.

Then, once the weak form of the problem is defined, the Finite Element Method (FEM) is applied to discretise and to solve the discrete mechanical problem, which is a discrete representation of the continuum mechanical problem.

1.3 Discrete formulation (Finite Element Method)

The discretisation consist in solving the equation of the problem at some given spatial locations (nodes) and interpolate between these locations with relatively simple functions. The latter approximation permits to simplify the continuum problem with complex solution-functions that must be valid for all the spatial locations of the domain. Thus, the equilibrium equation is solved at the nodes of the finite element mesh [Zienkiewicz et al., 1977, Belytschko et al., 2013] to obtain the displacements of the structure, $\mathbf{u}_p(\mathbf{p},\ t)$. Then, the continuum displacements are approximated as the product between a displacements interpolation matrix or shape functions matrix, $\mathbf{N(p)}$, and the nodal displacements vector, $\{\mathbf{u}_p(\mathrm{t})\}$,

$$\mathbf{u}_p(\mathbf{p},\ t) \approx \sum_{i=1}^{Nodes} N_i\left(\mathbf{p}\right)\left\{u_{p_i}(t)\right\} = \mathbf{N(p)}\left\{\mathbf{u}_p(\mathrm{t})\right\} \ , \tag{1.57}$$

note that the "braces" $\{\cdot\}$ represent the value of the field $\cdot$ at the spatial locations of the nodes. The shape functions matrix is invariant with respect

to time, t. The latter only depends on the spatial discretisation, type of Finite Element (bar, triangular, hexahedral...) or its interpolation degree (linear, quadratic...) which is related to the number of nodes of each element. Figure 1.6 shows a library of different *Finite Elements* used by an industrial finite element software.

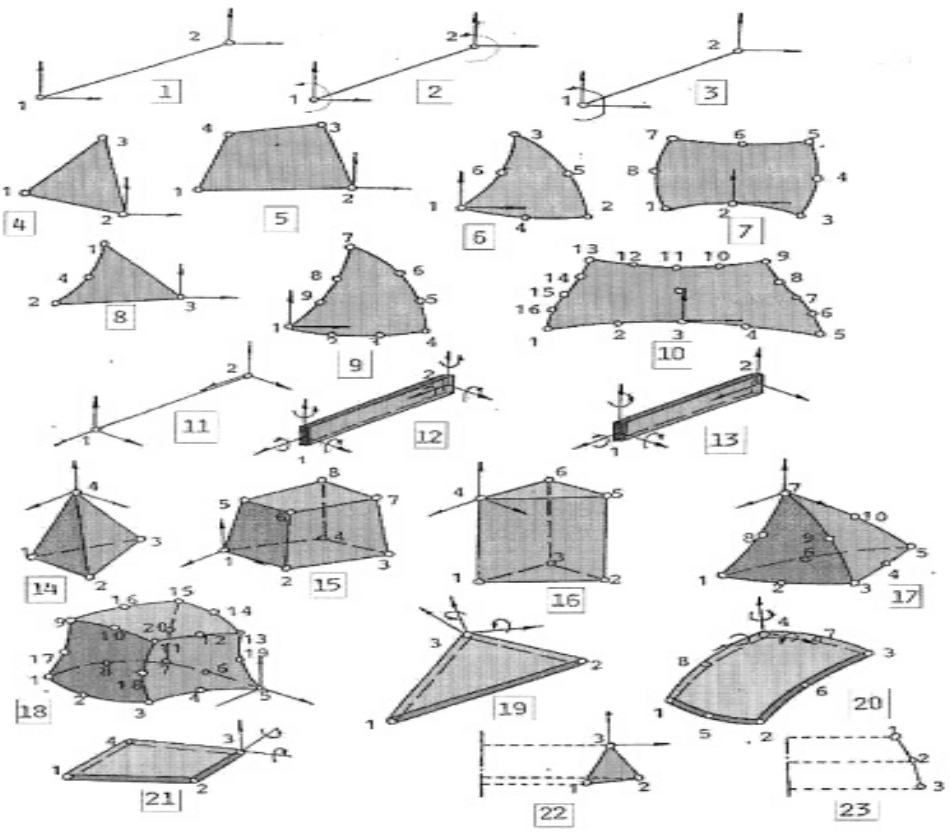

Figure 1.6: Example of a finite element library that could be found in a finite element software [Avilés, 2002].

Furthermore, the nodal displacements vector depends exclusively on the time, t. This approximation simplifies the complexity of the problem as for linear problems space and time discretisations are uncoupled. Note that the nodal displacements are a relative quantity relative to the initial configuration $\mathbf{p}$ of the structure. Thus, each value represent the deviation with respect to the initial value.

For a large number of nodal degrees of freedom, n, the construction of the displacements interpolation matrix becomes very expensive as each interpolation function depends on each spatial location of the system, as well as the integrations that are performed for each element. To avoid expensive constructions of the finite element system, the *iso-parametric* elements approximate the displacement field by means of a mapping, as shown in Fig. 1.7, between the

studied element in the global coordinates and a reference element with normalised coordinates for which the integration functions are standardised.

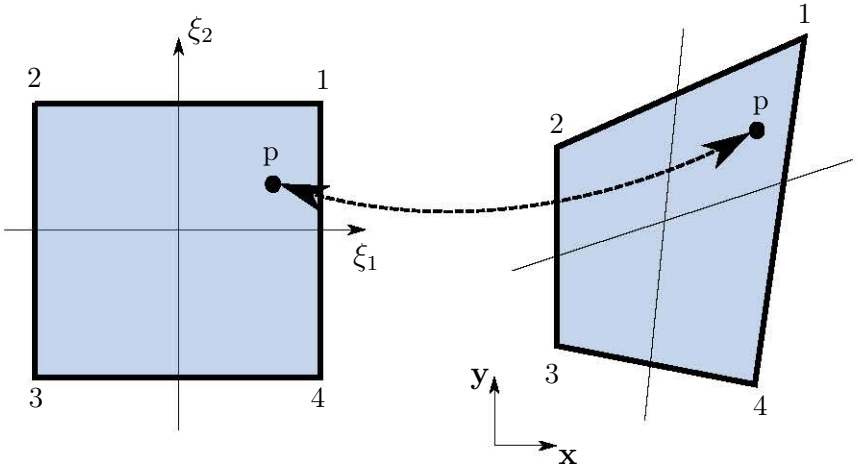

Figure 1.7: Mapping of P coordinate between the iso-parametric and the global coordinates.

1.3.1 Matrices and vectors of the discretised problem

The bilinear and linear forms of the continuum problem are associated to the following discrete matrices and vectors:

1. The symmetric, definite and positive *mass* matrix associated to the bilinear form of mass:

$$\mathbf{M} = \int_{V(0)} \rho_p(\mathbf{p})\, \mathbf{N}(\mathbf{p})^T \mathbf{N}(\mathbf{p}) \mathrm{d}V(0) \,. \tag{1.58}$$

2. The *gyroscopic coupling* matrix associated to the bilinear form of gyroscopic coupling which is skew-symmetric:

$$\mathbf{D}_g(t) = \int_{V(0)} 2\rho_p(\mathbf{p})\, \mathbf{N}(\mathbf{p})^T \boldsymbol{\Omega}(t) \mathbf{N}(\mathbf{p}) \mathrm{d}V(0) \,. \tag{1.59}$$

3. The skew-symmetric *centrifugal acceleration* matrix associated to the bilinear centrifugal acceleration:

$$\mathbf{K}_a(t) = \int_{V(0)} \rho_p(\mathbf{p})\, \mathbf{N}(\mathbf{p})^T \left(\frac{\mathrm{d}\boldsymbol{\Omega}(t)}{\mathrm{d}t} \right)(t)\, \mathbf{N}(\mathbf{p}) \mathrm{d}V(0) \tag{1.60}$$

4. The *centrifugal softening* matrix which is symmetric, definite and positive associated to the bilinear centrifugal softening:

$$\mathbf{K}_c(t) = \int_{V(0)} \rho_p(\mathbf{p})\, \mathbf{N}(\mathbf{p})^T \boldsymbol{\Omega}(t)^2 \mathbf{N}(\mathbf{p}) \mathrm{d}V(0) \,. \tag{1.61}$$

5. The *non-follower external inertial load* vector associated to the linear form of non-follower external inertial load:

$$\mathbf{f}_{ei}(t) = -\int_{V(0)} \rho_p\left(\mathbf{p}\right) \mathbf{N}(\mathbf{p})^T \left(\mathbf{\Omega}(t)^2 + \frac{\mathrm{d}\mathbf{\Omega}(t)}{\mathrm{d}t}\right) \mathbf{N}(\mathbf{p})\mathrm{d}V(0) \ . \tag{1.62}$$

6. The *internal forces* vector associated to the linear form of the internal efforts which is nonlinear with respect to $\mathbf{u}_p(\mathbf{p},\, t)$:

$$\mathbf{g}(\{\mathbf{u}_p(\mathrm{t})\}) = \int_{V(0)} \underbrace{\left(\frac{\partial \mathbf{N}}{\partial \mathbf{p}}\left(\mathbf{p}\right)\right)^T}_{\mathbf{B}(\mathbf{p})^T} : \mathbf{X}_p(\{\mathbf{u}_p(\mathrm{t})\})\mathbf{S}_p(\{\mathbf{u}_p(\mathrm{t})\})\mathrm{d}V(0) \ . \tag{1.63}$$

7. The *external forces* vector associated to the linear form of the external forces:

$$\begin{aligned} \mathbf{f}_e(t) = &-\int_{V(0)} \rho_p\left(\mathbf{p}\right) \mathbf{N}(\mathbf{p})^T \mathbf{N}(\mathbf{p}) \mathbf{f}_{v_p}(\mathrm{t})\mathrm{d}V(0) \\ &-\int_{\partial V(0)} \mathbf{N}(\mathbf{p})^T \mathbf{N}(\mathbf{p}) \mathbf{f}_{s_p}(\mathrm{t})\mathrm{d}S(0) \ . \end{aligned} \tag{1.64}$$

8. The *contact forces* vector is obtained by combining the normal, the tangential stick and the tangential sliding contributions. Each of them are constructed from the discretisation of the surface. First, the continuum, $\mathbf{A}$, $\mathbf{H}$, δg_n, $\delta\underset{\sim}{\xi}$ and $\Delta\xi^{\bullet}$ quantities are defined, then, the expressions of the normal force and of the tangential forces are defined.

   (a) The first covariant fundamental surface metric matrix, $\mathbf{A}$, is,

$$\mathbf{A} = \frac{\partial \mathbf{w}}{\partial \xi} \cdot \frac{\partial \mathbf{w}^T}{\partial \xi} \ . \tag{1.65}$$

   (b) The second covariant fundamental surface metric matrix, $\mathbf{H}$, is,

$$\mathbf{H} = \mathbf{n} \cdot \frac{\partial^2 \mathbf{w}}{\partial \xi^2} \ . \tag{1.66}$$

   (c) The variation of the *normal gap* is,

$$\delta g_n = \left(\mathbf{S}_0{}^T - \mathbf{N}^m(\underset{\sim}{\xi})^T\right) \mathbf{n} \cdot \delta \mathbf{u}_p^c = [\bigtriangledown g_n]^T \cdot \delta \mathbf{u}_p^c \ , \tag{1.67}$$

   where $\mathbf{S}_0$ is a selection vector for the slave nodal components, $\mathbf{N}^m(\underset{\sim}{\xi})$ are the shape functions of the master in the local surface coordinates system, $\mathbf{n}$ is the normal vector of the master surface at the contact node and $\delta\mathbf{u}_p^c$ is the virtual displacements vector in the contact surface.

(d) The variation of the *surface parameter* is,

$$\begin{aligned}\delta\underset{\sim}{\xi}_i &= (\mathbf{A} - g_n\mathbf{H})^{-1}_{ij}\left(\left(\mathbf{S}_0^T - \mathbf{N}^m(\underset{\sim}{\xi}^T)\right)\mathbf{B}^m_j(\underset{\sim}{\xi})^T\mathbf{u}^c_p + g_n\mathbf{B}^m_j(\underset{\sim}{\xi})^T\mathbf{n}\right)\cdot\delta\mathbf{u}^c_p \\ &= [\bigtriangledown\xi_i]^T\cdot\delta\mathbf{u}^c_p\,.\end{aligned} \tag{1.68}$$

(e) The *normal contact force* vector is:

$$\mathbf{f}_{c_n}(\{\mathbf{u}_p(\mathrm{t})\}) = \int_{\overline{\Gamma}^1_c}\varepsilon_n\,(-g_n)\,[\bigtriangledown g_n]^T\,\mathrm{d}\overline{\Gamma}^1_c\,. \tag{1.69}$$

(f) The *tangential stick force* vector is:

$$\mathbf{f}_{c_{stick}}(\{\mathbf{u}_p(\mathrm{t})\},\,\{\dot{\mathbf{u}}_p(\mathrm{t})\}) = -\int_{\overline{\Gamma}^{1\bullet}_c}\epsilon_t\,[\bigtriangledown\xi_i]^\bullet\,[\bigtriangledown\xi_i]^T\,\mathrm{d}\overline{\Gamma}^1_c\,. \tag{1.70}$$

(g) The *tangential slip force* vector is:

$$\mathbf{f}_{c_{slip}}(\{\mathbf{u}_p(\mathrm{t})\},\,\{\dot{\mathbf{u}}_p(\mathrm{t})\}) = -\int_{\overline{\Gamma}^{1*}_c}\mu\underset{\sim}{s}^T\,[\bigtriangledown\xi_i]^T\,\mathrm{d}\overline{\Gamma}^1_c\,. \tag{1.71}$$

Thus, the *contact force* vector is,

$$\begin{aligned}\mathbf{f}_c(\{\mathbf{u}_p(\mathrm{t})\},\,\{\dot{\mathbf{u}}_p(\mathrm{t})\}) = \mathbf{f}_{c_n}(\{\mathbf{u}_p(\mathrm{t})\}) + \mathbf{f}_{c_{stick}}(\{\mathbf{u}_p(\mathrm{t})\},\,\{\dot{\mathbf{u}}_p(\mathrm{t})\}) \\ + \mathbf{f}_{c_{slip}}(\{\mathbf{u}_p(\mathrm{t})\},\,\{\dot{\mathbf{u}}_p(\mathrm{t})\})\,.\end{aligned} \tag{1.72}$$

1.3.2 Discretised form of the weak problem for geometrically nonlinear rotating structures with contact

The discretised form of the mechanical problem is formulated as follows:

Find $\{\mathbf{u}_p(\mathrm{t})\}\in\mathcal{H}^1$ *such that* $\forall\{\delta\boldsymbol{u}_p\}\in\mathcal{H}^1$*, and that the residue vector satisfies the relation,* $\{\mathbf{R}(\{\mathbf{u}_p(\mathrm{t})\})\} = \{0\}$.

Where the definition of the discretised residue is,

$$\begin{aligned}\{\mathbf{R}(\{\mathbf{u}_p(\mathrm{t})\})\} = \mathbf{M}\frac{\mathrm{d}^2\{\mathbf{u}_p\}}{\mathrm{d}t^2}(t) + \mathbf{D}_g(\mathbf{t})\frac{\mathrm{d}\{\mathbf{u}_p\}}{\mathrm{d}t}(t) + \mathbf{K}_a(\mathbf{t})\{\mathbf{u}_p(\mathrm{t})\} \\ + \mathbf{K}_c(\mathbf{t})\{\mathbf{u}_p(\mathrm{t})\} + \mathbf{g}(\{\mathbf{u}_p(\mathrm{t})\}) - \mathbf{f}_e(\mathrm{t}) - \mathbf{f}_{ei}(\mathrm{t}) - \mathbf{f}_c(\{\mathbf{u}_p(\mathrm{t})\},\,\{\dot{\mathbf{u}}_p(\mathrm{t})\})\,.\end{aligned} \tag{1.73}$$

1.4 Full Order Model of a geometrically nonlinear rotating structure with contact

In the previous section the weak form of the mechanical problem is discretised to study the dynamics of rotating structures with contact type nonlinearities. The discretised equation of motion of a *high fidelity* model of a rotating

structure is defined in Eqn. (1.74) considering the rotating frame of reference. The latter model, also called Full Order Model (FOM) provides accurate results at a computationally expensive cost.

In the following, it is considered that the rotating velocity has a constant modulus and that the axis of rotation does not vary, $\mathbf{K}_a = \mathbf{0}$. In order to magnify the influence of geometric nonlinearities, the gyroscopic and the Coriolis effects are neglected with respect to the external inertial loading, $\mathbf{D}_g = \mathbf{0}$. Furthermore, to simplify the notation, a) the time dependency of the displacement vector is not explicitly represented, b) as the rotating velocity is considered as constant in time, centrifugal external forces, $\mathbf{f}_{ei}(\Omega)$, and the centrifugal softening matrix, $\mathbf{K}_c(\Omega)$, are time independent, and c) all the quantities presented hereinafter belong to the discretised problem, thus, the "braces" notation is avoided, i.e. $\{\mathbf{u}_p(\mathrm{t})\} \equiv \mathbf{u}_p$.

$$\mathbf{M}\ddot{\mathbf{u}}_p + \mathbf{C}\dot{\mathbf{u}}_p + \mathbf{K}_c(\Omega)\mathbf{u}_p + \mathbf{g}(\mathbf{u}_p) = \mathbf{f}_e(t) + \mathbf{f}_{ei}(\Omega) + \mathbf{f}_c(\mathbf{u}_p, \dot{\mathbf{u}}_p) \ , \tag{1.74}$$

where $\mathbf{M}$ is the mass matrix, $\mathbf{C}$ is the viscous damping matrix, $\mathbf{K}_c(\Omega)$ is the centrifugal softening matrix, $\mathbf{g}(\mathbf{u}_p)$ is the nonlinear internal efforts vector, $\mathbf{f}_e(t)$ is the external forces vector, $\mathbf{f}_{ei}(\Omega)$ is the non-follower external inertial load vector and $\mathbf{f}_c(\mathbf{u}_p, \dot{\mathbf{u}}_p)$ is the nonlinear forces due to friction contact.

The viscous damping effects are introduced by the *viscous damping* matrix. The classical viscous damping matrices are assembled by means of Caughery series [Caughey, 1960], that is a generalisation of the Rayleigh damping matrix [Strutt and Rayleigh, 1945] and by the summation of modal damping matrices [Wilson and Penzien, 1972]. Optimal Caughery series were proposed to study nonlinear analyses [Luco and Lanzi, 2017]. The identification by means of a generalised proportional damping [Adhikari and Phani, 2004] permits to capture the variations of the modal damping factor, ξ_j. Within the scope of proportional damping [Géradin and Rixen, 2014] proposed a method to obtain the damping matrix by means of Caughery series. Other authors propose the implementation of hysteretic mechanisms instead of using proportional damping matrices.

As the accuracy of the damping matrix is out of the scope of this work, hereinafter, the viscous damping effect is modelled by means of a Rayleigh damping matrix that considers a linear combination of the mass and stiffness matrices, that is,

$$\mathbf{C} = \beta_m \mathbf{M} + \alpha_K \mathbf{K} \ , \tag{1.75}$$

where the coefficients β_m and α_K are parameters that need to be identified. In [Adhikari and Phani, 2004] a method for identifying the damping parameters is presented by means of an experimental modal analysis.

Then, the modal damping factor is defined as,

$$\xi_j = \frac{1}{2}\left(\frac{\beta_m}{\omega_j} + \alpha_K\right) , \tag{1.76}$$

where ω_j represent the j-th natural frequency of the structure.

To reduce the complexity of Eqn. (1.74) the physical displacements are defined as the sum of an initial pre-stressed static equilibrium state, $\mathbf{u}_s$, induced by rotation and the relative displacements, $\mathbf{u}$, around the pre-stressed static equilibrium state, $\mathbf{u}_p = \mathbf{u}_s + \mathbf{u}$, as shown in Fig. 1.8.

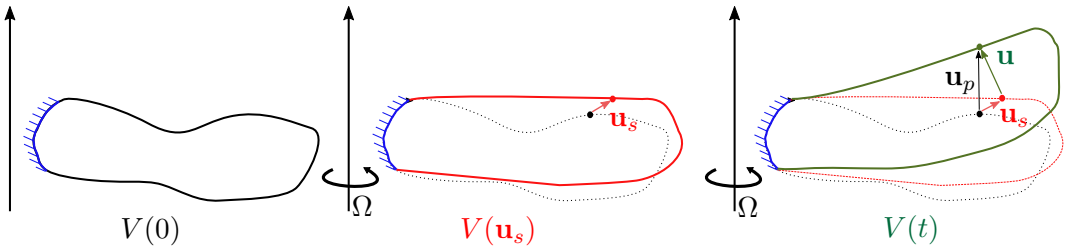

Figure 1.8: Representation of the static displacements and the relative displacements of the structure.

The static equilibrium state is obtained by solving the nonlinear system of Eqn. (1.77).

$$\mathbf{K}_c(\Omega)\mathbf{u}_s + \mathbf{g}(\mathbf{u}_s) = \mathbf{f}_{ei}(\Omega) . \tag{1.77}$$

Depending on the characteristics of the studied contact nonlinearity (tip shroud, rub...) contact effects should be considered in Eqn. (1.77). This equation is solved by an iterative procedure (i.e. Newton-Raphson method). In the classical approach [Henry, 1981] the static state of equilibrium, $\mathbf{u}_s$, due to the rotating velocity, Ω, is obtained by considering the geometrically nonlinear effects (large displacements) and the dynamic state around the static state is **linearised** by means of the tangent stiffness matrix. In the approach presented here, not only the static state is considered with a nonlinear behaviour but also the dynamic vibrations around the static state, keeping the nonlinear behaviour of the internal forces. The latter is represented by a purely nonlinear forces term, $\mathbf{g}_{nl}(\mathbf{u})$, as shown in Eqn. (1.88). In the following, the classical linearised approach is referred to as the "Linear FOM/ROM".

The nonlinear tangent stiffness matrix, $\mathbf{K}_t(\mathbf{u}_p)$, and the elastic linear stiffness matrix, $\mathbf{K}_e$, which corresponds to the value of the tangent stiffness matrix for the non deformed structure ($\mathbf{u}_p$= 0) are defined as follows,

$$\begin{aligned}\mathbf{K}_t(\mathbf{u}_p) = \frac{\partial \mathbf{g}(\mathbf{u}_p)}{\partial \mathbf{u}_p} = &\int_{V(0)} \left[\mathbf{B}(\mathbf{p})^T \cdot (\mathbb{D} : \mathbf{E}_p(\{\mathbf{u}_p\}))\right] : \mathbf{B}(\mathbf{p}) \mathrm{d}V(0) \\ &+ \int_{V(0)} \left[\mathbb{D} : \left(\mathbf{B}(\mathbf{p})^T \mathbf{X}_p(\{\mathbf{u}_p(\mathrm{t})\})\right)\right] : \left(\mathbf{B}(\mathbf{p})^T \mathbf{X}_p(\{\mathbf{u}_p(\mathrm{t})\})\right) \mathrm{d}V(0) ,\end{aligned} \tag{1.78}$$

$$\mathbf{K}_e = \mathbf{K}_t(\mathbf{0}) = \left.\frac{\partial \mathbf{g}(\mathbf{u}_p)}{\partial \mathbf{u}_p}\right|_{\mathbf{u}_p=0} = \int_{V(0)} \mathbf{B}(\mathbf{p})^T : \mathbb{D} : \mathbf{B}(\mathbf{p}) \mathrm{d}V(0) \ . \tag{1.79}$$

The tangent stiffness matrix with respect to the static displacements is defined hereunder,

$$\mathbf{K}_s = \mathbf{K}_t(\mathbf{u}_s) = \left.\frac{\partial \mathbf{g}(\mathbf{u}_p)}{\partial \mathbf{u}_p}\right|_{\mathbf{u}_p=\mathbf{u}_s} \ , \tag{1.80}$$

that is also written as the sum of a linear stiffness and a nonlinear stiffness related to the initial state of the structure [Schotte, 2001, Schotté and Ohayon, 2009].

$$\mathbf{K}_s = \mathbf{K}_e + \mathbf{K}_{nl}(\mathbf{u}_s) \approx \mathbf{K}_e + \mathbf{K}_g(\mathbf{u}_s) \ , \tag{1.81}$$

Then, if the tangent stiffness matrix is evaluated around the pre-stressed state, the nonlinear term corresponds to the sum of a pre-stressed geometrical stiffness, $\mathbf{K}_g(\mathbf{u}_s)$, induced by rotation and a pre-deformed stiffness, $\mathbf{K}_\varepsilon(\mathbf{u}_s)$, that reflects the variation of the structure's stiffness due to the change of the geometry in the initial state,

$$\mathbf{K}_{nl}(\mathbf{u}_s) = \mathbf{K}_g(\mathbf{u}_s) + \underbrace{\mathbf{K}^L_\varepsilon(\mathbf{u}_s) + \mathbf{K}^Q_\varepsilon(\mathbf{u}_s)}_{\mathbf{K}_\varepsilon(\mathbf{u}_s)} \approx \mathbf{K}_g(\mathbf{u}_s) \ , \tag{1.82}$$

where $\mathbf{K}^L_\varepsilon(\mathbf{u}_s)$ and $\mathbf{K}^Q_\varepsilon(\mathbf{u}_s)$ are the linear and quadratic terms of the pre-deformed stiffness matrix. Considering that $\mathbf{E}^L_p$ and $\mathbf{E}^{NL}_p$ are respectively the linear and nonlinear terms of the Green-Lagrange strain tensor, Eqn. (1.10), the geometrical stiffness and the pre-deformed stiffness are defined as,

$$\mathbf{K}_g(\mathbf{u}_s) = \int_{V(0)} \mathbf{BS}(\mathbf{u}_s) : \mathbf{B} \mathrm{d}V(0) \ , \tag{1.83}$$

$$\begin{aligned} \mathbf{K}_\varepsilon(\mathbf{u},\, \delta\mathbf{u}) &= 2\int_{V(0)} \mathbb{D}\mathbf{E}^L_p(\delta\mathbf{u}) : \mathbf{E}^{NL}_p(\mathbf{u}_s,\, \mathbf{u}) + \mathbb{D}\mathbf{E}^L_p(\mathbf{u}) : \mathbf{E}^{NL}_p(\mathbf{u}_s,\, \delta\mathbf{u}) \mathrm{d}V(0) \\ &+ 4\int_{V(0)} \mathbb{D}\mathbf{E}^{NL}_p(\mathbf{u}_s,\, \mathbf{u}) : \mathbf{E}^{NL}_p(\mathbf{u}_s,\, \delta\mathbf{u}) \mathrm{d}V(0) \ . \end{aligned} \tag{1.84}$$

When the strain of the structure in the initial state is small, the pre-deformed matrix is neglected, $\mathbf{K}_\varepsilon(\mathbf{u}_s) \approx \mathbf{0}$, and the nonlinear contribution of the tangent matrix corresponds to the pre-stressed geometrical stiffness, $\mathbf{K}_g(\mathbf{u}_s)$. In the following, this assumption is considered as valid.

Then, introducing the Eqn. (1.77) in the Eqn. (1.74), the equation of motion of the structure with respect to the static equilibrium state position is obtained,

$$\mathbf{M}\ddot{\mathbf{u}} + \mathbf{C}\dot{\mathbf{u}} + \mathbf{K}_c(\Omega)\mathbf{u} + \mathbf{g}(\mathbf{u}_s + \mathbf{u}) - \mathbf{g}(\mathbf{u}_s) = \mathbf{f}_e(t) + \mathbf{f}_c(\mathbf{u}{+}\mathbf{u}_s,\, \dot{\mathbf{u}}) \ , \tag{1.85}$$

where the external inertial forces $\mathbf{f}_{ei}(\Omega)$ are eliminated.

The development of the nonlinear forces $\mathbf{g}(\mathbf{u}_s + \mathbf{u})$ in the neighbourhood of the static displacements, $\mathbf{u}_s$, is the sum of a constant, a linear part and a purely nonlinear part,

$$\mathbf{g}(\mathbf{u}_\mathrm{s} + \mathbf{u}) = \mathbf{g}(\mathbf{u}_\mathrm{s}) + \left.\frac{\partial \mathbf{g}(\mathbf{u}_\mathrm{p})}{\partial \mathbf{u}_p}\right|_{\mathbf{u}_p=\mathbf{u}_s} \mathbf{u} + \mathbf{g}_{nl}(\mathbf{u}) = \mathbf{g}(\mathbf{u}_\mathrm{s}) + \mathbf{K}_s\mathbf{u} + \mathbf{g}_{nl}(\mathbf{u}) \ . \quad (1.86)$$

The stiffness matrix function of the rotating velocity, Ω, and the static displacements, $\mathbf{u}_s$, is defined hereunder,

$$\mathbf{K}(\Omega) = \mathbf{K}(\Omega,\, \mathbf{u}_s) = \mathbf{K}_c(\Omega) + \mathbf{K}_s = \mathbf{K}_c(\Omega) + \mathbf{K}_e + \mathbf{K}_{nl}(\mathbf{u}_s) \ , \quad (1.87)$$

composed of the linear elastic stiffness matrix, of the centrifugal softening matrix and of the nonlinear part of the tangent matrix which includes the geometrical pre-stressed stiffness matrix, $\mathbf{K}_g(\mathbf{u}_s)$.

Then the equation of motion is defined in terms of the relative displacements, $\mathbf{u}$, [Balmaseda et al., 2018],

$$\mathbf{M}\ddot{\mathbf{u}} + \mathbf{C}\dot{\mathbf{u}} + \mathbf{K}(\Omega)\mathbf{u} + \mathbf{g}_{nl}(\mathbf{u}) = \mathbf{f}_e(t) + \mathbf{f}_c(\mathbf{u}+\mathbf{u}_s,\, \dot{\mathbf{u}}) \ . \quad (1.88)$$

The FOM has an expensive time cost for large number of computations (i.e. design, control...). In order to significantly reduce the computational time in exchange of an acceptable loss in precision reduced order model techniques are an interesting solution.

1.5 Conclusions

The physical problem described in this chapter is the dynamics of a rotating structure with large displacements and friction contact nonlinearities. The strong form of the problem is transformed into its weak form, suitable for discretisation. After presenting some classical friction laws and models, the penalty method is used to solve the variational inequality of the friction contact problem and other techniques are presented. For the studied applications, the contact region is *a priori* known and the variational inequality is transformed into a variational equality.

Then the continuum formulation is discretised by means of the Finite Element Method (FEM). Furthermore, the matrices and vectors that are used in the discretised equation of motion are defined. This formulation is adapted to be a function of the vibrations, $\mathbf{u}$, around the static displacements induced by rotation, $\mathbf{u}_s$. Moreover, the Full Order Model (FOM) of the structure is introduced. The FOM provides accurate results to the studied physical problem, however, the resolution time is very expensive for nonlinear structures (considering industrial standards). Hereinafter, the results obtained with the

FOM are considered as the reference solution.

In the next chapter, some reduced order models to study the dynamics of rotating structures with large displacement and contact nonlinearities are developed. These methods improve the time performances of the FOM and provide acceptable accuracy with respect to the FOM results. Thus, they are meant to represent the best compromise between computational time and accuracy.

The following hypothesis are considered hereinafter:

1. With respect to the material behaviour and its properties:
   (a) The material is homogeneous, isotropic, non-dissipative and elastic.
   (b) The energy dissipation is induced by a Rayleigh viscous damping matrix, $\mathbf{C}$, in the discrete formulation. Only the mass contribution is considered, $\alpha_K = 0$.
2. With respect to the rotation of the structure:
   (a) The rotating velocity of the structure is supposed to be constant in module and direction.
   (b) The effect of the gyroscopic coupling, $\mathbf{D}_g$, and the centrifugal acceleration, $\mathbf{K}_a$, are considered as negligible.
   (c) The physical displacements of the structure, $\mathbf{u}_p$, are the sum of the static state induced by rotation, $\mathbf{u}_s$, and the vibrations, $\mathbf{u}$, around that static state.
   (d) Both $\mathbf{u}_s$ and $\mathbf{u}$ are considered as geometrically nonlinear.
3. With respect to the friction contact:
   (a) The friction contact boundary is supposed to be *a priori* known.
   (b) A macroslip Coulomb's law is considered.
   (c) The penalisation method is used.
   (d) The structure is in contact with an object that rotates solidarily to it. Only the vibrations, $\mathbf{u}$, affect the contact state.
   (e) A node to node contact is supposed. Due to the limitations of the penalisation method for large displacements, the contact boundary is placed in a region where the displacement of the structure are small. No large slip states are studied.
   (f) The geometry of the contact surfaces are not taken into consideration.
   (g) A detailed analysis of the contact surface discretisation is out of the scope of this study.

Chapter 2

Construction and resolution of the reduced order model

IN THIS SECOND CHAPTER the construction of reduced order models that represent the discretised nonlinear physical model (FOM) for rotating structures, defined in the previous chapter, are developed. First, the reduced order technique is introduced and some of the classical reduced order bases are presented. Second, the Galeking projection is implemented to build the reduced order model (ROM). Third, the inflation (classical) and STEP (polynomial) methods used to evaluate the nonlinear generalised forces are presented and an original POD based correction is proposed in order to solve the inaccuracy of the classical ROM methods, to study the forced response of nonlinear slender structures. Fourth, the proposed ROMs are parametrised in order to prevent the OFFline computational cost of constructing a reduced order model for each rotating velocity. Finally, the solution methods that are used to evaluate the time response of the proposed reduced order models are presented.

Contents

2.1 Introduction

The finite element discretisation of the weak form of the studied physical problem presented in the previous chapter is considered as the reference solution and hereinafter is referred as the Full Order Model (FOM). This model is capable of providing accurate results, however, for repetitive design or control processes, where several computations of the FOM are performed, the computational cost (directly related to the financial cost) can easily exceed the industrial standards for "acceptable costs" to evaluate a given solution. The latter statement is specially true in multi-parametric and optimization processes with measurement uncertainties where the average and the standard deviation of the solution are obtained by performing a very large series of FOM computations such as in the Monte Carlo method [Metropolis and Ulam, 1949].

To reduce the computational cost of the high fidelity finite element nonlinear models, some investigators have developed the construction of nonlinear reduced order models (ROM) [Hollkamp and Gordon, 2008, Sampaio and Soize, 2007]. However, without special techniques to create an efficient ROM able to evaluate the system matrices when the structure deforms, the computational cost of this process may become equivalent to the time to perform the full order finite element analysis and the advantages of the reduction are counteracted. An efficient approach to nonlinear structural analysis was carried out by [Rizzi and Muravyov, 2001, Muravyov and Rizzi, 2003] representing the internal forces by a third order polynomial formulation of displacements. This method is known as the Stiffness Evaluation Procedure (STEP). The stiffness coefficients of the polynomial representation are obtained by a series of static results obtained with the full order finite element model. As an extension to the STEP method "non intrusive" reduced order models have been reviewed by [Mignolet et al., 2013] and validated for the prediction of fatigue [Radu et al., 2004], nonlinear stochastic computations [Capiez-Lernout et al., 2012, Capiez-Lernout et al., 2017], post-buckling analyses [Capiez-Lernout et al., 2014] and complex structures [Perez et al., 2014]. The Element-wise Stiffness Evaluation Procedure (E-STEP) generalizes the STEP to optimization problems enabling the parametrization of the stiffness evaluation procedure. The hyper-reduction [Ryckelynck, 2005, Farhat et al., 2015, Chapman et al., 2017] and the piecewise linearisation [Bond and Daniel, 2007, Yuan and Jiang, 2017] are alternative techniques to ease the system matrix computation issues.

In the framework of rotating structures, the vibration of linear rotating beams has been widely studied [Boyce et al., 1954, Pnueli, 1972, Stafford and Giurgiutiu, 1975], extended to the study of nonlinear geometrical fixed beam models [da Silva and Hodges, 1986] and adapted to rotating structures [Beley et al., 2017, Du et al., 1994]. The effect of nonlinear rotation creates a coupling between the axial and transverse motions. Based on a von Karman formula-

tion, a reduction model of a rotating beam is performed by nonlinear modes and invariant manifolds [Pesheck et al., 2002, Jiang et al., 2005]. The free vibrations of non-uniform fixed geometrically nonlinear beams with variable cross section and material properties along the axial direction are carried out by [Kumar et al., 2015]. A comparison between several models of a rotating cantilever beam in terms of accuracy and validity is presented by [Thomas et al., 2016]. These models are mainly used in the study of helicopter and turbo-machinery blades [Tang and Dowell, 1996, Pesheck et al., 2001, Vakakis, 1992, Grolet and Thouverez, 2010, Beley et al., 2017], modelisations of slender beams or thin shells [Sénéchal et al., 2009, Hodges et al., 1996, Huang and Han, 2010] and structure-fluid interactions [Zhang et al., 2014]. A finite element formulation of the rotating problem is presented in [Sternchüss, 2009] and the necessity to develop 3D finite element models for the study of rotordynamics is highlighted in [Genta and Silvagni, 2014].

The remainder of this chapter is structured as follows: first, the reduced order model concept is introduced and some of the classical reduced order bases are presented. Second, *the projection based* reduced order models are defined and a discussion of the reduced order bases used in this work is carried out. The validity of the latter bases is discussed with respect to each of the considered nonlinearities. Third, the geometrically nonlinear effects are studied with the application to a 1D Duffing oscillator and the techniques to represent the nonlinear forces in the reduced order model are presented. Then, the limitations of combining the later techniques with the classical reduced order bases is highlighted for the application of slender structures. An original POD based correction technique is proposed to solve these limitations. Fourth, the contact nonlinearity effects are discussed for a modified 1D Duffing oscillator and the coupled influence between the geometrical nonlinearity and the friction contact type nonlinearities is studied. Fifth, the parametrisation with respect to the rotating velocity of the nonlinear reduced order model is presented. Finally, some concluding remarks are drawn to justify the hypotheses to be considered in the following chapters.

2.2 Reduced order techniques

In most of the reduction techniques, the nodal displacements of the FOM are approximated by a linear product between an approximation basis, $\mathbf{Q}_{app.}$ and the generalised displacements vector, $\mathbf{q}$,

$$\mathbf{u} = \mathbf{Q}_{app.}\mathbf{q} \, . \tag{2.1}$$

The construction of the reduced order model is carried out in an *OFFline* phase where expensive FOM computations are performed. Then, once the reduced order model is defined, the solution of the problem is obtained during

the *ONline* phase with a minimal computational cost.

For some techniques, the OFFline phase is more expensive than a single FOM computation, however, over a given number of computations, the combination of the time consumption between the OFFline and ONline phases of the reduced order model is more rapid than the FOM computations as it is shown in Fig. 2.1.

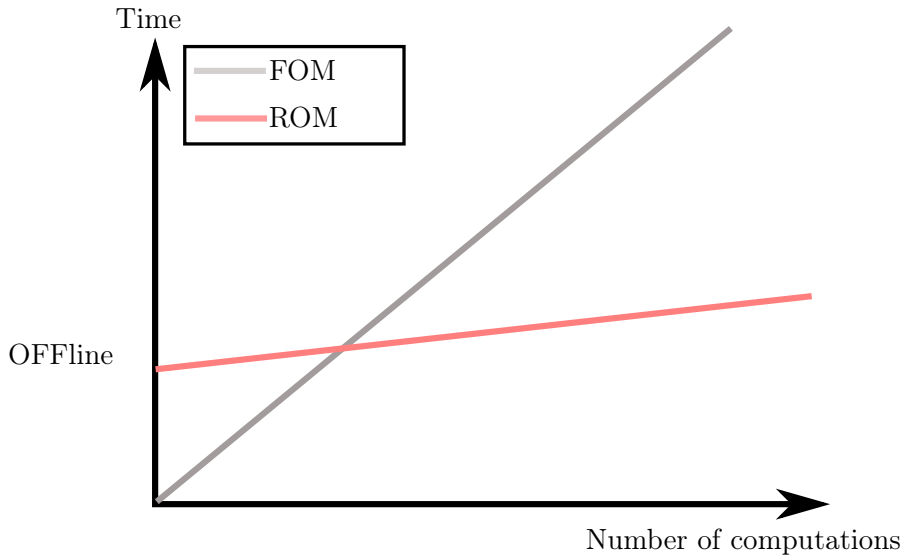

Figure 2.1: Computational time of the FOM vs the ROM.

Hereunder, some of the most common approaches for the approximation basis and for the reduction techniques are presented. The approximation basis, $\mathbf{Q}_{app.}$, also called the *reduced basis*, is equally represented as $\mathbf{\Phi}$.

2.2.1 Linear normal modes (LNM)

The Linear Normal Modes are obtained by evaluating the eigenvalues and eigenvectors of the underlying linearised system,

$$\mathbf{K\Phi} = \mathbf{M\Phi\omega}^2 \,, \tag{2.2}$$

where $\mathbf{K}$ is the stiffness matrix at the equilibrium configuration.

The construction of the LNM basis is very simple and widely implemented in industrial finite element codes (i.e. Nastran, Code_Aster,...). For very large number of degrees of freedom, the eigenvalue problem computational time is optimised by means of iterative methods such as the Sorensen method [Maschho and Sorensen, 1996] capable of computing directly the first r eigenvalues and eigenvectors.

LNM at given displacement

The linear normal modes at a given displacement configuration are performed by taking into consideration the stiffness properties of a nonlinear deformed configuration, $\hat{\mathbf{u}}$. Thus, the stiffness matrix is defined as,

$$\mathbf{K} = \left.\frac{\partial \mathbf{g}(\mathbf{u})}{\partial \mathbf{u}}\right|_{\hat{\mathbf{u}}} . \tag{2.3}$$

A common choice is to consider that $\hat{\mathbf{u}}$ corresponds to the maximum displacement configuration or to a pre-computed stress configuration of the structure. This case is a generalisation of the LNM for rotating structures where the structure is considered to be pre-stressed by the effect of rotation.

LNM for rotating structures

To compute the Linear Normal Modes basis, the hypothesis of small vibrations around the static displacements is applied to the equation of motion of the structure,

$$\mathbf{M}\ddot{\mathbf{u}} + \mathbf{C}\dot{\mathbf{u}} + \mathbf{K}(\Omega)\mathbf{u} = \mathbf{f}_e(t) . \tag{2.4}$$

Then, the natural frequencies of the structure and its corresponding Linear Normal Modes are computed as the solution of the eigenvalue and eigenvector problem presented in Eqn. (2.5) without considering viscous damping effects,

$$\mathbf{K}(\Omega)\mathbf{\Phi} = \mathbf{M}\mathbf{\Phi}\boldsymbol{\omega}^2 , \tag{2.5}$$

where $\boldsymbol{\omega} = \text{diag}\,[\omega_1, \ldots, \omega_r]$ with $\omega_1 \leq \ldots \leq \omega_r$ the first r natural frequencies and $\mathbf{\Phi} = [\mathbf{\Phi}_1, \ldots, \mathbf{\Phi}_r]$ the linear normal modes associated to those natural frequencies. The group of first r normal linear modes form the reduced LNM basis $\mathbf{\Phi}$ around the pre-stressed static equilibrium induced by the rotation.

LNM with second order terms (Taylor basis)

In order to expand the use of LNM to nonlinear systems [Slaats et al., 1995, Grolet and Thouverez, 2010, Martin and Thouverez, 2019] the reduced basis is enhanced with the derivatives of the LNM defined previously. Thus, the derivatives of a linear normal mode are defined as,

$$\Phi_{i,k} = \left(\frac{\partial \Phi_k}{\partial q_i} + \frac{\partial \Phi_i}{\partial q_k}\right) , \tag{2.6}$$

then, the reduced basis is formed by the linear normal modes defined in Eqn. (2.2), (2.3) and (2.5) enhanced by the modes derivatives.

$$\mathbf{\Phi} = [\underbrace{\Phi_1, \ldots, \Phi_r}_{\text{LNM}}, \underbrace{\Phi_{1,1}, \ldots, \Phi_{r,r}}_{\text{LNM derivatives}}] . \tag{2.7}$$

In order to avoid increasing too much the basis size with modes derivatives, the key of this technique is to choose the correct combination between the modes derivatives and the behaviour of the structure. Numerically, the derivatives of the modes are obtained by introducing a finite displacement around the modal shape, Δq_k, and performing a numerical derivative,

$$\frac{\partial \Phi_i}{\partial q_k} = \frac{\Phi_i \left(\mathbf{u}_0 + \Phi_k \Delta q_k\right) - \Phi_i \left(\mathbf{u}_0\right)}{\Delta q_k} \ , \tag{2.8}$$

which is based on the finite difference of the modal coordinate under consideration.

2.2.2 Ritz Vectors

The Ritz vectors are an extension to the Lanzcos [Lanczos, 1950] algorithm for the estimation of eigenvectors. For some cases, the computation of the Ritz vectors is quicker than the computation of the LNM as the last ones evaluate the eigenproblem of full dimension while the computation of Ritz vectors is performed with an iterative method [Kapania and Byun, 1993].

The Ritz vectors correspond to the static response to a given loading state of the system,

$$\Phi_1 = \mathbf{K}^{-1}\mathbf{f}_e \ , \tag{2.9}$$

where $\mathbf{K}$ is the tangent stiffness matrix. The latter eigenvector can be normalised with respect to the mass or with respect to any other norm. In literature, the mass normalisation is privileged as the normalisation of the stiffness matrix leads to the square of the modal frequencies of the linearised system. Thus, the Ritz vector is normalised as follows,

$$\mathbf{\Phi}_1 = \frac{\Phi_1}{\sqrt{\Phi_1^T \mathbf{M} \Phi_1}} \ . \tag{2.10}$$

The following Ritz vectors are obtained based on the previously generated vectors, thus,

$$\mathbf{\Phi}_{k+1} = \mathbf{K}^{-1}\mathbf{M}\Phi_k - \sum_{j=1}^{k-1} \Phi_j^T \mathbf{M}\mathbf{K}^{-1}\mathbf{M}\Phi_k\Phi_j \ , \quad \forall\ 1 \leq k \leq r \ . \tag{2.11}$$

The latter equation is normalised as shown in Eqn. (2.10). Similarly to the LNM, the Ritz vectors are assembled in a reduced basis matrix, $\mathbf{\Phi}$. The number of retained modes r should be large enough to accurately represent the behaviour of the structure and small enough to highlight the reduction in the computational effort.

Furthermore, following the same logic as for the second order terms to enhance the basis of the LNM, the Ritz vectors basis can be enriched by their derivatives [Idelsohn and Cardona, 1985, Engblom and Chang, 1991],

$$\frac{\partial \Phi_i}{\partial q_k} = -\mathbf{K}^{-1} \frac{\Delta \mathbf{K}}{\Delta q_k} \Phi_i \ . \tag{2.12}$$

2.2.3 Proper Orthogonal Decomposition (POD)

The Proper Orthogonal Decomposition (POD) is a widely developed reduced order technique that uses a meaningful set of physical data obtained by means of a set of experiments [Bellizzi and Sampaio, 2009] or by a set of FOM computations [Lenaerts et al., 2003, Sirovich, 1987] to extract the characteristics of the solution in order to construct the reduced basis. This technique focuses on the inherent physics of the studied problem rather than on its mathematical properties. Most of the developments of this methods are performed in the field of fluid dynamics [Kunisch and Volkwein, 2002, Couplet et al., 2005, Amsallem et al., 2009, Placzek, 2009], however, it is also valid for the study of structural dynamics [Carassale and Solari, 2002, Han and Feeny, 2003, Azam and Mariani, 2013].

Thus, to build the POD reduced basis, a set of data is collected from the numerical solution of the FOM at a given number, m, of temporal instants (snapshots). All the data is stored in the snapshot matrix, $\mathbf{A}$, which is defined as,

$$\mathbf{A} = [\mathbf{u}(\mathrm{t}_1), \ldots, \mathbf{u}(\mathrm{t}_m)]_{n \times m} \ , \tag{2.13}$$

where $\mathbf{u}(t_i)$ represents the solution vector for the i-th considered instant, t_i.

If the mean values of $\mathbf{u}(t_i)$ are zero, the covariance matrix is then constructed as,

$$\mathbf{R}_{cov.n \times n} = \mathbf{A}\mathbf{A}^T \ . \tag{2.14}$$

The number of snapshots, m, and the number of degrees of freedom, n, determine the algorithm to optimally compute the POD basis [Kirby et al., 1990]. For large values of n, the evaluation of the Eqn. (2.14) becomes very expensive.

The eigenvalue problem related to the correlation matrix is solved to obtain the associated eigenvectors and eigenvalues,

$$\mathbf{R}_{cov.} \Phi_i = \lambda_i \Phi_i \ , \tag{2.15}$$

which leads to n eigenvectors and n eigenvalues. As the correlation matrix is symmetric and positive, the latter eigenvectors and eigenvalues are real and positive.

The direct method presented in Eqn. (2.15) is only applicable when the number of degrees of freedom of the structure n is small. For all the other cases, the two methods presented in the following are applied.

a) Singular value decomposition (SVD)

The singular value decomposition (SVD) [Strang, 1980] is a factorisation of the snapshots matrix, $\mathbf{A}$. The latter factorisation is a generalisation of the eigendecomposition problem of a positive semi-definite normal matrix. The form of the factorisation is $\mathbf{A} = \mathbf{U}\Sigma\mathbf{V}^T$, where $\mathbf{U}$ is a $n \times n$ orthogonal matrix $\left(\mathbf{U}^T\mathbf{U} = \mathbf{I}\right)$, Σ is a $n \times m$ matrix whose first $s = \text{rank}\,(\mathbf{A}) \leq \min(n, m)$ diagonal values correspond to the singular values of the snapshots matrix, $\mathbf{A}$, and $\mathbf{V}^T$ is a $m \times m$ orthogonal matrix. Then due to the particular form of the singular values matrix, Σ, the SVD problem is computed by truncating to the s first columns of $\mathbf{U}$ and $\mathbf{V}^T$ respectively. Thus,

$$\mathbf{A} = \mathbf{U}_s\Sigma_s\mathbf{V}_s^T \ . \tag{2.16}$$

Then, by analogy with Eqn. (2.15), $\mathbf{R}\ \mathbf{U}_s = \mathbf{A}\ \mathbf{A}^T\ \mathbf{U}_s$, thus, the eigenproblem is solved as,

$$\mathbf{R}\mathbf{U}_s = \mathbf{U}_s\Sigma_s^2 \Rightarrow \mathbf{\Phi} = \mathbf{U}_s \text{ and } \boldsymbol{\lambda} = \Sigma_s^2 \ . \tag{2.17}$$

b) Snapshot POD method

Another technique to solve the eigenvalue problem, that is specially useful when the number of snapshots m is smaller than the number of degrees of freedom of the structure n is the Snapshot POD method [Sirovich, 1987]. In this method, the covariance matrix with a dimension of $m \times m$ is defined as,

$$\mathbf{R}_{cov.m\times m} = \mathbf{A}^T\mathbf{A} \ . \tag{2.18}$$

Thus, the eigenproblem to be solved is reformulated in terms of the right singular eigenvectors of $\mathbf{R}_{cov.m\times m}$,

$$\mathbf{R}_{cov.m\times m}\mathbf{V}_s = \mathbf{V}_s\Sigma_s^2 \ , \tag{2.19}$$

and the POD eigenvectors are obtained from Eqn. (2.16), $\mathbf{\Phi} = \mathbf{A}\mathbf{V}_s$, considering Σ_s^{-1} matrix as a scaling factor.

The main objective is to increase the computational performances of the FOM, thus, the obtained solution is truncated to a number r of eigenvectors that are used to form the reduced basis.

$$\mathbf{\Phi} = [\Phi_1, \ldots, \Phi_r] \ . \tag{2.20}$$

In literature, the value of r is generally obtained with the energy contained in the truncated space evaluated from the ratio of the eigenvalues spectrum,

$$\mathscr{E}_r = \frac{\sum_{i=1}^{r} \lambda_i}{\sum_{j=1}^{s} \lambda_j} , \tag{2.21}$$

considering that $\lambda_1 < \lambda_2 < \cdots < \lambda_s$. Thus the energy ratio is defined as the energy contained in the modes that form the truncated basis with respect to the total energy of the full order system. The objective is to ensure a value of $\mathscr{E}_r$ as close to 1 as possible.

2.2.4 Component mode synthesis

The component mode synthesis allows to study complex configurations of structures by decomposing the whole structure into different substructures. These substructures are represented by Ritz vectors that include linear normal modes, rigid body motion modes, static modes, interface modes, etc. The equation of movement of each substructure is then projected to build the reduced order model of the substructure. In order to couple the reduced order models of each substructure, the interfaces boundaries between the substructures are kept in the generalised displacements as shown in the following. Then, the coupled model of all substructures is capable of reproducing the behaviour of the whole structure for modal analysis or forced response analysis.

With respect to the type of boundary conditions that are applied at the interfaces of substructures, four main groups of component mode synthesis methods are differenciated: a) methods with fixed interfaces [Hurty, 1960, Hurty, 1965, Craig and Bampton, 1968, Craig Jr, 1985], methods with free interface [Rubin, 1975, Bamford, 1967, MacNeal, 1971, Rubin, 1975, Martinez et al., 1985], methods with mixed interface [MacNeal, 1971, Farvaque et al., 1984, Tran, 1992, Tran, 1993] and with loaded interfaces [Benfield and Hruda, 1971].

In the classical methods of component mode synthesis linear normal modes of substructures are enhanced with the so called *static displacements*. These methods are capable of saving the physical displacements in the generalised coordinates which is specially interesting for localised boundary conditions such as the friction contact problem. However, the reduction given by these methods is limited as all the degrees of freedom of the interface are kept in the generalised displacements of the reduced order model. Thus, to handle this issue, the *interface mode* component mode synthesis method have been developed to provide a significant reduction of the boundary dimension. However, the physical meaning of the boundary displacements is erased. In order to keep the physical meaning at some given positions of the boundary, the partial interface modes have been developed [Tran, 2009b, Tran, 2009a]. The

latter method combines the advantages of the interface reduction of the interface methods and the physical displacements at some given positions as in the classical component mode methods.

Hereunder the classical *fixed interface* method of Craig-Bampton and the *free interface* method are presented. In the following chapters, only the fixed interface Craig-Bampton method is used.

Fixed interface methods

The physical displacements for the Craig-Bampton fixed interface method are split into the inner d.o.f., $\mathbf{u}_i$, and the boundary interface d.o.f., $\mathbf{u}_b$. With this method, stiffness and mass matrices are partitioned with respect to inner and boundary d.o.f.,

$$\mathbf{K}(\Omega) = \begin{bmatrix} \mathbf{K}_{ii} & \mathbf{K}_{ib} \\ \mathbf{K}_{bi} & \mathbf{K}_{bb} \end{bmatrix} \quad , \quad \mathbf{M} = \begin{bmatrix} \mathbf{M}_{ii} & \mathbf{M}_{ib} \\ \mathbf{M}_{bi} & \mathbf{M}_{bb} \end{bmatrix} . \tag{2.22}$$

The same partition is applicable to all the elements in the equation of motion of the structure, Eqn. (1.74).

Then, as for any reduced order model based on a reduction basis, the relative physical displacements of the FOM are approximated as a linear combination between the reduction basis and the generalised displacements as,

$$\mathbf{u} = \mathbf{Q}\mathbf{q} = \Phi_{CB} \begin{Bmatrix} \mathbf{q}_i \\ \mathbf{u}_b \end{Bmatrix} = [\Phi_c \ \Psi_c] \begin{Bmatrix} \mathbf{q}_i \\ \mathbf{u}_b \end{Bmatrix} . \tag{2.23}$$

In the Craig-Bampton method the reduced basis, $\mathbf{Q} = \Phi_{CB}$, is composed of r_c fixed interface linear normal modes Φ_c and r_b constraint modes Ψ_c, while the generalised coordinates, $\mathbf{q}$, are composed of the modal coordinates $\mathbf{q}_i$ and the d.o.f. of the boundary interface, $\mathbf{u}_b$. The number of vectors in the reduced basis, $\mathbf{Q}$, is $r = r_c + r_b$.

Fixed interface Linear Normal Modes

The stiffness of a rotating structure depends on the rotating velocity and on the nonlinear static deformation of the pre-stressed equilibrium state. Thus, the natural frequencies and the modes of the structure depend on the rotating velocity. To compute the fixed interface linear normal modes, the pre-stressed equilibrium state is obtained by solving a nonlinear problem that only considers the effect of the centrifugal forces induced by rotation. Then, as shown in Eqn. (2.24) the linearised LNM are computed by considering that the structure is clamped at the boundary interface d.o.f.,

$$\mathbf{K}(\Omega)\mathbf{\Phi}_c = \mathbf{M}\mathbf{\Phi}_c\boldsymbol{\omega}^2 \quad , \quad \mathbf{\Phi}_c|_{u_b} = \mathbf{0} \, , \tag{2.24}$$

The fixed interface linear normal modes basis is formed by truncating the solution basis to the first r_c modes, $\mathbf{\Phi}_c = [\Phi_{c_1}, \ldots, \Phi_{c_{r_c}}]$. The associated natural frequencies of the fixed interface structure are $\boldsymbol{\omega} = \text{diag}\,[\omega_1, \ldots, \omega_{r_c}]$.

Constraint modes

The static deformation solution to unitary displacements at boundary d.o.f of the structure represent the constraint modes,

$$\mathbf{K}(\Omega) \left\{ \begin{array}{c} \Psi_{c_i} \\ \mathbf{I} \end{array} \right\} = \left[\begin{array}{cc} \mathbf{K}_{ii} & \mathbf{K}_{ib} \\ \mathbf{K}_{bi} & \mathbf{K}_{bb} \end{array} \right] \left\{ \begin{array}{c} \Psi_{c_i} \\ \mathbf{I} \end{array} \right\} = \left\{ \begin{array}{c} \mathbf{0} \\ \mathbf{R} \end{array} \right\} . \tag{2.25}$$

The constraint modes Ψ_c are then obtained from Eqn. (2.25), thus,

$$\Psi_c = \left\{ \begin{array}{c} -\mathbf{K}_{ii}^{-1}\mathbf{K}_{ib} \\ \mathbf{I} \end{array} \right\} . \tag{2.26}$$

Craig-Bampton reduced order basis

The Craig-Bampton reduced basis presented in Eqn. (2.23) is formed by the fixed interface linear normal modes and the constraint modes of the structure.

$$\mathbf{\Phi}_{CB} = [\Phi_c \; \Psi_c] = \left[\begin{array}{cc} \Phi_{c_i} & \Psi_{c_i} \\ \mathbf{0} & \mathbf{I} \end{array} \right] . \tag{2.27}$$

Free interface methods

Very similar to the fixed interface method, the matrix of the system are also partitioned as in Eqn. (2.22).

Then, the relative physical displacements of the FOM are approximated as a linear combination between the reduction basis and the generalised displacements as,

$$\mathbf{u} = \mathbf{Q}\mathbf{q} = \mathbf{\Phi}_{free} \left\{ \begin{array}{c} \mathbf{q}_i \\ \mathbf{u}_b \end{array} \right\} . \tag{2.28}$$

In the free interfaces method the reduced basis, $\mathbf{Q} = \Phi_{free}$, is derived from r_l free interface linear normal modes $\mathbf{\Phi}$ and r_b attachment modes Ψ_a, while the generalised coordinates, $\mathbf{q}$, are composed of the modal coordinates $\mathbf{q}_i$ and the d.o.f., $\mathbf{u}_b$, of the boundary interface. The number of vectors in the reduced basis, $\mathbf{Q}$, is $r = r_l + r_b$.

Free interface Linear Normal Modes

The free interface modes of the structure are the normal modes of the structure computed when the interface is not constrainted. Thus, the free interface modes of the structure correspond to the Linear Normal Modes of the structure defined in Eqn. (2.5).

Attachment modes

For constrained structures, the solution to an opposite unitary force applied at boundary d.o.f of the structure represent the attachment modes,

$$\mathbf{K}(\Omega)\Psi_a = \begin{bmatrix} \mathbf{K}_{ii} & \mathbf{K}_{ib} \\ \mathbf{K}_{bi} & \mathbf{K}_{bb} \end{bmatrix} \Psi_a = \begin{Bmatrix} \mathbf{0} \\ \mathbf{-I} \end{Bmatrix} . \tag{2.29}$$

The attachment modes Ψ_a are then defined as,

$$\Psi_a = \mathbf{K}^{-1}(\Omega) \begin{Bmatrix} \mathbf{0} \\ \mathbf{-I} \end{Bmatrix} . \tag{2.30}$$

Free interface reduced order basis

The free interface reduced order basis is obtained from the expression of the displacements with this method, thus,

$$\mathbf{u} = \mathbf{\Phi}\mathbf{q}_i + \Psi_a \boldsymbol{\mu} \, , \tag{2.31}$$

where $\boldsymbol{\mu}$ are the generalised displacements of the interface. The displacements of the interface are defined as,

$$\mathbf{u}_b = {}^a\mathbf{\Phi}\mathbf{q}_i + {}^a\Psi_a \boldsymbol{\mu} \, , \tag{2.32}$$

where the upper-index ${}^a(\,)$ makes reference to the restriction to $(\,)$ in the interface boundary. Thus, identifying the value of $\boldsymbol{\mu}$ and introducing it into Eqn. (2.31) the displacements of the structure are defined as,

$$\begin{aligned} \mathbf{u} &= \mathbf{\Phi}\mathbf{q}_i + \Psi_a \, {}^a\Psi_a^{-1} \left(\mathbf{u}_b - {}^a\mathbf{\Phi}\mathbf{q}_i \right) \\ &= \left(\Phi - \Psi_a \, {}^a\Psi_a^{-1} \, {}^a\mathbf{\Phi} \right) \mathbf{q}_i + \Psi_a \, {}^a\Psi_a^{-1} \mathbf{u}_b \\ &= \mathbf{\Phi}'\mathbf{q}_i + \Psi'_a \mathbf{u}_b \, , \end{aligned} \tag{2.33}$$

where $\Psi'_a = \Psi_a \, {}^a\Psi_a^{-1}$ and $\mathbf{\Phi}' = \mathbf{\Phi} - \Psi'_a \, {}^a\mathbf{\Phi}$. Furthermore, the properties ${}^a\Psi'_a = \mathbf{I}$ and ${}^a\mathbf{\Phi}'_a = 0$ are fulfilled.

Then, the fixed interface reduced basis is defined as,

$$\mathbf{\Phi}_{free} = [\mathbf{\Phi}' \; \Psi'_a] = \begin{bmatrix} \mathbf{\Phi}'_i & \Psi'_{a_i} \\ \mathbf{0} & \mathbf{I} \end{bmatrix} , \tag{2.34}$$

which keeps a similar form compared to the reduced basis of the fixed interface methods, Eqn. (2.27).

2.2.5 Proper Generalised Decomposition (PGD)

The Proper Generalised Decomposition (PGD) [Ammar et al., 2007, Chinesta et al., 2010, Chinesta et al., 2011] is a reduced order technique assuming that the solution of a multiparametric problem can be expressed in terms of separate variables of the form,

$$\mathbf{u} \approx \mathbf{U}^N(x_1, x_2, \ldots, x_p) = \sum_{i=1}^{N} \mathbf{X}_1(\mathbf{x}_1)\mathbf{X}_2(\mathbf{x}_2)\ldots\mathbf{X}_p(\mathbf{x}_p) \ , \tag{2.35}$$

where the number of terms N and the functions $\mathbf{X}$ are a priori unknowns and obtained with a Greedy algorithm based in a fixed point procedure [Ammar et al., 2006]. The PGD is well adapted for multiparametric problems or for optimisation problems as the cost of evaluating one parameter dependant function is less expensive than the evaluation of multiparameter functions.

2.3 Projection based reduced order models

In this section, the *projection based* type of reduced order models are introduced. As shown in the previous section, the physical displacements of the FOM are approximated by the linear product between an approximation basis, $\mathbf{Q}_{app.}$, and the generalised displacements of the structure, $\mathbf{q}$. It is considered that the number of equations, r, to be solved in the reduced order model are considerably smaller than the number of degrees of freedom (equal to the number of equations) in the FOM, $r \ll n$. Then, introducing the latter approximation in Eqn. (1.88), the equation of motion is rewritten as follows,

$$\mathbf{M}\mathbf{Q}_{app.}\ddot{\mathbf{q}} + \mathbf{C}\mathbf{Q}_{app.}\dot{\mathbf{q}} + \mathbf{K}(\Omega)\mathbf{Q}_{app.}\mathbf{q} + \mathbf{g}_{nl}(\mathbf{Q}_{app.}\mathbf{q}) = \mathbf{f}_e(\mathrm{t}) + \mathbf{f}_c(\mathbf{Q}_{app.}\mathbf{q} + \mathbf{u}_s,\ \mathbf{Q}_{app.}\dot{\mathbf{q}}) \ . \tag{2.36}$$

However, in order to reduce the number of equations to be solved the latter expression is pre-multiplied by a projection basis, $\mathbf{Q}_{proj.}$, and the reduced order equation of motion is defined as,

$$\tilde{\mathbf{M}}\ \ddot{\mathbf{q}} + \tilde{\mathbf{C}}\ \dot{\mathbf{q}} + \tilde{\mathbf{K}}(\Omega)\mathbf{q} + \tilde{\mathbf{g}}_{nl}(\mathbf{q}) = \tilde{\mathbf{f}}_e(t) + \tilde{\mathbf{f}}_c(\mathbf{q}, \dot{\mathbf{q}}) \ , \tag{2.37}$$

where $\tilde{\mathbf{M}} = \mathbf{Q}_{proj.}^T\mathbf{M}\mathbf{Q}_{app.}$, $\tilde{\mathbf{C}} = \mathbf{Q}_{proj.}^T\mathbf{C}\mathbf{Q}_{app.}$, and $\tilde{\mathbf{K}}(\Omega) = \mathbf{Q}_{proj.}^T\mathbf{K}(\Omega)\mathbf{Q}_{app.}$ are the generalized mass, damping and stiffness matrices, $\tilde{\mathbf{f}}_e(t)$ is the generalized external force vector, $\tilde{\mathbf{g}}_{nl}(\mathbf{q})$ is the generalized purely nonlinear force vector and $\tilde{\mathbf{f}}_c(\mathbf{q}, \dot{\mathbf{q}})$ is the generalised contact forces vector. On the one hand, when the projection basis is the same as the approximation basis, $\mathbf{Q}_{proj.} = \mathbf{Q}_{app.}$, the projecting procedure is called a *Galerkin projection*. On the other hand, when both bases differ, $\mathbf{Q}_{proj.} \neq \mathbf{Q}_{app.}$, the projection takes the name of a *Petrov-Galerkin projection*. Hereinafter, the proposed reduced order models are obtained by a *Galerkin projection*.

2.3.1 Discussion on the choice of the reduced basis

The reduced order models (ROMs) constructed by projection on a reduced basis are widely developed in literature. These methods differentiate between an expensive "OFFline" stage where the reduced bases are computed and an efficient "ONline" stage where the problem is solved.

One of these methods whose "OFFline" stage is computationally efficient and is widely developed in commercial finite element codes is the basis formed by the Linear Normal Modes (LNM) of the structure. The latter basis is used in the following to build the geometrically nonlinear ROMs due to its computational simplicity and physical meaning. An optimised version of this basis is performed by intelligently choosing the modes that best fit the expected solution by means of the Modal Assurance Criteria (MAC), Eqn. (3.1). Moreover, the POD basis used in the MAC is also an adequate basis to represent the behaviour of the structure.

However, the latter techniques are inefficient to solve contact problems as none of the generalised coordinates represents a physical displacement. In order to develop ROMs that solve interface problems such as contact, the component mode synthesis techniques that provide appropriate reduced bases as some degrees of freedom (d.o.f.) of interest on the interface are kept in the generalised coordinates are used. Hereinafter, the Craig-Bampton fixed interface method is implemented due to its simplicity.

Thus, depending on the studied nonlinearity, one of the following reduced order bases is chosen: a) LNM, b) LNM+MAC (chapter 3), c) POD or d) Craig-Bampton.

2.4 Geometrical nonlinearities in the ROM

The reduced order models should be capable of representing the nonlinear behaviour of the structure. In this section, the effects induced by the large displacements (geometrical) nonlinearity are studied with a 1D Duffing oscillator study-case. Furthermore, the techniques to consider the latter nonlinearity into the reduced order model are presented. Then, a new technique based on the correction of the nonlinear forces with a POD forces basis is proposed to remove the limitations of the classical methods and to study the forced response of slender structures. The effects of the contact type nonlinearity and of a coupled geometrical/contact nonlinearities are then studied with a modified Duffing oscillator.

2.4.1 Geometrically nonlinear effect

When a structure is submitted to large displacements, it is vital to characterise its geometrically nonlinear behaviour to ensure a reduced probability of failure under external excitations.

For *linear structures*, the forced response is unique for each excitation magnitude, F_e, and frequency, ω_e. Thus, the maximum displacements are expected at *resonance* with the modes of the structure (when the excitation frequency matches the natural frequency, $\omega_e = \boldsymbol{\omega}_i$). The resonant frequencies correspond to the frequencies computed from the eigenvalue problem of the Linear Normal Modes (LNM), Eqn. (2.5). Thus, the design of these structures is defined such that the stress constraints are fulfilled for the most critical displacement state induced by vibration. In turbomachinery, these critical vibration states are obtained by the intersection of the engine order lines and the natural frequencies function of the rotating velocity of the structure. The identification of these critical frequencies is performed with the Campbell diagram as shown in Fig. 3.

For *geometrically nonlinear* structures, in the neighbourhood of the nonlinear resonance state, the forced response is not unique for a given excitation magnitude and frequency as the solution depends also on the initial state of the structure. As shown in Fig. 2.2a, the resonant frequency varies with the value of the normalised nonlinear stiffness, $\overline{\gamma}$. Furthermore, for some excitation frequencies multiple responses are observed, two stable (solid line) and one unstable (dashed line). The response tends to one or the other stable configuration depending on its initial state. Figure 2.2b represent the forced response of the structure when the damping ratio is varied keeping constant the value of the nonlinear stiffness and the value of the applied force. For linear structures, when the value of the normalised damping ratio $\overline{\xi}$ changes, the amplitude of the response is modified in a direct relation and the resonant frequency remains constant. However, for nonlinear structures, not only the value of the response's magnitude is modified but also the value of the resonant frequency (frequency where the maximum displacements are observed).

The nonlinear forced response is obtained with *continuation techniques*. The classical *sequential continuation* consists in introducing the last computed solution as the initial conditions to the next frequency computation. By implementing this method, the solution is only capable of reproducing the stable solutions. To compute the stable branches a double scan procedure is performed varying the excitation frequency (scanning from low to high frequencies and then from high to low frequencies). The last technique leads to the arrow path shown in Fig. 2.2c. The unstable solution is computed by the arc-length continuation technique [Abbott, 1978, Chan and Keller, 1982].

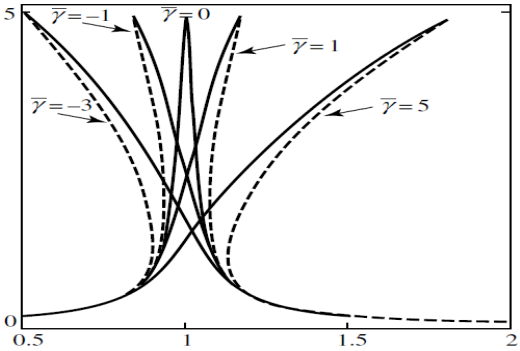

(a) Effect of varying the nonlinear stiffness with constant excitation magnitude and viscous damping ratio.

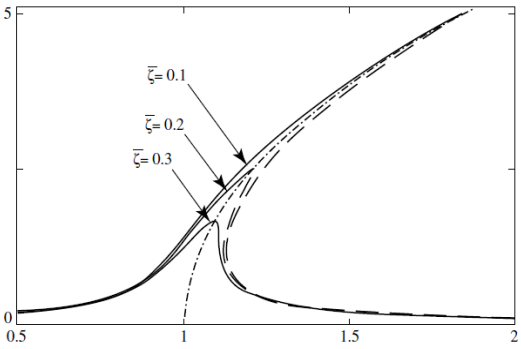

(b) Effect of varying the viscous damping ratio with a constant excitation magnitude and nonlinear stiffness.

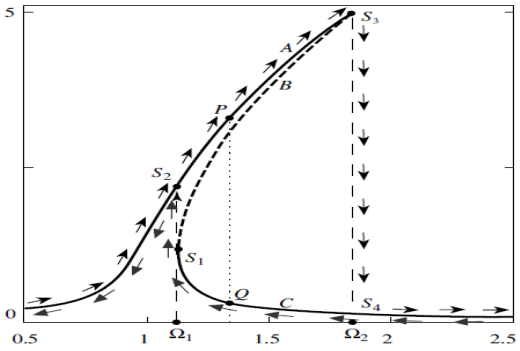

(c) Nonlinear forced response with a representation of the hysteresis loop.

Figure 2.2: Geometrically nonlinear effect on the forced response of the structure [Kalmár-Nagy and Balachandran, 2011].

Duffing oscillator

To study the coupled influence between the geometrical nonlinearity and the friction contact nonlinearity, a modified 1D Duffing oscillator is studied in the following, Figure 2.3. In this section, the contact effects are negligible, $f_c(u, \dot{u}) = 0$, while the coupled nonlinear response is studied in section 2.5.

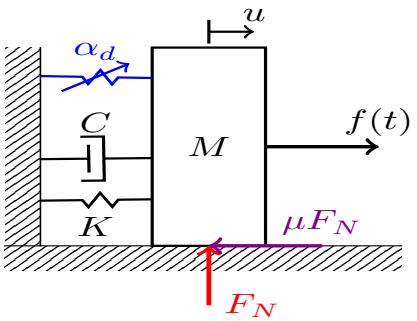

Figure 2.3: Scheme of a nonlinear oscillator.

The Duffing oscillator and the effects of bifurcation are widely studied in literature [Kovacic and Brennan, 2011, Nayfeh and Sanchez, 1989, Brennan et al., 2008]. The Duffing oscillator has a third order nonlinear behaviour represented by the nonlinear force, $g_{nl}(u) = \alpha_D u^3$, where α_D represents the nonlinear stiffness coefficient. The equation of motion of the latter oscillator is classically modified to depend on three normalised parameters, however, in order to maintain the form of the Eqn. (1.88) and (2.37), the equation of motion of the Duffing oscillator is defined as,

$$M\ddot{u} + C\dot{u} + K\,u + \alpha_D\,u^3 = f(t) + f_c(u, \dot{u})\ . \tag{2.38}$$

The following values are considered in the numerical application: mass M is 0.3 Kg, the viscous damping C is 0.605 Nsm^{-1}, the linear rigidity of the oscillator is $K = 12.19$ kNm^{-1} and the external excitation, $f_e = f_{max}\cos(\omega t)$, magnitude is $f_{max} = 50$ N.

Figure 2.4 represents the forced response curve (displacements of the structure with respect to the excitation frequency). In order to ensure that the periodic regime is reached, the final time is equal to 500 excitation periods. The resonant frequency of the linear case, $\alpha_D = 0$ corresponds to the natural frequency of the structure $\omega_1 = \frac{1}{2\pi}\sqrt{K/M} = 32.08$ Hz. The influence of the geometrical nonlinearity is studied by a variation of the nonlinear stiffness coefficient between a value of 10^4 Nm^{-3} and 10^7 Nm^{-3}. For each value of α_D a sequential continuation is performed from $\omega_e = 25$ Hz to $\omega_e = 70$ Hz by introducing as initial conditions the previously computed state. The reverse frequency scanning is not performed.

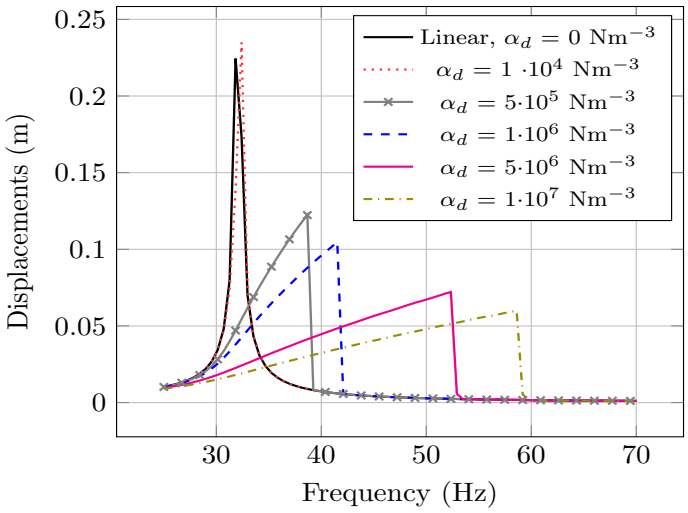

Figure 2.4: Forced response of the geometrically nonlinear Duffing oscillator for different nonlinear stiffness coefficient values, α_D.

The observed behaviour is similar to the one in Fig. 2.2a. When the value

of the nonlinear stiffness is increased the resonant frequency tends to higher values and the maximum amplitude of the response is reduced. However, even if the peak value of the nonlinear response is smaller than the linear case, the frequency range where the response is important is considerably larger than for the linear response. Thus, for design purposes, the nonlinear behaviour of the structure should be taken into consideration in order to avoid unexpected displacement in the neighbourhood of the nonlinear resonance and not to oversize the structure which would imply an increment of weight and prize.

2.4.2 Evaluation of the generalised nonlinear forces

In order to study the geometrically nonlinear effect into the reduced order model, the generalised nonlinear forces are evaluated with different techniques: the *inflation method* (classical) method which is implementable by using commercial finite element codes where for every nonlinear force evaluation, the nonlinear forces are computed in the FOM and then projected to obtain the generalised forces of the ROM. This method produces computationally inefficient ROMs that depend on the size of the FOM. The POD/DEIM method [Barrault et al., 2004, Chaturantabut and Sorensen, 2010] uses a second basis for the nonlinear term. Then the nonlinear forces are evaluated by the FOM but only at DEIM interpolation points and the nonlinear term is approximated through collocation in the nonlinear POD basis. The hyper-reduction [Ryckelynck, 2005] technique is adapted to problems involving internal variables. The constitutive equations are solved in a reduced domain and the internal variables are extrapolated by using POD vectors related to the internal variables similarly to the DEIM.

In order to avoid carrying out FOM computations within the "ONline" stage, hereinafter, the *STiffness Evaluation Procedure (STEP)* that approximates the nonlinear forces as a third degree polynomial is used. Furthermore, to improve the solution of the nonlinear forces projection, a new *POD based correction* is proposed. The latter correction is adapted for all the studied bases.

In the techniques presented hereunder, the reduced basis is defined as $\mathbf{\Phi}$ which traditionally represent the LNM of the structure. However, the methods presented in the following are valid for any reduced basis, $\mathbf{Q}$. Moreover, as traditionally the reduced order basis is denoted by $\mathbf{\Phi}$, this notation is kept to represent the reduced order basis, thus, $\mathbf{Q} \Leftrightarrow \mathbf{\Phi}$.

Inflation method

The computation of the generalized nonlinear forces by the inflation method consists in the evaluation of the purely nonlinear force $\mathbf{g}_{nl}$ in the FOM and

projecting the solution into the ROM,

$$\tilde{\mathbf{g}}_{nl}(\mathbf{q}) = \mathbf{\Phi}^T \mathbf{g}_{nl}(\mathbf{\Phi q}) = \mathbf{\Phi}^T \mathbf{g}(\mathbf{u}_s + \mathbf{\Phi q}) - \mathbf{\Phi}^T \mathbf{g}(\mathbf{u}_s) - \tilde{\mathbf{K}}_s \mathbf{q} \,, \tag{2.39}$$

where $\tilde{\mathbf{K}}_s = \Phi^T \mathbf{K}_s \Phi$.

Thus, for each computation of the generalised forces inside the solution algorithm, first, the FOM displacements, $\mathbf{u}(t_i)$, are obtained from the generalised coordinates, $\mathbf{q}(t_i)$, by means of Eqn. (2.1). Second, a FOM nonlinear static computation is carried out with a finite element software to compute the nonlinear, $\mathbf{g}(\mathbf{u}_s + \mathbf{\Phi q})$, forces in the FOM and the FOM purely nonlinear forces are evaluated, $\mathbf{g}_{nl}(\mathrm{u}) = \mathbf{g}_{nl}(\mathbf{\Phi q})$. Finally, the latter forces are projected through a Galerking projection, $\mathbf{\Phi}^T$.

This method is simple to implement, however, as the computation of the nonlinear forces is performed in the FOM, the ROM directly depends on the size of the FOM. Thus, the ROM of Eqn. (2.37) is not autonomous and the computational cost remains significant due to the evaluation of the nonlinear forces.

STiffness Evaluation Procedure (STEP)

In order to build an autonomous ROM fully independent of the FOM the STiffness Evaluation Procedure (STEP) [Rizzi and Muravyov, 2001, Muravyov and Rizzi, 2003] develops a polynomial approximation to compute the generalised nonlinear forces, $\tilde{\mathbf{g}}_{nl}(\mathbf{q})$, as a function of the generalised displacements, $\mathbf{q}$. An extension to evaluate the nonlinear forces of structures under rotation is presented in the following.

Each component p (with $p = 1, \ldots, r$) of the generalized purely nonlinear forces vector, $\tilde{\mathbf{g}}_{nl}(\mathbf{q})$, is expressed as a polynomial approximation of third degree in terms of the r number of variables that form the generalized coordinates $\mathbf{q} = [q_1, \ldots, q_r]$,

$$\begin{aligned} \tilde{g}^p_{nl}(q_1, \ldots, q_r) &= \tilde{g}^p_{nl_{Quad.}} + \tilde{g}^p_{nl_{Cub.}} \\ &= \sum_{i=1}^{r} \sum_{j=i}^{r} A^p_{ij} q_i q_j + \sum_{i=1}^{r} \sum_{j=i}^{r} \sum_{m=j}^{r} B^p_{ijm} q_i q_j q_m \,. \end{aligned} \tag{2.40}$$

Once the A^p_{ij} and B^p_{ijm} stiffness coefficients are calculated, the generalized purely nonlinear forces $\tilde{\mathbf{g}}_{nl}(\mathbf{q})$ are directly obtained by Eqn. (2.40). The ROM is independent of the FOM and the computational cost is considerably improved.

Computation of the polynomial coefficients

The polynomial coefficients A^p_{ij} and B^p_{ijm} are obtained by identification using a finite element software (i.e. NASTRAN, ABAQUS, Code_Aster, Z-

Set,...) to compute the nonlinear forces $\mathbf{g}(\mathbf{u}_s + \mathbf{u})$ associated to a given number of imposed displacements, $\mathbf{u}_s + \mathbf{u}$. Then, the purely nonlinear part is identified from Eqn. (1.86),

$$\mathbf{g}_{nl}(\mathbf{u}) = \mathbf{g}(\mathbf{u}_s + \mathbf{u}) - \mathbf{g}(\mathbf{u}_s) - \mathbf{K}_s\mathbf{u} \,, \tag{2.41}$$

In the following, the latter procedure is used to evaluate the purely nonlinear forces, however, some finite element codes restrict the access to the system matrices, thus, to avoid this problem the purely nonlinear forces, $\mathbf{g}_{nl}$, are evaluated with an alternative method. The latter forces are computed by means of the stiffness matrix, $\mathbf{K}(\Omega)$, which is used in the computation of the LNM. To this aim, the displacements $\mathbf{u}_s$ and $\mathbf{u}_s$+$\mathbf{u}$ are imposed to the structure and the static reactions $\mathbf{r}(\mathrm{u}_s)$ and $\mathbf{r}(\mathbf{u}_s$+$\mathbf{u})$ are extracted as,

$$\mathbf{K}_c(\Omega)\mathbf{u}_s + \mathbf{g}(\mathbf{u}_s) = \mathbf{r}(\mathbf{u}_s) \,, \tag{2.42}$$

$$\mathbf{K}_c(\Omega)\,(\mathbf{u}_s + \mathbf{u}) + \mathbf{g}(\mathbf{u}_s + \mathbf{u}) = \mathbf{r}(\mathbf{u}_s + \mathbf{u}) \,. \tag{2.43}$$

Thus, from Eqn. (2.42), (2.43) and (2.41) the alternative expression to obtain the purely nonlinear force is defined as follows,

$$\mathbf{g}_{nl}(\mathbf{u}) = \mathbf{r}(\mathbf{u}_s + \mathbf{u}) - \mathbf{r}(\mathbf{u}_s) - \mathbf{K}(\Omega)\mathbf{u} \,. \tag{2.44}$$

Then, its projection with respect to the p-th mode $\mathbf{\Phi}_p$ is,

$$\tilde{g}^p_{nl}(\mathbf{u}) = \mathbf{\Phi}_p^T \mathbf{g}_{nl}(\mathbf{u}) \,, \tag{2.45}$$

equivalent to Eqn. (2.39).

The imposed displacements vectors, $\mathbf{u}$, used to obtain the polynomial coefficients are a linear combination of one, two and three modes under the form of $\mathbf{u}_1$ to $\mathbf{u}_6$ as defined hereafter.

a) Combination of one mode

For $i = 1, \ldots, r$, the nonlinear forces induced by the following vectors are calculated,

$$\mathbf{u}_1 = \mathbf{\Phi}_i q_i \,, \tag{2.46}$$

$$\mathbf{u}_2 = -\mathbf{\Phi}_i q_i \,, \tag{2.47}$$

with the same value of q_i in $\mathbf{u}_1$ and $\mathbf{u}_2$. This leads to consider that just the i-th component of the generalized coordinates vector, $\mathbf{q}$, is different from zero and equal to q_i for $\mathbf{u}_1$ and equal to $-q_i$ for $\mathbf{u}_2$.

Then, the Eqn. (2.40) evaluated for $\mathbf{u}_1$ and $\mathbf{u}_2$ takes the form,

$$\tilde{g}^p_{nl}(\mathbf{u}_1) = A^p_{ii} q_i^2 + B_{iii} q_i^3 \,, \tag{2.48}$$

$$\tilde{g}^p_{nl}(\mathbf{u}_2) = A^p_{ii} q_i^2 - B_{iii} q_i^3 \,. \tag{2.49}$$

For every fixed p and i, Eqn. (2.48) and (2.49) form a linear system of two equations with the unknowns A^p_{ii} and B_{iii}. Then, it is deduced that,

$$A^p_{ii} = \frac{1}{2q_i^2}\left[\tilde{g}^p_{nl}(\mathbf{u}_1) + \tilde{g}^p_{nl}(\mathbf{u}_2)\right] , \tag{2.50}$$

$$B^p_{iii} = \frac{1}{2q_i^3}\left[\tilde{g}^p_{nl}(\mathbf{u}_1) - \tilde{g}^p_{nl}(\mathbf{u}_2)\right] . \tag{2.51}$$

The computation of coefficients A^p_{ii} and B^p_{iii} for $p = 1, \ldots, r$ needs $2r$ static computations of the nonlinear forces $\mathbf{g}_{nl}(\mathbf{u}_1)$ and $\mathbf{g}_{nl}(\mathbf{u}_2)$.

b) Combination of two modes

For $i = 1, \ldots, r$ and $j = 1, \ldots, r$ with $i < j$, the nonlinear forces are computed for the following displacements,

$$\mathbf{u}_3 = \mathbf{\Phi}_i q_i + \mathbf{\Phi}_j q_j , \tag{2.52}$$

$$\mathbf{u}_4 = -\mathbf{\Phi}_i q_i - \mathbf{\Phi}_j q_j , \tag{2.53}$$

$$\mathbf{u}_5 = \mathbf{\Phi}_i q_i - \mathbf{\Phi}_j q_j , \tag{2.54}$$

where q_i and q_j are the same for $\mathbf{u}_3$, $\mathbf{u}_4$ and $\mathbf{u}_5$. Thus, $\mathbf{q} = [0, \ldots, q_i, \ldots, q_j, \ldots, 0]^T$ for $\mathbf{u}_3$, $\mathbf{q} = [0, \ldots, -q_i, \ldots, -q_j, \ldots, 0]^T$ for $\mathbf{u}_4$ and $\mathbf{q} = [0, \ldots, q_i, \ldots, -q_j, \ldots, 0]^T$ for $\mathbf{u}_5$. Then, from the Eqn. (2.40) the expression of the purely nonlinear forces becomes,

$$\begin{aligned}\tilde{g}^p_{nl}(\mathbf{u}_3) = {} & A^p_{ii}q_i^2 + A^p_{ij}q_iq_j + A^p_{jj}q_j^2 \\ & + B^p_{iii}q_i^3 + B^p_{iij}q_i^2q_j + B^p_{ijj}q_iq_j^2 + B^p_{jjj}q_j^3 ,\end{aligned} \tag{2.55}$$

$$\begin{aligned}\tilde{g}^p_{nl}(\mathbf{u}_4) = {} & A^p_{ii}q_i^2 + A^p_{ij}q_iq_j + A^p_{jj}q_j^2 \\ & - B^p_{iii}q_i^3 - B^p_{iij}q_i^2q_j - B^p_{ijj}q_iq_j^2 - B^p_{jjj}q_j^3 ,\end{aligned} \tag{2.56}$$

$$\begin{aligned}\tilde{g}^p_{nl}(\mathbf{u}_5) = {} & A^p_{ii}q_i^2 - A^p_{ij}q_iq_j + A^p_{jj}q_j^2 \\ & + B^p_{iii}q_i^3 - B^p_{iij}q_i^2q_j + B^p_{ijj}q_iq_j^2 - B^p_{jjj}q_j^3 .\end{aligned} \tag{2.57}$$

For each p and for each fixed couple (i, j), A^p_{ii}, A^p_{jj}, B_{iii} and B_{jjj} are previously defined by the Eqn. (2.50) and (2.51). Then, the unknowns A^p_{ij}, B^p_{ijj} and B^p_{iij} are obtained from the Eqn. system formed by Eqn. (2.55) to (2.57),

$$A^p_{ij} = \frac{1}{2q_iq_j}\left[\tilde{g}^p_{nl}(\mathbf{u}_3) + \tilde{g}^p_{nl}(\mathbf{u}_4) - 2A^p_{ii}q_i^2 - 2A^p_{jj}q_j^2\right] , \tag{2.58}$$

$$B^p_{ijj} = \frac{1}{2q_iq_j^2}\left[\tilde{g}^p_{nl}(\mathbf{u}_3) + \tilde{g}^p_{nl}(\mathbf{u}_5) - 2A^p_{ii}q_i^2 - 2A^p_{jj}q_j^2 - 2B^p_{iii}q_i^3\right] , \tag{2.59}$$

$$B^p_{iij} = \frac{1}{2q_i^2q_j}\left[-\tilde{g}^p_{nl}(\mathbf{u}_4) - \tilde{g}^p_{nl}(\mathbf{u}_5) + 2A^p_{ii}q_i^2 + 2A^p_{jj}q_j^2 - 2B^p_{jjj}q_j^3\right] . \tag{2.60}$$

The polynomial coefficients A^p_{ij}, B^p_{ijj} and B^p_{iij}, for $i = 1, \ldots, r$ and $j = 1, \ldots, r$ with $i < j$ are obtained after $\frac{3}{2}r(r-1)$ static computations of the nonlinear forces $\mathbf{g}_{nl}(\mathbf{u}_3)$, $\mathbf{g}_{nl}(\mathbf{u}_4)$ and $\mathbf{g}_{nl}(\mathbf{u}_5)$.

c) Combination of three modes

For $i = 1, \ldots, r$, $j = 1, \ldots, r$ and $m = 1, \ldots, r$ with $i < j < m$ the purely nonlinear forces are obtained for the imposed displacements $\mathbf{u}_6$,

$$\mathbf{u}_6 = \Phi_i q_i + \Phi_j q_j + \Phi_m q_m \ , \tag{2.61}$$

where only the i-th, j-th and m-th elements of the generalized coordinates $\mathbf{q}$ are different from zero, $\mathbf{q} = [0, \ldots, q_i, \ldots, q_j, \ldots, q_m, \ldots, 0]^T$. Then, from the Eqn. (2.40) the expression of the purely nonlinear forces is,

$$\begin{aligned} \tilde{g}^p_{nl}(\mathbf{u}_6) = \ & A^p_{ii} q_i^2 + A^p_{ij} q_i q_j + A^p_{im} q_i q_m + A^p_{jj} q_j^2 + A^p_{jm} q_j q_m + A^p_{mm} q_m^2 \\ & + B^p_{iii} q_i^3 + B^p_{iij} q_i^2 q_j + B^p_{iim} q_i^2 q_m + B^p_{ijj} q_i q_j^2 + B^p_{ijm} q_i q_j q_m \\ & + B^p_{imm} q_i q_m^2 + B^p_{jjj} q_j^3 + B^p_{jjm} q_j^2 q_m + B^p_{jmm} q_j q_m^2 + B^p_{mmm} q_m^3 \ . \end{aligned} \tag{2.62}$$

For every fixed p, the Eqn. (2.62) has a single unknown B^p_{ijm}, then,

$$\begin{aligned} B^p_{ijm} = \frac{1}{q_i q_j q_m} \big[& \tilde{g}^p_{nl}(\mathbf{u}_6) - A^p_{ii} q_i^2 - A^p_{ij} q_i q_j - A^p_{im} q_i q_m - A^p_{jj} q_j^2 \\ & - A^p_{jm} q_j q_m - A^p_{mm} q_m^2 - B^p_{iii} q_i^3 - B^p_{iij} q_i^2 q_j - B^p_{iim} q_i^2 q_m \\ & - B^p_{ijj} q_i q_j^2 - B^p_{imm} q_i q_m^2 - B^p_{jjj} q_j^3 - B^p_{jjm} q_j^2 q_m \\ & - B^p_{jmm} q_j q_m^2 - B^p_{mmm} q_m^3 \big] \ . \end{aligned} \tag{2.63}$$

To obtain the B^p_{ijm} polynomial coefficients for $i = 1, \ldots, r$, $j = 1, \ldots, r$ and $m = 1, \ldots, r$ with $i < j < k$, the number of static computations of the nonlinear force $\mathbf{g}_{nl}(\mathbf{u}_6)$ that are needed is $\binom{r}{3} = \frac{1}{6} r(r-1)(r-2)$.

Then, the number of nonlinear static FOM simulations (computational cost) that are necessary to obtain all the polynomial coefficients of the STEP is,

$$2r + \frac{3}{2} r(r-1) + \frac{1}{6} r(r-1)(r-2) = \frac{1}{6}(r^3 + 6r^2 + 5r) \ . \tag{2.64}$$

2.4.3 Derivatives of the nonlinear forces

In order to build the Jacobian matrix to solve the time response of the equations of motion regardless the system is FOM or ROM, the gradient of the nonlinear forces with respect to the displacements or with respect to the generalized coordinates needs to be evaluated.

The gradient of the nonlinear forces $\mathbf{g}(\mathbf{u}_p)$ for the FOM, Eqn. (1.74), in relation to the physical displacements $\mathbf{u}_p$ is obtained from the Eqn. (1.78), (1.81) and (1.82),

$$\frac{\partial \mathbf{g}}{\partial \mathbf{u}_p}(\mathbf{u}_p) = \mathbf{K}_t(\mathbf{u}_p) = \mathbf{K}_e + \mathbf{K}_{nl}(\mathbf{u}_p) = \mathbf{K}_e + \mathbf{K}_g(\mathbf{u}_p) + \ldots \ . \tag{2.65}$$

The dynamics of the rotating structure is observed from the static equilibrium state, thus for the FOM the gradient depends on the relative displacements $\mathbf{u}$. From equation (1.86) the derivative matrix of the purely nonlinear forces $\mathbf{g}_{nl}(\mathbf{u})$ with respect to the relative displacements is expressed as follows,

$$\frac{\partial \mathbf{g}_{nl}}{\partial \mathbf{u}}(\mathbf{u}) = \frac{\partial \mathbf{g}(\mathbf{u}_s + \mathbf{u})}{\partial \mathbf{u}}(\mathbf{u}) - \mathbf{K}_s \ , \tag{2.66}$$

considering $\mathbf{u}_p = \mathbf{u}_s + \mathbf{u}$,

$$\begin{aligned} \frac{\partial \mathbf{g}(\mathbf{u}_s + \mathbf{u})}{\partial \mathbf{u}}(\mathbf{u}) &= \frac{\partial \mathbf{g}}{\partial \mathbf{u}_p}(\mathbf{u}_s + \mathbf{u}) \frac{\partial \mathbf{u}_p}{\partial \mathbf{u}}(\mathbf{u}) = \frac{\partial \mathbf{g}}{\partial \mathbf{u}_p}(\mathbf{u}_s + \mathbf{u}) \\ &= \mathbf{K}_t(\mathbf{u}_s + \mathbf{u}) = \mathbf{K}_e + \mathbf{K}_{nl}(\mathbf{u}_s + \mathbf{u}) \ , \end{aligned} \tag{2.67}$$

thus,

$$\frac{\partial \mathbf{g}_{nl}}{\partial \mathbf{u}}(\mathbf{u}) = \mathbf{K}_t(\mathbf{u}_s + \mathbf{u}) - \mathbf{K}_s = \mathbf{K}_{nl}(\mathbf{u}_s + \mathbf{u}) - \mathbf{K}_{nl}(\mathbf{u}_s) \ . \tag{2.68}$$

Then, using the definition of matrix $\mathbf{K}(\Omega)$ from Eqn. (1.87), the derivative of the nonlinear forces matrix with respect to the relative displacements is obtained from Eqn. (1.88),

$$\begin{aligned} \frac{\partial \left(\mathbf{K}\mathbf{u} + \mathbf{g}_{nl}\right)}{\partial \mathbf{u}} &= \mathbf{K}_c(\Omega) + \mathbf{K}_t(\mathbf{u}_s + \mathbf{u}) \\ &= \mathbf{K}_c(\Omega) + \mathbf{K}_e + \mathbf{K}_{nl}(\mathbf{u}_s + \mathbf{u}) \\ &= \mathbf{K}_c(\Omega) + \mathbf{K}_e + \mathbf{K}_g(\mathbf{u}_s + \mathbf{u}) + \dots \ . \end{aligned} \tag{2.69}$$

The derivative matrix of the ROM's generalised nonlinear forces, $\tilde{\mathbf{g}}_{nl}(\mathbf{u})$ is obtained by the projection of the FOM derivative matrix by means of the inflation formulation or by the STEP polynomial approximation.

Derivatives of the nonlinear forces with the inflation method

The derivative matrix of the generalized purely nonlinear forces $\tilde{\mathbf{g}}_{nl}$ with respect to the generalized coordinates $\mathbf{q}$ is obtained by the relation given in Eqn. (2.1) and the inflation formulation in Eqn. (2.39),

$$\begin{aligned} \frac{\partial \tilde{\mathbf{g}}_{nl}}{\partial \mathbf{q}}(\mathbf{q}) &= \mathbf{\Phi}^T \frac{\partial \mathbf{g}_{nl}(\mathbf{\Phi}\mathbf{q})}{\partial \mathbf{q}}(\mathbf{q}) = \mathbf{\Phi}^T \frac{\partial \mathbf{g}_{nl}}{\partial \mathbf{u}}(\mathbf{\Phi}\mathbf{q}) \frac{\partial \mathbf{u}}{\partial \mathbf{q}}(\mathbf{q}) \\ &= \mathbf{\Phi}^T \frac{\partial \mathbf{g}_{nl}}{\partial \mathbf{u}}(\mathbf{\Phi}\mathbf{q}) \, \mathbf{\Phi} \ . \end{aligned} \tag{2.70}$$

Then, the inflation formulation to obtain the derivative matrix of the generalised nonlinear forces is defined as follows,

$$\begin{aligned} \frac{\partial \left(\tilde{\mathbf{K}}\mathbf{q} + \tilde{\mathbf{g}}_{nl}\right)}{\partial \mathbf{q}}(\mathbf{q}) &= \mathbf{\Phi}^T \left[\frac{\partial \left(\mathbf{K}\mathbf{u} + \mathbf{g}_{nl}\right)}{\partial \mathbf{u}}(\mathbf{\Phi}\mathbf{q})\right] \mathbf{\Phi} \\ &= \tilde{\mathbf{K}}_c(\Omega) + \tilde{\mathbf{K}}_t(\mathbf{u}_s + \mathbf{\Phi}\mathbf{q}) \\ &= \tilde{\mathbf{K}}_c(\Omega) + \tilde{\mathbf{K}}_e + \tilde{\mathbf{K}}_{nl}(\mathbf{u}_s + \mathbf{\Phi}\mathbf{q}) \\ &= \tilde{\mathbf{K}}_c(\Omega) + \tilde{\mathbf{K}}_e + \tilde{\mathbf{K}}_g(\mathbf{u}_s + \mathbf{\Phi}\mathbf{q}) + \dots \ , \end{aligned} \tag{2.71}$$

where $\tilde{\mathbf{K}}_c = \mathbf{\Phi}^T \mathbf{K}_c \mathbf{\Phi}$, $\tilde{\mathbf{K}}_t = \mathbf{\Phi}^T \mathbf{K}_t \mathbf{\Phi}$, $\tilde{\mathbf{K}}_e = \mathbf{\Phi}^T \mathbf{K}_e \mathbf{\Phi}$, $\tilde{\mathbf{K}}_{nl} = \mathbf{\Phi}^T \mathbf{K}_{nl} \mathbf{\Phi}$ and $\tilde{\mathbf{K}}_g = \mathbf{\Phi}^T \mathbf{K}_g \mathbf{\Phi}$.

Derivatives of the nonlinear forces with the STEP method

The derivative matrix of the generalised nonlinear forces computed by the STEP method is defined as,

$$\frac{\partial \left(\tilde{\mathbf{K}}\mathbf{q} + \tilde{\mathbf{g}}_{nl} \right)}{\partial \mathbf{q}} (\mathbf{q}) = \tilde{\mathbf{K}} \ + \left[\frac{\partial \tilde{\mathbf{g}}_{nl}}{\partial \mathbf{q}} \right] (\mathbf{q}) \ . \tag{2.72}$$

The derivative matrix of the generalized purely nonlinear forces $\tilde{\mathbf{g}}_{nl}$ with respect to the generalized coordinates $\mathbf{q}$ is obtained by derivating the polynomial expression of equation (2.40). Thus, for $p = 1, \ldots, r$ and $l = 1, \ldots, r$,

$$\begin{aligned} \left[\frac{\partial \tilde{\mathbf{g}}_{nl}}{\partial \mathbf{q}} \right]_{(p,l)} &= \frac{\partial \tilde{g}^p_{nl}}{\partial q_l} (q_1, ..., q_r) \\ &= \sum_{i=1}^{r} \sum_{j=i}^{r} A^p_{ij} \left(\delta_{il} q_j + q_i \delta_{jl} \right) \\ &+ \sum_{i=1}^{r} \sum_{j=i}^{r} \sum_{m=j}^{r} B^p_{ijm} \left(\delta_{il} q_j q_m + q_i \delta_{jl} q_m + q_i q_j \delta_{ml} \right) \ , \end{aligned} \tag{2.73}$$

where δ_{ij} is the Kronecker delta which is defined as,

$$\delta_{ij} \begin{cases} = 1 & \text{if } i = j \\ = 0 & \text{if } i \neq j \end{cases} \ . \tag{2.74}$$

2.4.4 Correction of the geometrical nonlinear forces

The use of inflation and the STEP methods for slender structures

The bases that are considered are not a priori capable of representing the nonlinear displacements of a slender structure such as cantilever beams or turbine blades with a reduced number of modes (i.e. for aeroelastic coupling). The nonlinear forces of the structure are not well represented in the reduced space, the displacement responses amplitudes are significantly reduced and, for some cases, the response exhibits spurious oscillations (high harmonic components) as shown in [Grolet and Thouverez, 2010, Andersen and Poulsen, 2014]. Furthermore, the STEP method is not adapted for applications with slender structures such as cantilever beams [Rizzi and Muravyov, 2001]. However, the simplicity of the studied bases and the time performances of the STEP combined together, provide a ROM that is simple to construct using any commercial finite element software. Some authors solve this problem by taking into consideration the second derivative terms of the LNM, Eqn. (2.6), $\frac{\partial \mathbf{\Phi}_i}{\partial q_i}$

[Grolet and Thouverez, 2010, Martin and Thouverez, 2019]. The dual modes [Mignolet et al., 2013, Radu et al., 2004, Capiez-Lernout et al., 2012] improve the representativity of the reduced base performing static nonlinear computations and extracting the purely nonlinear displacements vector. The latter is used to enhance the reduced basis. These methods, have been validated for beam type finite elements, however, if twist or geometrical complexities of these structures need to be considered, 3D finite elements are needed. Other promising reduced order techniques to study geometrically nonlinear structures are the Nonlinear Normal Modes (NNM) [Rosenberg, 1962, Shaw and Pierre, 1992, Jezequel and Lamarque, 1991, Touzé and Amabili, 2006]. These techniques are still in development for complex structures with many degrees of freedom. Reduction techniques like hyper-reduction [Ryckelynck, 2005] or Discrete Empirical Interpolation Method (DEIM) [Chaturantabut and Sorensen, 2010] provide accurate results to asses the nonlinear forces in the reduced space by means of a previously computed force basis, $\mathbf{\Phi}_f$, and the assessment of the FOM nonlinear forces on a small set of chosen nodes of the structure. However, these techniques do not provide a fully autonomous ROMs as for each time step the nonlinear forces are re-evaluated at some chosen nodes of the FOM.

POD based correction for nonlinear forces

To improve the accuracy of the response and to avoid the amplitude reduction, before projecting the nonlinear forces of the FOM on the reduced basis, the latter forces are approximated by means of a nonlinear forces POD basis, $\mathbf{\Phi}_f$, computed previously.

The concept of the proposed method is to *to filter the nonlinear force to restrict them to a more representative subpace inferred from the FOM nonlinear forces.*

The proposed correction is valid both for STEP and inflation methods as the correction is performed before the projection of the nonlinear forces. This procedure is divided in two phases: a) an OFFline phase where the nonlinear forces basis is constructed and b) an ONline phase where the nonlinear forces are computed. The ONline phase as presented hereunder corresponds to the correction of the inflation method presented previously. The correction for the STEP is carried out during the stiffness coefficient identification in the OFFline phase. Hereinafter, the ROMs associated to a correction of nonlinear forces are respectively referred to as InflationC ROM or StepC ROM (C representing the Correction, i.e. STEP with Correction $\equiv$ StepC).

OFFline phase: Construction of the nonlinear forces basis, $\mathbf{\Phi}_f$

The nonlinear basis that is used to approximate the FOM nonlinear forces, $\mathbf{\Phi}_f$, is computed by means of a POD procedure whose basis is computed by a SVD. As shown in Eqn. (2.75), the nonlinear forces are collected for a given number of snapshots that represent a set of characteristic displacements in the response. Then, for each snapshot the associated nonlinear forces are evaluated,

$$\mathbf{A} = [\mathbf{g}_{nl}(\mathbf{u}_1), \cdots, \mathbf{g}_{nl}(\mathbf{u}_m)] \ . \tag{2.75}$$

The set of snapshots can be obtained from experimental data or by other means (i.e. a set of nonlinear forces related to a displacement space formed by a linear combination of modes...).

Then, a truncated Singular Value Decomposition (SVD) [Hansen, 1990] is implemented as in Eqn. (2.16) and the *nonlinear forces basis* is formed by a truncation or by explicitly choosing a number, r_f, of nonlinear basis vectors,

$$\mathbf{A} = \mathbf{U}\Sigma\mathbf{V}^T \approx \mathbf{U}_{r_f}\Sigma_{r_f}\mathbf{V}_{r_f}^T \ . \tag{2.76}$$

The nonlinear basis consists in the truncation to r_f modes in the resulting left singular vectors of the SVD basis, $\mathbf{\Phi}_f = \mathbf{U}_{r_f}$ verifying $\mathbf{\Phi}_f^T\mathbf{\Phi}_f = \mathbf{I}$.

ONline phase (Inflation): Computing the nonlinear forces

Once the nonlinear forces basis is constructed, as defined in Eqn. (2.77), the nonlinear forces in the FOM are approximated as a linear combination between the nonlinear forces basis and the approximated force coordinates (similar to the concept of basis reduction, Eqn. (2.1)).

$$\mathbf{g}_{nl}(\mathbf{u}) \approx \mathbf{\Phi}_f\mathbf{q}_{nl}^f = \mathbf{g}_{nl}^f(\mathbf{u}) \, , \tag{2.77}$$

where the force coordinates are computed by a least-squares approach. The approximation of the FOM nonlinear forces in the FOM space is computed by,

$$\mathbf{g}_{nl}^f(\mathbf{u}) = \mathbf{\Phi}_f \left(\mathbf{\Phi}_f^T\mathbf{\Phi}_f\right)^{-1}\mathbf{\Phi}_f^T\mathbf{g}_{nl}(\mathbf{u}) = \mathbf{\Phi}_f\mathbf{\Phi}_f^T\mathbf{g}_{nl}(\mathbf{u}) \, . \tag{2.78}$$

Then, the generalised forces in the ROM space are computed as,

$$\tilde{\mathbf{g}}_{nl}(\mathbf{q}) = \mathbf{\Phi}^T\mathbf{g}_{nl}^f(\mathbf{u}) = \mathbf{\Phi}^T\mathbf{\Phi}_f\mathbf{\Phi}_f^T\mathbf{g}_{nl}(\mathbf{u}) = \mathbf{B}^T\mathbf{g}_{nl}(\mathbf{u}) \, . \tag{2.79}$$

where $B^T = \mathbf{\Phi}^T\mathbf{\Phi}_f\mathbf{\Phi}_f^T$ is the correction (filtering) matrix.

The proposed correction for nonlinear forces is a non intrusive technique as it only takes place in the projection of the nonlinear forces into the ROM space and does not require additional FOM computations once it is constructed. The latter correction might be understood as a filter for the directions and magnitude of the FOM nonlinear forces while performing the projection into the reduced space. The accuracy of the response depends on the quality of the nonlinear forces basis, $\mathbf{\Phi}_f$, and of the reduced order basis, $\mathbf{\Phi}$.

STEP with Correction (StepC)

Combining the STEP method and the proposed POD correction, the StepC ROM is constructed with the coeff A_{ij} and B_{ijm} identified from the **filtered** static forces $\mathbf{B}^T\mathbf{g}_{nl}(\mathbf{u})$ corresponding to Eqn. (2.79) instead of the original static forces $\mathbf{g}_{nl}(\mathbf{u})$, in the OFFline phase. With respect to the classical STEP method the identification of the nonlinear coefficients is, $\mathbf{B}_p^T$ being the p-th row of $\mathbf{B}^T$,

$$
\begin{aligned}
A^p_{ii} &= \frac{1}{2q_i^2}\left[\mathbf{B}_p^T\mathbf{g}_{nl}\left(\mathbf{u}_1\right)+\mathbf{B}_p^T\mathbf{g}_{nl}\left(\mathbf{u}_2\right)\right] \ , \\
A^p_{ij} &= \frac{1}{2q_iq_j}\left[\mathbf{B}_p^T\mathbf{g}_{nl}\left(\mathbf{u}_3\right)+\mathbf{B}_p^T\mathbf{g}_{nl}\left(\mathbf{u}_4\right)-2A^p_{ii}q_i^2-2A^p_{jj}q_j^2\right] \ , \\
B^p_{iii} &= \frac{1}{2q_i^3}\left[\mathbf{B}_p^T\mathbf{g}_{nl}\left(\mathbf{u}_1\right)-\mathbf{B}_p^T\mathbf{g}_{nl}\left(\mathbf{u}_2\right)\right] \ , \\
B^p_{ijj} &= \frac{1}{2q_iq_j^2}\left[\mathbf{B}_p^T\mathbf{g}_{nl}\left(\mathbf{u}_3\right)+\mathbf{B}_p^T\mathbf{g}_{nl}\left(\mathbf{u}_5\right)-2A^p_{ii}q_i^2-2A^p_{jj}q_j^2-2B^p_{iii}q_i^3\right] , \\
B^p_{iij} &= \frac{1}{2q_i^2q_j}\left[-\mathbf{B}_p^T\mathbf{g}_{nl}\left(\mathbf{u}_4\right)-\mathbf{B}_p^T\mathbf{g}_{nl}\left(\mathbf{u}_5\right)+2A^p_{ii}q_i^2+2A^p_{jj}q_j^2-2B^p_{jjj}q_j^3\right] , \\
B^p_{ijm} &= \frac{1}{q_iq_jq_m}\left[\mathbf{B}_p^T\mathbf{g}_{nl}(\mathbf{u}_6)-A^p_{ii}q_i^2-A^p_{ij}q_iq_j-A^p_{im}q_iq_m-A^p_{jj}q_j^2\right. \\
&\quad -A^p_{jm}q_jq_m-A^p_{mm}q_m^2-B^p_{iii}q_i^3-B^p_{iij}q_i^2q_j-B^p_{iim}q_i^2q_m \\
&\quad -B^p_{ijj}q_iq_j^2-B^p_{imm}q_iq_m^2-B^p_{jjj}q_j^3-B^p_{jjm}q_j^2q_m \\
&\quad \left.-B^p_{jmm}q_jq_m^2-B^p_{mmm}q_m^3\right] \ .
\end{aligned}
\tag{2.80}
$$

Then the nonlinear forces are computed in the ONline phase by Eqn. (2.40). Figure 2.5 represents the flow chart to identify the corrected stiffness coefficients, A_{ij} and B_{ijk}.

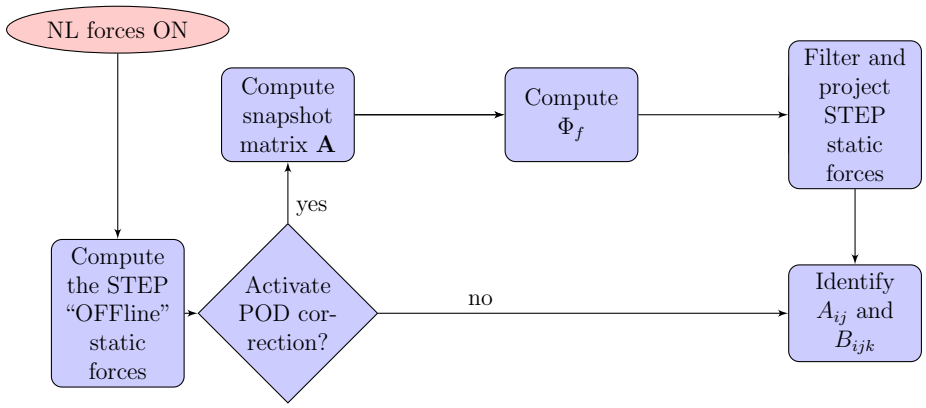

Figure 2.5: Flow chart of the identification process of the nonlinear stiffness force coefficients by STEP and StepC POD correction methods.

Summary of the Linear, STEP and StepC ROMs

Figure 2.6 presents the flowchart to build the StepC ROM that is used in the ONline phase. During the OFFline phase the correction matrix, $\mathbf{B}^T$, is constructed and the reduction bases can be optimised. Both are introduced in the STEP method to obtain the generalised nonlinear forces, $\tilde{\mathbf{g}}_{nl}(\mathbf{q})$. The latter combined with the reduced basis permits to create the StepC ROM that corresponds to Eqn. (2.37).

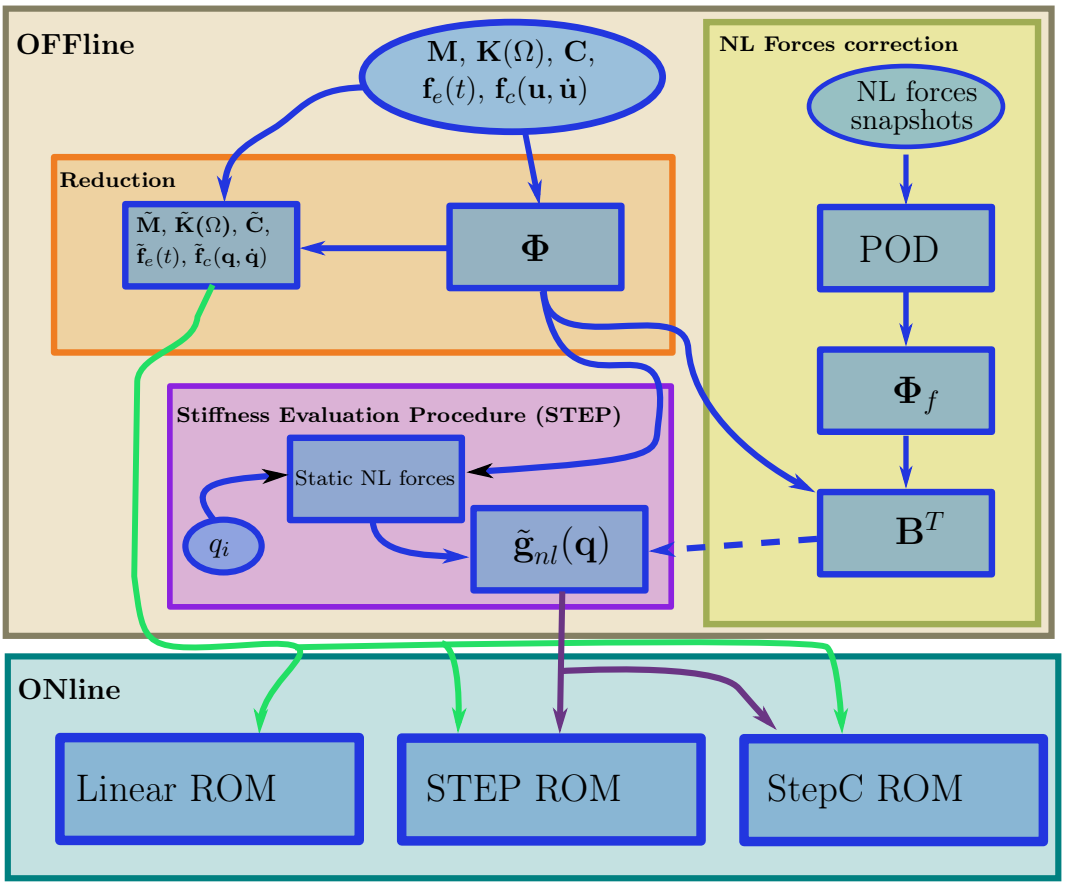

Figure 2.6: Summary of construction for the studied ROMs.

2.5 Friction contact nonlinear forces in the reduced order model

The friction contact is a localised phenomena (contact boundary) that occurs due to the contact between solids. The weak form of the friction contact problem and its discretisation are introduced in the previous chapter. In the following, the expression of the nonlinear forces for the penalisation method is introduced.

Considering that the gap function, g_n, that evaluates the distance between the master and the slave surfaces is known, the normal contact force that opposes to the interpenetration between solids by means of the penalisation method is defined as,

$$f_n = \begin{cases} 0 & \text{if} \quad g_n \geq 0 \\ -\varepsilon_n g_n & \text{if} \quad gn < 0 \end{cases} , \tag{2.81}$$

where ε_n is the normal penalisation factor and the negative value of g_n means that there exists an interpenetration between solids.

The relation between the tangential friction force and the normal contact force computed with Eqn. (2.81) is obtained by means of a friction law (section 1.2.4).

The effect of friction contact leads, among others, to wear, to induced vibrations or to a cracking propagations phenomena. Thus, the quantification of the contact effect is vital for design purposes. Furthermore, the friction induces a loss of mechanical energy due to dissipation, and, as a consequence the structure's response is modified. In turbomachinery, rubbing elements permit to reduce the amplitude of the blades by means of friction contact dissipation.

Hereunder, the coupling between geometrically nonlinear and friction contact effects is studied by means of the modified Duffing oscillator defined in Eqn. (2.38) and in Fig. 2.3.

Due to the low dimensionality of the problem the normal contact force is supposed as known, thus, a Tresca type of friction law is considered with an static friction coefficient, $\mu_s = 0.75$ and a dynamic friction coefficient, $\mu_d = 0.6$. Figures 2.7a to 2.7c represent the forced response of the structure for $\alpha_D = 0$ Nm^{-3}, 10^6 Nm^{-3} and 10^7 Nm^{-3} values of the nonlinear stiffness coefficient and for an imposed normal contact force of value, $\mathrm{f}_N = 0$ N, 30 N, 45 N and 60 N. The unstable solution is not computed, however, the frequency sweep is performed in both directions so that both nonlinear stable branches are evaluated. The dark lines in Fig. 2.7d represent the forced response of the Duffing oscillator for a variable nonlinear stiffness coefficient constant contact force, $f_N = 10$ N. The light lines correspond to the solution presented in Fig. 2.4 representing the forced response for a variable nonlinear stiffness without contact nonlinearity, $f_N = 0$ N.

For all the cases, an increment of the normal contact force induces a reduction of the amplitude on the displacements response. When the structure behaves nonlinearly, the contact shifts the nonlinear resonance frequency towards the value of the linear natural frequency. The influence of the contact normal force is greater for low values of displacements than when the oscillator

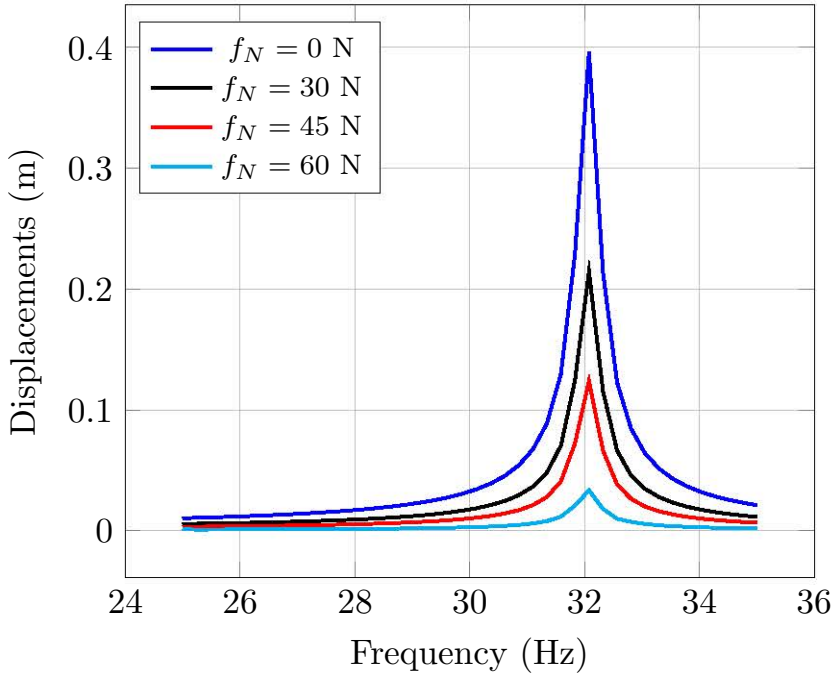

(a) Forced response of the Duffing oscillator for a variable normal contact force, case of a linear structure, $\alpha_D = 0$.

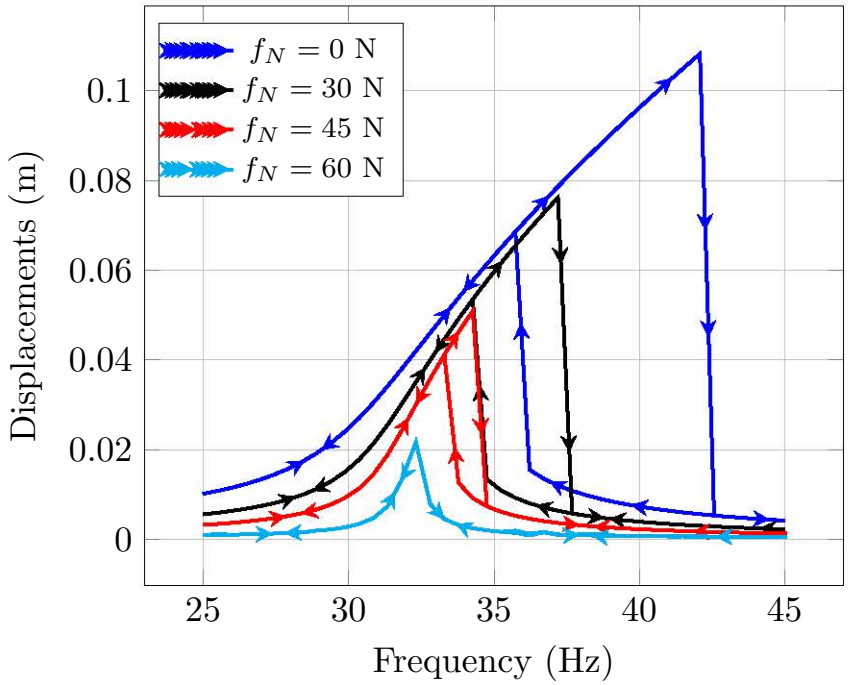

(b) Forced response of the Duffing oscillator for a variable normal contact force, case of a geometrically nonlinear structure, $\alpha_D = 10^6$ Nm^{-3}.

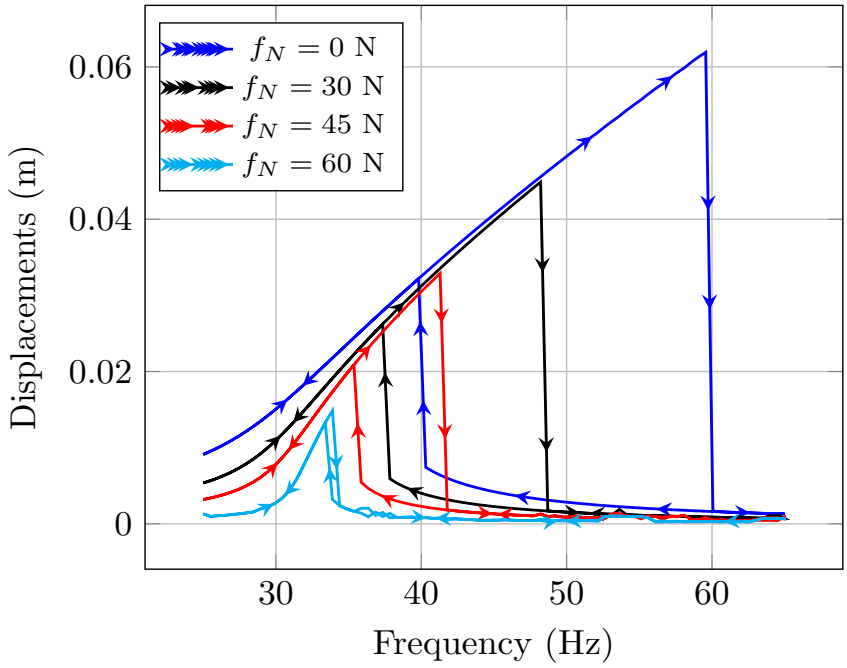

(c) Forced response for a variable normal contact force, case of a geometrically nonlinear structure, $\alpha_D = 10^7$ Nm^{-3}.

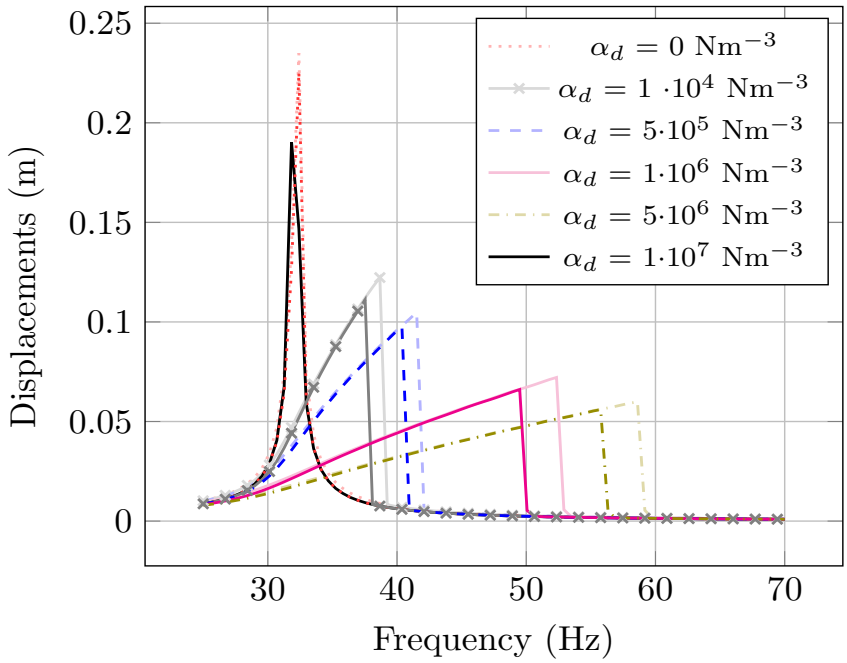

(d) Forced response for variable nonlinear stiffness coefficient, α_d and a normal force of 10 N.

Figure 2.7: Forced response for different values of α_D and for different values of the normal contact force.

presents large displacements. In the latter case, the nonlinear solutions tend to behave similarly (even if the displacements peak value is reduced when the normal contact force is increased).

When the structure behaves linearly, Fig. 2.7a, for very low excitation frequencies, $\omega_e \ll \omega_n$, the excitation force and the solution are in phase. However, when the excitation frequency tends towards the resonant frequency $\omega_e \to \omega_n$, the excitation and the solution phase difference is increased until the value of $\pi/2$ rad observed at resonance. For excitation frequencies over the resonant value, the shift between the excitation and response is increased until a phase difference of π rad for $\omega_e \gg \omega_n$. When the structure behaves nonlinearly, the phase does not vary until the solution changes from one stable branch to the other, where the phase is abruptly changed. For low values of the contact normal force, the effect on the solution phase does not vary with respect to the non contact configuration. However, when the contact force takes greater values, the solution for low amplitude regimes is quasi-periodic or chaotic. The latter could induce unwanted spurious vibrations and accelerated wear effects. However, the displacements of the oscillator remain small.

The implementation of friction devices provides the advantage that the observed response amplitude is reduced, however, the shift of the nonlinear resonant frequency should be computed and the excitation frequencies should avoid the excitation frequencies where the response behaves chaotically.

The reduced order model presented in the previous sections is capable of reproducing the nonlinear behaviour of the structure with geometrical and friction contact nonlinearities at a given rotating velocity. However, for any other rotating velocity, the reduced order models would not be adapted and it should be constructed again. Thus, the latter could lead to very expensive computations to build a series of reduced order models for different rotating velocities. To avoid that problem, in the next section, a parametrisation of the nonlinear reduced order model is proposed. Thus, the construction of the reduced order model is once performed for a range of rotating velocities increasing the time performances of the OFFline phase.

2.6 Parametric reduced order model

The proposed ROM is obtained by solving the reduced basis for each of the considered rotating velocities. Thus, reconstructions of the ROM is required for analysing the response at different rotating velocities and could limit the analysis for loadings that depend on the rotating velocity, i.e. engine order excitations. To reduce the latter limitation, a parametrization of the ROM is

carried out as proposed in [Hong et al., 2011, Kurstak et al., 2018].

First the parametrisation of the reduced order bases is presented. Then, the parametrisation of the nonlinear forces is preformed for which three different techniques are proposed and discussed.

2.6.1 Reduced basis and linear stiffness parametrisation

The parametrised reduced order basis is obtained by carrying out a Singular Value Decomposition (SVD) of the chosen type of reduced basis at three pre-computed rotating velocities, $\mathbf{Q}_{\Omega=p_0}$, $\mathbf{Q}_{\Omega=p_0+\Delta p}$, $\mathbf{Q}_{\Omega=p_0+2\Delta p}$ where p_0, $p_0+\Delta p$ and $p_0+2\Delta p$ represent the rotating velocities used for interpolation. The proposed basis is valid inside the range $[\Omega = p_0,\ \Omega = p_0 + 2\Delta p]$.

$$\mathbf{X} \overset{SVD}{\leftarrow} \mathbf{Q}_{expanded} = [\mathbf{Q}_{\Omega=p_0}, \mathbf{Q}_{\Omega=p_0+\Delta p}, \mathbf{Q}_{\Omega=p_0+2\Delta p}] \ , \tag{2.82}$$

where $\mathbf{X}$ is the parametrised basis that corresponds to the left singular vectors of the SVD. As presented previously, the ROM's construction performances are improved by truncating the latter basis to a given number of vectors. The later basis does not correspond any longer to the LNM of the structure.

Furthermore, the stiffness matrix is defined as a function of the rotating velocity by a quadratic interpolation,

$$\mathbf{K}(\Omega) = \mathbf{K}(p0) + \left.\frac{\partial \mathbf{K}}{\partial \Omega}\right|_{\Omega=p_0} (\Omega - p_0) + \frac{1}{2} \left.\frac{\partial^2 \mathbf{K}}{\partial \Omega^2}\right|_{\Omega=p_0} (\Omega - p_0)^2 \ , \tag{2.83}$$

where the derivatives are identified by means of finite order differences,

$$\left.\frac{\partial \mathbf{K}}{\partial \Omega}\right|_{\Omega=p_0} = \frac{\mathbf{K}(p_0+2\Delta p) + 4\mathbf{K}(p_0+\Delta p) - 3\mathbf{K}(p_0)}{\Delta p} \ , \tag{2.84}$$

$$\left.\frac{\partial^2 \mathbf{K}}{\partial \Omega^2}\right|_{\Omega=p_0} = \frac{\mathbf{K}(p_0+2\Delta p) - 2\mathbf{K}(p_0+\Delta p) + \mathbf{K}(p_0)}{\Delta p^2} \ , \tag{2.85}$$

where $\mathbf{K}(p_0+2\Delta p)$, $\mathbf{K}(p_0+\Delta p)$ and $\mathbf{K}(p_0)$ are computed in the FOM.

2.6.2 Parametrisation of the nonlinear forces

The expression of the purely nonlinear forces, Eqn. (2.41), depends on the rotating velocity. Thus, a parametrisation is needed to avoid computing the OFFline stage of the STEP method for each rotating velocity. For values of the imposed vibration greater than the static displacements induced by rotation, $||\mathbf{Xq}|| \gg ||\mathbf{u}_s||$, the nonlinear forces $\mathbf{g}(\mathbf{u}_s + \mathbf{Xq})$ are very similar as shown in Fig. 2.8. Thus, for all the considered rotating velocities, one single

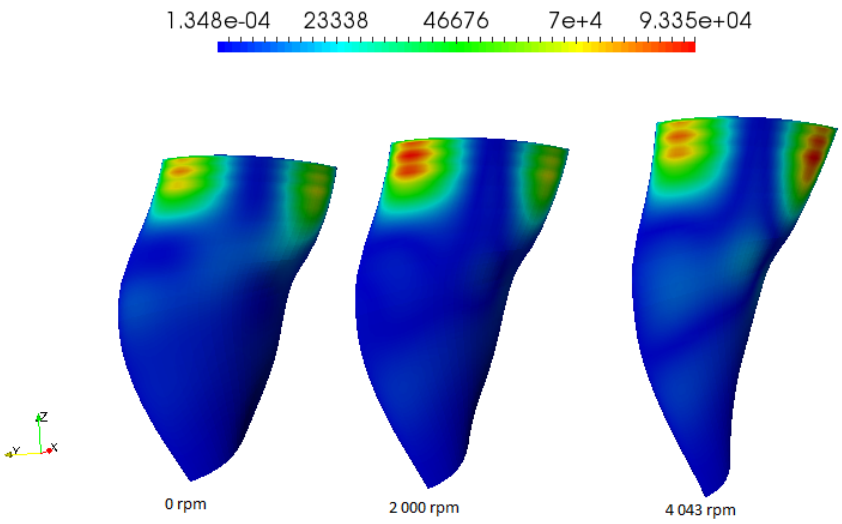

(a) Nonlinear force, $\mathbf{g}(\mathbf{u}_s - \mathbf{X}_4 q_4 - \mathbf{X}_7 q_7)$.

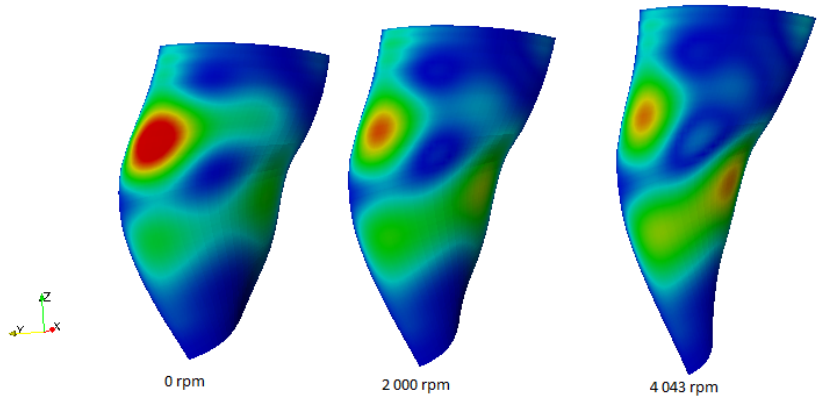

(b) Nonlinear force, $\mathbf{g}(\mathbf{u}_s + \mathbf{X}_8 q_8 + \mathbf{X}_{10} q_1 0)$.

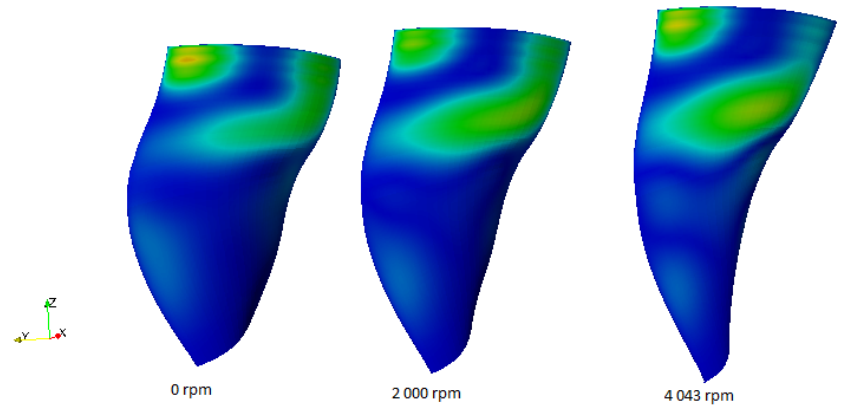

(c) Nonlinear force, $\mathbf{g}(\mathbf{u}_s + \mathbf{X}_4 q_4 + \mathbf{X}_7 q_7 + \mathbf{X}_8 q_8)$.

Figure 2.8: Nonlinear static forces due to an imposed displacement state extracted form the STEP procedure for $\Omega = 0$ rpm, 2000 rpm and 4043 rpm.

computation of the nonlinear forces would lead to an acceptable results of the nonlinear forces of the structure.

Thus, considering the nonlinear forces as those of the velocity that corresponds to $\Omega = p_0 + \Delta p$ leads to an accurate approximation of the nonlinear forces.

$$\mathbf{g}(\mathbf{u}_s(\Omega) + \mathbf{X}\mathbf{q}) \approx \mathbf{g}(\mathbf{u}_s(\mathrm{p}_0 + \Delta\mathrm{p})) \tag{2.86}$$

Then, the purely nonlinear forces of the structure are identified by parametrising matrix $\mathbf{K}_s$ as well as the static displacements of the structure, $\mathbf{u}_s$, following a similar procedure as for the parametrisation of the linear stiffness matrix, Eqn. (2.83) to (2.85). Then, for matrix $\mathbf{K}_s$,

$$\mathbf{K}_s(\Omega) = \mathbf{K}_s(p_0) + \left.\frac{\partial \mathbf{K}_s}{\partial \Omega}\right|_{\Omega=p_0} (\Omega - p_0) + \frac{1}{2}\left.\frac{\partial^2 \mathbf{K}_s}{\partial \Omega^2}\right|_{\Omega=p_0} (\Omega - p_0)^2 \ , \tag{2.87}$$

where the derivatives are identified by means of finite order differences,

$$\left.\frac{\partial \mathbf{K}_s}{\partial \Omega}\right|_{\Omega=p_0} = \frac{\mathbf{K}_s(p_0 + 2\Delta p) + 4\mathbf{K}_s(p_0 + \Delta p) - 3\mathbf{K}_s(p_0)}{\Delta p} \ , \tag{2.88}$$

$$\left.\frac{\partial^2 \mathbf{K}_s}{\partial \Omega^2}\right|_{\Omega=p_0} = \frac{\mathbf{K}_s(p_0 + 2\Delta p) - 2\mathbf{K}_s(p_0 + \Delta p) + \mathbf{K}_s(p_0)}{\Delta p^2} \ , \tag{2.89}$$

where $\mathbf{K}_s(p_0+2\Delta p)$, $\mathbf{K}_s(p_0+\Delta p)$ and $\mathbf{K}_s(p_0)$ are computed in the FOM. And similarly for the static displacements forces induced by rotation,

$$\mathbf{g}(\mathbf{u}_s(\Omega)) = \mathbf{g}(\mathbf{u}_s(p_0)) + \left.\frac{\partial \mathbf{g}(\mathbf{u}_s)}{\partial \Omega}\right|_{\Omega=p_0} (\Omega - p_0) + \frac{1}{2}\left.\frac{\partial^2 \mathbf{g}(\mathbf{u}_s)}{\partial \Omega^2}\right|_{\Omega=p_0} (\Omega - p_0)^2 \ , \tag{2.90}$$

where the derivatives are identified by means of finite order differences,

$$\left.\frac{\partial \mathbf{g}(\mathbf{u}_s)}{\partial \Omega}\right|_{\Omega=p_0} = \frac{\mathbf{g}(\mathbf{u}_s(\mathrm{p}_0 + 2\Delta\mathrm{p})) + 4\mathbf{g}(\mathbf{u}_s(\mathrm{p}_0 + \Delta\mathrm{p})) - 3\mathbf{g}(\mathbf{u}_s(\mathrm{p}_0))}{\Delta p} \ , \tag{2.91}$$

$$\left.\frac{\partial^2 \mathbf{g}(\mathbf{u}_s)}{\partial \Omega^2}\right|_{\Omega=p_0} = \frac{\mathbf{g}(\mathbf{u}_s(\mathrm{p}_0 + 2\Delta\mathrm{p})) - 2\mathbf{g}(\mathbf{u}_s(\mathrm{p}_0 + \Delta\mathrm{p})) + \mathbf{g}(\mathbf{u}_s(\mathrm{p}_0))}{\Delta p^2} \ , \tag{2.92}$$

where $\mathbf{g}(\mathbf{u}_s(p_0 + 2\Delta p))$, $\mathbf{g}(\mathbf{u}_s(p_0 + \Delta p))$ and $\mathbf{g}(\mathbf{u}_s(p_0))$ are computed in the FOM.

As shown in Fig. 2.8, the nonlinear forces are similar for all rotating velocities for a given imposed displacements. Thus, the nonlinear forces for a given rotating velocity, Ω, are computed as,

$$\mathbf{g}_{nl}(\mathbf{u}) = \mathbf{g}(\mathbf{u}_s(\mathrm{p}_0 + \Delta\mathrm{p}) + \mathbf{X}\mathbf{q}) - \mathbf{g}(\mathbf{u}_s(\Omega)) - \mathbf{K}_s(\Omega)\mathbf{X}\mathbf{q} \ . \tag{2.93}$$

2.7 Resolution methods

The equation of motion of the structure is evaluated for each time step in order to obtain the time-response of the structure under a given time-dependant external loading and a considered nonlinearity. In literature many methods to compute the solution of a nonlinear system can be found. Regarding the time integration methods, the implicit, the explicit or the ImEx (implicit-explicit) schemes are widely used. With respect to computations of the time response in the frequency domain, the Harmonic Balance method (HBM) is largely developed. In the following, first, the classical Newmark time integration scheme is introduced. Then, the HHT-α time integration method is presented which is very similar to the Newmark scheme. Finally, the Harmonic Balance Method is developed.

2.7.1 Newmark time integration methods

The Newmark scheme [Newmark, 1959] is a numerical time integration scheme used to solve the linear and nonlinear second degree differential equations. The principle of the present method is to determine the displacements, velocity and acceleration of an instant $t + \Delta t$ from the values of the position $\mathbf{u}^t$, velocity $\dot{\mathbf{q}}^t$ and acceleration $\ddot{\mathbf{q}}^t$ at the instant t.

Linear Newmark scheme

For the linear equation system presented as,

$$\begin{cases} \tilde{\mathbf{M}}\ \ddot{\mathbf{q}} = f\left(\mathbf{q}, \dot{\mathbf{q}}, t\right) \\ \mathbf{q}\left(t=0\right) = \mathbf{q}_0 \\ \dot{\mathbf{q}}\left(t=0\right) = \dot{\mathbf{q}}_0 \end{cases} , \tag{2.94}$$

the Newmark scheme takes the following form and the displacements, velocities and accelerations for the time step $t + \Delta t$ are obtained as follows,

$$\ddot{\mathbf{q}}^{t+\Delta t} = \tilde{\mathbf{M}}^{-1} f\left(\mathbf{q}^t, \dot{\mathbf{q}}^t, t + \Delta t\right) , \tag{2.95}$$

$$\dot{\mathbf{q}}^{t+\Delta t} = \dot{\mathbf{q}}^t + \Delta t \left[(1-\gamma)\,\ddot{\mathbf{q}}^t + \gamma \ddot{\mathbf{q}}^{t+\Delta t}\right] , \tag{2.96}$$

$$\mathbf{q}^{t+\Delta t} = \mathbf{q}^t + \Delta t \dot{\mathbf{q}}^t + \frac{\Delta t^2}{2}\left[(1-2\beta)\,\ddot{\mathbf{q}}^t + 2\beta \ddot{\mathbf{q}}^{t+\Delta t}\right] , \tag{2.97}$$

where β and γ are the parameters that define the stability and convergence rate of the scheme as shown in the Tab. 2.1.

However, to solve a nonlinear equation system, Eqn. (2.95) to (2.97) are no longer valid.

Range	Stability
$\gamma \leq \frac{1}{2}$	Unstable
$\frac{1}{2} \leq \gamma$ and $2\beta \leq \gamma$	Conditionally stable
$\frac{1}{2} \leq \gamma$ and $\gamma \leq 2\beta$	Unconditionally stable

Table 2.1: Stability of the linear Newmark method.

Nonlinear Newmark scheme

The procedure to solve nonlinear equation systems with Newmark scheme is presented in [Krenk, 2009]. Hence, an important prerequisite is the assumption that the external forces $\mathbf{f}_e(\mathrm{t})$ are known at each time step and do not depend on the displacements $\mathbf{u}$. This excludes the contact problems between multiple bodies, for which special procedures would have to be implemented. For contact or aerodynamic forces, the procedure is to introduce the contact/aerodynamic solver into the Newmark algorithm in order to compute the unknown loadings that depend on the current state of the structure.

Hereunder the ROM formulation of the nonlinear Newmark scheme for the study of a rotating structure with geometrical and contact nonlinearities is developed. In order to solve the dynamic response of the Eqn. (2.37) by the nonlinear Newmark scheme, the following steps are required: i) initial conditions, ii) initial prediction for the instant $t + \Delta t$, iii) computation of the increment, iv) computation of the generalized coordinates, velocities and accelerations and v) test of convergence.

i) Initial conditions

The initial conditions for the ROM's generalized coordinates $\mathbf{q}_0$ and generalized velocities $\dot{\mathbf{q}}_0$ are obtained by means of a least-squares approximation. The accelerations are obtained from Eqn. (2.37),

$$\mathbf{q}_0 = \left(\Phi^T\Phi\right)^{-1}\Phi^T\mathbf{u}_0 \,, \tag{2.98}$$

$$\dot{\mathbf{q}}_0 = \left(\Phi^T\Phi\right)^{-1}\Phi^T\dot{\mathbf{u}}_0 \,, \tag{2.99}$$

$$\ddot{\mathbf{q}}_0 = \tilde{\mathbf{M}}^{-1}\left(\tilde{\mathbf{f}}_e\left(t_0\right) - \tilde{\mathbf{C}}\ \dot{\mathbf{q}}_0 - \tilde{\mathbf{K}}\ \mathbf{q} - \tilde{\mathbf{g}}_{nl}(\mathbf{q}_0) - \tilde{\mathbf{f}}_c(\mathbf{q}_0)\right) . \tag{2.100}$$

ii) Initial prediction for time $t + \Delta t$

The residue $\tilde{\mathbf{r}}_{n=1}^{t+\Delta t}$ used as a reference in the test of convergence is defined as follows,

$$\tilde{\mathbf{r}}_{n=1}^{t+\Delta t} = \tilde{\mathbf{f}}_e\left(t + \Delta t\right) - \tilde{\mathbf{M}}\ \ddot{\mathbf{q}}_n^t - \tilde{\mathbf{C}}\ \dot{\mathbf{q}}_n^t - \tilde{\mathbf{K}}\ \mathbf{q}_n^t - \tilde{\mathbf{g}}_{nl}(\mathbf{q}_n^t) - \tilde{\mathbf{f}}_c(\mathbf{q}_n^t) \,. \tag{2.101}$$

The initial predictive values for the internal Newton-Raphson loop are initialized by the prediction of the solution for time $t + \Delta t$,

$$\ddot{\mathbf{q}}_{n=1}^{t+\Delta t} = \ddot{\mathbf{q}}^{t} \,, \tag{2.102}$$

$$\dot{\mathbf{q}}_{n=1}^{t+\Delta t} = \dot{\mathbf{q}}^{t} + \Delta t \ddot{\mathbf{q}}^{t} \,, \tag{2.103}$$

$$\mathbf{q}_{n=1}^{t+\Delta t} = \mathbf{q}^{t} + \Delta t \dot{\mathbf{q}}^{t} + \frac{\Delta t^2}{2} \ddot{\mathbf{q}}^{t} \,, \tag{2.104}$$

with $\mathbf{q}^{t=0} = \mathbf{q}_0$, $\dot{\mathbf{q}}^{t=0} = \dot{\mathbf{q}}_0$ and $\ddot{\mathbf{q}}^{t=0} = \ddot{\mathbf{q}}_0$.

iii) Computation of the increment

The generalized residue $\tilde{\mathbf{r}}_n^{t+\Delta t}$ for time $t+\Delta t$ and Newton-Raphson iteration index n is,

$$\begin{aligned} \tilde{\mathbf{r}}_n^{t+\Delta t} = \tilde{\mathbf{f}}_e\,(t+\Delta t) - \tilde{\mathbf{M}}\ \ddot{\mathbf{q}}_n^{t+\Delta t} - \tilde{\mathbf{C}}\ \dot{\mathbf{q}}_n^{t+\Delta t} - \tilde{\mathbf{K}}\ \mathbf{q}_n^{t+\Delta t} - \tilde{\mathbf{g}}_{nl}(\mathbf{q}_n^{t+\Delta t}) \\ - \tilde{\mathbf{f}}_c(\mathbf{q}_n^{t+\Delta t}) \,, \end{aligned} \tag{2.105}$$

where the nonlinear forces are obtained by the methods presented previously.

Then, the Jacobian matrix for the n-th iteration $\mathbf{J}_n$ is used to compute the increment $\Delta\mathbf{q}_n^{t+\Delta t}$ of the generalized coordinates:

$$\mathbf{J}_n = \frac{\partial\left(\tilde{\mathbf{K}}\mathbf{q}_n + \tilde{\mathbf{g}}_{nl} - \tilde{\mathbf{f}}_c(\mathbf{q})\right)}{\partial \mathbf{q}}\left(\mathbf{q}_n^{t+\Delta t}\right) + \frac{\gamma}{\beta\Delta t}\tilde{\mathbf{C}} + \frac{1}{\beta\Delta t}\tilde{\mathbf{M}} \,, \tag{2.106}$$

where $\frac{\partial\left(\tilde{\mathbf{K}}\mathbf{q}+\tilde{\mathbf{g}}_{nl}-\tilde{\mathbf{f}}_c(\mathbf{q})\right)}{\partial \mathbf{q}}\left(\mathbf{q}_n^{t+\Delta t}\right)$ is the derivative matrix of the nonlinear forces. Then, the increment of the generalized coordinates $\Delta\mathbf{q}_n^{t+\Delta t}$ takes the expression,

$$\Delta\mathbf{q}_n^{t+\Delta t} = \mathbf{J}_n^{-1}\tilde{\mathbf{r}}_n^{t+\Delta t} \,. \tag{2.107}$$

iv) Computation of the generalized coordinates, velocities and accelerations

The values of the generalized coordinates $\mathbf{q}_{n+1}^{t+\Delta t}$, the generalized velocities $\dot{\mathbf{q}}_{n+1}^{t+\Delta t}$ and the generalized accelerations $\ddot{\mathbf{q}}_{n+1}^{t+\Delta t}$ for the n-th Newton-Raphson iteration and for the instant $t + \Delta t$ are obtained from $\Delta\mathbf{q}_n^{t+\Delta t}$ as follows,

$$\mathbf{q}_{n+1}^{t+\Delta t} = \mathbf{q}_n^{t+\Delta t} + \Delta\mathbf{q}_n^{t+\Delta t} \,, \tag{2.108}$$

$$\dot{\mathbf{q}}_{n+1}^{t+\Delta t} = \dot{\mathbf{q}}_n^{t+\Delta t} + \frac{\gamma}{\beta\Delta t}\Delta\mathbf{q}_n^{t+\Delta t} \,, \tag{2.109}$$

$$\ddot{\mathbf{q}}_{n+1}^{t+\Delta t} = \ddot{\mathbf{q}}_n^{t+\Delta t} + \frac{1}{\beta\Delta t^2}\Delta\mathbf{q}_n^{t+\Delta t} \,, \tag{2.110}$$

where β and γ are the Newmark scheme parameters that define the stability of the integration. Some examples of these parameters are given in Tab. 2.2.

Method	γ	β	Stability
Linear acceleration	$\frac{1}{2}$	$\frac{1}{6}$	$\Delta t \leq 0.551\ \max(T_i)$
Constant average acceleration	$\frac{1}{2}$	$\frac{1}{4}$	Unconditionally
Bathe [Bathe, 2006]	$\geq \frac{1}{2}$	$\geq \frac{1}{4}\left(\frac{1}{2}+\gamma\right)^2$	-
Verification of energy fluctuation	$\frac{3}{5}$	$\frac{2}{5}$	$\Delta t \leq \frac{2\pi}{\omega_{max}}$

Table 2.2: The integration parameters for the nonlinear Newmark scheme.

v) Test of convergence

The generalized residual force $\tilde{\mathbf{r}}_{n+1}^{t+\Delta t}$ is evaluated by means of the values obtained by Eqn. (2.108) to (2.110). The solution $\mathbf{q}_{n+1}^{t+\Delta t}$ reaches the convergence when the following condition is satisfied,

$$\| \tilde{\mathbf{r}}_{n}^{t+\Delta t} \| \leq \epsilon \| \tilde{\mathbf{r}}_{n=1}^{t+\Delta t} \| , \tag{2.111}$$

where the convergence parameter $\epsilon \ll 1$.

If the convergence is not reached a new Newton-Raphson iteration is performed in order to obtain the solution for the present time instant (stages *iii* to *v*). Once the convergence condition is fulfilled the computation of the next time instant is started from stage *ii*.

2.7.2 HHT-α method

The α-methods are a generalisation of the nonlinear Newmark scheme. The latter is a special case of the α-methods when α is equal to 1. These methods improve the stability of the solution and permit to solve a wider variety of problems (i.e. transient solution of structural dynamic systems). There are two types of α-methods: i) the Hilber-Hughes-Taylor-α method, or HHT-α, [Hilber et al., 1977] that weights the displacements and the velocities at $t+\alpha\Delta t$ and calculates the accelerations at $t+\Delta t$, and ii) the Generalized-α method [Hulbert, 1993] which considers a second parameter α_M to weight the mass matrix and to calculate the accelerations at time $t+\alpha_M\Delta t$. Furthermore, the application of the methods to nonlinear problems are presented by [Wood et al., 1980, Kuhl and Ramm, 1996, Chang, 2008, Bransch and Lehmann, 2011, Klarmann and Wagner, 2015]. Hereafter, only the HHT-α method is considered and developed for the case of a nonlinear rotating structure's ROM. The parameter α used in the present developments is not the same as the original in [Hilber et al., 1977], but is based on the formulation taken from [Erlicher et al., 2002]: $\alpha_{HHT-\alpha_{original}} - 1 = \alpha$.

The HHT-α method introduces an extra prediction inside the Newton-Rapshon loop of the nonlinear Newmark scheme. Hence, the following steps are

required in order to solve the nonlinear system: i) initial conditions, ii) initial prediction for time $t+\Delta t$, iii) predictive values for the inner Newton-Raphson loop, iv) computation of the increment, v) computation of the generalized coordinates, velocities and accelerations and vi) test of convergence.

i) Initial conditions

The initial conditions for the ROM's generalized coordinates $\mathbf{q}_0$, generalized velocities $\dot{\mathbf{q}}_0$ and generalized accelerations $\ddot{\mathbf{q}}_0$ are obtained by means of Eqn. (2.98) to (2.100).

ii) Initial prediction for time $t+\Delta t$

The initial predictive values for the internal Newton-Raphson loop are initialized by the prediction of the solution for time $t+\Delta t$, see Eqn. (2.102) to (2.104). The residue $\tilde{\mathbf{r}}_{n=1}^{t+\Delta t}$ used as a reference in the test of convergence is defined in Eqn. (2.101).

iii) Predictive values for the Newton-Raphson inner loop

The predictive values for the Newton-Raphson iterations for the generalised displacements $\mathbf{q}_n^{t+\alpha\Delta t}$ and generalized velocities $\dot{\mathbf{q}}_n^{t+\alpha\Delta t}$ are obtained for time $t+\alpha\Delta t$,

$$\mathbf{q}_n^{t+\alpha\Delta t} = (1-\alpha)\,\mathbf{q}^t + \alpha\mathbf{q}_n^{t+\Delta t}\,, \tag{2.112}$$

$$\dot{\mathbf{q}}_n^{t+\alpha\Delta t} = (1-\alpha)\,\dot{\mathbf{q}}^t + \alpha\dot{\mathbf{q}}_n^{t+\Delta t}\,, \tag{2.113}$$

where α is the parameter of the HHT-α method. This method is unconditionally stable for any value of α for linear problems. The Newmark parameters γ and β are defined as a function of α in order to ensure the second order accuracy and the unconditional stability [Hilber et al., 1977],

$$\beta = \frac{(2-\alpha)^2}{4}\,, \tag{2.114}$$

$$\gamma = \frac{3}{2}-\alpha\,, \tag{2.115}$$

where the values of α are between $\frac{2}{3}$ and 1, $\frac{2}{3}\leq\alpha\leq 1$. From [Hulbert, 1993] if $\beta\geq\frac{1}{4}+\frac{1}{2}(1-\alpha)$ the range of validity of α is extended to $\frac{1}{2}\leq\alpha\leq 1$.

iv) Computation of the increment

The generalized residue $\tilde{\mathbf{r}}_n^{t+\Delta t}$ for the instant $t+\Delta t$ and Newton-Raphson iteration index n is defined as follows,

$$\begin{aligned}\tilde{\mathbf{r}}_n^{t+\Delta t} = \tilde{\mathbf{f}}_e\,(t+\Delta t) - \tilde{\mathbf{M}}\;\ddot{\mathbf{q}}_n^{t+\Delta t} - \tilde{\mathbf{C}}\;\dot{\mathbf{q}}_n^{t+\alpha\Delta t} \\ - \tilde{\mathbf{K}}\;\mathbf{q}_n^{t+\alpha\Delta t} - \tilde{\mathbf{g}}_{nl}(\mathbf{q}_n^{t+\alpha\Delta t}) - \tilde{\mathbf{f}}_c(\mathbf{q})\,.\end{aligned} \tag{2.116}$$

Then, the Jacobian matrix for the n-th iteration $\mathbf{J}_n$ is used to compute the increment $\Delta\mathbf{q}_n^{t+\Delta t}$ of the generalized coordinates,

$$\mathbf{J}_n = \frac{\partial\left(\tilde{\mathbf{K}}\mathbf{q}_n + \tilde{\mathbf{g}}_{nl} - \tilde{\mathbf{f}}_c(\mathbf{q})\right)}{\partial\mathbf{q}}\left(\mathbf{q}_n{}^{t+\alpha\Delta t}\right) + \frac{\alpha\gamma}{\beta\Delta t}\tilde{\mathbf{C}} + \frac{1}{\beta\Delta t}\tilde{\mathbf{M}} \quad . \tag{2.117}$$

v) Computation of the generalized coordinates, velocities and accelerations

The values of the generalized coordinates $\mathbf{q}_{n+1}^{t+\Delta t}$, the generalized velocities $\dot{\mathbf{q}}_{n+1}^{t+\Delta t}$ and the generalized accelerations $\ddot{\mathbf{q}}_{n+1}^{t+\Delta t}$ for the n-th Newton-Raphson iteration and for the instant $t+\Delta t$ are obtained from $\Delta\mathbf{q}_n^{t+\Delta t}$ as defined in Eqn. (2.108) to (2.110).

vi) Test of convergence

The generalized residual force $\tilde{\mathbf{r}}_{n+1}^{t+\Delta t}$ is evaluated by means of the values obtained by the Eqn. (2.108) to (2.110). The solution $\mathbf{q}_{n+1}^{t+\Delta t}$ reaches the convergence when the condition of the equation (2.111) is satisfied.

If the convergence is not reached, a new Newton-Raphson iteration is performed in order to obtain the solution for the present time instant (stages *iii* to *vi*). Once the convergence condition is fulfilled, the computation of the next time is started from stage *ii*.

Hereunder a the nonlinear Newmark and the HHT-α schemes are presented. In order to simplify the notation, a nonlinear static structure ($\Omega = 0$) ROM with the internal linear or nonlinear forces $\tilde{\mathbf{g}}(\mathbf{q})$ is considered.

Initial conditions: $\mathbf{q}_0$, $\dot{\mathbf{q}}_0$
$\ddot{\mathbf{q}}_0 = \tilde{\mathbf{M}}^{-1}\left(\tilde{\mathbf{f}}_0 - \tilde{\mathbf{C}}\,\dot{\mathbf{q}}_0 - \tilde{\mathbf{g}}\,(\mathbf{q}_0)\right)$
While $t + \Delta t \leq t_{max}$ **:**
  $\tilde{\mathbf{r}}_{n=1}^{t+\Delta t} = \tilde{\mathbf{f}}_e\,(t+\Delta t) - \tilde{\mathbf{M}}\,\ddot{\mathbf{q}}^t - \tilde{\mathbf{C}}\,\dot{\mathbf{q}}^t - \tilde{\mathbf{K}}\,\mathbf{q}^t - \tilde{\mathbf{g}}_{nl}(\mathbf{q}^t)$
  Prediction step:
    $\ddot{\mathbf{q}}_{n=1}^{t+\Delta t} = \ddot{\mathbf{q}}^t$
    $\dot{\mathbf{q}}_{n=1}^{t+\Delta t} = \dot{\mathbf{q}}^t + \Delta t\ddot{\mathbf{q}}^t$
    $\mathbf{q}_{n=1}^{t+\Delta t} = \mathbf{q}^t + \Delta t\dot{\mathbf{q}}^t + \frac{\Delta t^2}{2}\ddot{\mathbf{q}}^t$
  While $\| \tilde{\mathbf{r}}_n^{t+\Delta t} \| \geq \epsilon \| \tilde{\mathbf{r}}_{n=1}^{t+\Delta t} \|$ **:**
    Computation of the increment:
      If HHT-α:
        Predictive values:
          $\mathbf{q}_n^{t+\alpha\Delta t} = (1-\alpha)\mathbf{q}^t + \alpha\mathbf{q}_n^{t+\Delta t}$
          $\dot{\mathbf{q}}_n^{t+\alpha\Delta t} = (1-\alpha)\dot{\mathbf{q}}^t + \alpha\dot{\mathbf{q}}_n^{t+\Delta t}$
      $\tilde{\mathbf{r}}_n^{t+\Delta t} = \tilde{\mathbf{f}}_e\,(t+\Delta t) - \tilde{\mathbf{M}}\,\ddot{\mathbf{q}}_n^{t+\Delta t} - \tilde{\mathbf{C}}\,\dot{\mathbf{q}}_n^{t+\alpha\Delta t} - \tilde{\mathbf{g}}(\mathbf{q}_n^{t+\alpha\Delta t})$
      $\mathbf{J}_n = \frac{\partial\tilde{\mathbf{g}}(\mathbf{q})}{\partial\mathbf{q}}\Big|_{\mathbf{q}=\mathbf{q}_n^{t+\alpha\Delta t}} + \frac{\alpha\gamma}{\beta\Delta t}\tilde{\mathbf{C}} + \frac{1}{\beta\Delta t}\tilde{\mathbf{M}}$
      $\Delta\mathbf{q}_n^{t+\Delta t} = \mathbf{J}_n^{-1}\tilde{\mathbf{r}}_n^{t+\Delta t}$
    Compute: $\mathbf{q}_{n+1}^{t+\Delta t}$, $\dot{\mathbf{q}}_{n+1}^{t+\Delta t}$ **and** $\ddot{\mathbf{q}}_{n+1}^{t+\Delta t}$
      $\mathbf{q}_{n+1}^{t+\Delta t} = \mathbf{q}_n^{t+\Delta t} + \Delta\mathbf{q}_n^{t+\Delta t}$
      $\dot{\mathbf{q}}_{n+1}^{t+\Delta t} = \dot{\mathbf{q}}_n^{t+\Delta t} + \frac{\gamma}{\beta\Delta t}\Delta\mathbf{q}_n^{t+\Delta t}$
      $\ddot{\mathbf{q}}_{n+1}^{t+\Delta t} = \ddot{\mathbf{q}}_n^{t+\Delta t} + \frac{1}{\beta\Delta t^2}\Delta\mathbf{q}_n^{t+\Delta t}$

Algorithm 1: Newmark and HHT-α schemes algorithms.

2.7.3 Harmonic balance method

The harmonic balance method (HBM) is used to solve the dynamics steady-state forced response of nonlinear systems under periodic excitations $\mathbf{f}_e(\omega, t)$ where ω is the angular frequency of excitation. The forces and displacements are approximated by truncated Fourier series and the time dependent problem is computed in the frequency domain. This method's computational cost is generally lower than the one of the traditional time integration methods for the FEM [Newmark, 1959, Hilber et al., 1977]. The HBM is able to solve algebraic autonomous and non-autonomous differential equation systems [Belén-dez et al., 2007, Mickens, 1996, Mickens, 1984, Wu et al., 2006, Lim and Lai, 2006, Alam et al., 2007, Hosen et al., 2012].

First, the generalized coordinates, the purely nonlinear internal forces and the external excitation of the reduced equation of movement, Eqn. (2.37), are

approximated by a Fourier series truncated to N harmonics,

$$\mathbf{q}(\mathrm{t}) = \mathrm{X}_0 + \sum_{k=1}^{N} \mathrm{X}_{a_k} \cos(k\omega t) + \mathrm{X}_{b_k} \sin(k\omega t) = \mathbf{q}(\mathrm{X},\, t) \;, \quad (2.118)$$

$$\tilde{\mathbf{f}}_e\,(t) = \mathrm{F}_0 + \sum_{k=1}^{N} \mathrm{F}_{a_k} \cos(k\omega t) + \mathrm{F}_{b_k} \sin(k\omega t) = \tilde{\mathbf{f}}_e(\mathrm{F_e}, t) \;, \quad (2.119)$$

$$\tilde{\mathbf{g}}_{nl}\,(\mathbf{q}, t) = \mathrm{G}_0 + \sum_{k=1}^{N} \mathrm{G}_{a_k} \cos(k\omega t) + \mathrm{G}_{b_k} \sin(k\omega t) = \tilde{\mathbf{g}}_{nl}(\mathrm{G}_{nl}, t) \quad (2.120)$$

where N is the number of harmonics taken into consideration, X_0, F_0 and G_0 are the Fourier constant terms vectors of the generalized coordinates, external force and the purely nonlinear forces respectively , $\mathbf{X}_{a_k}$, $\mathbf{F}_{a_k}$ and $\mathbf{G}_{a_k}$ are the Fourier odd terms vectors and $\mathbf{X}_{b_k}$, $\mathbf{F}_{b_k}$ and $\mathbf{G}_{b_k}$ are the Fourier even terms vectors.

The Fourier coefficients vectors for the generalized coordinates, external excitations and the purely nonlinear forces are defined as follows,

$$\begin{aligned} \mathrm{X} &= \left[\mathrm{X}_0^T, \mathrm{X}_{a_1}^T, \mathrm{X}_{b_1}^T, \ldots, \mathrm{X}_{a_N}^T, \mathrm{X}_{b_N}^T\right]^T \\ &= \left[a_0^1, \ldots, a_0^r, a_1^1, \ldots, a_1^r, b_1^1, \ldots, b_1^r, \ldots, a_N^1, \ldots, a_N^r,\right. \\ &\quad \left. b_N^1, \ldots, b_N^r\right]^T \;, \end{aligned} \quad (2.121)$$

$$\begin{aligned} \mathrm{F}_e &= \left[\mathrm{F}_0^T, \mathrm{F}_{a_1}^T, \mathrm{F}_{b_1}^T, \ldots, \mathrm{F}_{a_N}^T, \mathrm{F}_{b_N}^T\right]^T \\ &= \left[F_0^1, \ldots, F_0^r, F_{a_1}^1, \ldots, F_{a_1}^r, F_{b_1}^1, \ldots, F_{b_1}^r, \ldots, F_{a_N}^1, \ldots, F_{a_N}^r,\right. \\ &\quad \left. F_{b_N}^1, \ldots, F_{b_N}^r\right]^T \;, \end{aligned} \quad (2.122)$$

$$\begin{aligned} \mathrm{G}_{nl}\,(\mathrm{X}) &= \left[\mathrm{G}_0^T, \mathrm{G}_{a_1}^T, \mathrm{G}_{b_1}^T, \ldots, \mathrm{G}_{a_N}^T, \mathrm{G}_{b_N}^T\right]^T \\ &= \left[G_0^1, \ldots, G_0^r, G_{a_1}^1, \ldots, G_{a_1}^r, G_{b_1}^1, \ldots, G_{b_1}^r, \ldots, G_{a_N}^1, \ldots, G_{a_N}^r,\right. \\ &\quad \left. G_{b_N}^1, \ldots, G_{b_N}^r\right]^T \;. \end{aligned} \quad (2.123)$$

The Fourier coefficients vectors X, F_e and $\mathrm{G}_{nl}(\mathrm{X})$ are obtained from the definition of the Fourier coefficients, i.e. the expression to obtain the constant, odd and even Fourier coefficients of the generalized coordinates is,

$$\mathrm{X}_0 = \frac{1}{T}\int_0^T \mathbf{q}\,\mathrm{d}t \;, \quad (2.124)$$

$$\mathrm{X}_{a_k} = \frac{2}{T}\int_0^T \mathbf{q}\cos(k\omega t)\,\mathrm{d}t \;, \quad (2.125)$$

$$\mathrm{X}_{b_k} = \frac{2}{T}\int_0^T \mathbf{q}\sin(k\omega t)\,\mathrm{d}t \;. \quad (2.126)$$

The matrix form of the generalized coordinates, external forces and the purely nonlinear forces are obtained by the use of $\mathbf{A}(\omega,\, t) = \text{diag}\,[\mathbf{I}_d, \mathbf{I}_d\, \cos(\omega t), \mathbf{I}_d\, \sin(\omega t), \ldots, \mathbf{I}_d\, \cos(N\omega t), \mathbf{I}_d\, \sin(N\omega t)]$ base matrix and the coefficient vectors defined in Eqn. (2.121) to (2.123).

$$\begin{aligned} \mathbf{q}(\mathrm{X},\, t) &= \mathbf{A}(\omega,\, t)\mathrm{X}\,, & (2.127)\\ \tilde{\mathbf{f}}_e(\mathrm{F_e}, t) &= \mathbf{A}(\omega,\, t)\mathrm{F}_e\,, & (2.128)\\ \tilde{\mathbf{g}}_{nl}(\mathrm{X}, t) &= \mathbf{A}(\omega,\, t)\mathrm{G_{nl}}(\mathrm{X}) & (2.129)\\ \tilde{\mathbf{f}}_c(\mathrm{X}, t) &= \mathbf{A}(\omega,\, t)\mathrm{F_c}(\mathrm{X})\,. & (2.130) \end{aligned}$$

The residue of the reduced order equation of motion is defined as,

$$\mathbf{r}(\mathbf{q}, t) = \tilde{\mathbf{M}}\ddot{\mathbf{q}} + \tilde{\mathbf{C}}\dot{\mathbf{q}} + \tilde{\mathbf{K}}(\mathbf{q},\, \Omega)\mathbf{q} + \tilde{\mathbf{g}}_{nl}(\mathbf{q}) - \tilde{\mathbf{f}}_c(\mathbf{q}) - \tilde{\mathbf{f}}_e(t) = 0\,. \qquad (2.131)$$

Then, substituting the expression of $\mathbf{q}$ and its time derivatives, $\tilde{\mathbf{f}}_e$ and $\tilde{\mathbf{g}}_{nl}$, the reduced order equation of motion residue becomes,

$$\mathrm{R}(\mathrm{X}, \mathrm{t}) = \mathbf{A}(\omega,\, t)\,(\mathbf{Z}(\omega)\mathrm{X} + \mathrm{G_{nl}}(\mathrm{X}) - \mathrm{F_c}(\mathrm{X}) - \mathrm{F}_e) = 0\,, \qquad (2.132)$$

where:

$$\mathbf{Z}(\omega) = \begin{bmatrix} \tilde{\mathbf{K}} & 0 & 0 & \cdots & 0 & 0 \\ 0 & \tilde{\mathbf{K}} - \omega^2\tilde{\mathbf{M}} & \omega\tilde{\mathbf{C}} & \cdots & 0 & 0 \\ 0 & -\omega\tilde{\mathbf{C}} & \tilde{\mathbf{K}} - \omega^2\tilde{\mathbf{M}} & \cdots & 0 & 0 \\ \vdots & \vdots & \vdots & \ddots & \vdots & \vdots \\ 0 & 0 & 0 & \cdots & \tilde{\mathbf{K}} - N^2\omega^2\tilde{\mathbf{M}} & N\omega\tilde{\mathbf{C}} \\ 0 & 0 & 0 & \cdots & -N\omega\tilde{\mathbf{C}} & \tilde{\mathbf{K}} - N^2\omega^2\tilde{\mathbf{M}} \end{bmatrix}_{r(2N+1)\times r(2N+1)}$$

Second, the *harmonic balance* procedure is performed. The latter consists in balancing the temporal dependence by a Galerkin procedure. Thus, Eqn. (2.132) is multiplied by the ($\frac{1}{2}$, $\cos(l\omega t)$ and $\sin(l\omega t)$ for $l = 1, \ldots, N$) trigonometrical weight functions and integrated over a period of time,

$$\frac{2}{T}\int_0^T \mathrm{R}(\mathrm{X}, \mathrm{t}) \cdot \text{weight function}\; \mathrm{d}t\,. \qquad (2.133)$$

Finally, the nonlinear algebraic equation system in the frequency domain is obtained as shown in Eqn. (2.134). The dimension of the algebraic system ($r(2N+1)$) is bigger than the initial differential equation system dimension (r). The new unknowns are the components of the generalized coordinates Fourier coefficients vector, X,

$$\mathrm{R}(\omega, \mathrm{X}) = \mathbf{Z}(\omega)\mathrm{X} + \mathrm{G_{nl}}(\mathrm{X}) - \mathrm{F}_e = 0\,. \qquad (2.134)$$

If the system conditioning and the convergence velocity are interesting, the following methods for solving the nonlinear algebraic equation systems might

be implemented: Newton-Raphson method, modified Newton method, Broyden method, fixed point method, secant method... However, the method of Newton-Raphson is widely developed and it is usually used due to its convergence and implementation properties. Then, the solution for an iteration $i+1$ is based on the values of the previous iteration i as ,

$$\mathrm{X}^{i+1} = \mathrm{X}^{i} + \Delta\mathrm{X}^{i\to i+1} = \mathrm{X}^{i} - \mathbf{J}(\omega,\ \mathrm{X}^{i})^{-1}\,\mathrm{R}(\omega,\mathrm{X}^{\mathrm{i}})\ , \tag{2.135}$$

where $\mathbf{J}(\omega,\ \mathrm{X}^{i})$ is the Jacobian matrix, $\mathrm{R}(\omega,\mathrm{X}^{\mathrm{i}})$ is the residue and $\Delta\mathrm{X}^{i\to i+1}$ is the increment of the solution and,

$$\mathbf{J}(\omega,\ \mathrm{X}^{i}) = \mathbf{Z}(\omega) + \frac{\partial \mathrm{G}_{nl}}{\partial \mathrm{X}}(\mathrm{X}^{i}) - \frac{\partial \mathrm{F}_{c}}{\partial \mathrm{X}}(\mathrm{X}^{i})\ . \tag{2.136}$$

Many engineering problems have pointed out the necessity to perform parametric studies (i.e. response of a turbine blade for different rotating velocities). If the chosen parameter is the excitation force frequency, the HBM for nonlinear systems needs the implementation of continuation methods [Sundararajan and Noah, 1997, Allgower and Georg, 2003] in order to solve the bifurcation problem. Furthermore, the HBM is also applied to contact problems in turbomachinery [Von Groll and Ewins, 2000, Petrov and Ewins, 2002, Yajie et al., 2006, Peletan, 2012, Peletan et al., 2014].

The main difficulty with the HBM is the evaluation of the Fourier vector of nonlinear forces $\mathrm{G}_{nl}(\mathbf{X})$. To this aim, two methods are presented: the AFT method and the polynomial approximation.

AFT (Alternating Frequency Time) method

The AFT (Alternating Frequency Time) method [Griffin, 1989] is useful when the expression of the nonlinear force is known in the time domain. Thus, for every Newton-Raphson iteration the generalized coordinates in the frequency domain X are brought back to the time domain by means of the inverse Fourier transform FFT^{-1} (the Fast Fourier Tansform (FFT) is an algorithm that computes the discrete Fourier transforms). Then, the nonlinear force is evaluated in the time domain and transformed back to the frequency domain using the direct FFT as shown in the Fig. 2.9.

The main advantage of the AFT method is the possibility to solve complex nonlinear forces in the time domain that do not have an analytical expression or this one is difficult to define in the frequency domain. However, due to the time-frequency domain switch and to the "every time instant" evaluation of the purely nonlinear force, the computational time performances are decreased. However, the properties of the FFT might be applied to improve the time performances of this method. Thus, it is preferable to consider at least $10N$ number of instants during the period T. The accuracy of the method

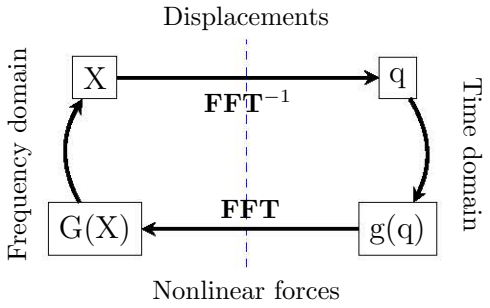

Figure 2.9: Alternating time frequency method.

has a direct relation with the highest order harmonic taken into consideration and the number of instants is preferably to be power of two, $2^m, \forall m \in \mathbb{N}$. The AFT method is widely implemented [Wang and Chen, 1992, Rook, 2002, Yajie et al., 2006, Guskov et al., 2008, Peletan, 2012, Martin and Thouverez, 2019].

In order to solve the equation (2.134) by the Newton-Raphson method, the computation of the Jacobian is needed as of two approaches are considered.

a) Direct Jacobian computation

This method evaluates the nonlinear part of the Jacobian at "every iteration" without transforming into the frequency domain the expression of the nonlinear force,

$$\mathbf{J}_{nl}(\mathrm{X}) = \frac{\partial \mathrm{G_{nl}}(\mathrm{X})}{\partial \mathrm{X}} = \overline{\mathbf{A}}(\omega,\, t)\frac{\partial \tilde{\mathbf{g}}_{nl}(\mathbf{q})}{\partial \mathbf{q}}\mathbf{A}(\omega,\, t)\ , \tag{2.137}$$

where $\mathbf{A}(\omega,\, t)$ and $\overline{\mathbf{A}}(\omega,\, t)$ are respectively the inverse and direct Fourier transformation matrices.

For this purpose, the nonlinear Jacobian matrix is computed from the derivative matrix $\frac{\partial \tilde{\mathbf{g}}_{nl}(\mathbf{q})}{\partial \mathbf{q}}$ by means of an established relation between $\frac{\partial \mathrm{G_{nl}}(\mathrm{X})}{\partial \mathrm{X}}$ and $\frac{\partial \tilde{\mathbf{g}}_{nl}(\mathbf{q})}{\partial \mathbf{q}}$.

First, from the equation (2.118) the following relations are deduced for $p = 1, \ldots, r$ and $v = 1, \ldots, N$,

$$\frac{\partial g_{nl}^p}{\partial a_0^z} = \sum_{i=1}^{r} \frac{\partial g_{nl}^p}{\partial q_i}\frac{\partial q_i}{\partial a_0^z} = \sum_{i=1}^{r} \frac{\partial g_{nl}^p}{\partial q_i}\delta_{iz} = \frac{\partial g_{nl}^p}{\partial q_z}\ , \tag{2.138}$$

$$\frac{\partial g_{nl}^p}{\partial a_v^z} = \sum_{i=1}^{r} \frac{\partial g_{nl}^p}{\partial q_i}\frac{\partial q_i}{\partial a_v^z} = \sum_{i=1}^{r} \frac{\partial g_{nl}^p}{\partial q_i}\delta_{iz}\cos(v\omega t) = \frac{\partial g_{nl}^p}{\partial q_z}\cos(v\omega t)\ , \tag{2.139}$$

$$\frac{\partial g_{nl}^p}{\partial b_v^z} = \sum_{i=1}^{r} \frac{\partial g_{nl}^p}{\partial q_i}\frac{\partial q_i}{\partial b_v^z} = \sum_{i=1}^{r} \frac{\partial g_{nl}^p}{\partial q_i}\delta_{iz}\sin(v\omega t) = \frac{\partial g_{nl}^p}{\partial q_z}\sin(v\omega t)\ . \tag{2.140}$$

Second, from the equation (2.120) the following relations are obtained for $p = 1, \ldots, r$ and $v = 1, \ldots, N$,

$$\frac{\partial g^p_{nl}}{\partial a^z_0} = \frac{\mathrm{G}^p_0(X)}{\partial a^z_0} + \sum_{k=1}^{N} \frac{\partial \mathrm{G}^p_{a_k}}{\partial a^z_0} \cos(k\omega t) + \frac{\mathrm{G}^p_{b_k}}{\partial a^z_0} \sin(k\omega t) \,, \tag{2.141}$$

$$\frac{\partial g^p_{nl}}{\partial a^z_v} = \frac{\mathrm{G}^p_0(X)}{\partial a^z_v} + \sum_{k=1}^{N} \frac{\partial \mathrm{G}^p_{a_k}}{\partial a^z_v} \cos(k\omega t) + \frac{\mathrm{G}^p_{b_k}}{\partial a^z_v} \sin(k\omega t) \,, \tag{2.142}$$

$$\frac{\partial g^p_{nl}}{\partial b^z_v} = \frac{\mathrm{G}^p_0(X)}{\partial b^z_v} + \sum_{k=1}^{N} \frac{\partial \mathrm{G}^p_{a_k}}{\partial b^z_v} \cos(k\omega t) + \frac{\mathrm{G}^p_{b_k}}{\partial b^z_v} \sin(k\omega t) \,. \tag{2.143}$$

Finally, the expression of the nonlinear Jacobian matrix is obtained from the equations (2.124) to (2.126). For $p = 1, \ldots, r$, $v = 1, \ldots, N$ and $k = 1, \ldots, N$,

$$\frac{\partial G^p_0}{\partial a^z_0} = \frac{1}{T}\int_0^T \frac{\partial g^p_{nl}}{\partial a^z_0}\,\mathrm{d}t = \frac{1}{T}\int_0^T \frac{\partial g^p_{nl}}{\partial q_z}\mathrm{d}t \,, \tag{2.144}$$

$$\frac{\partial G^p_0}{\partial a^z_v} = \frac{1}{T}\int_0^T \frac{\partial g^p_{nl}}{\partial a^z_v}\,\mathrm{d}t = \frac{1}{T}\int_0^T \frac{\partial g^p_{nl}}{\partial q_z}\cos\left(v\omega t\right)\mathrm{d}t \,, \tag{2.145}$$

$$\frac{\partial G^p_0}{\partial b^z_v} = \frac{1}{T}\int_0^T \frac{\partial g^p_{nl}}{\partial b^z_v}\,\mathrm{d}t = \frac{1}{T}\int_0^T \frac{\partial g^p_{nl}}{\partial q_z}\sin\left(v\omega t\right)\mathrm{d}t \,, \tag{2.146}$$

$$\frac{\partial G^p_{a_k}}{\partial a^z_0} = \frac{2}{T}\int_0^T \frac{\partial g^p_{nl}}{\partial a^z_0}\cos(k\omega t)\,\mathrm{d}t = \frac{2}{T}\int_0^T \frac{\partial g^p_{nl}}{\partial q_z}\cos\left(k\omega t\right)\mathrm{d}t \,, \tag{2.147}$$

$$\begin{aligned}\frac{\partial G^p_{a_k}}{\partial a^z_v} &= \frac{2}{T}\int_0^T \frac{\partial g^p_{nl}}{\partial a^z_v}\cos(k\omega t)\,\mathrm{d}t \\ &= \frac{2}{T}\int_0^T \frac{\partial g^p_{nl}}{\partial q_z}\cos\left(v\omega t\right)\cos\left(k\omega t\right)\mathrm{d}t \,,\end{aligned} \tag{2.148}$$

$$\begin{aligned}\frac{\partial G^p_{a_k}}{\partial b^z_v} &= \frac{2}{T}\int_0^T \frac{\partial g^p_{nl}}{\partial b^z_v}\cos(k\omega t)\,\mathrm{d}t \\ &= \frac{2}{T}\int_0^T \frac{\partial g^p_{nl}}{\partial q_z}\sin\left(v\omega t\right)\cos\left(k\omega t\right)\mathrm{d}t \,,\end{aligned} \tag{2.149}$$

$$\frac{\partial G^p_{b_k}}{\partial a^z_0} = \frac{2}{T}\int_0^T \frac{\partial g^p_{nl}}{\partial a^z_0}\sin(k\omega t)\,\mathrm{d}t = \frac{2}{T}\int_0^T \frac{\partial g^p_{nl}}{\partial q_z}\sin\left(k\omega t\right)\mathrm{d}t \,, \tag{2.150}$$

$$\begin{aligned}\frac{\partial G^p_{b_k}}{\partial a^z_v} &= \frac{2}{T}\int_0^T \frac{\partial g^p_{nl}}{\partial a^z_v}\sin(k\omega t)\,\mathrm{d}t \\ &= \frac{2}{T}\int_0^T \frac{\partial g^p_{nl}}{\partial q_z}\cos\left(v\omega t\right)\sin\left(k\omega t\right)\mathrm{d}t \,,\end{aligned} \tag{2.151}$$

$$\begin{aligned}\frac{\partial G^p_{b_k}}{\partial b^z_v} &= \frac{2}{T}\int_0^T \frac{\partial g^p_{nl}}{\partial b^z_v}\sin(k\omega t)\,\mathrm{d}t \\ &= \frac{2}{T}\int_0^T \frac{\partial g^p_{nl}}{\partial q_z}\sin\left(v\omega t\right)\sin\left(k\omega t\right)\mathrm{d}t \,.\end{aligned} \tag{2.152}$$

b) Modified Newton method

In order to avoid the computation of the Jacobian at "every iteration", this method considers a constant prediction matrix. The main disadvantage of this method is that the number of iterations to convergence is greater than those needed for the direct Jacobian computation and that for some cases the solution might not reach convergence. Nevertheless, this procedure is more rapid as the Jacobian is not evaluated at every iteration, thus,

$$\mathbf{J} = \mathbf{Z}(\omega) \ . \tag{2.153}$$

A hybrid method that combines the direct Jacobian computation and the modified Newton method provides the advantage of reaching convergence while the Jacobian is not computed at every iterations. The computation of the Jacobian would be triggered by a condition established previously, i.e. the value of the residue increases with respect to the previous iteration.

STEP method in the frequency domain

The polynomial form of the STEP method provides the possibility of transforming the time dependant function into a frequency dependant function by means of a Fourier series transformation of the displacements. Thus, a relation between the time dependant nonlinear stiffness coefficients and the frequency dependant stiffness coefficients is established. Furthermore, the computation of the Jacobian matrix is performed in the frequency domain which reduces the time consumption with respect to the AFT method. The particularities of this method are not numerically implemented in this work, however, the equations that define the nonlinear forces vector and the Jacobian matrix in the frequency domain are presented in the Appendix A.

2.8 Conclusions

In order to reduce the computational cost of the full order model of nonlinear structures described in chapter 1, classical reduced order models have been introduced. In this work, the projection based reduced order model technique is implemented. Thus the displacements are approximated as a linear product between a basis and the low dimensional generalised displacements, $r \ll n$. Furthermore, the linear normal modes (LNM), the POD and the component mode synthesis bases are presented. The nonlinear forces and its derivatives are represented in the reduced order model by means of the inflation or by means of the STEP methods. The classical reduced order bases are not well adapted for the study of the dynamics of slender structures. Thus, the nonlinear forces representation in the ROM leads to inaccurate solutions. In order to avoid the latter problem, an original POD based correction is proposed to filter the nonlinear forces before projecting them into the reduced space. The

computational cost of constructing a ROM for each rotating velocity could reduce the interest of using a reduced order model as it would lead to expensive ROM constructions. Thus, a parametrisation of the ROM with respect to the rotating velocity is proposed in order to reduce the computational cost of the OFFline stage and to provide a ROM capable of carrying out accurate results within a range of rotating velocities. The time response of the proposed models is obtained by means of the HHT-α or the Newmark time integration schemes or by means of the harmonic balance method (HBM) coupled with the AFT technique that evaluates the nonlinear forces in the time domain. Furthermore, the equations to compute the nonlinear stiffness coefficients of the STEP method in the frequency domain are developed in the Appendix A.

In the next chapter, the proposed ROMs are tested for two academic beam structures and for a complex structure of a fan blade. The accuracy of the proposed ROM is studied for non rotating and for rotating cases and different techniques of constructing the nonlinear forces basis are discussed. Furthermore, the solutions obtained with the HHT-α and HBM methods are discussed.

The following hypotheses are considered hereinafter:

1. With respect to the reduced order basis:
   (a) Projection based reduced order model are considered.
   (b) The projection and approximation bases are the same (Galerkin projection).
   (c) LNM, LNM+MAC, POD and Craig-Bampton basis are used.
   (d) With respect to the nonlinearities of the ROM:
      i. For geometrical nonlinearities any basis is used.
      ii. For friction contact nonlinearities only the Craig-Bampton basis is used.
2. With respect to the generalised forces:
   (a) The inflation, STEP and StepC methods are used.
   (b) Due to the time consumption of the inflation method, the use of this method is limited to a simple case.
   (c) The nonlinear forces basis is constructed in an OFFline phase:
      i. The snapshots are obtained from a FOM dynamic solution.
      ii. The snaphots are obtained from a FOM static solution.
3. With respect to the parametrisation:
   (a) The reduced order model is constructed for three rotating velocities.
   (b) The range of validity is $p_0 \leq \Omega \leq p_0 + 2\Delta p$.

4. With respect to the solution methods:
   (a) Newmark, HHT-α and HBM + AFT methods are implemented.
   (b) The stiffness coefficients of the STEP method are developed in the frequency domain (Appendix A).

Chapter 3

Numerical applications

THE REDUCED ORDER MODELS developed in the previous chapter are now evaluated for three different structures. The first structure is a thick cantilever beam that is used to highlight the necessity of the POD based correction associated with the StepC ROM. The second structure is a thin cantilever beam where its nonlinear behaviour is significant. In this application the contruction of the StepC ROM is analysed in terms of the influence of the reduced basis and the nonlinear forces basis on the solution. Furthermore, the StepC ROM is validated for a dynamic resonant case. The contact nonlinearity is also implemented for a simple case. The third structure, is a complex case study representing a fan blade developed at ONERA. Moreover, the ROM is parametrised with respect to the rotating velocity in order to reduce the construction time.

Contents

3.1 Introduction

The validity and accuracy of the reduced order models presented and developed in the previous chapter are tested in the following by means of three different slender structures submitted to static or dynamic loadings: a) a thick cantilever beam, b) a thin cantilever beam and c) a complex structure representing a fan blade.

The objective of the first application is to highlight the interest of using the StepC ROM with a POD based correction. The second structure is considered to present an optimised construction of the StepC ROM and to show that the StepC ROM can provide accurate results for different loading cases. The third structure demonstrates the validity of the StepC ROM for a complex structure with a parametrisation of the reduced basis.

3.1.1 Reminder of the theoretical methods

In this section the basic concept presented in Chapter 2 are reminded.

FOM/ROM models

The reference solution is obtained by computing the solution of the studied problem with a finite element software (Code_Aster). This solution is refereed as the **Full Order Model (FOM)** and provides a precise solution of the physical phenomena that are studied. Its computation is expensive in time.

The **Linear/Linearised reduced order model (Linear ROM)** is the classical approximation for the study of rotating structures that considers linear vibrations around the nonlinear pre-stressed equilibrium state. Thus, the geometrical nonlinearities are only due to the pre-stressed state induced by rotation.

The **Stiffness Evaluation Procedure reduced order model (STEP ROM)** is the classical STEP method [Muravyov and Rizzi, 2003] without a POD based nonlinear forces correction. The solutions obtained with this method produce spurious artefacts in the solution for the studied slender structures.

The **Stiffness Evaluation Procedure with POD based Correction reduced order model (StepC ROM)** is the original method proposed in this work that is capable of providing an improved representativity of the solution with respect to the other ROMs.

Approximation basis

The physical displacements of the structure are approximated by the linear product between the reduced basis and the generalised displacements.

The **Linear Normal Modes (LNM)** are obtained from the eigenvalue problem of the structure at a given rotating velocity.

The **Proper Orthogonal Decomposition (POD)** modes are obtained from a set of displacements that are representative of the displacements state of the structure. These snapshots are obtained from the solution of FOM computations.

The **Linear Normal Modes with Modal Assurance Criteria (LNM + MAC)** provide a judicious choice of the LNM that are representative of the structure's dynamics. It is a combination between the previous reduced bases. The MAC represents the similarity of the LNM with respect to the POD. Thus, when the MAC number is close to unity, the shape of the studied modes is almost the same. Furthermore, when the MAC number is close to zero, the modes that are compared are independent one to another. The Modal Assurance Criteria (MAC) is defined as,

$$MAC(\mathbf{POD}_i, \mathbf{\Phi}_j) = \frac{|\mathbf{POD}_i^T \mathbf{\Phi}_j|^2}{\mathbf{POD}_i^T \mathbf{POD}_i \mathbf{\Phi}_j^T \mathbf{\Phi}_j} \tag{3.1}$$

In practice, the identification of the retained LNM is carried out as follows: first, the MAC number is computed for all the combinations of the most energetic (largest eigenvalues) POD vectors and with all the LNM. Second, *the candidate LNM* are obtained by imposing a minimum MAC criteria. Third, the candidate LNM are sorted given priority to those LNM that are related to the highest energy level POD vectors. The latter procedure provides a priority between the candidate modes. Finally, the sorted candidate modes are retained up to the chosen basis size. An illustrative example is presented in Fig. 3.1 where the first 65 LNM are compared to the 30 most energetic POD vectors in order to retain the best 15 LNM to form the reduction basis.

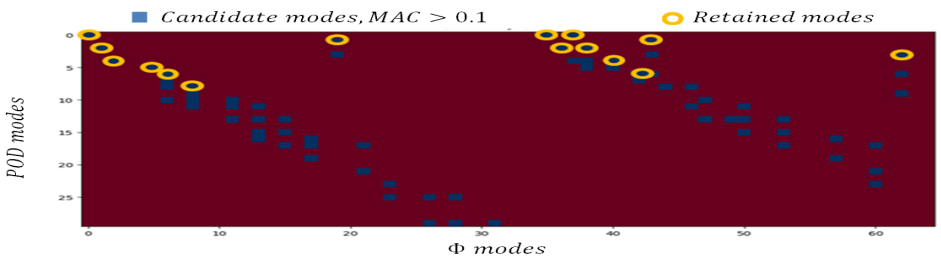

Figure 3.1: Illustrative case to present the modes selection procedure.

The **Craig-Bampton (C-B)** basis is capable of saving into the generalised coordinates some of the physical displacements of the structure. This reduced basis is used when the contact non linearity is activated.

StepC ROM

The StepC ROM is constructed in this chapter by using different reduced order bases and types of nonlinear forces snapshots. The correction is performed by means of a POD nonlinear forces basis, $\mathbf{\Phi}_f$, obtained from a series of snapshots. These snapshots are obtained here by two different type of FOM simulations, either dynamic with an harmonic forcing or static with an incremental loading. In Tab. 3.1, the different constructions of the StepC ROM used to study the behaviour of each structure of this chapter are defined in terms of the reduced order bases, the nonlinear forces basis construction techniques and the parametric basis activation.

Table 3.1: Construction elements of the StepC ROM

	Structure 1	Structure 2	Structure 3
LNM	x	x	x
LNM+MAC		x	
POD		x	
C-B		x	x
$\mathbf{\Phi}_f$ Dynamic	x	x	x
$\mathbf{\Phi}_f$ Static	x	x	
Parametric			x

Some of the questions that might be arisen when constructing the StepC ROM are presented hereunder and answered in this chapter,

1. Does the POD based forces correction improve the obtained solution regardless the reduced basis, $\mathbf{Q}$?
2. By choosing an optimal reduced basis is there any improvement in the solution by implementing the POD based forces correction?
3. How is obtained the nonlinear forces basis, $\mathbf{\Phi}_f$?
4. What are the techniques that could be used to obtain the snapshots?
5. Could the snapshots be obtained from a FOM static/dynamic solution?
6. What is the validity of, $\mathbf{\Phi}_f$, for other loading intensities, excitation frequency or rotating velocities?
7. How many vectors should be retained in the nonlinear forces basis, $\mathbf{\Phi}_f$?
8. Does the number of vectors vary with the choice of the snapshots?
9. Is the proposed correction valid for complex structures? What are the limits of the proposed correction?

3.1.2 Computational implementation of the models

The results presented in this chapter are obtained using the finite element software Code_Aster [EDF, 1989] and the programming languages Python [van Rossum, 1995] and Fortran. Code_Aster is capable of executing Python code providing an integrated environment for the FOM and the ROM. All the computations in the FOM are evaluated by means of Code_Aster commands while the ROM is coded in a python module. The computationally expensive parts of the code such as evaluating the Jacobian matrix or computing the polynomial nonlinear forces during the ONline stage (where many loops are involved) are carried out by python modules previously compiled in Fortran and translated by the F2PY program.

3.2 Structure 1: Thick cantilever beam

3.2.1 Mesh and boundary conditions

The proposed ROMs are validated for a 3D model of a rotating titanium cantilever beam ($E = 104\,GPa$, $\nu = 0.3$) of dimensions 0.4 m $\times$0.03 m $\times$0.01 m. The beam is modelled by a set of $20 \times 2 \times 1$ quadratic hexahedral (Hexa20) finite elements, Fig. 3.3.

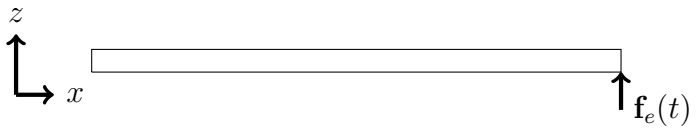

Figure 3.2: Clamped-free beam rotating around z axis.

The viscous damping is modelled by only considering the mass contribution of the classical Rayleigh damping, $\mathbf{C} = \beta_m \mathbf{M}$ where β_r is the Rayleigh damping coefficient equal to $\beta_r = 2\pi\omega_i\xi$. The external loading, $\mathbf{f}_e(t)$, is applied at every node on the tip surface of the beam in the direction of the z axis. The beam is clamped at one of its ends and rotates at a distance of $0.1\,m$ around the vertical z axis as shown in Fig. 3.2. The central node of the tip surface is used to asses the accuracy of proposed ROMs.

3.2.2 Reduced basis

The first ten mode shapes of the structure are presented in Fig. 3.4. The vertical loading leads to a bending motion coupled with a longitudinal motion of the structure, thus, modes 2, 5, 6, and 8 do not provide any additional information to the reduced basis. To improve the quality of the reduced basis one option is to substitute the latter modes by those modes that represent the vertical bending or longitudinal (Fig. 3.4j) motions of the structure as

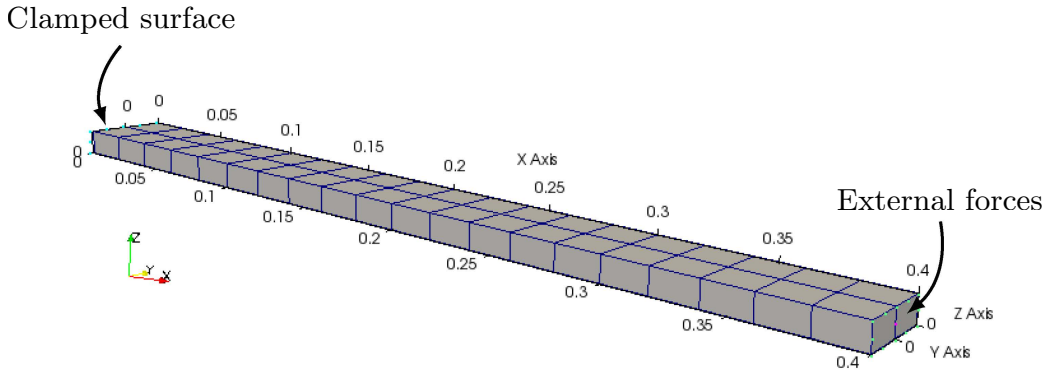

Figure 3.3: Mesh and boundary conditions of the thick beam.

they would provide additional information to the reduced basis and the ROMs accuracy would be improved.

The reduced basis is formed by the first ten LNM of the beam defined in section 2.2.1.

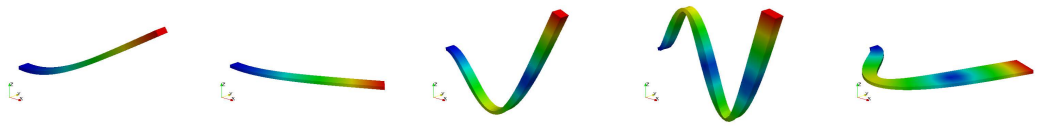

(a) Mode 1 (b) Mode 2 (c) Mode 3 (d) Mode 4 (e) Mode 5

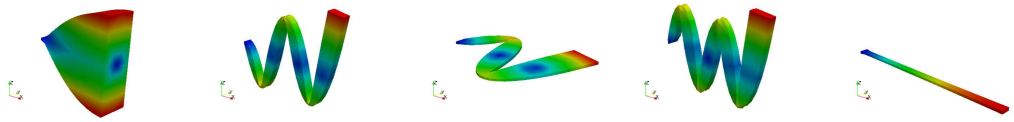

(f) Mode 6 (g) Mode 7 (h) Mode 8 (i) Mode 9 (j) Mode 10

Figure 3.4: Fist 10 linear normal modes of the structure, $\Omega = 0$ rpm.

3.2.3 Loading case 1: Out of resonance

In this loading case [Balmaseda et al., 2018] the proposed ROMs are evaluated for 20 external loading cases under an out of resonance external excitation, $\omega_e = \frac{\omega_1(\Omega=0)}{8}$ with $\omega_1(\Omega = 0) = 49.62$ Hz. Five rotating velocities, Ω, are considered (0 rpm, 1000 rpm, 2000 rpm, 3000 rpm and 4000 rpm). The last velocity corresponds to the maximum allowed Ω in orderto remain in the elastic range of the material under the effect of rotation. Furthermore, for each rotating velocity four force intensity factors, α_f, are examined

(0.1, 0.3, 0.5, 0.7) where the nominal force, f_N, is equal to 150 N. The aim of these force intensity factors is to asses the ROMs from light to intense loadings. To evaluate the static nonlinear forces in the STEP procedure and identify the nonlinear stiffness coefficients of the polynomial approximation, defined in section 2.4.2 and Eqn. (2.40), the coefficient vector used in Eqn. (2.46) to Eqn. (2.63) that is combined with the modes of the structure is $q = [0.8\,,\, 2.66{\cdot}10^{-3}\,,\, 0.13\,,\, 0.13\,,\, 0.13\,,\, 2.66{\cdot}10^{-3}\,,\, 0.13\,,\, 0.016\,,\, 8{\cdot}10^{-3}\,,\, 0.64]^T$. The external harmonic excitation is defined as,

$$\mathbf{f}_e(\mathrm{t}) = f_N \alpha_f \sin(\omega_e t) \ . \tag{3.2}$$

To highlight the need of a POD based correction, first, the accuracy of the generalised nonlinear forces obtained with the STEP and StepC ROMs is evaluated. If the nonlinear forces are accurate enough, the nonlinear displacements response should be accurate. Second, the displacements of the structure are studied in order to proof the validity of the last assumption and to asses the influence of the number of vectors retained in the nonlinear forces basis, $\mathbf{\Phi}_f$. Last, a phenomenological study of the structure's behaviour is performed in order to highlight the physical representativity of the proposed StepC ROM. Due to the thickness of the structure the nonlinear behaviour in the vertical displacements does not differ considerably from the linearised case, however, the nonlinear behaviour of the structure induces a non negligible coupling between the vertical and the longitudinal motions.

Comparison of the nonlinear generalised forces

In order to compare the nonlinear generalised forces, first, a time response is performed with the FOM and with both STEP and StepC ROMs. The nonlinear forces obtained with the FOM are projected into the reduced space by $\mathbf{\Phi}^T$. Then, for all the generalised nonlinear forces a Fast Fourier Transform (FFT) is performed in order to obtain the harmonic properties (spectrum) computed by each model. The spectrum of the generalised nonlinear forces is evaluated for the strongest force intensity, $\alpha_f = 0.7$ and at rest. The generalised nonlinear component spectra are compared in Fig. 3.5.

It is observed that for all the generalised nonlinear forces components the StepC ROM provides a more precise representation of the generalised nonlinear forces than the STEP ROM. The latter is specially highlighted in the case of the 10^{th} component (Fig. 3.5j) where the FOM and StepC models provide very similar values. The 10^{th} component is related to the longitudinal LNM, thus, the nonlinear behaviour of the structure in the longitudinal direction computed with the StepC ROM is expected to be more accurate than with the STEP ROM. Thus, to obtain an accurate solution of the response provided by the ROM, the generalised forces obtained with the ROMs and the projection by $\mathbf{\Phi}$ of the nonlinear forces of the FOM should be similar.

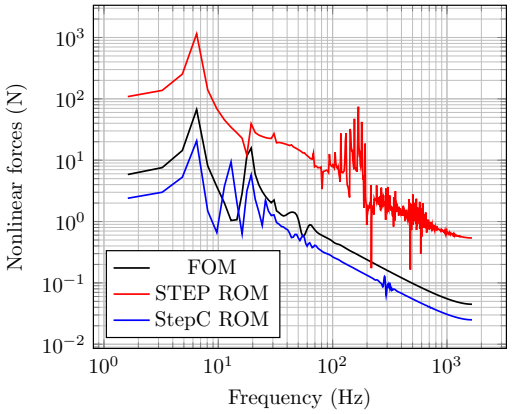

(a) Component 1 of $\tilde{\mathbf{g}}_{nl}$.

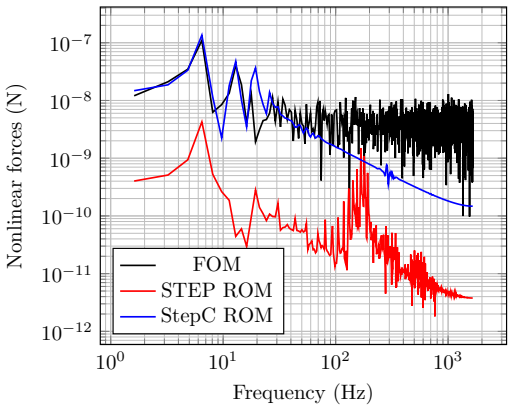

(b) Component 2 of $\tilde{\mathbf{g}}_{nl}$.

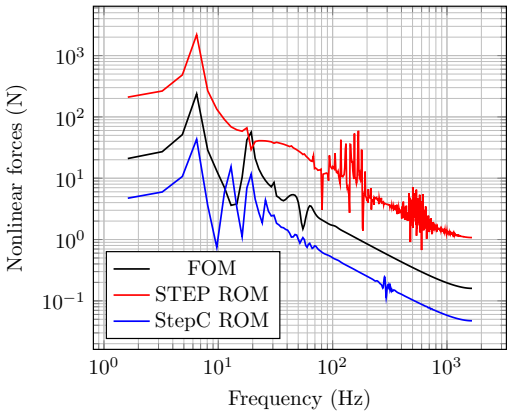

(c) Component 3 of $\tilde{\mathbf{g}}_{nl}$.

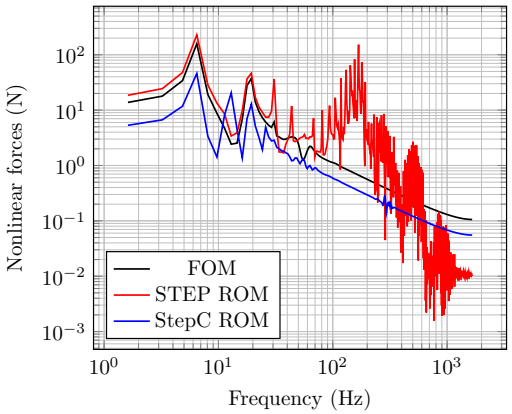

(d) Component 4 of $\tilde{\mathbf{g}}_{nl}$.

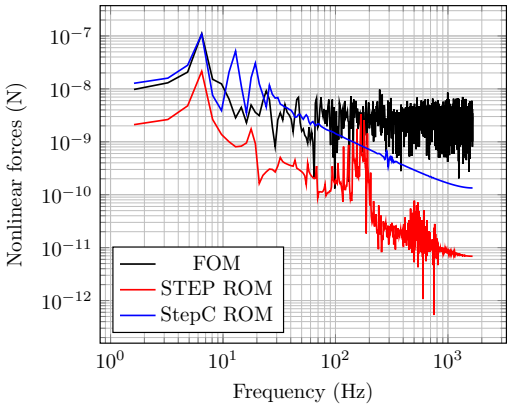

(e) Component 5 of $\tilde{\mathbf{g}}_{nl}$.

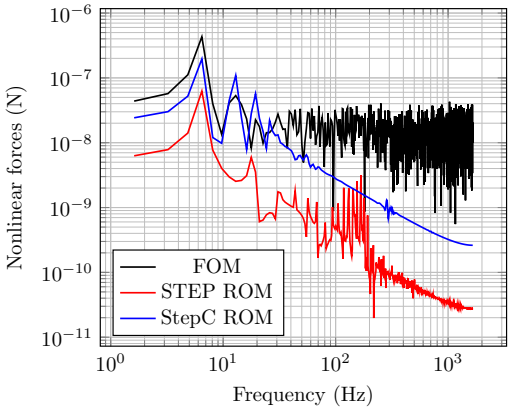

(f) Component 6 of $\tilde{\mathbf{g}}_{nl}$.

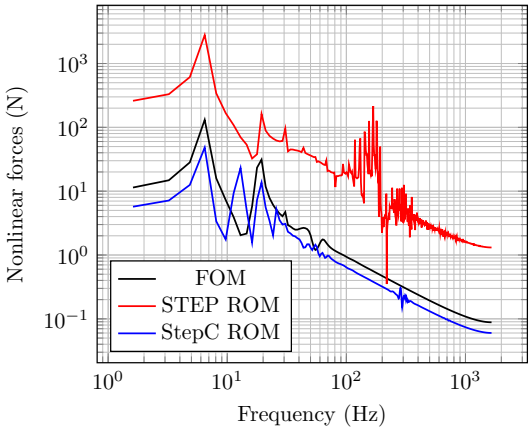

(g) Component 7 of $\tilde{\mathbf{g}}_{nl}$.

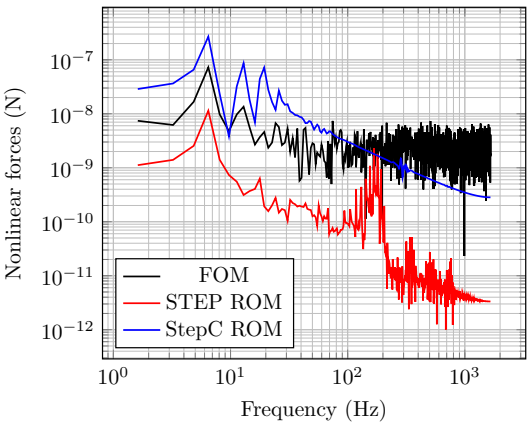

(h) Component 8 of $\tilde{\mathbf{g}}_{nl}$.

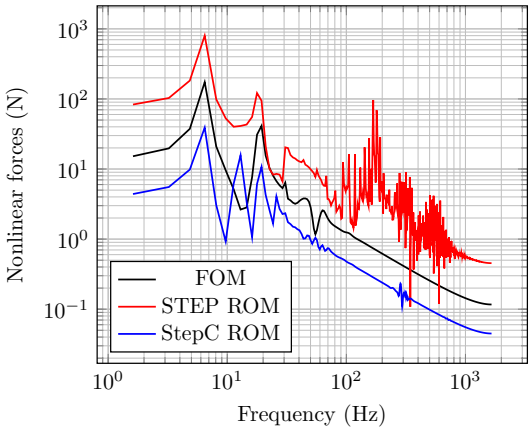

(i) Component 9 of $\tilde{\mathbf{g}}_{nl}$.

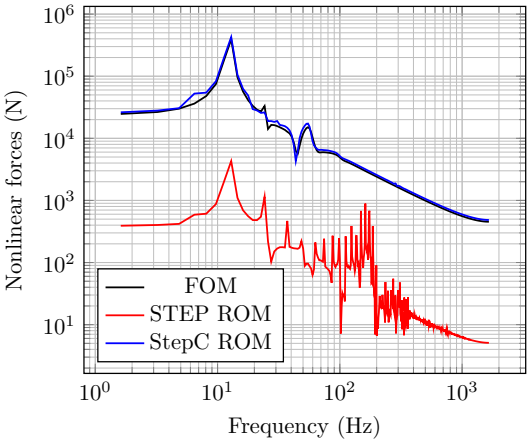

(j) Component 10 of $\tilde{\mathbf{g}}_{nl}$.

Figure 3.5: Comparison of the spectrum of the generalised nonlinear forces for $\alpha_f = 0.7$ and $\Omega = 0$ rpm.

Influence of the number of vectors in $\mathbf{\Phi}_f$

The influence of the number of vectors that form the nonlinear forces basis $\mathbf{\Phi}_f$ in the solution of the proposed Correction based ROM, defined in section 2.4.4, is studied hereunder.

The Singular Value Decomposition (SVD), Eqn. (2.76), is performed to obtain the nonlinear forces basis $\mathbf{\Phi}_f$. The latter is carried out with the snapshot matrix, $\mathbf{A}$ defined in Eqn. (2.75), obtained by computing the geometrically nonlinear FOM forces for the case with the greatest displacements for a non rotating structure, $\alpha_f = 0.7$ and $\Omega = 0\,$rpm. Thus, the computation of nonlinear forces is performed only once as it provides valid results for any loading intensity level, α_f, smaller than the loading intensity considered to construct the snapshot matrix and for any rotating velocity, Ω.

Figure 3.6b highlights the necessity to correctly asses the nonlinear forces of the ROM. When a simple projection over $\mathbf{\Phi}$ is performed to obtain the nonlinear forces, the response of the structure is stiffened, the maximum displacements of the FOM are not reached and higher order harmonics contribute to the response. When the POD based nonlinear forces correction is performed, the quality of the response directly depends on the number, m, of chosen vectors to construct $\mathbf{\Phi}_f$ as shown in Fig. 3.6a. However, there is a value of m for which the ROM accurately approaches the FOM response. In this case, the optimal value of m is 6. Its been observed that the latter value of m corresponds to an eigenvalue spectrum ratio, Eqn. (2.21), between 99.99% and 100%.

Furthermore, when $m \to m_{max}$ the StepC ROM (STEP with Correction defined in section 2.4.4) solution tends towards the response obtained with the STEP ROM (STEP without correction defined in section 2.4.2) as shown in Fig. 3.6a. Thus, the correction provides an improvement in accuracy.

In the following the nonlinear force projection matrix $\mathbf{B}^T$ (Eqn. 2.79) is constructed with the greatest loading case and with $m = 6$ as is the $\mathbf{\Phi}_f$ that provides the best results for this loading case.

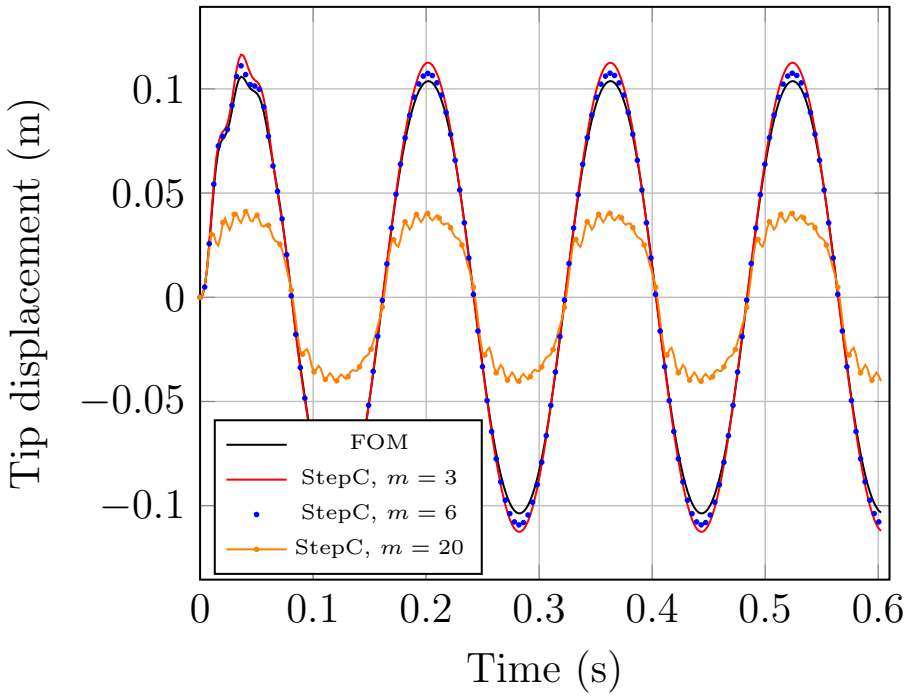

(a) Influence of m to construct $\mathbf{\Phi}_f$.

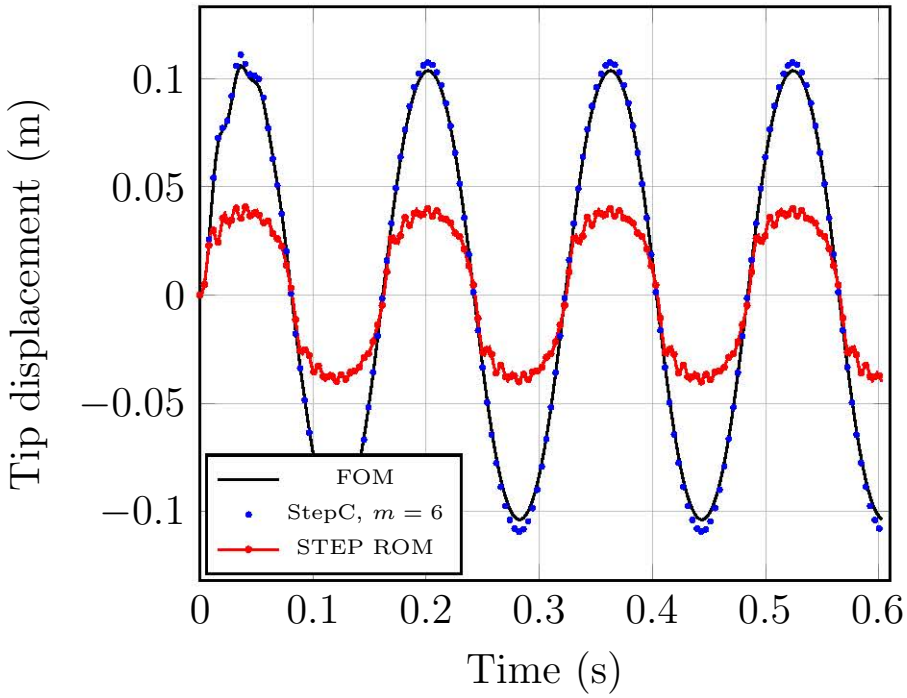

(b) StepC ROM vs. STEP ROM, $\alpha_f = 0.7$.

Figure 3.6: Influence of the POD based correction of nonlinear forces on the time response displacements at the tip of the rotating beam for $\Omega = 0$ rpm.

Solution for different values of force intensity and rotating velocity

The dynamic response of the structure is computed by the solution methods presented in section 2.7: (i) the HHT-α method and (ii) the HBM-AFT method. As the results obtained with both methods are equivalent , only the time response computed by the HHT-α method are presented here. Figure 3.7 shows the vertical displacement of the central node of the tip surface for different loading intensities and at rest and at 2000 rpm rotating velocity.

The inflation method for computing the generalised nonlinear forces gives almost the same results as the STEP ROM or the StepC ROM depending on the activation or not of the POD based nolinear forces correction.

Both Linear ROM and StepC ROMs provide an accurate response when the loading intensity is small. Furthermore, at rest, $\Omega = 0$ rpm, StepC ROM provides better results for high loading intensities. For a rotating velocity equal to $\Omega = 2000$ rpm, both methods provide similar results for vertical displacements for all the loading intensities. However, the StepC ROM is capable of reproducing the coupling between the longitudinal and vertical motions. Furthermore, when nonlinearities due to the external force are *negligible* with respect to the rotating effects, both methods provide accurate responses.

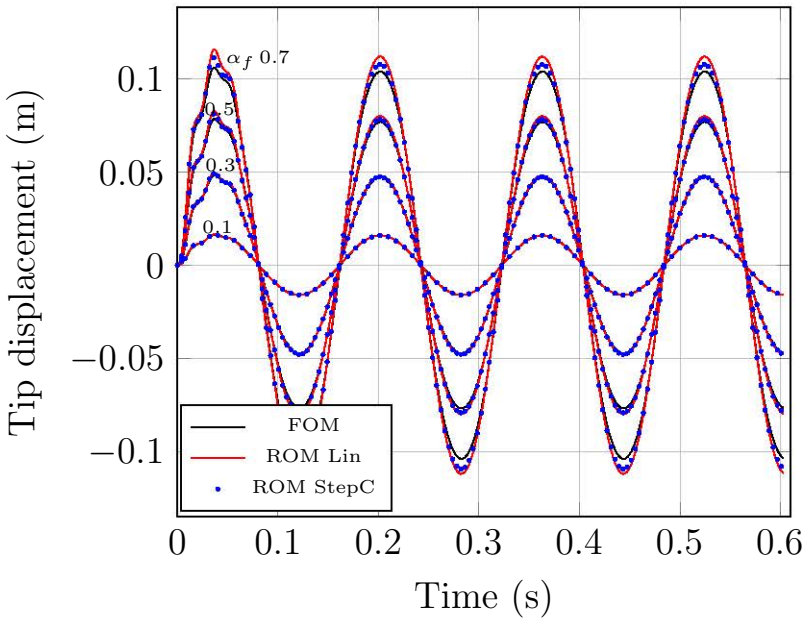

(a) Time response for different loading levels without rotating velocity, $\Omega = 0$ rpm.

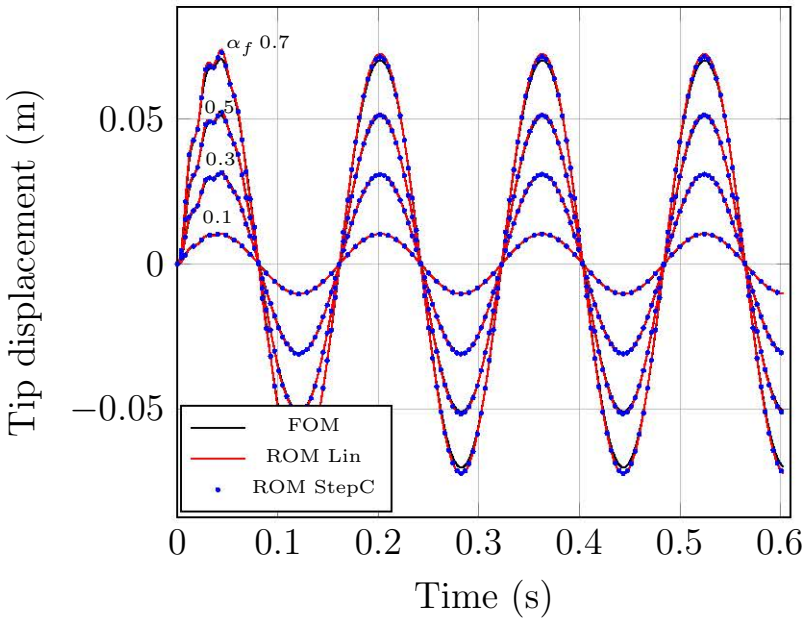

(b) Time response for different loading levels with constant rotating velocity, $\Omega = 2000$ rpm.

Figure 3.7: Tip displacements time response for a harmonic excitation.

Accuracy and computational time consumption

In order to asses the accuracy of the StepC ROM and of the Linear ROM, the time average relative error with respect to the FOM solution is performed

for all the loading cases and solution methods at each degree of freedom of the structure,

$$e_r(\%) = \frac{1}{n_t} \sum_{i=0}^{n_t} \frac{\|\mathbf{u}_{ROM}(t_i) - \mathbf{u}_{FOM}(t_i)\|}{\|\mathbf{u}_{FOM}(t_i)\|} \cdot 100 \ . \tag{3.3}$$

The relative error for the HHT-α is computed considering all the time steps of the response. However, the relative error of the HBM method is computed for a single period once the steady state of the FOM is attempt. For the HBM, the solution is compared such that the solutions are in phase.

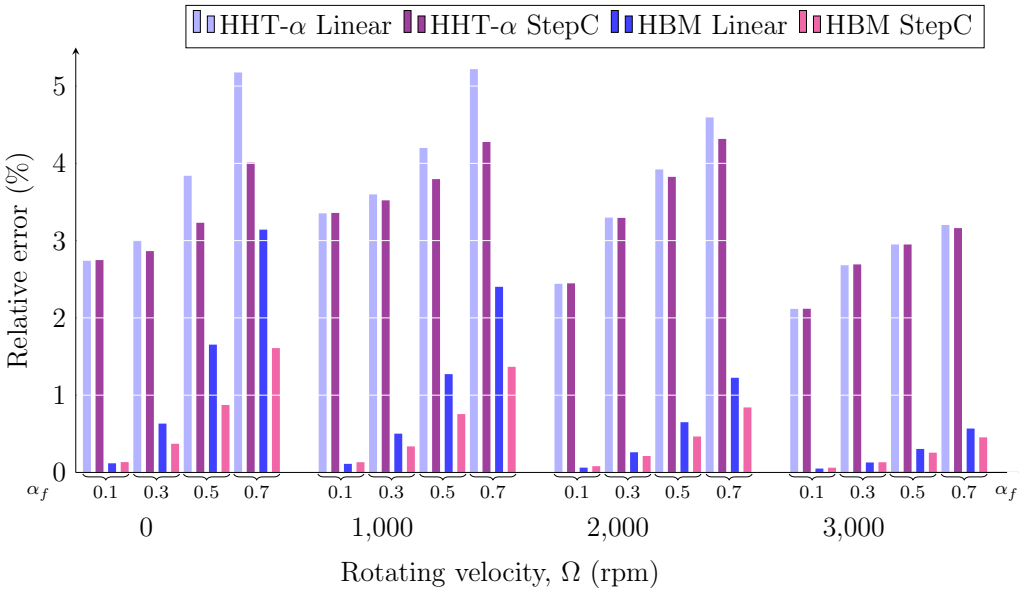

Figure 3.8: Comparative chart that presents the relative error with respect to different rotating velocities, loading intensities and time integration methods.

As shown in Fig. 3.8, for all the considered loading intensities and rotating velocities, the StepC ROM provides more precise results than the Linear ROM. However, for small loading intensities and high rotating velocities, both ROMs provide accurate results with respect to the FOM solution taken as reference. The latter is specially highlighted in the HBM results. Thus, the proposed StepC ROM is valid here for any external loading intensity and for any rotating velocity.

Time performances

As shown in Tab. 3.2 both ROMs have a similar ONline computational cost equivalent to the $\approx 3\%$ of the time to carry out a FOM computation. The construction of the StepC ROM is more expensive than the construction of the Linear ROM, however, the improved accuracy of the StepC ROM justifies the additional cost of the proposed ROM.

Table 3.2: Computational cost in seconds for a single simulation with 3000 time steps, $\Omega = 0\,\text{rpm}$ and $\alpha_f = 0.7$.

	FOM	Linear	t_{FOM}/t_{Lin}	StepC	t_{FOM}/t_{StepC}
HHT-α	1147.18	34.76	33	53.76	21
HBM	-	24.48	47	32.09	36

Physical representation of the structure's behaviour

In this section, the objective is to asses if by means of the POD based nonlinear forces correction, the ROM is capable of reproducing the vertical and the longitudinal coupling induced by the nonlinear behaviour of the structure. The geometrically nonlinear FOM presents a longitudinal coupling when bending occurs. If the structure behaves linearly, the latter effect does not take place and both movements are independent (uncoupled).

Hereunder, the $\alpha_f = 0.3$ and $\alpha_f = 0.7$ cases are studied. The computation is carried out for 2000 time steps between the initial time, $t_i = 0$, and the final time, $t_f = 0.604$ s. The HHT-α integration method is used to compute the forced time response of the structure. Figure 3.9a and 3.9b represent the displacement of the ROMs in the longitudinal and vertical directions. The StepC ROM provides longitudinal displacements that are of the same order of magnitude as the FOM longitudinal displacements. Furthermore, the vertical displacements are slightly more accurate than the linearised case. However, the maximum values of vertical displacements obtained with the StepC ROM are similar to those of the linear ROM, while for the minimum vertical displacements values the StepC ROM provides better results.

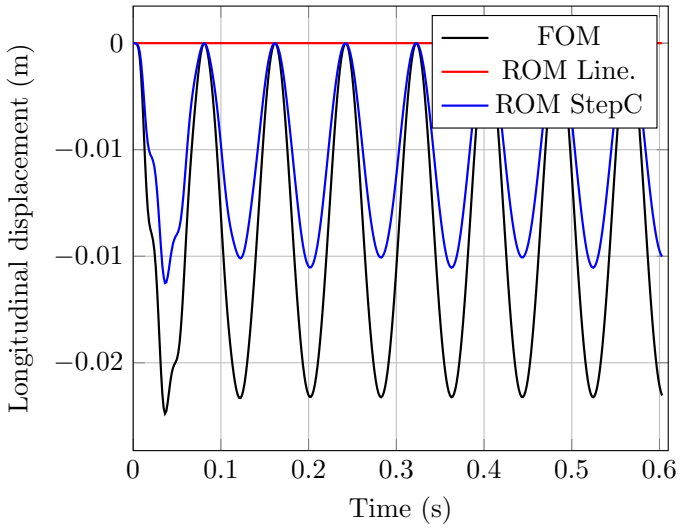

(a) Longitudinal displacements of the tip of the beam.

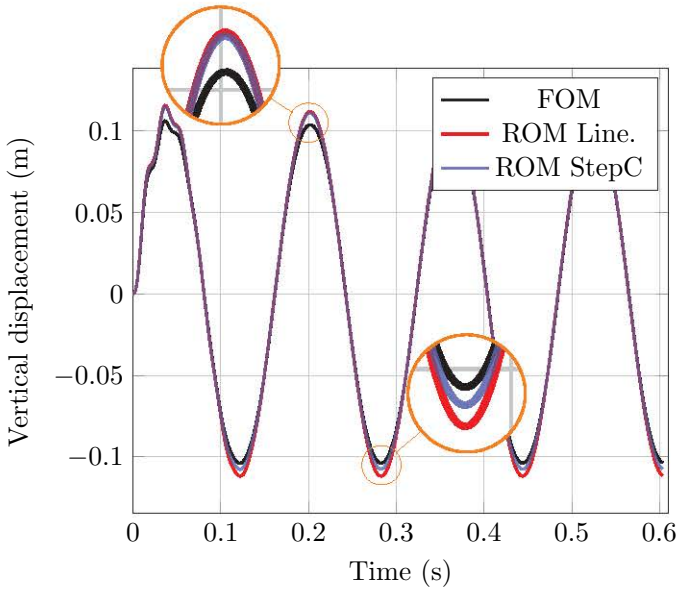

(b) Vertical displacements of the tip of the beam.

Figure 3.9: Displacements time response in x and z directions and their corresponding spectrum.

The behaviour of the tip node is represented in Fig. 3.10 where the vertical displacements are plotted vs. the longitudinal displacements for different loading intensities. Even if the longitudinal behaviour is not fully represented, the StepC ROM provides more representative results than the Linear ROM as it is able to reproduce the coupled behaviour of the structure. For all the presented solutions one single force basis, $\mathbf{\Phi}_f$, is used. The latter is computed for a loading intensity, $\alpha_f = 0.7$, and for a non rotating structure, $\Omega = 0$ rpm. The same $\mathbf{\Phi}_f$ is considered later for the case where the structure rotates at $\Omega = 4000$ rpm.

When the structure rotates, the effect of rotation reduces the influence of the external loadings on the behaviour of the structure. As shown in Fig. 3.11, for a rotating velocity, $\Omega = 4000$ rpm, and a loading intensity, $\alpha_f = 0.7$, the StepC model provides more accurate responses than the Linear ROM, specially in the longitudinal direction, but as the overall behaviour of the structure due to the external loading is closer to linearity, the Linear ROM also provides an accurate solution to the FOM displacements in the vertical direction.

Thus, the proposed StepC ROM is able to reproduce the nonlinear coupling between the vertical and the longitudinal motions of the structure for both studied rotating velocities providing a better physical representation of the structure's behaviour than with the classical ROMs.

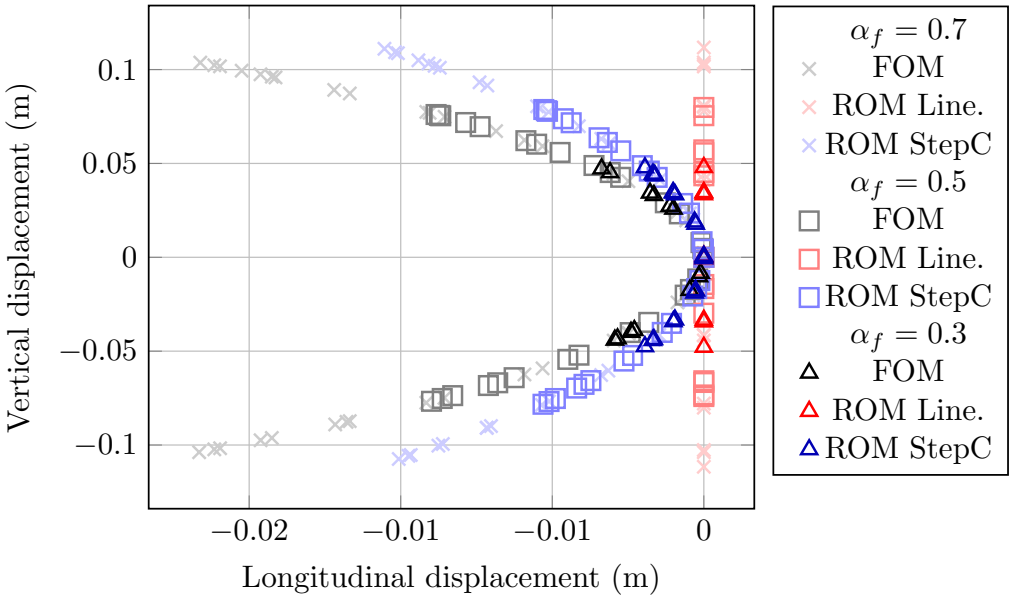

Figure 3.10: Longitudinal versus vertical displacements of the tip of the beam for different loading intensities, $\Omega = 0$ rpm..

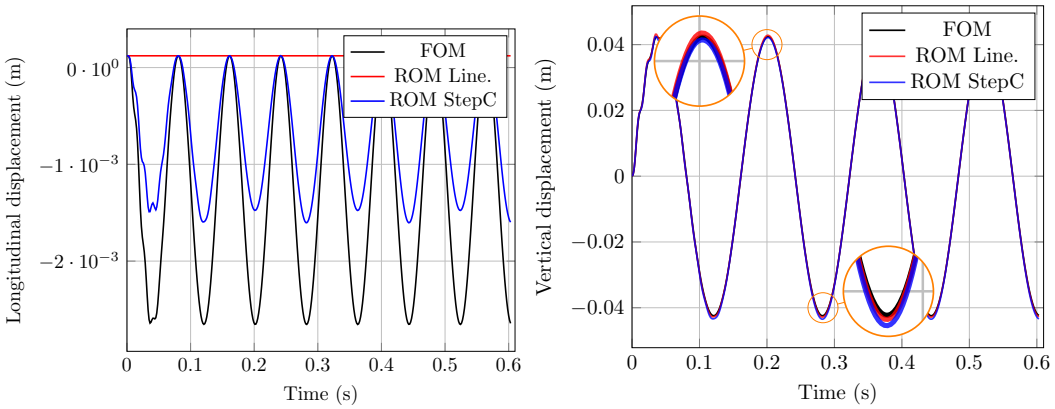

(a) Longitudinal displacements.

(b) Vertical displacements.

Figure 3.11: Displacements of the tip of the beam for a rotating velocity $\Omega = 4000$ rpm.

Error estimation and computational time

To compare the ROMs accuracy, the Root Mean Squares Error (RMSE) is computed. As the time solutions between models can present a time shift, the RMSE error is computed in the frequency domain. The error is evaluated only for the periodic regime without considering the transient dynamic solution. Thus, before computing the RMSE, a Fast Fourier Transform (FFT) is performed to the periodic solution in order to compute the error in the frequency domain. Then the RMSE_{dof}, error of each degree of freedom of the structure,

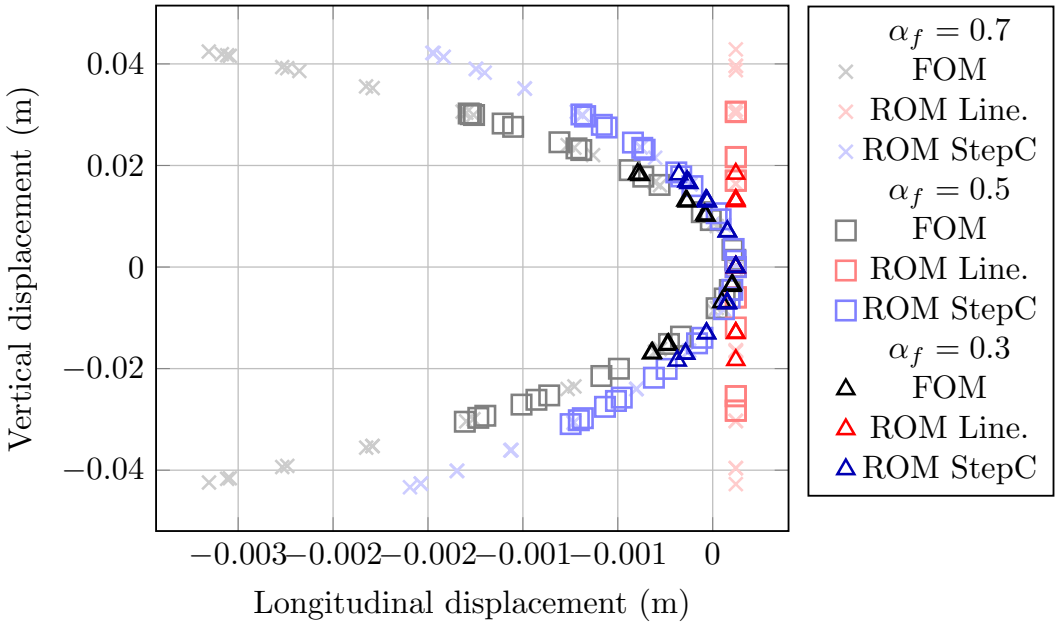

Figure 3.12: Longitudinal and/vs. vertical displacements of the tip of the beam for a rotating velocity $\Omega = 4000$ rpm.

is computed as,

$$RMSE_{dof} = \sqrt{\frac{1}{n_{freq}} \sum_{\omega=\omega_i}^{\omega_f} \left(\mathbf{U}_{ROM}(\omega) - \mathbf{U}_{FOM}(\omega)\right)^2}\,, \tag{3.4}$$

and the module of the RMSE error related to each node is computed with,

$$RMSE_i = \sqrt{RMSE_x^2 + RMSE_y^2 + RMSE_z^2}\,, \tag{3.5}$$

note that the computed error is not a relative value and that represents the square of error averaged in time.

Table 3.3 presents the maximum RMSE for the Linear ROM, StepC ROM and the Inflation ROM. The results obtained with the StepC ROM are more accurate than the Linear ROM for all the considered cases and the inflation method provides similar results with respect to the StepC ROM. When the rotating velocity increases, the overall error of all the models is reduced. Furthermore, when the effects of external loadings are not significant compared to the rotating inertial effects, the StepC ROM provides more accurate results than the Linear ROM, up to 2.3 times more accurate. The inflation method provides almost the same results as the StepC ROM. However, the time consumption is extremely expensive.

The ONline computational time of the Linear ROM, of the StepC ROM and of the FOM is compared in Tab. 3.4. The reduced order models have the same

Table 3.3: Maximum Root Mean Square Error (RMSE) for the periodic displacements of the thick beam for an excitation frequency $\omega_e = 6.12$ Hz and a nominal force of $f_n = 150$ N at each node.

$\Omega = 0$ rpm		
Force intensity	Linear ROM (10^-5)	StepC ROM (10^-5)
$\alpha_f = 0.3$	15.10	6.55
$\alpha_f = 0.5$	41.41	18.07
$\alpha_f = 0.7$	79.70	35.25
$\Omega = 1000$ rpm		
Force intensity	Linear ROM (10^-5)	StepC ROM (10^-5)
$\alpha_f = 0.3$	10.69	4.72
$\alpha_f = 0.5$	29.71	12.95
$\alpha_f = 0.7$	57.63	25.04
$\Omega = 2000$ rpm		
Force intensity	Linear ROM (10^-5)	StepC ROM (10^-5)
$\alpha_f = 0.3$	4.47	2.36
$\alpha_f = 0.5$	13.58	6.48
$\alpha_f = 0.7$	27.10	12.57
$\Omega = 3000$ rpm		
Force intensity	Linear ROM (10^-5)	StepC ROM (10^-5)
$\alpha_f = 0.3$	1.18	1.09
$\alpha_f = 0.5$	4.82	3.06
$\alpha_f = 0.7$	10.77	5.98
$\Omega = 4000$ rpm		
Force intensity	Linear ROM (10^-5)	StepC ROM (10^-5)
$\alpha_f = 0.3$	1.05	0.55
$\alpha_f = 0.5$	1.65	1.43
$\alpha_f = 0.7$	3.51	2.94

order of magnitude in terms of ONline computational time. The StepC ROM provides more precise results but its OFFline computational time is greater than the one of the Linear ROM. However, the latter cost is mainly due to the construction of the nonlinear forces basis as a FOM computation is performed

in order to construct the snapshots matrix. However, a single computation of the nonlinear forces basis, $\mathbf{\Phi}_f$, allows computations for different rotating velocities and for smaller loading intensities.

Table 3.4: Online computation time comparison between the FOM, the Linear ROM and the StepC ROM. Loading conditions: $\alpha_f = 0.7$, $\Omega = 0$ rpm.

Integration method	FOM	Linear ROM	t_{FOM}/t_{Lin}	StepC ROM	t_{FOM}/t_{StepC}
HHT-α	5916 s	11.35 s	521.23	16.10 s	367.45

3.2.4 Loading case 2: First mode resonance

With the second loading case the capacity of the ROMs to reproduce the dynamic response at first mode linear in resonance is evaluated. Thus the excitation frequency corresponds to $\omega_e = \omega_1(\Omega)$. The ROMs are evaluated for four rotating velocities $\Omega \in (0\text{rpm}, 1000\text{rpm}, 2000\text{rpm}, 3000\text{rpm}$ and $4000\text{rpm})$. In this numerical application only the loading intensity $\alpha_f = 0.7$ is considered and the stiffness coefficients vector is the same as the one chosen in the previous application.

When a structure is excited at resonance, small excitation forces might result in very large displacements of the structure. Thus, the study of the response at resonance of different modes is vital for design purposes. In the present loading case, just the first bending mode resonance is considered. The value of the natural frequency depends on the rotating velocity. Thus, in order to excite the structure at the linear resonance, for every new rotating velocity, the exciting frequency is adapted to match the resonance frequency. In nonlinear dynamics, the maximum value of the resonant response is not ensured to be at the linearised natural frequency, however, at this frequency the structure is usually overexcited, see section 2.4.1. The study of the nonlinear resonance is out of the scope of the present application. However, to study the nonlinear resonance behaviour of the structure, when the exciting frequency varies, continuation techniques might be applied.

For the forced response submitted to the resonant loading, 8000 time steps are considered between the initial time, $t_i = 0$, and the final time, $t_f = 30/\omega_1(\Omega)$ s. The HHT-α integration method is used to compute the forced response of the structure. For the resonant case, the maximum loading case defined by $f_N = 30$ N and $\alpha_f = 0.7$ is considered. Figure 3.13 represents the displacement of the ROMs in the vertical and longitudinal directions for two rotating velocities, 0 rpm and 3000 rpm. The StepC ROM provides a longitudinal response of the same order of magnitude as the FOM longitudi-

nal displacements and its vertical displacements are more accurate than the linearised case for the non rotating case.

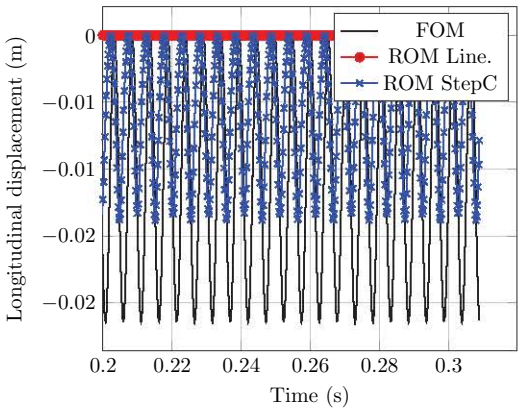

(a) Longitudinal resonant displacements of the tip of the beam, $\Omega = 0$ rpm.

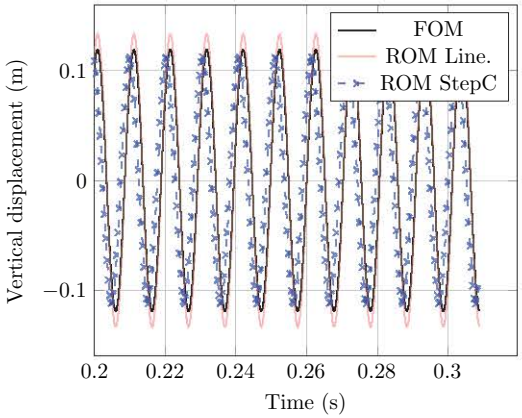

(b) Vertical resonant displacements of the tip of the beam, $\Omega = 0$ rpm.

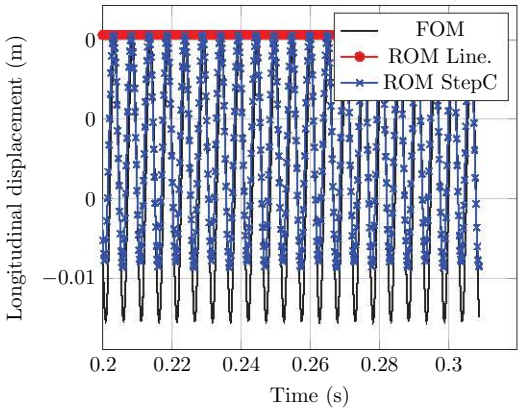

(c) Longitudinal resonant displacements of the tip of the beam, , $\Omega = 3000$ rpm.

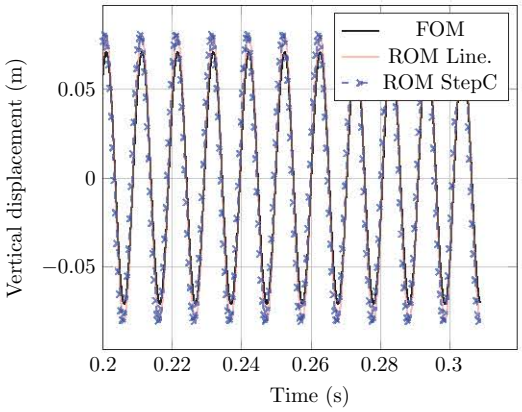

(d) Vertical resonant displacements of the tip of the beam, $\Omega = 3000$ rpm.

Figure 3.13: Periodic time response displacement in x and z directions without rotation and with $\Omega = 3000$ rpm.

Error estimation and computational time

Table 3.5 presents the maximum RMSE for the Linear ROM and StepC ROM. The results obtained with the StepC nonlinear model are more accurate for low rotating velocities and tend to obtain similar results to those given by the Linear ROM for high rotating velocities. However, these solutions are carried out considering that $\mathbf{\Phi}_f$ is not adapted to the frequency change. Thus, a parametrised $\mathbf{\Phi}_f$ might provide improved results. Even when the computational error becomes similar, the StepC ROM is capable to reproduce the longitudinal displacements. Thus, the StepC ROM is capable of providing the physical representation of the coupling between the bending and longitudinal

motions.

Table 3.5: Maximum Root Mean Square Error for the periodic displacements of the thick beam, a resonant excitation frequency and a nominal force at each node of $f_N = 30$ N.

$\mathbf{\Phi}_f$: modes 1 and 3				
Rotating velocity Ω (rpm)	Excitation frequency $\omega_e = \omega_0(\Omega)$ (Hz)	Linear ROM (10^{-5})	StepC ROM (10^{-5})	$\frac{\text{RMSE}_{\text{Lin}}}{\text{RMSE}_{\text{StepC}}}$
0	49.62	61.48	36.02	1.71
1000	53.90	52.53	22.49	2.33
2000	65.01	37.41	18.02	2.08
3000	80.04	26.93	21.10	1.28
4000	97.08	21.14	19.13	1.10

The ONline computational time of the Linear ROM and the StepC ROM is compared in Table 3.6 with respect to the computational time of the FOM. Similar conclusions to those presented in the previous case might be arisen from the study of the OFFline stage computational time.

Table 3.6: Online computation time comparison between the FOM, the Linear ROM and the StepC ROM. Loading conditions: Resonance, $\alpha_f = 0.7$, $\Omega = 0$ rpm.

Integration method	FOM	Linear ROM	t_{FOM}/t_{Lin}	StepC ROM	t_{FOM}/t_{StepC}
HHT-α	29481 s	39 s	755.92	84 s	350.96

3.2.5 Discussion and feedback

The main conclusions that are arisen from the study of the thick cantilever structure are:

1. The StepC with the POD based correction provides an improved representativity of the nonlinear coupling between the motions of the structure.

2. The StepC with the POD based correction avoids the spurious artefacts observed with the STEP ROM solution.

3. The construction of $\mathbf{\Phi}_f$ and the number of vectors is crucial to represent the behaviour of the structure.

4. The StepC ROM provides more accurate solutions than the Linear ROM and than the STEP ROM.

5. The proposed POD based correction is valid for both resonant and out of resonance excitation frequencies.

6. When the structure behaves linearly both StepC and Linear ROMs provide similar results.

With this application, the interest of implementing the POD based correction is highlighted. However, the construction of the nonlinear forces basis $\mathbf{\Phi}_f$ might be very expensive for complex structures. Furthermore, even if the coupled motion is represented and the proposed ROM represents the best accuracy performances between the studied ROMs, the longitudinal displacements are not accurate enough. As discussed in section 3.2.2 some of the modes that form the reduced basis do not provide any information to the studied motion, thus an improvement of the reduced basis would lead to a better representativity of the structure's behaviour. In addition, a deep study of the nonlinear forces and its construction would lead to an optimised nonlinear forces basis, with a reduced construction time and easier calibration.

The difference between the linear and nonlinear behaviour of the structure is not significant within the elastic displacements range of the studied thick cantilever beam. Thus, in order to validate the proposed method to highly nonlinear cases, in the next section, an application to a thin cantilever beam where the vertical displacements are significantly nonlinear is considered. Furthermore, the influence in accuracy of the chosen reduced basis and of the nonlinear forces basis is discussed.

3.3 Structure 2: Thin cantilever beam

3.3.1 Mesh and boundary conditions

In the present section, the proposed ROM is evaluated for a thin beam structure. The main objective is to show that the proposed StepC ROM provides the best compromise between the computational time and the accuracy of the model and that it improves the results obtained with the Linear ROM and with the STEP ROM. Furthermore, the influence of the reduced basis and the construction of the nonlinear forces basis is discussed. The chosen structure is widely studied in literature [Powell, 1969, Thomas et al., 2016, Beley et al., 2017] to develop analytical formulations and to study its behaviour using beam type Finite Elements. It is recalled here that when the finite element model is formed by three dimensional elements, thin structures are submitted to the risk of presenting shear locking effects.

This structure is the clamped-free thin cantilever beam shown in Fig. 3.14, of dimensions $1\,\mathrm{m} \times 0.1\,\mathrm{m} \times 0.005\,\mathrm{m}$ rotating around the z axis. The distance between the rotating axis and the clamped end of the beam is $b = 0.1\,\mathrm{m}$.

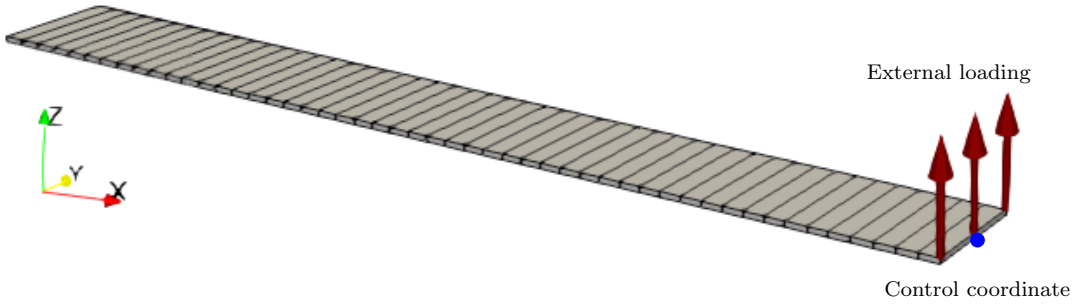

Figure 3.14: Mesh and boundary conditions of the thin beam.

The finite element mesh is formed by 50 hexahedral quadratic elements and 608 nodes. The first end of the beam (the closest to the rotating axis) is clamped and the external loadings are applied at every node of the second end. The maximum rotating velocity before plastic deformations appear is $\Omega_{max} =$ 3000 rpm. The material is a Titanium-Aluminium (TiAl) alloy with 104 GPa Young's Modulus, 0.34 Poisson's Ratio, 4400 $\mathrm{Kg/m^3}$ density, 1% damping ratio and 828 MPa Yield strength [Cardarelli, 2000]. A Rayleigh damping is considered to model the structural viscous damping, $\mathbf{C} = \beta_m\ \mathbf{M} = 2\xi\omega_0\mathbf{M}$. The time responses provided by the ROMs are studied at the control coordinate (highlighted in Fig. 3.14) as it is one of the regions where the geometrically nonlinear effects are expected.

The external force applied at each node, $\mathbf{f}_e(\mathrm{t})$, is defined as a linear product between an intensity factor, α_f, a nominal force,f_N, and a time dependant function where the direction of the forces is considered as parallel to the z axis,

$$\mathbf{f}_e(\mathrm{t}) = f_N \alpha_f f(t)\ , \tag{3.6}$$

where $f(t)$ is a time dependant loading function that defines the loading case.

Two different loading functions are considered: the first loading case corresponds to an incremental static loading formed by a ramp function from $t_0 = 0\,s$ to $t_f = 200\,s$ with a force that varies linearly between 0% and 100% of the nominal force, f_N, times the loading coefficient α_f. The ramp is subdivided into 5000 increments in order to obtain a significant number of force snapshots, thus, the loading function is, $f(t) = t_f^{-1} t$. The second loading function is a sinusoidal loading that excites the rotating structure at the frequency corresponding to the first mode resonance, $f(t) = \sin(\omega_e t)$ with $\omega_e = \omega_1(\Omega)$.

3.3.2 Linear normal modes of the structure

The first ten linear normal modes of the thin beam are presented hereunder.

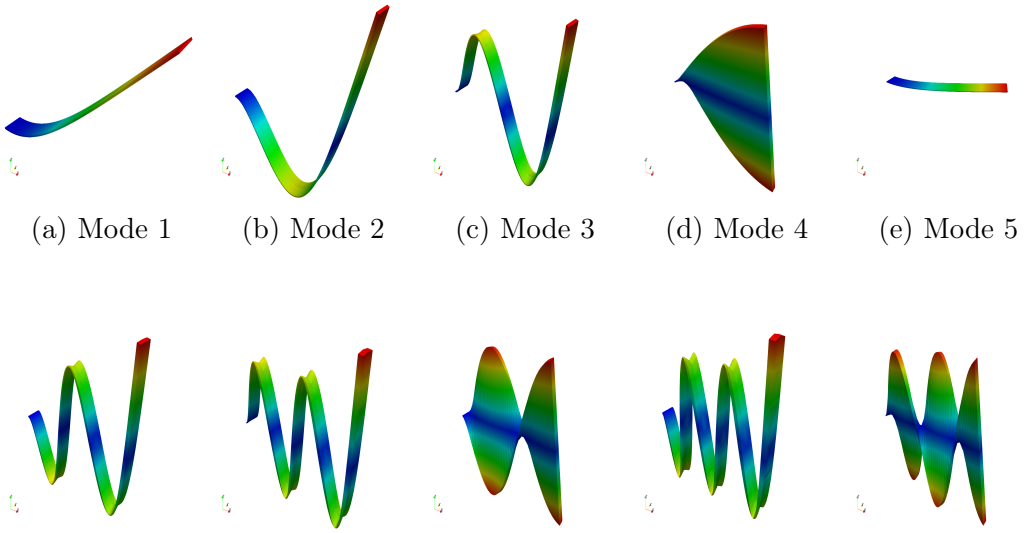

(a) Mode 1 (b) Mode 2 (c) Mode 3 (d) Mode 4 (e) Mode 5

(f) Mode 6 (g) Mode 7 (h) Mode 8 (i) Mode 9 (j) Mode 10

Figure 3.15: Fist 10 linear normal modes of the structure, $\Omega = 0$ rpm.

It is worth mentioning that in this reduced basis there are no modes that represent the longitudinal displacements of the structure, thus, by only using the first LNM the obtained results would not be representative of the longitudinal motion of the structure.

3.3.3 Influence of the coefficient vector q in the STEP procedure

The stiffness coefficients of STEP are obtained by the identification of the static forces induced by a given number of imposed displacements. These displacements are a combination of the modes of the reduced basis as shown in section 2.4.2 (i.e. for one mode combination $\mathbf{u}_1^p = \phi_p q_p$, where ϕ_p is the p-th mode of the basis and q_p is a loading factor related to the p-th modal coordinate). In the following, the same value $q_p = 0.3$ is chosen for all the nodal components as it represents the average displacement expected for the vertical solution. An analysis to determine if the chosen value of q_p influences the solution accuracy was carried out arising the following remarks:

1. Imposed hypothesis and constraints of the study:

   (a) For all the studied values of $\mathbf{q}$, all the vector components q_p were supposed to be the same.

(b) Five different values of q_p were proposed (1, 0.3, 0.03, 0.003, 0.0003).

(c) The accuracy of the solutions was studied with respect to the FOM solution considering that the reduction and the nonlinear forces bases were not modified.

2. Arisen observations:

(a) The STEP identification was impossible due to lack of convergence for values of $q_p > 1$.

(b) The results remained unchanged for values of q_p between the range $1 > q_p > 0.003$.

(c) For values under $0.0003 > q_p$ the response is modified and depends on the value of q_p which leads to a difficult identification of q_p and the solution is dependant of q_p's value.

(d) Thus, the value of q_p is chosen in order to satisfy the expected order of magnitude of the largest displacements of the structure.

3.3.4 Construction of the nonlinear forces basis, $\mathbf{\Phi}_f$

In this section the construction of the nonlinear forces basis $\mathbf{\Phi}_f$ is discussed.

To build the StepC ROM, the computation of a nonlinear forces basis that is representative of the structure nonlinear forces is needed. Figure 3.16 shows the maximum purely nonlinear forces of the structure for the loading case 1. Thus, the nonlinear forces basis, $\mathbf{\Phi}_f$ should be formed of those force vectors whose shape is representative of the nonlinear force states of the structure.

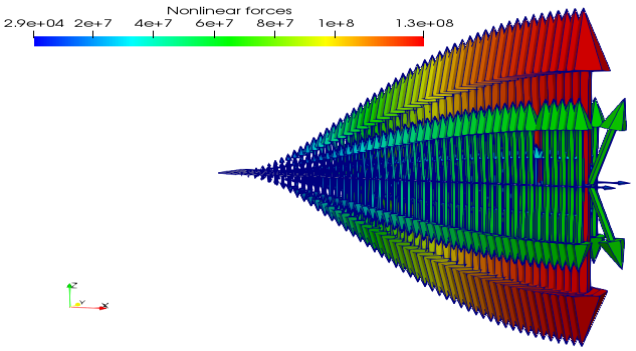

Figure 3.16: Purely nonlinear forces related to the maximum displacement of the structure.

Dynamic construction of the snapshots

As the nonlinear forces only depend on the displacement state of the structure, the snapshots should represent a large variety of nonlinear forces states

from linear to nonlinear states. In this section this is done by computing a dynamic FOM solution. The deformed shape of the static loading case is similar to the one observed during a first bending mode resonance. Thus, the computation of the nonlinear forces set is obtained through a FOM simulation for an excitation of first mode resonance (first bending) with an amplitude of the vertical displacements at the free-end of the beam similar to the displacements of the studied loading case ($\approx 0.5\,\mathrm{m}$).

The first four nonlinear forces vectors candidates to form the nonlinear forces basis are shown in Fig. 3.17. It is observed that the shape of the first vector of $\mathbf{U}_{r_f}$ is similar to the maximum nonlinear forces. Combining it with the other vectors, an approximate representation of the nonlinear forces is expected. A combination of the first four vector of $\mathbf{U}_{r_f}$ is proposed as candidate basis to be studied.

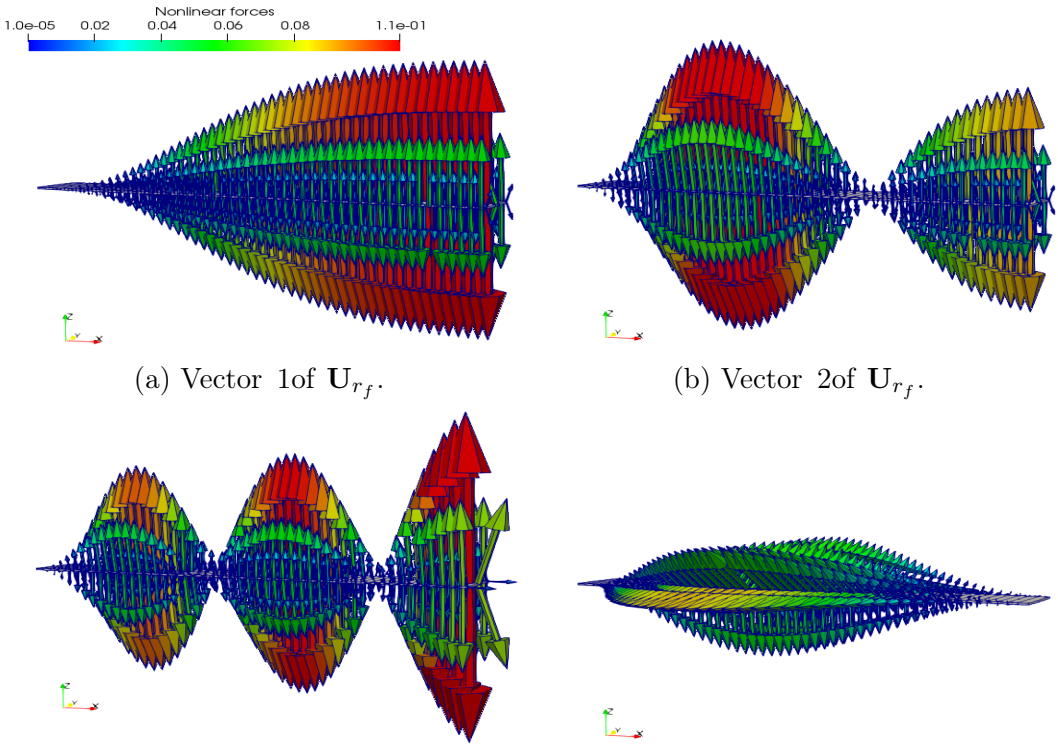

(a) Vector 1of $\mathbf{U}_{r_f}$. (b) Vector 2of $\mathbf{U}_{r_f}$.

(c) Vector 3of $\mathbf{U}_{r_f}$. (d) Vector 4of $\mathbf{U}_{r_f}$.

Figure 3.17: First four vectors of $\mathbf{U}_{r_f}$.

Table 3.7 presents the combination of vectors of $\mathbf{U}_{r_f}$ that are candidate to form the nonlinear forces basis, $\mathbf{\Phi}_f$.

Table 3.7: The possible vectors of $\mathbf{U}_{r_f}$ combination to form $\mathbf{\Phi}_f$.

Candidate basis	First vector of $\mathbf{U}_{r_f}$	Second vector of $\mathbf{U}_{r_f}$	Third vector of $\mathbf{U}_{r_f}$	Fourth vector of $\mathbf{U}_{r_f}$
$\mathbf{\Phi}_{f1}$	x			
$\mathbf{\Phi}_{f2}$	x	x		
$\mathbf{\Phi}_{f3}$	x		x	
$\mathbf{\Phi}_{f4}$	x			x

Static construction of the snapshots

The nonlinear forces do not have a dynamic component as they only depend on the vibrations of the structure at a given rotating velocity. Thus, the snapshot nonlinear forces are obtained from a static loading. Furthermore, the construction of the nonlinear forces basis by means of a dynamic FOM computation is very expensive to carry out, specially for refined meshes, in addition, spurious vectors might appear in the basis. As the nonlinear forces depend only on the displacements of the structure and not on the excitation type, the forces snapshots are obtained from a FOM static computation solution to an imposed force in the direction of the external dynamic forces in order to attain a given value of displacements which is representative of the expected dynamic solution.

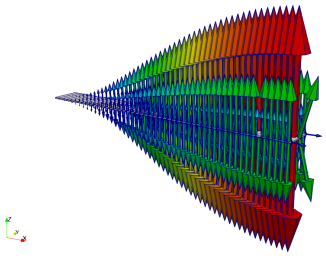

(a) Vector 1 ,of $\mathbf{U}_{r_f}$

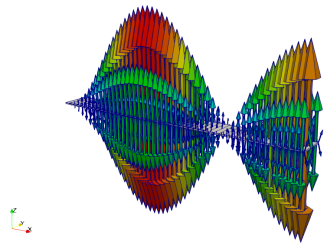

(b) Vector 2 ,of $\mathbf{U}_{r_f}$

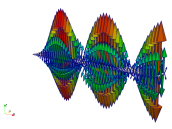

(c) Vector 3 of $\mathbf{U}_{r_f}$

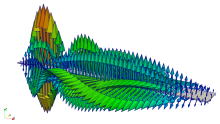

(d) Vector 4 of $\mathbf{U}_{r_f}$

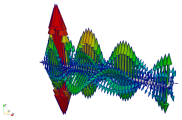

(e) Vector 5 of $\mathbf{U}_{r_f}$

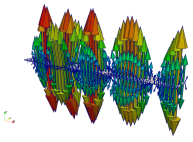

(f) Vector 6 of $\mathbf{U}_{r_f}$

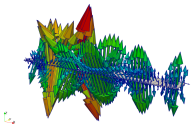

(g) Vector 7 of $\mathbf{U}_{r_f}$

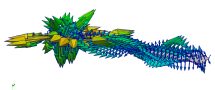

(h) Vector 8 of $\mathbf{U}_{r_f}$

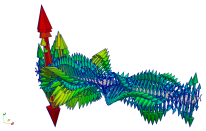

(i) Vector 9 of $\mathbf{U}_{r_f}$

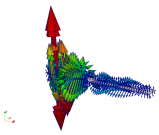

(j) Vector 10 of $\mathbf{U}_{r_f}$

Figure 3.18: Fist 10 vectors of $\mathbf{U}_{r_f}$ obtained with an incremental static loading at $\Omega = 0$ rpm.

During the static computation, 5000 increments are used to enrich the snapshot matrix, $\mathbf{A}$. The first ten nonlinear forces vectors related to this loading provide a continuum solution without force localization effects as shown in Fig. 3.18. The shape of the first nonlinear forces vector corresponds exactly to the one of the nonlinear forces Fig. 3.16. Thus, with this procedure, the obtained nonlinear forces basis is more accurate. As a consequence, the nonlinear forces basis is formed by the first vector of $\mathbf{U}_{r_f}$.

3.3.5 Numerical results for loading case 1: Static

The objective of developing ROMs is to provide the best compromise between the time consumption and the accuracy of the system. Thus, the obtained ROMs solutions should provide an error smaller than 10% in order to be considered as valid.

The objective of this loading case is to study the influence of the correction and its implementation in the solution. An advised construction of the StepC ROM is then presented in section 3.3.6. For all the considered cases, the reduced basis is normed such as the maximum norm is equal to unity, $||\mathbf{\Phi}||_{\text{inf}} = 1$. Thus, four different cases are studied hereinafter:

First, the reduced basis is formed by the first 10 LNM and the nonlinear forces basis is formed by Φ_{f_4} obtained dynamically without taking into account the shape of the modes in the reduced basis, $\mathbf{\Phi}$. Second, for the same reduced basis, the influence of the vectors that form Φ_f is assessed. Third, in order to improve the representativity of the reduced basis, the MAC+LNM basis is chosen. Fourth, the POD reduced basis and a static construction of the nonlinear forces basis is evaluated. For the first three cases, only the non rotating structure case is considered. The fourth case additionally consideres $\Omega = 0$ rpm, $\Omega = 1000$ rpm and $\Omega = 3000$ rpm rotating velocities.

LNM + dynamic construction with $\mathbf{\Phi}_{f_4}$

Here it is considered that the reduced order basis is formed by the first 10 LNMs in order to keep a reduced computational cost of the OFFline stage and that the nonlinear forces basis is formed by two of the first four vectors of $\mathbf{U}_{r_f}$ constructed dynamically, vectors 1 and 4. The latter combination of vectors provides an improved accuracy with respect to the Linear and STEP ROMs.

Figure 3.19 shows the vertical and longitudinal displacements of the Linear ROM and the StepC ROM compared to the FOM solution. The solution obtained with the StepC ROM is considerably improved with respect to the Linear ROM for the vertical displacements. The longitudinal displacements

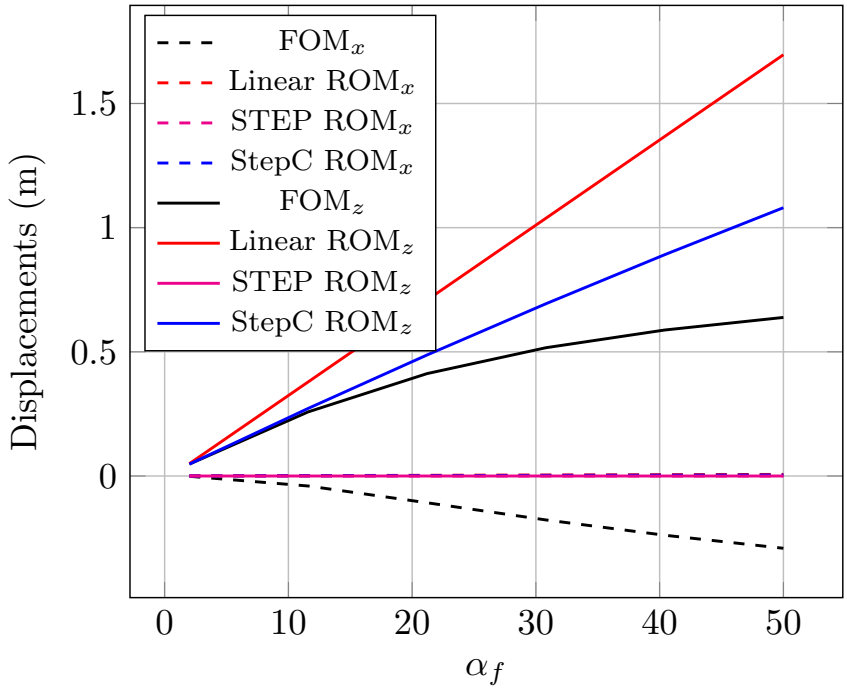

Figure 3.19: Vertical (- -) and longitudinal (-) displacements of the tip.

are not well represented by any of the ROMs. This is because none of the longitudinal modes of the structure are kept in the reduced basis. Even if the solution accuracy is improved with respect to the classical ROMs, the solution still presents a large error as shown in Tab. 3.8.

In order to obtain accurate result the influence of the nonlinear forces basis and of the reduction basis is studied in the following. First, the influence of the vectors combination that forms the nonlinear forces basis is studied. Then, by means of the MAC the representativity of the reduced basis is improved. The latter provides more accurate results when the solution converges, however, reduces its numerical stability.

LNM + dynamic construction of $\mathbf{\Phi}_f$ with different vectors combination

It has been observed that for most of the studied cases, the first nonlinear vector must be retained in $\mathbf{\Phi}_f$ as it provides the main characteristics of the nonlinear forces. The shape of the first vector shown in Fig. 3.17.a is similar to the nonlinear forces of Fig. 3.16. However, the latter vector does not reproduce the longitudinal forces nor the amplitude in the neighbourhood of the free-end where the maximum nonlinear effects occur.

When the number of retained vectors of $\mathbf{U}_{r_f}$ tends to one the solution of the StepC ROM usually tends to the solution of the Linear ROM. However,

if the retained number of vectors of $\mathbf{U}_{r_f}$ is high enough, the solution tends to the STEP ROM solution (if convergence is reached). When the number of retained vectors is increased sequentially, there is a value of retained vectors for whom the StepC ROM diverges for all the loading intensities for the first time. This value separates the optimal candidates and the disturbing candidates. All the vectors of $\mathbf{U}_{r_f}$ over the first disturbing vector, if contained by $\mathbf{\Phi}_f$, provide results that tend to the STEP ROM solution or that tend to numerical instabilities (diverge).

The construction of the $\mathbf{\Phi}_f$ basis is computationally expensive as a FOM computation is carried out. Thus, the objective is to use the same $\mathbf{\Phi}_f$ for different intensities of the loading (driven by α_f). The displacements of the structure are studied for six loading intensities. The total force applied at the free-end of the structure varies linearly from $f_N\alpha_{f1} = 50\,\mathrm{N}$ to $f_N\alpha_{f6} = 600\,\mathrm{N}$. The intensity factors $\alpha_f = \{4.166, \ldots, 50\}$ are chosen such that the structure is submitted from linear to highly nonlinear states. The average of the MAE_r^i error for each nonlinear basis is shown in Tab. 3.8.

The ROMs are considered as accurate when *the average* and *the maximum* of the error of each node related to the length of the structure ($MAE_{L_x}^i$, where i represents the evaluated node), Eqn. (3.7), are under or close to 10 %. Furthermore, to reduce the ONline/OFFline computational time the reduced basis is formed by a maximum of 10 vector components. The allowed limit nonlinear displacement corresponds to a case where the structure remains elastic but the stress is close to yield (a vertical displacement of $\approx 50\,\%$ of the beam length).

$$MAE_{L_x}^i(\%) = \frac{MAE^i}{L_x}(\%) = \frac{\sum_{j=1}^{n_{step}} |\mathrm{u}_{\mathrm{ROM}}^{\mathrm{i}}(t_j) - \mathrm{u}_{\mathrm{FOM}}^{\mathrm{i}}(t_j)\,|}{n_{step}L_x} \cdot 100\,, \tag{3.7}$$

where $\mathrm{u}_{\mathrm{ROM}}^{\mathrm{i}}(t_j)$ and $\mathrm{u}_{\mathrm{FOM}}^{\mathrm{i}}(t_j)$ represent the module of the i-th node of the ROM and of the FOM at the time step t_j.

Table 3.8: Average MAE_r^i (%) for the StepC ROM $\mathbf{\Phi}_f$candidate basis and for the Linear ROM, the lowest error value for each loading intensity is highlighted.

	$\mathbf{U}_{r_f}$	α_{f1}	α_{f2}	α_{f3}	α_{f4}	α_{f5}	α_{f6}
StepC ROM $\mathbf{\Phi}_{f1}$	1	Diverges	Diverges	Diverges	Diverges	Diverges	Diverges
StepC ROM $\mathbf{\Phi}_{f2}$	1,2	**0.41**	**3.69**	**9.12**	**15.54**	**22.16**	28.95
StepC ROM $\mathbf{\Phi}_{f3}$	1,3	3.02	Diverges	Diverges	Diverges	Diverges	Diverges
StepC ROM $\mathbf{\Phi}_{f4}$	1,4	3.93	12.27	17.76	21.28	23.72	**25.45**
Linear ROM		0.43	4.32	11.34	20.21	30.08	40.58

The solution does not converge for all the combinations of $\mathbf{\Phi}_f$ and loading intensities. When the loading intensity is small most of the cases converge.

However, only the $\mathbf{\Phi}_{f_2}$ basis is capable of providing more precise results than the Linear ROM. When the loading intensity increases, for some special cases, the solution does not converge due to numerical instabilities. For the cases where the solution does converge, the results that are obtained are always more accurate than the Linear ROM.

Thus, the best nonlinear forces basis is chosen as the one for which the average MAE_r^i error is minimum. The nonlinear force basis corresponds to the second candidate basis, $\mathbf{\Phi}_f = \mathbf{\Phi}_{f2}$, that is formed by the first two vectors of $\mathbf{U}_{r_f}$. The nonlinear forces basis, $\mathbf{\Phi}$, is then applied to Eqn. (2.79) and by introducing the correction into the STEP procedure the StepC ROM is constructed.

The results obtained with the proposed StepC ROM are up to 1.3 times more accurate than the Linear ROM. However, the average MAE_r^i error is considerably higher than the chosen design constraints ($MAE_r^i \lessapprox 10\,\%$), thus, the StepC ROM formed with the first 10 LNM and the POD forces correction provides an improved representation but its error remains over the design constraints. This is due to the lack of representativity of the reduced basis. If a given displacement component (i.e. longitudinal vertical) is not represented by the modes that form the reduction basis, $\mathbf{\Phi}$, the ROM is not capable of reproducing that behaviour. Thus, to improve the representativeness of the ROM the reduced bases are formed by the modes that best fit the expected displacements. In order to judiciously choose these optimal LNMs the Modal Assurance Criteria (MAC) is evaluated.

LNM+MAC + Dynamic construction of $\mathbf{\Phi}_f$

As the correction of the nonlinear forces depends on the nonlinear forces basis, $\mathbf{\Phi}_f$ and on the reduced basis, $\mathbf{\Phi}$, the accuracy of each of them has an influence on the capacity to represent the nonlinear forces and the displacements of the structure. Thus, to ensure that the chosen modes are able of reproducing the FOM solution, the Modal Assurance Criterion (MAC) is implemented.

First, a FOM computation is carried out to obtain a set of displacements that are representative of the response of the structure. The latter are saved in a snapshot matrix, $\mathbf{S}$. Then, a Proper Orthogonal Decomposition (POD) is computed with a SVD and the POD modes of the displacements are obtained. The latter modes are then compared to the LNM that are candidates to form the reduced basis by using the MAC, Eqn. (3.1).

A large number of compared modes increases the capacity of reproducing the displacement of the structure of the new reduced basis. Here, the number of LNM that are compared is chosen to be 300. Furthermore, the modes that are candidates to form the reduced basis are those for which the MAC is greater than 0.1. The objective of choosing a MAC greater than 0.1 is that

the modes that are totally different to the structure's behaviour are discarded. If the MAC is increased in order to choose those modes that exactly match the behaviour of the structure, the basis representatitivy is reduced and the solutions tend to the first case where the vertical displacements are accurately represented but the longitudinal displacements are not represented. The first POD modes capture the main features of the structure's displacements, thus, the LNM that best fit the first POD vectors are retained as presented in section 3.1.1.

Following the latter assumptions, the reduction basis is formed by $\mathbf{\Phi} = [\mathbf{\Phi}_1, \mathbf{\Phi}_{36}, \mathbf{\Phi}_{38}, \mathbf{\Phi}_{20}, \ \mathbf{\Phi}_{44}, \mathbf{\Phi}_{206}, \mathbf{\Phi}_{210}, \mathbf{\Phi}_2, \mathbf{\Phi}_{37}, \mathbf{\Phi}_{63}]$. Then, the identification of the nonlinear forces basis, $\mathbf{\Phi}_f$ is carried out leading to the average MAE_r^i error shown in Tab. 3.9.

Table 3.9: Average MAE_r^i (%) for the StepC ROM candidate basis and for the Linear ROM.

	$\mathbf{U}_{r_f}$	α_{f1}	α_{f2}	α_{f3}	α_{f4}	α_{f5}	α_{f6}
StepC ROM $\mathbf{\Phi}_{f1}$	1	0.15	4.05	Diverges	Diverges	Diverges	Diverges
StepC ROM $\mathbf{\Phi}_{f2}$	1,2	**0.07**	2.58	10.96	Diverges	Diverges	Diverges
StepC ROM $\mathbf{\Phi}_{f3}$	1,3	0.13	**0.70**	**2.27**	**3.81**	**5.21**	**6.43**
StepC ROM $\mathbf{\Phi}_{f4}$	1,4	0.31	Diverges	Diverges	Diverges	Diverges	Diverges
Linear ROM		0.43	4.32	11.34	20.21	30.08	40.58

Three main conclusions are arisen from the optimal choice of the LNM to form a representative reduced basis. First the converged solutions are significantly more accurate than the reduced basis without an optimal choice of LNM. Second, for loadings that induce large nonlinear behaviour just one of the candidate basis is capable of convergence. In this case, the latter simplifies the identification of the nonlinear forces basis, $\mathbf{\Phi}_f = \mathbf{\Phi}_{f3}$. Third, for small displacements, any of the proposed nonlinear forces bases are valid and more accurate than the Linear ROM and than the reduced bases without an optimal choice of LNM.

Figure 3.20 represents a comparison between the StepC ROM and the Linear ROM with respect to the reference solution obtained with the FOM. The colormap corresponds to the MAE_r^i error at each node. The solution displacements and shape is correctly represented until very intense loadings appear. For those cases, when the absolute displacement of the free-end is greater than the 70 % of the length of the structure, even if the desgin constraints are fulfilled, ($MAE_r^i \lessapprox 10\,\%$), the shape of the structure determined by the StepC ROM does not fully correspond to the deformed shape of the FOM. This can be due to the fact that for these displacements the forces are not fully represented as the nonlinear force basis, $\mathbf{\Phi}_f$, is initially evaluated for a lower displacements case, thus, the solutions loose their accuracy. However, for

all the loading cases, the StepC ROM provides results that are more accurate than the Linear ROM.

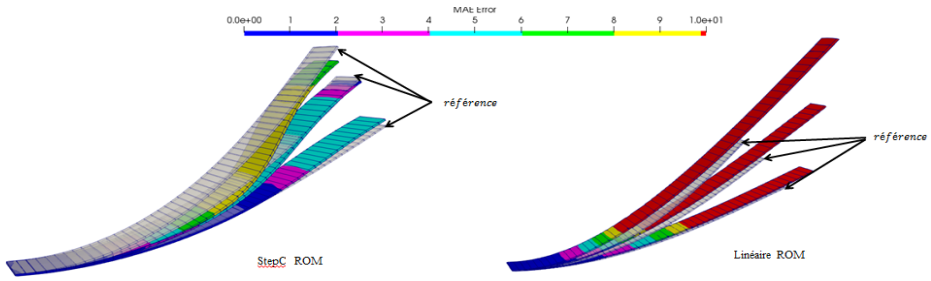

Figure 3.20: Deformed shaped for α_{f2}, α_{f4} and α_{f6}.

Influence of the number of modes in the reduction basis

The influence of the number of modes retained in the reduced basis is studied for the loading intensity α_{f_4}, the optimal $\mathbf{\Phi}_{f_3}$ basis determined previously. Thus, the number of retained optimal LNM that form the reduced basis varies. Thus, the maximum MAE_r^i error is obtained for each size of the reduced bases. As shown in Fig. 3.21, the maximum error obtained with the StepC ROM is reduced when the number of optimal LNM that is retained in the reduced basis increases. However, the larger the size of the reduced basis, the greater the cost to construct the ROM and to perform the ONline computations.

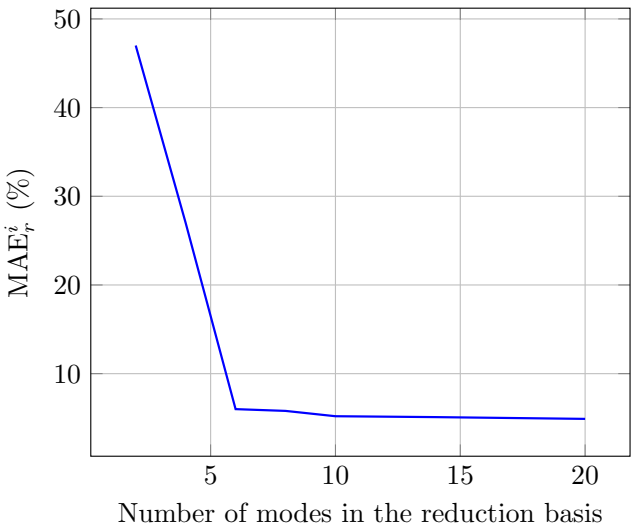

Figure 3.21: Maximum MAE_r^i of the StepC ROM with respect to the number of optimal LNM that form the reduced basis for the α_{f4} loading intensity.

POD + static construction of $\mathbf{\Phi}_f$

Here an alternative construction of the nonlinear forces basis, $\mathbf{\Phi}_f$, is evaluated. The nonlinear forces basis is formed by the first POD vector of $\mathbf{U}_{r_f}$ obtained from a static simulation.

Unlike the previous cases where the LNM reduced basis was used, hereunder, a POD reduced basis is chosen as it is representative of the observed phenomena. Between the studied reduced bases the POD is the one that provides the best results, however, its construction leads to non reasonable computational time. When computing POD basis is not reasonable, the LNM+MAC reduced basis is interesting due to its construction cost and improved representativity with respect to the LNM without MAC. In order to prove the validity of the StepC ROM, hereunder, the response of the structure is presented for a static loading with different loading intensities at three rotating velocities (at rest, 1000 rpm and 3000 rpm).

For all the loading cases and rotating velocities, Fig. 3.22 to 3.24 the StepC ROM provides accurate results and improves the solution that is provided by the Linear ROM. The Linear ROM does not capture the coupling between motions while the StepC ROM provides an accurate representation of the coupling and of the observed amplitudes. Thus, the construction of the StepC ROM with the POD basis and the static construction of the nonlinear forces basis provides the best solution for the first loading case.

When the structure does not rotate, as shown in Fig. 3.22, the StepC ROM provides almost the same response as the FOM except for the last loading. The last loading corresponds to a displacement that induces a stress level over the elastic limit thus, it is out of the scope of the present work. The latter is shown in order to proof the model's behaviour in extreme cases.

When the structure rotates at $\Omega = 1000$ rpm, as shown in Fig. 3.23, the StepC ROM provides almost the same response as the FOM for all the loading intensities. The longitudinal displacements are overestimated for the last loading case. Similar conclusions are arisen as in the non rotating case. The amplitude of the displacements is reduced due to the rotation of the structure. Even if the Linear ROM provides inaccurate values, the error in the vertical displacements is considerably reduced with respect to the non rotating case. Since the rotation of the structure increases its stiffness, the nonlinear behaviour of the vertical displacements is reduced.

When the structure rotates at $\Omega = 3000$ rpm, as shown in Fig. 3.24. The nonlinear coupling is well represented and the longitudinal and vertical displacements amplitudes are accurately captured. The Linear ROM provides an acceptable approximation for the vertical displacements while the nonlinear

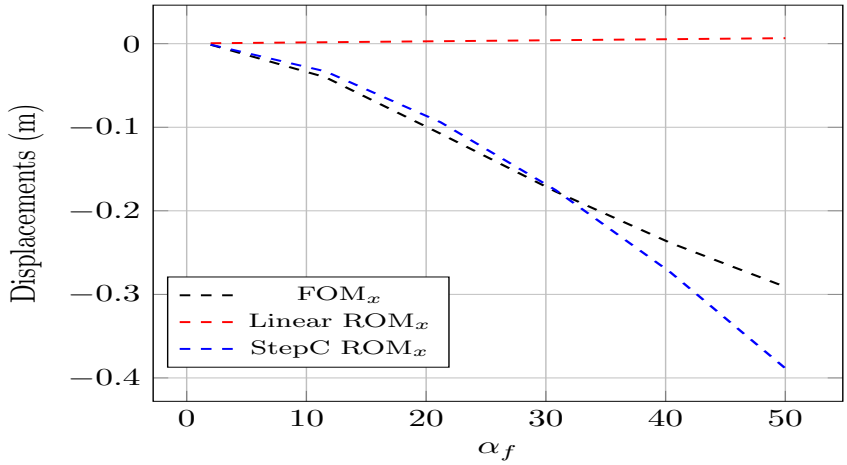

(a) Longitudinal displacements vs external force intensity.

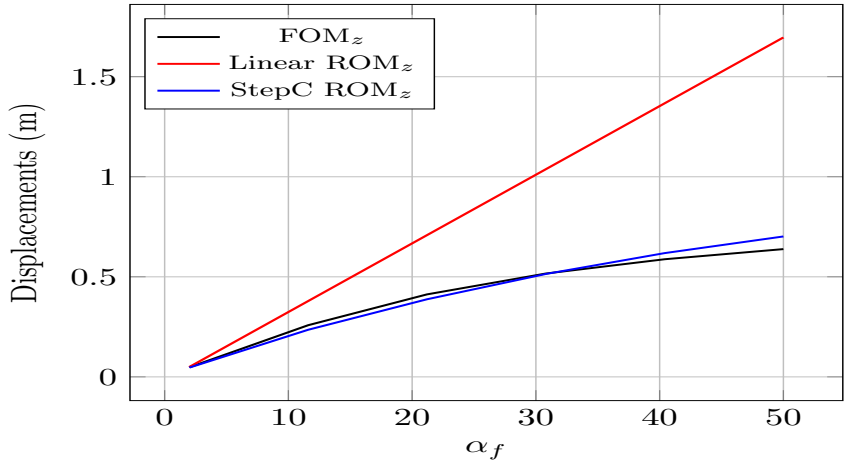

(b) Vertical displacements vs external force intensity.

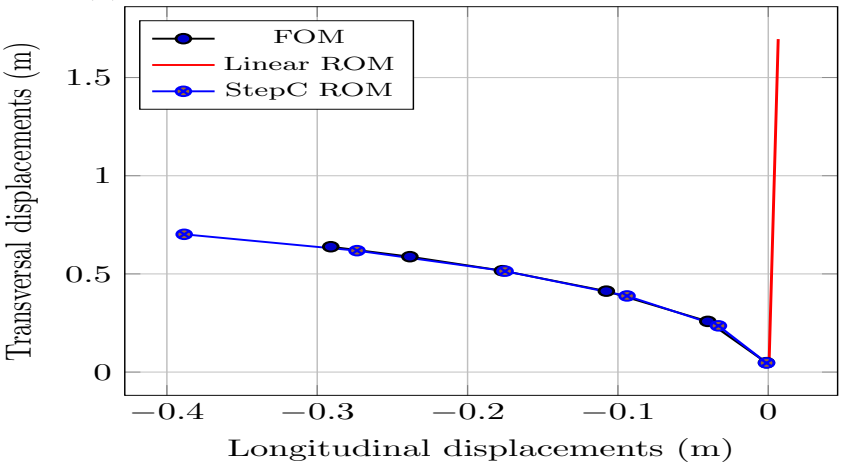

(c) Vertical vs longitudinal displacements.

Figure 3.22: Displacements of the structure for $\Omega = 0$ rpm.

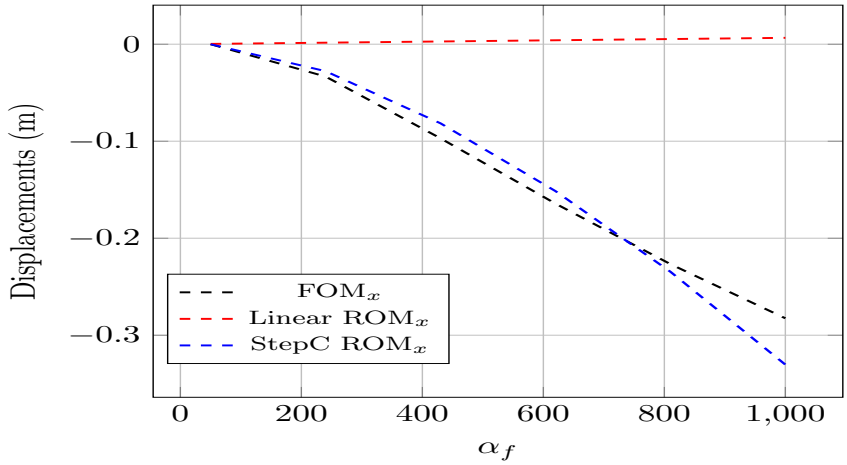

(a) Longitudinal displacements vs external force intensity.

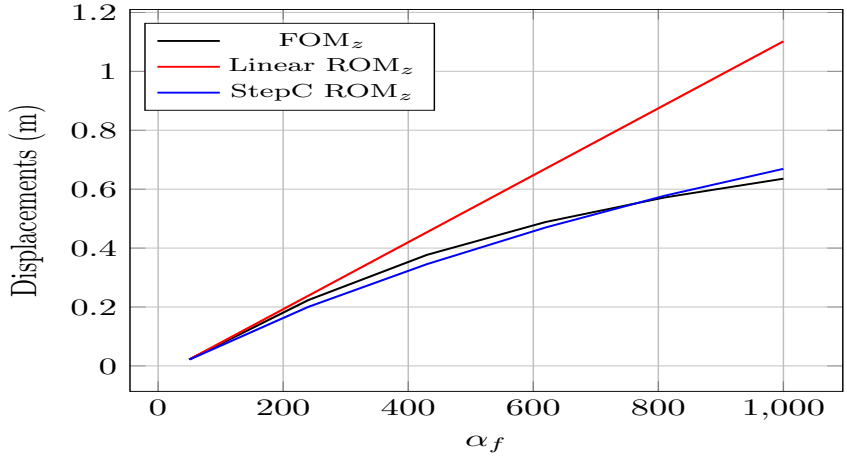

(b) Vertical displacements vs external force intensity.

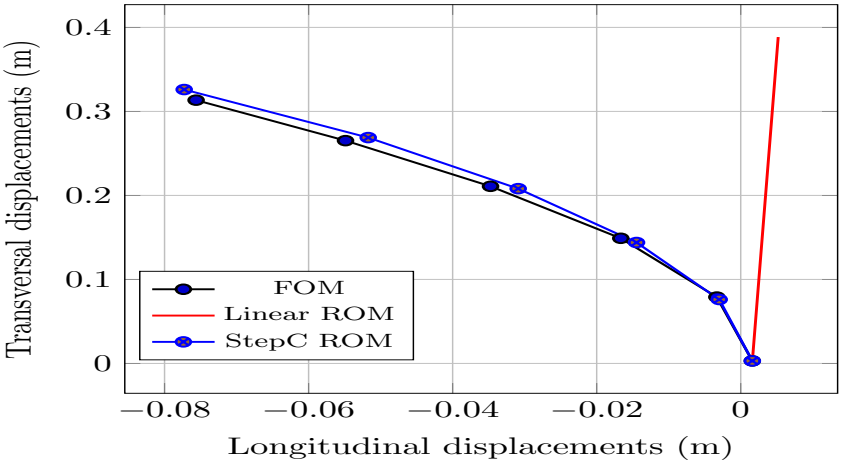

(c) Vertical vs longitudinal displacements.

Figure 3.23: Displacements of the structure for $\Omega = 1000$ rpm.

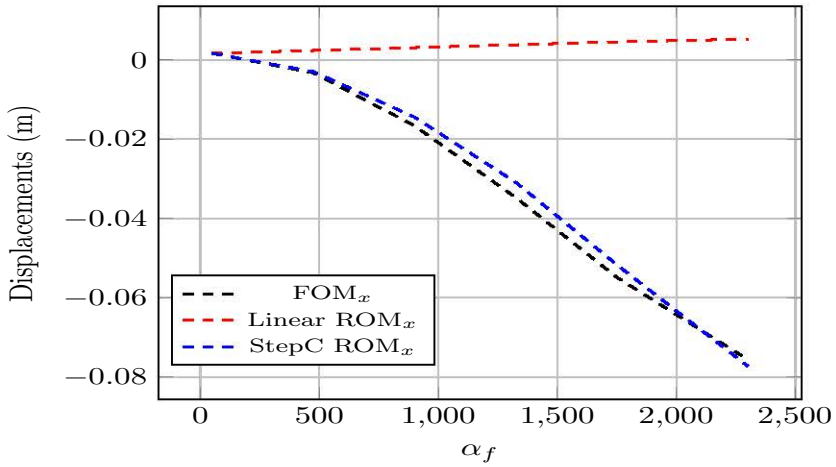

(a) Longitudinal displacements vs external force intensity.

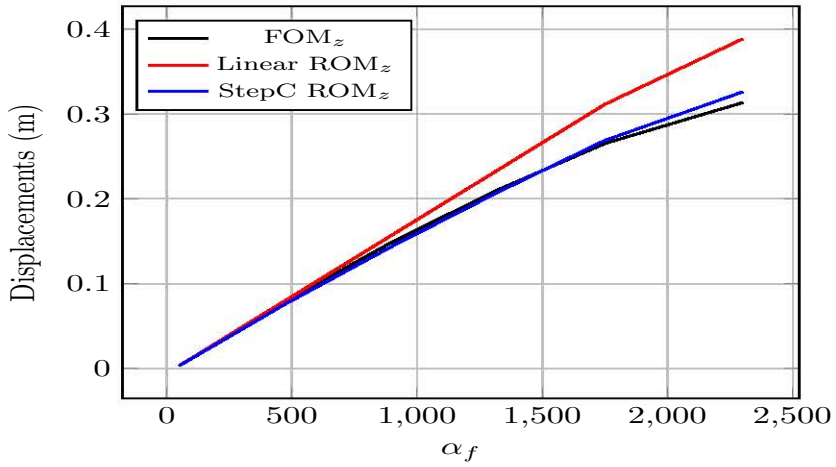

(b) Vertical displacements vs external force intensity.

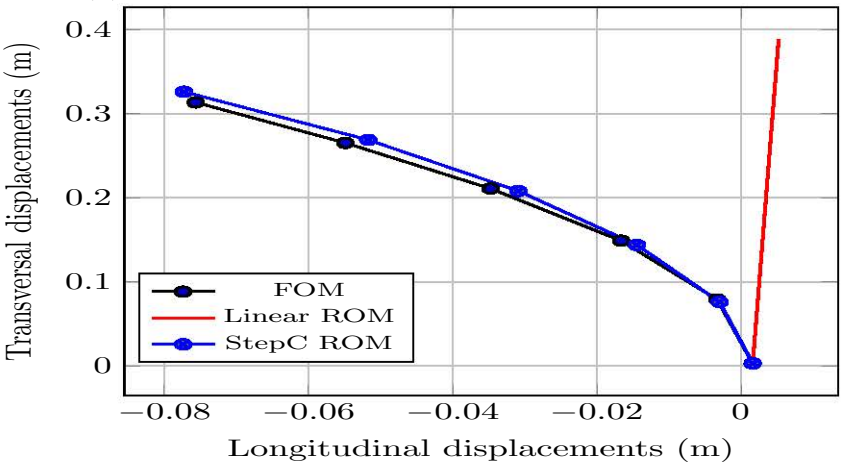

(c) Vertical vs longitudinal displacements.

Figure 3.24: Displacements of the structure for $\Omega = 3000$rpm.

coupling between the longitudinal and transversal directions is not captured.

Computational cost

The computational cost of the StepC ROM is obtained by adding the CPU time used by the OFFline and the ONline phases time.

On the one hand, the OFFline phase is performed once in order to construct the StepC ROM as presented previously. In order to compute the nonlinear forces basis, $\mathbf{\Phi}_f$ a complete FOM simulation is carried out (3h elapsed time). Furthermore, the construction of the reduced basis (5 min CPU time) and the evaluation of the static nonlinear forces for the STEP procedure (25 min elapsed time). Thus, the FOM construction has a total elapsed time cost of $\approx$ 3h30min.

On the other hand, the ONline phase solves the time-solution with 5000 time steps in $\approx 8s$, which consists in a computational cost up to 1545 times faster than the FOM. Table 3.11 presents a comparison of the CPU cost of the studied ROMs and the ONline time ratio with respect to the FOM CPU time. Furthermore, the time that is needed to perform all the considered loading (six loading intensities) is shown in order to highlight the interest of constructing the nonlinear StepC ROM. Both Linear ROM and StepC ROM have a similar ONline computational time, however, due to the accuracy of the second, the nonlinear ROM is proven to be a better choice.

Table 3.10: Comparison of the computational cost of the studied models for a single and multiple (6 loading cases) computations.

	t_{FOM}	$t_{Linear\ ROM}$	$t_{FOM}/t_{Linear\ ROM}$	$t_{StepC\ ROM}$	$t_{FOM}/t_{StepC\ ROM}$
Single loading	3h	5.29	2041	8.04 s	1343
Six loadings	17h3min	55 s	1105	52 s	1180

3.3.6 Advised construction of the StepC ROM

As presented previously, the procedure to construct the best StepC ROM is based in two procedures: first, the reduced basis, $\mathbf{\Phi}$, chosen for the reduction should provide an accurate representation of the nonlinear behaviour of the structure. Second, the construction of the nonlinear force basis should be such that the vectors in $\mathbf{\Phi}_f$ correspond to the shape of the nonlinear forces observed in the solution. Thus,

1. **Construction of the reduced basis:**
   (a) For computationally efficient FOMs $\rightarrow$ POD reduced basis.

(b) For computationally inefficient FOMs → LNM+MAC reduced basis.

2. **Construction of the nonlinear forces basis, $\mathbf{\Phi}_f$:**

   (a) Perform a static FOM computation considering an incremental static loading that deflects the structure to the expected level of displacements.

   (b) Extract the nonlinear forces at each increment

   (c) Perform a Singular Value Decomposition (SVD) compute the nonlinear forces POD vectors.

   (d) Form the $\mathbf{\Phi}_f$ basis with the first POD vector.

3. **Construct the StepC ROM with the chosen reduced basis and the nonlinear forces basis**

3.3.7 Numerical results for loading case 2: Resonance

The resonant excitation frequency corresponds to the natural frequency of the linearised model for each rotating velocity. The objective is to prove that the StepC ROM provides accurate results when the structure is submitted to dynamic loadings.

The dynamics of the structure is studied for two rotating velocities: at rest ($\Omega = 0$ rpm) and $\Omega = 1000$ rpm. As shown in the previous section, the POD reduced basis provides the best approximation to the studied case. Thus, in order to reduce the error obtained from reduction, a POD basis is chosen to approximate the displacements of the structure. For each rotating velocity, a new basis is computed. The nonlinear forces basis is obtained from static snapshots. Thus, the StepC ROM is formed by a POD reduced basis and by a nonlinear forces basis obtained by static loadings.

When the structure does not rotate, a nominal force of $f_N = 0.25$ N is applied at the first natural frequency of the structure. In order to reach the periodic steady state, the solution is computed for 100 excitation periods and 100 000 time steps. As shown in Fig. 3.25 the StepC ROM provides accurate results and is capable of representing the maximum amplitude both in the longitudinal and in the vertical directions. In the longitudinal direction, the StepC ROM presents two peaks of different amplitude while the peak value of the FOM is the same.The linear ROM is not capable of reproducing the coupling between the longitudinal and vertical directions. However, in the vertical direction provides more accurate results than the StepC ROM.

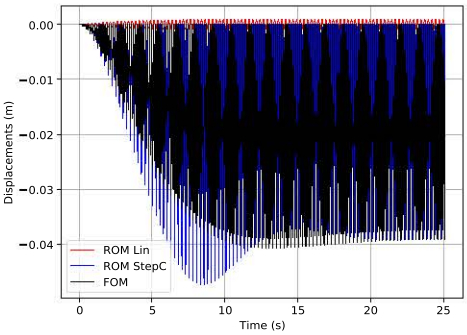

(a) Longitudinal displacements.

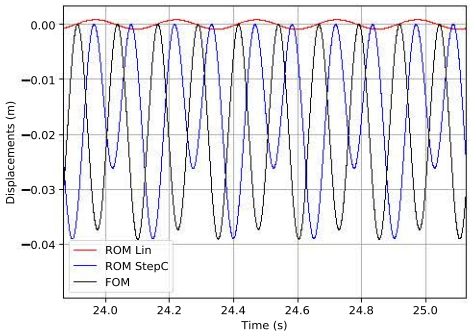

(b) Long. displacements (zoom).

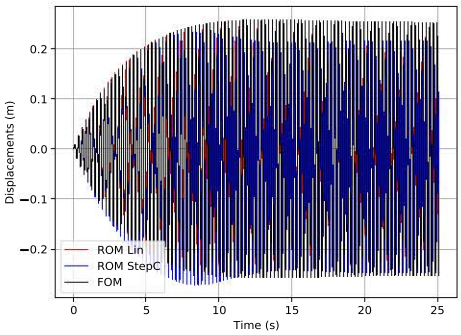

(c) Vertical displacements.

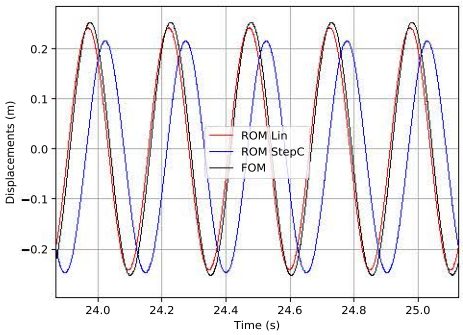

(d) Vertical displacements (zoom).

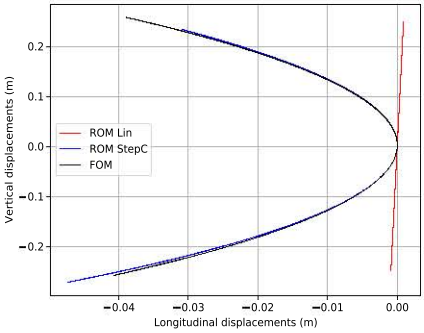

(e) Vertical vs long. displacements.

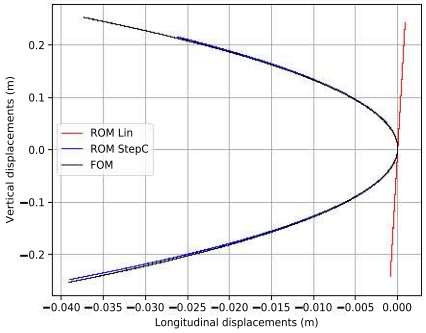

(f) Vertical vs long. displ. (zoom).

Figure 3.25: Displacements of the structure at resonant excitation for a rotating velocity, $\Omega = 0$ rpm.

When the structure rotates at 1000 rpm the nominal force that is applied in the nodes of the structure is $f_N = 12.5$ N. The nominal force is increased in order to keep a level of displacements where the nonlinearities are observed. The solution is evaluated for 100 periods with 30 000 time steps. As shown in Fig. 3.26 the StepC ROM provides more accurate results than the Linear ROM. Both longitudinal and vertical displacements are accurately reproduced with

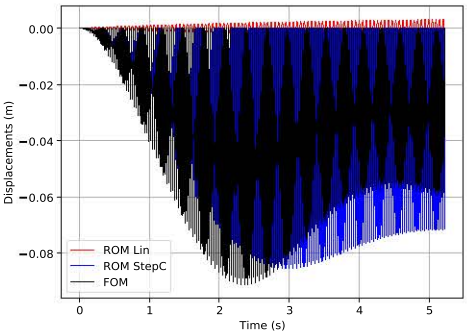

(a) Longitudinal displacements.

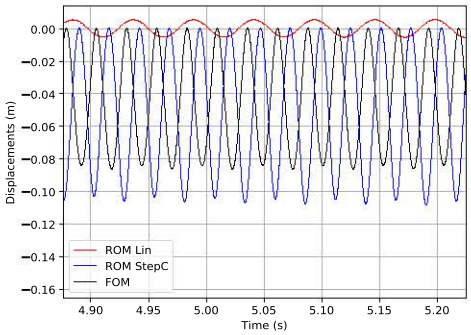

(b) Long. displacements (zoom).

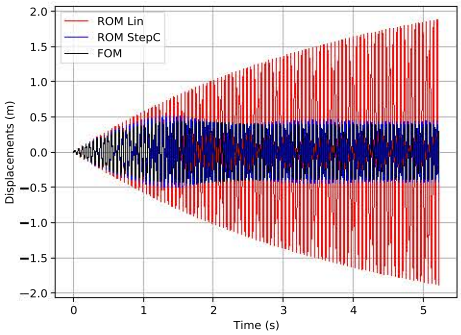

(c) Vertical displacements.

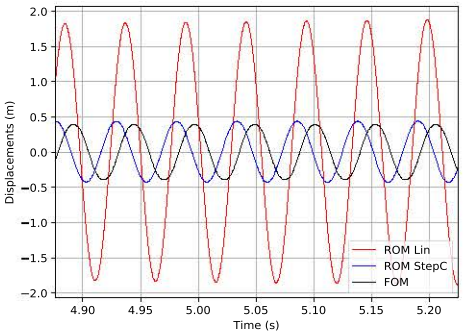

(d) Vertical displacements (zoom).

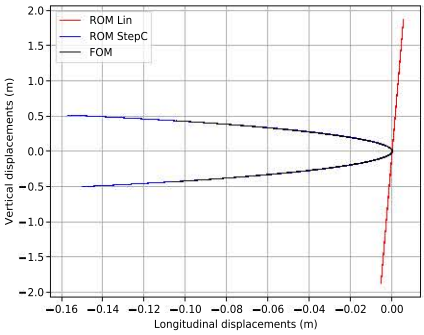

(e) Vertical vs long. displacements.

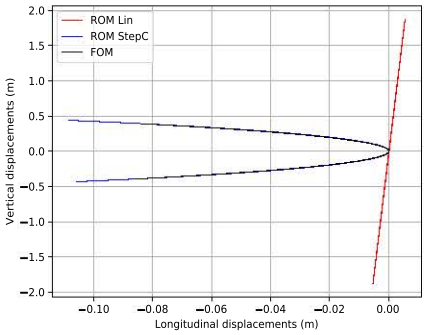

(f) Vertical vs long. displ. (zoom).

Figure 3.26: Displacements of the structure at resonant excitation for a rotating velocity, $\Omega = 1000$ rpm.

the StepC ROM. Thus, the importance of the construction of $\mathbf{\Phi}_f$ is highlighted. The Linear ROM is not capable of reproducing the longitudinal displacements and its vertical displacements representation is less accurate than at $\Omega = 0$ rpm.

Computational cost

Table 3.11 shows the ONline computational time of the proposed ROMs. A single FOM computation takes around 25h to be performed while each ROM has an approximative computational time of 80s providing a computation 767 times more rapid than the FOM. The computation of the StepC ROM is slower than the Linear ROM, however, the StepC ROM provides more accurate results.

Table 3.11: Comparison of the computational cost of the studied models for $\Omega = 0$ rpm and $\Omega = 1000$ rpm.

	t_{FOM}	$t_{Linear\ ROM}$	$t_{FOM}/t_{Linear\ ROM}$	$t_{StepC\ ROM}$	$t_{FOM}/t_{StepC\ ROM}$
$\Omega = 0$ rpm	24h15min	24.66 s	3540	113.76 s	767
$\Omega = 1000$ rpm	25h30min	79.54 s	1145	119.54 s	767

3.3.8 Friction contact nonlinearity

The objective of this section is to study the phenomenology of contact and to implement a contact model in the ROMs. Thus, just the results computed with the ROMs are presented. For the linear case, the solution of the ROMs and the FOMs are similar.

To study contact, the thin beam is modelled with a different mesh, shown in Fig. 3.27, in order to increase the number of nodes of the structure. The interface node is located at coordinates (0.22, 0, -0.0026) m. First the behaviour of the structure is supposed to be linear, just the contact nonlinearities are studied. For all the cases a Craig-Bampton reduced basis is used. The finite element mesh is formed by hexahedral quadratic elements (HEXA 20). The total number of degrees of freedom of the structure is 7149. The structure is clamped at one end and loaded at the other end by a vertical harmonic excitation.

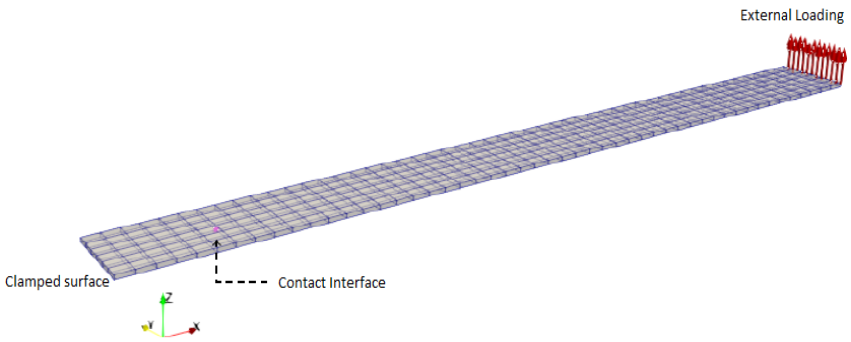

Figure 3.27: Mesh and boundary conditions of the beam.

The linear structure is excited at resonance by an external force whose nominal value is $f_N = 0.4$ N. Figure 3.28 shows the response spectrum (FFT of the time response) both when contact is activated and deactivated. When contact is taken into consideration, secondary harmonics appear as a result of the blocked motion. In addition, the amplitude of the main harmonics is attenuated by $\approx 50\%$.

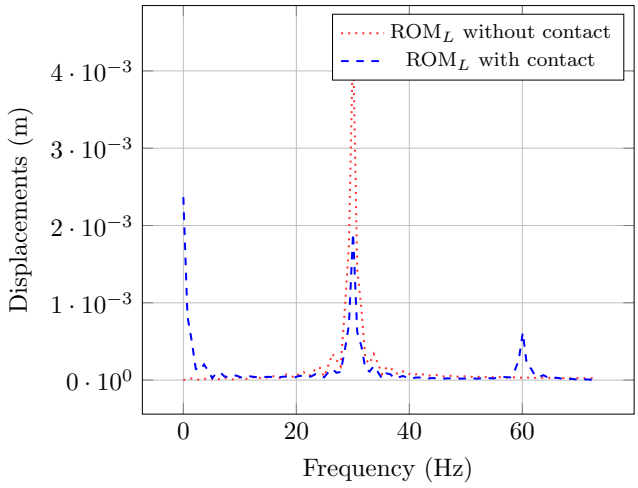

(a) Displacements at contact node.

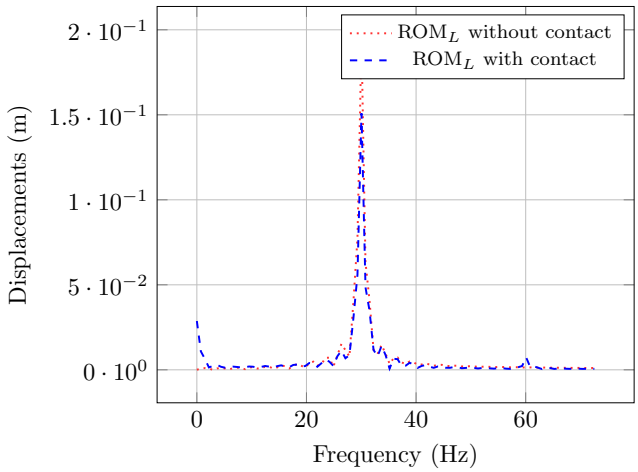

(b) Displacements at the loading end of the beam.

Figure 3.28: Displacements of the structure nodes with/without contact.

The phenomenology of contact nonlinearities with a large displacement is now studied, the nominal force that is applied corresponds to $f_N = 0.4$ N. The behaviour of the structure is studied by computing the forced response. As shown in Fig. 3.29 the resonant peak of the linear model is shifted towards higher frequencies (from 3.9 Hz to 4.25 Hz) when the contact is taken into consideration. The amplitude of the response is slightly reduced (80% of the

previous peak value). As per the linear case, the nonlinear response resonant peak is shifted towards higher values in frequency.

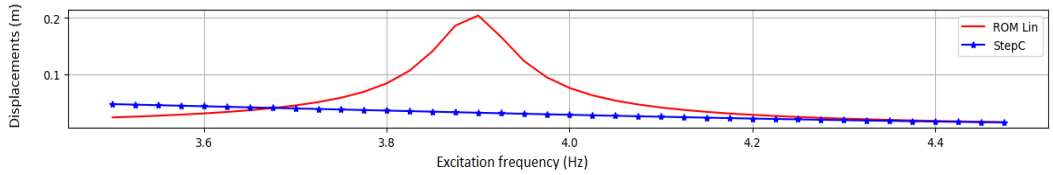

(a) Displacements vs excitation frequency without contact.

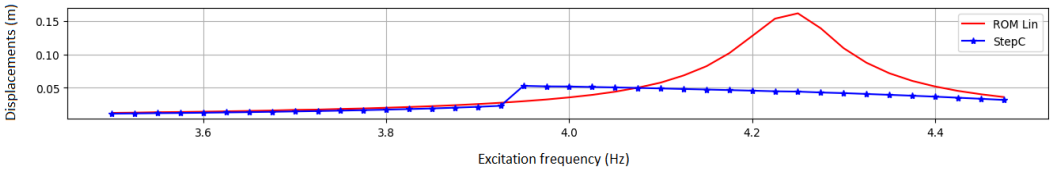

(b) Displacements vs excitation frequency with contact.

Figure 3.29: Forced response of the structure with/without contact.

Table 3.12 shows the computational time of the ROMs when contact type nonlinearities are considered or not. These computational time corresponds to a single resolution. Furthermore, it is observed that when the contact is activated the computational time is increased. This is due to the additional convergence iterations needed to fulfil contact and geometrical nonlinearities (if considered). The use of ROMs is of high interest as the solutions are computed very rapidly even when more than one nonlinearity is present.

Table 3.12: Computational time of the studied ROMs with/without contact.

	Lin. FOM	Lin. ROM	StepC ROM
Without contact	5h29min	2.31 s	7.99 s
With contact	10h36min	43.51 s	79.80 s

3.3.9 Discussion and feedback

This second structure is used to validate the optimal construction of the StepC ROM by carrying out a study of influence with respect to the reduced basis and with respect to the construction of the nonlinear forces POD basis. If the quality of the reduced basis is improved, the results obtained by the StepC ROM become more accurate. Furthermore, if the nonlinear forces basis is obtained by computing static loadings, the static/dynamic solution of the StepC ROM is capable of accurately reproduce the coupling behaviour of the structure. Nevertheless, the StepC ROM improves the solutions obtained with the Linear ROM and the STEP ROM. Besides, the StepC ROM it is used to study the phenomenology of contact when the structure behaves nonlinearly

observing that the contact induces a stiffening behaviour of the structure for the studied case.

3.4 Structure 3: Fan blade structure

3.4.1 Mesh and boundary conditions

The application in this section [Balmaseda et al., 2019] studies the validity of the proposed ROM for a complex structure. Two types of basis are chosen: the LNM, defined in section 2.2.1, and the Craig-Bampton basis, defined in section 2.2.4. The studied complex structure that represents the fan blade shown in Fig. 3.30, which is derived from the one designed in the frame of the activities devoted to the development of ONERA's NOVA configurations [Wiart et al., 2016, Wiart et al., 2015].

The finite element mesh is formed by 25872 hexahedral linear elements and 29681 nodes. The root of the blade is clamped and the external loadings are applied at every node of the tip surface. The structure rotates at a nominal velocity $\Omega_N = 4043$ rpm around the absolute x axis. The material is a Titanium-Aluminium (TiAl) alloy with 117.5 GPa Young's Modulus, 0.3 Poisson's Ratio, 4450 Kg/m^3 density, 1% damping ratio and 828 MPa Yield strength [Cardarelli, 2000]. An inertial Rayleigh damping is considered to model the structural viscous damping, $\mathbf{C} = \beta_m\ \mathbf{M} = 2\xi\omega_0\mathbf{M}$. The time responses provided by the ROMs are studied at the leading edge node (control coordinate), highlighted in Fig. 3.30, as it is one of the regions where the greatest geometrically nonlinear effects are expected. The contact interface in Fig. 3.30, where contact could be implemented, corresponds to boundary interface d.o.f. of the Craig-Bampton method. This type of contact interface could model the rubbing blade.

To study the periodic response under large displacements, induced for instance by mistuning or any instability, the structure is excited at its first linearised natural frequency that corresponds to the first bending mode. Thus, the external forces frequency is obtained from the eigenvalue analysis of the linearised model from Eqn. (2.24) with free interfaces. The external harmonic force is applied at every node of the tip surface in the axial direction as shown in Eqn. (3.8).

$$\mathbf{f}_e(\mathrm{t}) = \alpha_f \cdot \sin\left(\omega_e t\right)\ . \tag{3.8}$$

Due to the nonlinear behaviour of the structure, the linearised ROM and the nonlinear FOM responses differ significantly as shown in Fig. 3.35, thus, the necessity to build a more accurate nonlinear ROM is highlighted.

Two types of parametrised reduced bases are considered in this application: Linear Normal Modes and Craig-Bampton. In order to favour the "OF-

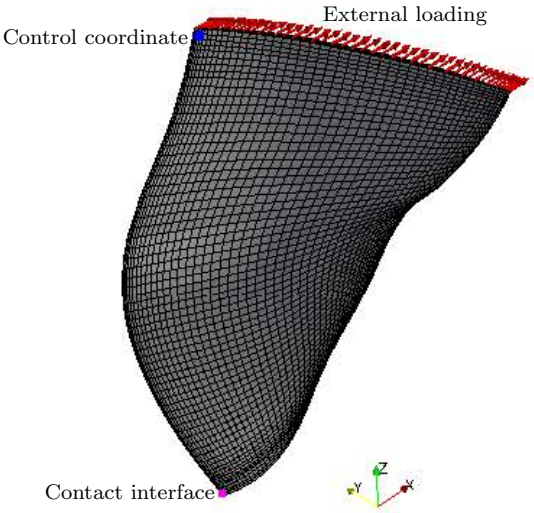

Figure 3.30: Mesh of the fan blade with the interface node and the control node highlighted.

Fline" computational time of the nonlinear force coefficients the total number of modes is chosen to be $r = 10$. In the case of Craig-Bampton basis, 7 fixed interface modes and 3 constraint modes are chosen (one for each d.o.f. of the studied interface node). For each basis type three different ROMs are studied. The linear ROMs do not take into consideration the purely nonlinear force term, the STEP ROMs consider the nonlinear term without any correction and the proposed StepC (Step with Correction) ROMs consider the nonlinear term with the POD correction developed previously. To avoid the construction of the projection basis at every rotating velocity, and to reduce the OFFline computational time, the reduced system is parametrised with respect to the rotating velocity.

The first three natural frequencies for the studied rotating velocities function of the nominal rotating velocity are presented in Tab. 3.13. It is observed that the stiffness of the structure increases with rotation and all the frequencies shift to higher frequency values when the rotation is increased. The latter is specially valid for the first two modes of the structure.

The nonlinear forces basis Φ_f is computed at 2000 rpm once for all the studied cases. The dynamic response of the structure is evaluated for two rotating velocities: for a rotating velocity of 2000 rpm and for 4043 rpm rotating velocity where the last corresponds to the nominal rotating velocity Ω_N of the blade. The periodic solutions are computed with the HHT-α method for 100 excitation periods and 3000 time steps.

Table 3.13: First three natural frequencies for different rotating velocities of the blade.

$\Omega(\%\,\Omega_N)$	ω_1 (Hz)	ω_2 (Hz)	ω_3 (Hz)
0	34.77	98.61	172.44
70	44.59	115.30	174.16
100	52.25	130.05	176.43

3.4.2 Parametric reduced order basis

The parametric ROM is constructed by evaluating the reduced order basis and the stiffness matrix of the FOM at 0 rpm, 2250 rpm and 4500 rpm. The reduced order basis are formed by the first 10 modes in order to keep a compromise between the OFFline computational cost and the accuracy of the ROMs. The parametric LNM basis modes are computed with Eqn. (2.82) are shown hereunder,

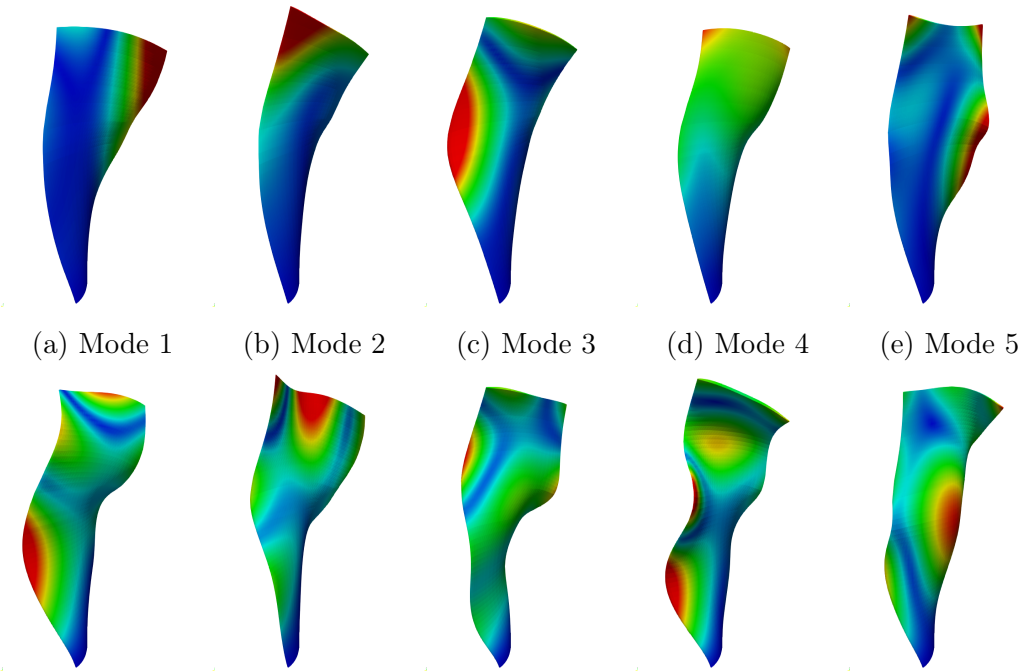

(a) Mode 1 (b) Mode 2 (c) Mode 3 (d) Mode 4 (e) Mode 5

(f) Mode 6 (g) Mode 7 (h) Mode 8 (i) Mode 9 (j) Mode 10

Figure 3.31: Fist 10 parametric linear normal modes of the structure.

3.4.3 Nonlinear forces basis $\mathbf{\Phi}_f$

The nonlinear forces basis is obtained by computing a FOM solution at the velocity of 2000 rpm. Then, following the procedure of section 2.4.4 the filtering matrix is obtained. The maximum nonlinear forces state of the structure is shown in Fig. 3.32.

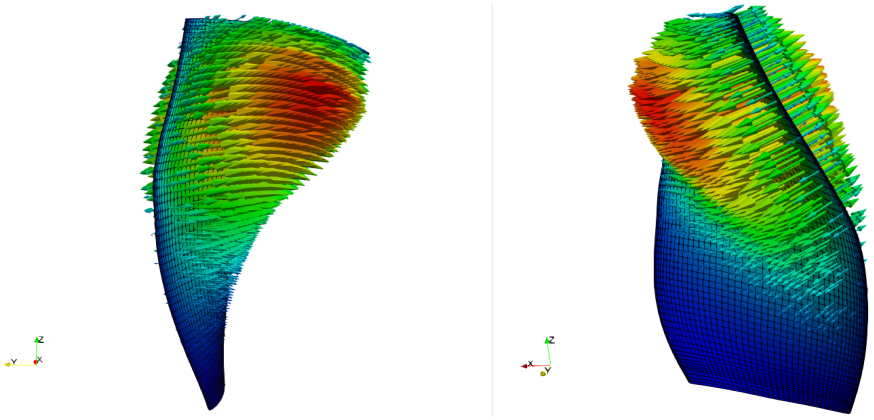

Figure 3.32: Maximum value of the purely nonlinear forces of the fan.

Normally, when rotating velocity varies, the nonlinear basis Φ_f should be recomputed to adapt the ROM to the new velocity, however, it was observed that the nonlinear basis obtained at a given velocity can be used for another rotating velocity. The interest of using the same nonlinear forces basis for several rotating velocities is that the FOM forces, that are computationally very expensive to obtain, are not re-evaluated. For the convergence analysis, the nonlinear forces basis is formed by the first two vectors in the resulting left singular vectors of the SVD computed by means of Eqn. (2.76), at a rotating velocity of 2000 rpm. The latter vectors are represented in Fig. 3.33.

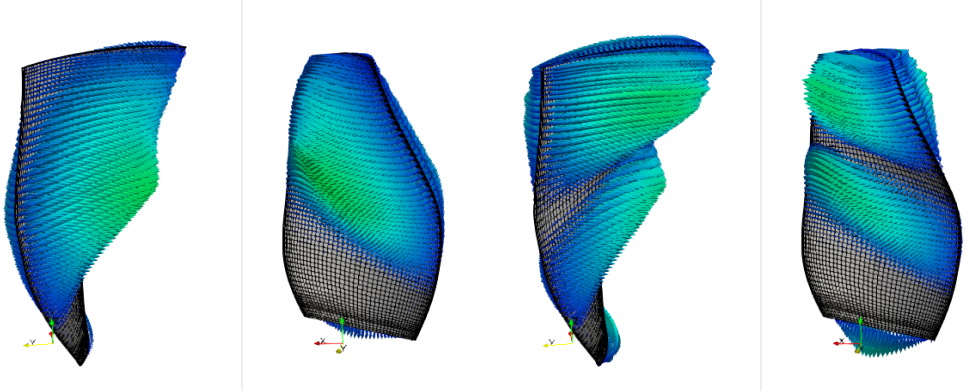

(a) 1^{st} nonlinear forces vector of $\mathbf{U}_{r_f}$. (b) 2^{nd} nonlinear forces vector of $\mathbf{U}_{r_f}$.

Figure 3.33: Nonlinear forces vectors that form $\mathbf{\Phi}_f$.

3.4.4 Convergence Analysis

Figure 3.34 presents the convergence analysis for the STEP and StepC methods with respect to the number of modes that form the reduced LNM basis. The relative error is evaluated for the periodic regime as shown in Eqn. (3.9) for three different rotating velocities. The loading factor α_f is chosen such that nonlinear effects are observed.

$$e_{Cconv}(\%) = \frac{|\max\{u_{ROM}(t)\} - \max\{u_{FOM}(t)\}|}{\max\{u_{ROM}(t)\}} \cdot 100 \,. \tag{3.9}$$

It is observed that the correction does not influence the accuracy for a low number of modes and provides similar results to the STEP method. However, from the 6th mode of the reduced basis the StepC correction with two nonlinear forces modes basis provide more accurate results for all the evaluated rotating velocities for a given basis size.

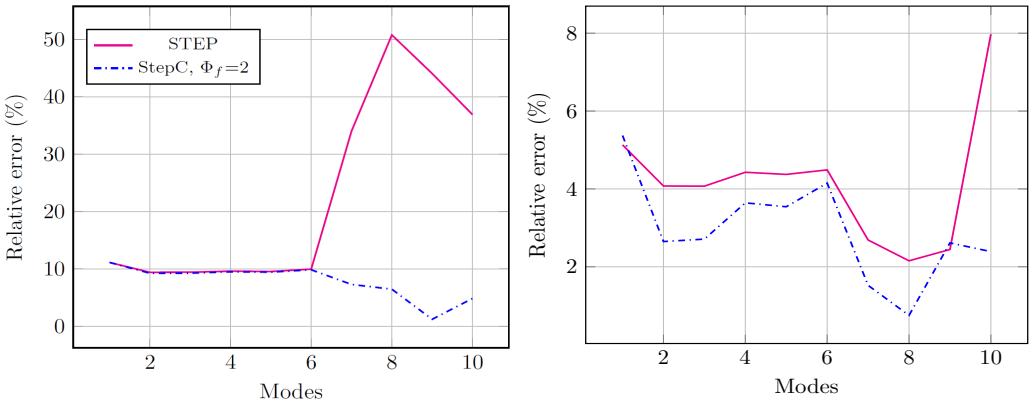

(a) $\Omega = 2000$ rpm, $\alpha_f = 0.5$. (b) $\Omega = 4043$ rpm, $\alpha_f = 1.5$.

Figure 3.34: Convergence analysis for different number of modes forming the reduced LNM basis.

3.4.5 First linearised mode resonance

In the following, it is considered that the nonlinear effects are significant when the difference between the linearised ROM and the nonlinear FOM periodic solutions differ by more than 10 %. For these cases, the cost of developing nonlinear ROMs is justified.

Figure 3.35 shows the periodic solution of the blade at 2000 rpm and 4043 rpm. The loading factor α_f is chosen to be 0.5 N for the first rotating velocity and 1.5 for second one in order to obtain a significant difference between the linearised and the nonlinear FOM solutions. The StepC nonlinear models provide more precise results than the linearised ROM and the STEP ROM for both reduced basis. It is observed that the solutions have a shift in time.

This effect is highlighted when Ω differs from the rotating velocity for which the nonlinear force basis is constructed. The objective is to accurately predict the response frequency and amplitude, thus, this effect remains out of the scope of the study. However, for aeroelastic coupling studies where the phase shift would influence in the accuracy of the solution, the nonlinear forces basis should be computed such that the phase between the FOM and the StepC ROM remain the same.

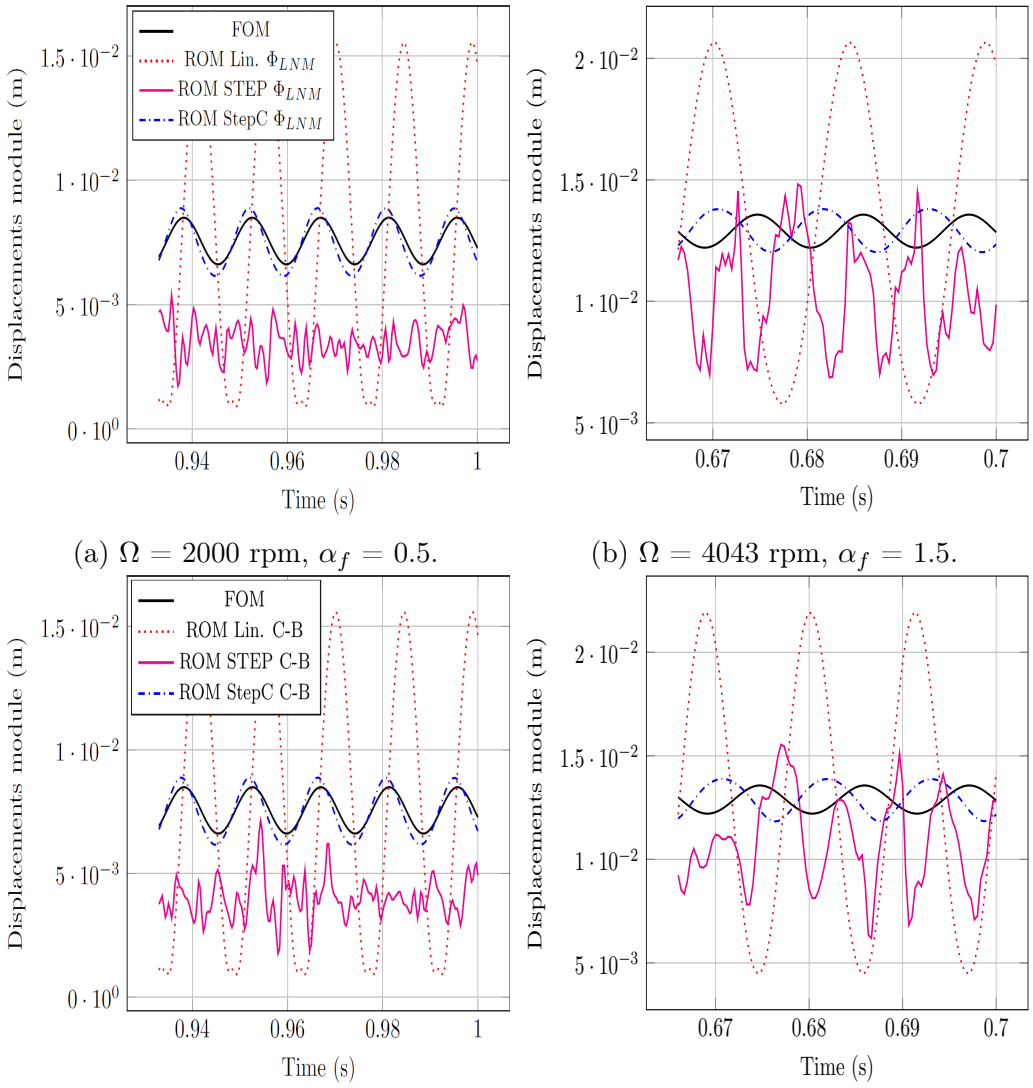

(a) $\Omega = 2000$ rpm, $\alpha_f = 0.5$.

(b) $\Omega = 4043$ rpm, $\alpha_f = 1.5$.

(c) $\Omega = 2000$ rpm, $\alpha_f = 0.5$.

(d) $\Omega = 4043$ rpm, $\alpha_f = 1.5$.

Figure 3.35: Periodic response for a first mode resonant harmonic excitation.

Figure 3.36 presents the global displacements of the structure at the maximum displacements instant amplified by a factor of 5 at $\Omega = 4043$ rpm. The Linear ROM presents a larger displacements than the reference FOM solution, however, the bending motion is well captured. The displacements of the

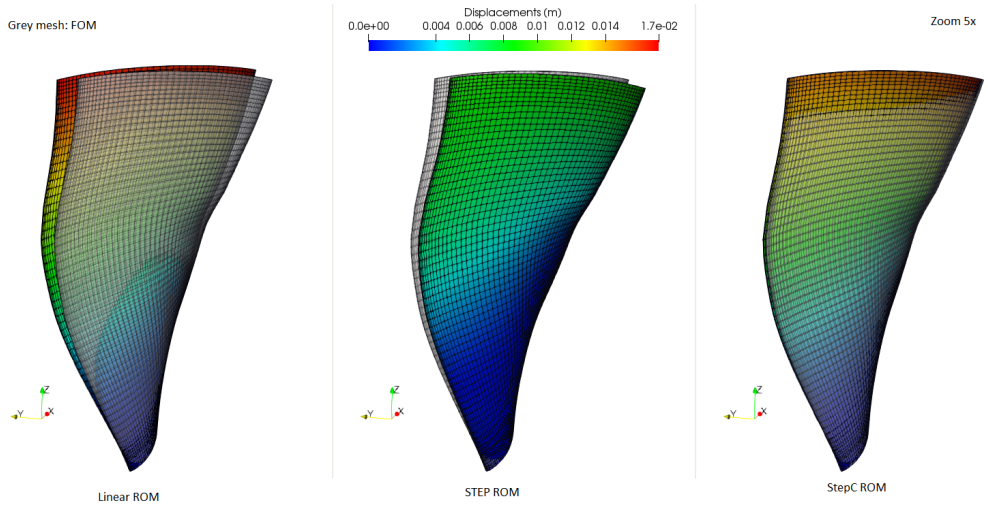

Figure 3.36: Displacements of the ROMs for $\Omega = 4043$ rpm and $\alpha_f = 1.5$.

STEP ROM have smaller amplitudes than the Linear ROM, thus, they provide a smaller error, however, the response does not represent the bending of the structure (the displacements shown in the figure is not fully representative) and is not periodic in time. The StepC ROM provides accurate results and the obtained displacements are of the same order of magnitude as the FOM taken as reference. Furthermore, the bending behaviour is correctly represented.

Error Analysis

The error of the ROMs periodic response is compared with respect to the FOM periodic response in terms of amplitude and response frequency. The POD based correction induces a time-shift in the response. Thus, the classical error computations cannot be carried out. In order to compare these solutions, the classical relative error is evaluated in the frequency domain. First, the periodic solution of the time-response is extracted, then, a Fast Fourier Transform (FFT) is carried out in order to transform the signals into frequency domain. Then, the error for each d.o.f. of the computed periodic response spectrum is performed as,

$$e_r(\%) = \frac{|u_{ROM}(\omega) - u_{FOM}(\omega)|}{\max\{|u_{FOM}(\omega)\}|} \cdot 100 \, . \tag{3.10}$$

Table 3.14 presents the spectrum based maximum relative error at the control coordinate. For both reduced bases and all the rotating velocities the nonlinear StepC ROM provides more accurate results (up to 39 times more accurate) than the linearised ROM. The STEP method on the other hand provides better results than the linearised ROM in terms of amplitude, however, the shape of the solution presents high level of undesirable harmonics. For most of the considered cases the Craig-Bampton basis provides more accurate results than the LNM basis as shown in Tab. 3.14. The latter might be due to

the presence of static deformations inside Craig-Bampton basis that provide a "knowledge" about the nonlinear behaviour of the structure in the reduced basis.

Table 3.14: Spectrum based relative error (%) of the ROMs.

	$\Omega = 0$ rpm		$\Omega = 2000$ rpm		$\Omega = 4043$ rpm	
Reduced basis	Φ_{LNM}	Φ_{CB}	Φ_{LNM}	Φ_{CB}	Φ_{LNM}	Φ_{CB}
Linear	268.74	272.70	40.51	40.68	28.41	25.43
STEP	50.51	53.25	54.2	47.23	20.49	15.88
StepC	11.84	8.97	2.64	2.58	2.09	3.29

Figure 3.37 shows the maximum value of the module of the MAE error for the Linear, STEP and StepC ROMs. The error values over the maximum allowed error (10%) are represented in red color. The area that overpasses this limit is similar for the Linear and the STEP ROMs (slightly larger for the last one). However, even if the behaviour is not representative, the maximum error obtained with the STEP ROM is smaller than the Linear ROM. For both rotating velocities the results obtained with the StepC ROM provide accurate results through all the nodes of the structure and none of the nodes overpasses the design constraint. Thus, the StepC ROM provides accurate results for all the nodes in the structure while with the Linear ROM and the STEP ROM only the behaviour in the neighbourhood of the clamped surface is accurately predicted.

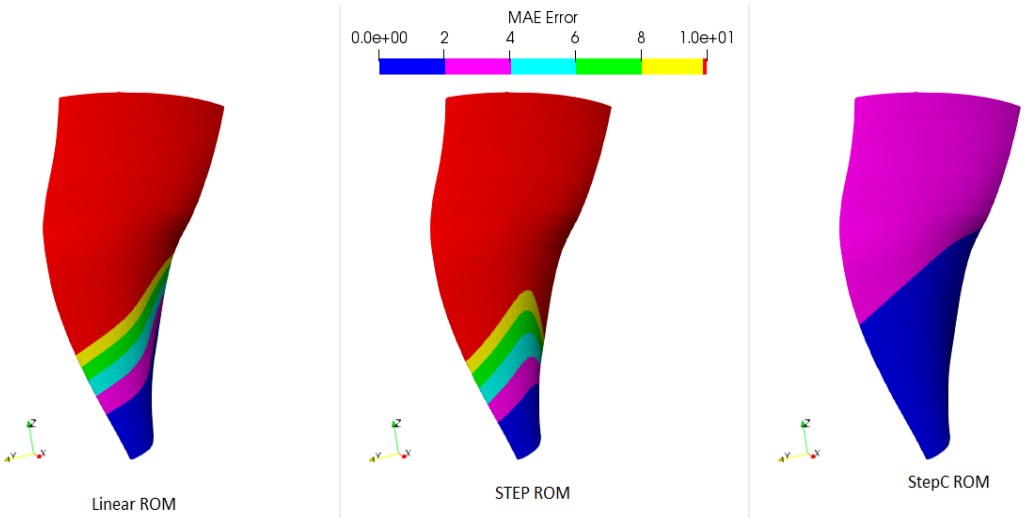

(a) Maximum value of the MAE error for a rotating velocity of 2000 rpm.

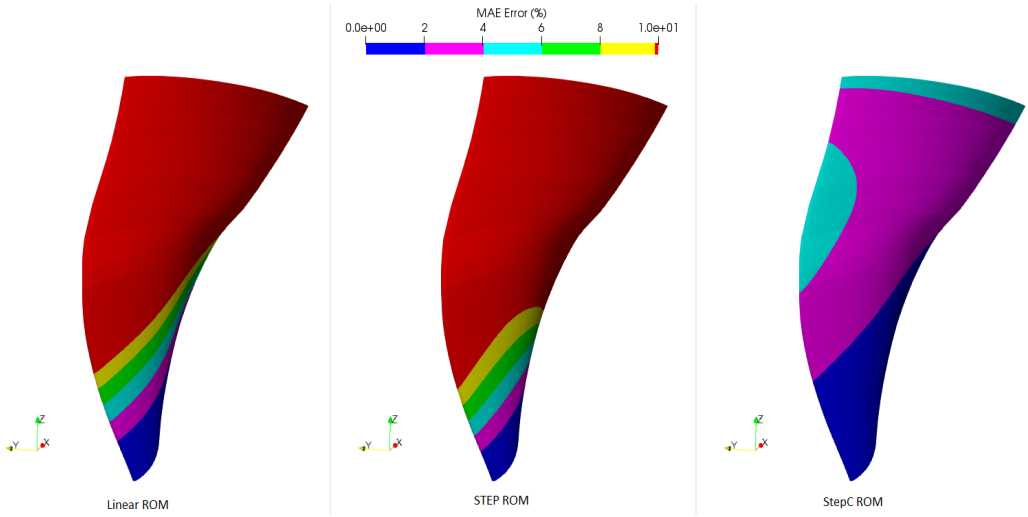

(b) Maximum value of the MAE error for a rotating velocity of 4043 rpm.

Figure 3.37: Maximum value of the MAE error for the displacements module at each node of the mesh.

Time Performances

The time performances of the ONline stage between the ROMs and the FOM are evaluated here and shown in Tab. 3.15. The computational time of the ROMs is similar regardless the chosen reduced basis. Thus, only the time performances of the LNM with $\Omega = 2000$ rpm and 3000 time steps are presented. Both ROM STEP and ROM StepC need the same computational ONline stage time to be solved. The Linear ROM is the quickest model with a 1.28 times factor with respect to nonlinear ROMs, however, the model is not precise enough. Then, the proposed StepC ROM provides the best compromise between accuracy and time consumption with a time gain of 16 523 times quicker ONline stage than the FOM. Note that the FOM time consumption corresponds to a single CPU sequential time, the real *clock time* of the FOM corresponds to a lower value (about 5h) if computations are carried out with 25 cores in parallel. However, even if multicore computations are implemented the StepC ROM is about 1500 times quicker than the parallelised FOM.

With respect to the construction of the ROMs, in addition to the reduced basis computation, the OFFline stage comprises the evaluation of the polynomial coefficients ($\approx$ 540 min CPU time). Furthermore, to construct the nonlinear force basis of StepC nonlinear ROMs, an additional FOM computation is carried out for 60 excitation periods and 2000 time steps ($\approx$ 64 h CPU time).

Table 3.15: Computational time of the ROMs.

Model	Time	t_{FOM} / t_{ROM}
FOM	90 h 52 min 48 s	
ROM Lin. Φ_{LNM}	15.2s	21 524
ROM STEP Φ_{LNM}	19.6s	16 692
ROM StepC Φ_{LNM}	19.8s	16 523

3.4.6 Forced response

The forced response of the structure for different excitation frequencies at a given rotation regime provides valuable information for the designer. For geometrically nonlinear structures, the value of the maximum amplitude and the resonant frequency may vary as shown in section 2.4.1. Furthermore, in the neighbourhood of the nonlinear resonance, the system can present more than one stable configuration for the same excitation frequency.

The forced response computed by the proposed ROMs is shown in Fig. 3.38 for 2000 rpm and 4043 rpm rotating velocities.

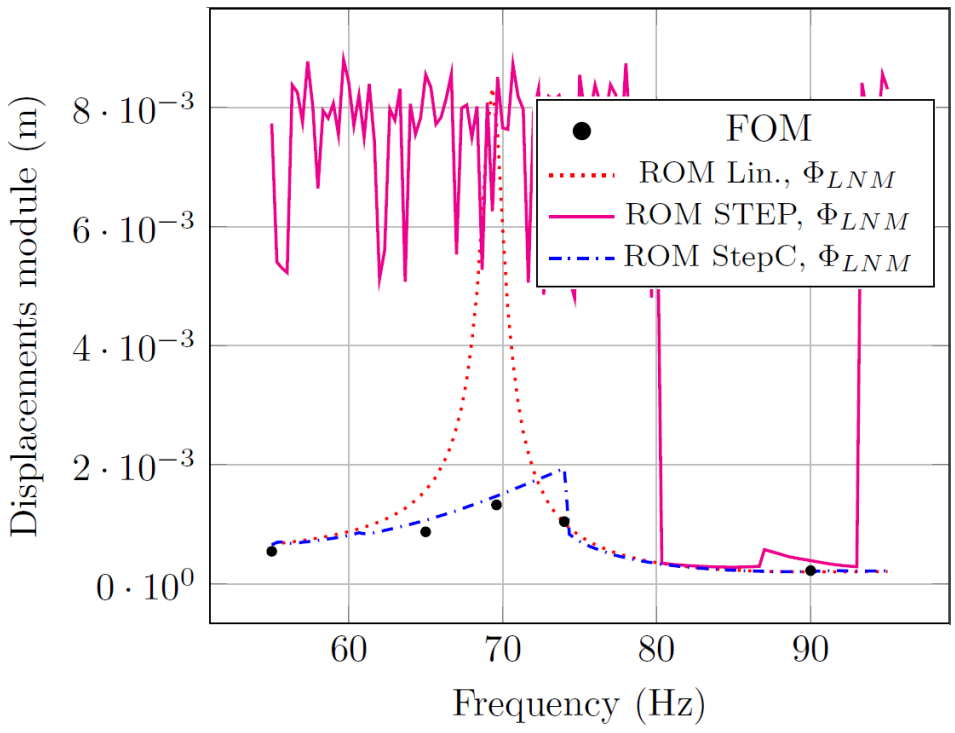

(a) $\Omega = 2000$ rpm, $\alpha_f = 0.5$.

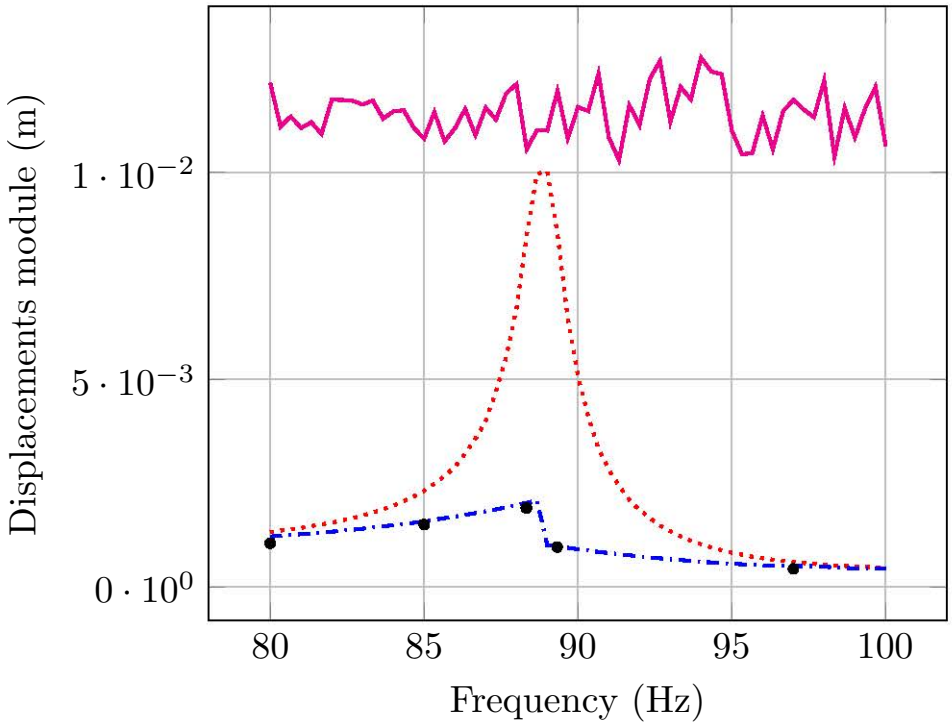

(b) $\Omega = 4043$ rpm, $\alpha_f = 0.5$.

Figure 3.38: Forced response of the structure.

The solutions are computed for 120 excitation frequencies equally distributed between 55 Hz and 95 Hz. In the present case, for each computation, the HHT-α time integration method is carried out, however, techniques like the Harmonic Balance Method (HBM) with continuation techniques properly capture the unstable branch of the solution. The study of the nonlinear force response is vital as the resonance peak is shifted in frequency. Furthermore, in the neighbourhood of the nonlinear resonance, the displacements of the StepC ROM are considerably larger than the displacements computed with the Linear ROM. The STEP solution is not capable of reproducing the forced response of the structure. The amplitude level is

It is observed that the nonlinear resonant frequency is slightly shifted with respect to the linear one. The StepC model for all rotating velocities outside resonance provides similar results as the linearised ROM.

3.4.7 Discussion and feedback

In this application the interest of implementing the StepC ROM for complex structures is highlighted. The parametrised reduced order basis are validated for different rotating velocities providing accurate results. The nonlin-

ear forces basis computed from snapshots obtained by a FOM computation are proven to be valid. The error of the StepC ROM is reduced with respect to the STEP ROM and to the Linear ROM. The Linear ROM is capable of representing the bending behaviour of the structure, however, the displacements are greater than the FOM. Furthermore, the StepC ROM also provides accurate results when computing the forced response. The advantages of the computational cost are specially highlighted as the ROMs are up to 16 500 - 21 500 times quicker than a single FOM computation.

3.5 Conclusions

In this chapter the need of a POD based correction is highlighted by means of three structures. Furthermore, the optimal construction of the StepC ROM is discussed and a detailed procedure is proposed (choosing the most representative reduced basis + constructing the POD nonlinear forces basis from static snapshots). Besides, the proposed StepC ROM provides a good representation of the nonlinear coupling between motions as well as an improved accuracy with respect to the classical Linearised ROM and STEP ROM.

The StepC ROM it has been validated for multiple numerical cases and structures with/without rotation. The StepC ROM is capable of reproducing the FOM's solution when the structure is submitted to different loadings (static, out of resonance, first mode resonance). And its parametrisation provides an improved construction time of the ROM.

Thus, the StepC ROM provides the best compromise between time consumption and accuracy satisfying the imposed design constraints.

Conclusions and perspectives

Rotating structures in industry such as fan or compressor blades, helicopter blades or wind turbine blades among others are submitted to large displacement nonlinearities during their life cycle. The latter is specially true in the actual context where the design trend is to create more flexible and larger slender structures leading to an amplification of the nonlinear effects due to larger displacements. These effects create a dependency of the structure's behaviour with respect to its displacement state. Furthermore, additional friction contact nonlinearities should be considered when studying the interaction between the disk and blade foot or between the blade and the rubber system. These interactions impact the behaviour of the structure as they lead to an energy dissipation as well as to possible surface effects such as wear or induced vibrations.

Four main contributions were presented in this work: i) the displacements around the pre-stressed equilibrium have been considered as nonlinear. Thus, the identification of the nonlinear stiffness coefficients of the STEP method was adapted in order to study the geometrically nonlinear vibrations. ii) The nonlinear forces within the structure were corrected by means of a nonlinear forces POD basis (before the projection was performed) in order to remove the spurious artefacts observed in the ROMs without correction. iii) The nonlinear ROM was parametrised with respect to the rotating velocity of the structure and was constructed in order to be valid for a given range of rotating velocities. iv) The geometrical nonlinearity was combined with the friction contact nonlinearity by means of a Craig-Bampton reduced basis that was capable of keeping some of the physical degrees of freedom as generalised displacements.

Projection based reduced order models have been developed in order to study the nonlinear dynamic analysis of rotating structures. To construct the reduced order models, four different reduction basis were considered: a) the Linear Normal Modes (LNM), b) the Proper Orthogonal Decomposition (POD), c) the LNM obtained with a MAC procedure with respect to the POD modes of the structure, and d) the Craig-Bampton reduced basis. The LNM are easy to compute, however, the nonlinear coupling behaviour is not captured. One method to improve the ROMs representativity is to judiciously choose the LNMs that best represent the behaviour of the structure. In order

to do so, a POD basis was constructed and the LNMs were compared to the POD basis by means of the MAC number. The POD basis is capable of providing accurate results, however, it can lead to very expensive constructions of the model.

The generalised nonlinear forces were obtained by means of the STEP procedure which is a third order polynomial approximation. The nonlinear stiffness coefficients were evaluated with a set of nonlinear FOM static computations. However, the classical STEP procedure combined with the considered reduced basis does not usually provide accurate results for slender structures. In order to improve the STEP ROM an original POD based nonlinear forces correction has been proposed by means of a nonlinear forces basis, $\mathbf{\Phi}_f$. For the studied structures, the best way to evaluate $\mathbf{\Phi}_f$ is to carry out a FOM static computation with an external load applied in the direction of the dynamic loading until the expected deflection amplitude is reached. Then a POD of the nonlinear forces vectors is obtained by means of a singular value decomposition (SVD). The nonlinear forces basis is then constructed with the first vector. For some cases, two vectors might be needed. However for most cases, a single vector was valid.

Three reduced order models are studied for each reduction basis. The Linear ROM corresponds to the classical linearised model where the pre-stress is considered as nonlinear but the vibration are supposed as linear, the STEP ROM corresponds to the classical STEP procedure without correction and the StepC ROM (STEP with Correction) is the original ROM proposed in this work. The latter ROMs are evaluated for three different rotating structures:

1. The first structure corresponds to a thick cantilever beam. In this study case, the interest of the POD based nonlinear forces correction is highlighted.

2. The second structure is a thin cantilever beam where the nonlinear behaviour of the structure significantly differs from the linear behaviour. In this application, the representativity of the coupling between the vertical and the longitudinal displacements is well captured with the StepC ROM providing more accurate results than with the studied classical ROMs. The choice of the reduced basis has a great influence on the ROM accuracy which is significantly improved when the reduced basis represents accurately the structure's behaviour. Furthermore, the quality of the nonlinear forces basis is improved when the snapshots are obtained from static computations. They can also be obtained from the FOM dynamic solution, but, the identification of the vectors that from the nonlinear forces basis is more complex on the cases studied.

3. The third numerical application corresponds to a complex structure representing a fan blade. The parametrisation of the ROMs is implemented and the dynamic response of the StepC ROM provides significantly more accurate results than the Linear or the STEP ROMs. The time response at first mode resonance provide accurate results in terms of amplitude and frequency of the solution. Furthermore, the forced response of the structure is well represented and the computational time of the ROMs is about 15 500 times quicker than a single FOM computation.

Two resolution methods are implemented in this work: the HHT-α method which is a time integration methods of the Newmark's method family and the Harmonic Balance Method (HBM) which computes the solution in the frequency domain. The correction of the nonlinear forces basis involved in the StepC ROM needs only a minor modification of these methods. The time solution is usually performed with the HHT-α method which provides the transient solution unlike the the HBM which computes only the converged periodic state.

In the future, the STEP ROM could be corrected by means of a stiffness weighted correction by projecting the FOM equation by $\mathbf{\Phi}^T\mathbf{K}(\Omega)$ (similar to a Petrov-Galerkin projection). This would lead to a regularisation of the solution that might reduce the spurious artefacts observed with the STEP ROM. Nevertheless, a stiffness coefficients identification without considering the quadratic terms, might lead to an improvement of the solution in case of a nonlinear behaviour where the quadratic terms do not have any influence. This could reduce the numerical error induced by these terms.

With respect to the construction of the nonlinear forces basis, new methods could be implemented: i) Using the nonlinear forces computed by the STEP solution as the snapshot matrix, ii) computing alternating stating loadings to obtain a symmetric response. iii) Combine the POD nonlinear forces vectors obtained from a static and dynamic FOM computations. iv) A general nonlinear forces basis, parametrised with respect to the excitation frequency or with respect to the excited mode at resonance.

The StepC ROM could be equally implemented for more complex study cases such as the dynamic study of a bladed disk by means of cyclic symmetry properties. Furthermore, for turbomachinery applications, the geometrically nonlinear behaviour of the bladed disk for tuned and mistuned cases could be studied. Furthermore, the imposed external loading could be obtained from an aeroelastic coupling by projecting the aerodynamic forces on the structure. If contact nonlinearities are also considered, the study of an industrial stage of turbomachinery could be implemented.

Bibliography

[Abbott, 1978] Abbott, J. P. (1978). An efficient algorithm for the determination of certain bifurcation points. *Journal of Computational and Applied Mathematics*, 4(1):19–27.

[Adhikari and Phani, 2004] Adhikari, S. and Phani, A. S. (2004). Rayleigh?s classical damping revisited.

[Al Sayed et al., 2011] Al Sayed, B., Chatelet, E., Baguet, S., and Jacquet-Richardet, G. (2011). Dissipated energy and boundary condition effects associated to dry friction on the dynamics of vibrating structures. *Mechanism and Machine Theory*, 46(4):479–491.

[Alam et al., 2007] Alam, M. S., Haque, M. E., and Hossain, M. B. (2007). A new analytical technique to find periodic solutions of non-linear systems. *International Journal of Non-Linear Mechanics*, 42(8):1035–1045.

[Allgower and Georg, 2003] Allgower, E. L. and Georg, K. (2003). *Introduction to numerical continuation methods*. SIAM.

[Ammar et al., 2006] Ammar, A., Mokdad, B., Chinesta, F., and Keunings, R. (2006). A new family of solvers for some classes of multidimensional partial differential equations encountered in kinetic theory modeling of complex fluids. *Journal of Non-Newtonian Fluid Mechanics*, 139(3):153–176.

[Ammar et al., 2007] Ammar, A., Mokdad, B., Chinesta, F., and Keunings, R. (2007). A new family of solvers for some classes of multidimensional partial differential equations encountered in kinetic theory modelling of complex fluids: Part ii: Transient simulation using space-time separated representations. *Journal of Non-Newtonian Fluid Mechanics*, 144(2-3):98–121.

[Amsallem et al., 2009] Amsallem, D., Cortial, J., Carlberg, K., and Farhat, C. (2009). A method for interpolating on manifolds structural dynamics reduced-order models. *International journal for numerical methods in engineering*, 80(9):1241–1258.

[Andersen and Poulsen, 2014] Andersen, S. and Poulsen, P. N. (2014). Reduction method for real-time simulations in hybrid testing. In *IX International Conference on Structural Dynamics (EURODYN 2014)*.

[Avilés, 2002] Avilés, R. (2002). *Métodos de análisis para diseño mecánico: diseño mecánico; tema II: análisis estático v. 2. Tema III: elementos finitos en estática v. 3. Tema IV: elementos finitos en dinámica v. 4. Tema V: análisis de fatiga*. Publicaciones-Escuela Superior de Ingenieros.

[Azam and Mariani, 2013] Azam, S. E. and Mariani, S. (2013). Investigation of computational and accuracy issues in pod-based reduced order modeling of dynamic structural systems. *Engineering structures*, 54:150–167.

[Balmaseda et al., 2018] Balmaseda, M., Jacquet-Richardet, G., Placzek, A., and Tran, D.-M. (2018). Reduced order models for dynamic analysis of nonlinear rotating structures. In *Proceedings of 6th European Conference on Computational Mechanics / 7th European Conference on Computational Fluid Dynamics*. Glasgow, UK.

[Balmaseda et al., 2019] Balmaseda, M., Jacquet-Richardet, G., Placzek, A., and Tran, D.-M. (2019). Reduced order models for nonlinear dynamic analysis with application to a fan blade. In *Proceedings of ASME Turbo Expo 2019*. American Society of Mechanical Engineers.

[Bamford, 1967] Bamford, R. (1967). A modal combination program for dynamic analysis of structures. *Jet Propulsion Laboratory Technical Memorandum*, (33-290).

[Barrault et al., 2004] Barrault, M., Maday, Y., Nguyen, N. C., and Patera, A. T. (2004). An 'empirical interpolation'method: application to efficient reduced-basis discretization of partial differential equations. *Comptes Rendus Mathematique*, 339(9):667–672.

[Bastien et al., 2007] Bastien, J., Michon, G., Manin, L., and Dufour, R. (2007). An analysis of the modified dahl and masing models: application to a belt tensioner. *Journal of Sound and Vibration*, 302(4-5):841–864.

[Batailly et al., 2014] Batailly, A., Legrand, M., Millecamps, A., and Garcin, F. (2014). High-pressure compressor blade dynamics under aerodynamic and blade-tip unilateral contact forcings. In *ASME Turbo Expo 2014: Turbine Technical Conference and Exposition*, pages V07BT33A010–V07BT33A010. American Society of Mechanical Engineers.

[Bathe, 2006] Bathe, K.-J. (2006). *Finite element procedures*. Klaus-Jurgen Bathe.

[Beléndez et al., 2007] Beléndez, A., Pascual, C., Gallego, S., Ortuño, M., and Neipp, C. (2007). Application of a modified he's homotopy perturbation method to obtain higher-order approximations of an x1/3 force nonlinear oscillator. *Physics Letters A*, 371(5):421–426.

[Beley et al., 2017] Beley, J.-D., Shen, Z., Chouvion, B., and Thouverez, F. (2017). Vibration non-linéaire de poutre en grande transformation. In *Conference: CSMA 2017, At Giens, France*.

[Bellizzi and Sampaio, 2009] Bellizzi, S. and Sampaio, R. (2009). Karhunen–loève modes obtained from displacement and velocity fields: assessments and comparisons. *Mechanical Systems and Signal Processing*, 23(4):1218–1222.

[Belytschko et al., 2013] Belytschko, T., Liu, W. K., Moran, B., and Elkhodary, K. (2013). *Nonlinear finite elements for continua and structures*. John wiley & sons.

[Benfield and Hruda, 1971] Benfield, W. and Hruda, R. (1971). Vibration analysis of structures by component mode substitution. *AIAA journal*, 9(7):1255–1261.

[Bond and Daniel, 2007] Bond, B. N. and Daniel, L. (2007). A piecewise-linear moment-matching approach to parameterized model-order reduction for highly nonlinear systems. *IEEE Transactions on Computer-Aided Design of Integrated Circuits and Systems*, 26(12):2116–2129.

[Boyce et al., 1954] Boyce, W., DiPrima, R., and Handelman, G. (1954). Vibrations of rotating beams of constant section. In *JOURNAL OF APPLIED MECHANICS-TRANSACTIONS OF THE ASME*, volume 21, pages 286–286. ASME-AMER SOC MECHANICAL ENG 345 E 47TH ST, NEW YORK, NY 10017.

[Bransch and Lehmann, 2011] Bransch, M. and Lehmann, L. (2011). A nonlinear hht-α method with elastic–plastic soil–structure interaction in a coupled sbfem/fem approach. *Computers and Geotechnics*, 38(1):80–87.

[Brennan et al., 2008] Brennan, M., Kovacic, I., Carrella, A., and Waters, T. (2008). On the jump-up and jump-down frequencies of the duffing oscillator. *Journal of Sound and Vibration*, 318(4-5):1250–1261.

[Burton et al., 1976] Burton, R., Kilaparti, S., and Heckmann, S. (1976). Modeling of turbine blade tip contact. *Journal of Engineering for Power*, 98(4):435–440.

[Capiez-Lernout et al., 2017] Capiez-Lernout, E., Soize, C., Akkaoui, Q., and Ohayon, R. (2017). Uncertainty propagation in a nonlinear reduced-order model in internal elasto-acoustics. In *Congrès Français de Mécanique (CFM 2017)*, volume 199, pages 1204–1209. Elsevier.

[Capiez-Lernout et al., 2014] Capiez-Lernout, E., Soize, C., and Mbaye, M. (2014). Geometric nonlinear dynamic analysis of uncertain structures with cyclic symmetry-application to a mistuned industrial bladed disk. In *International Conference on Uncertainty in Structural Dynamics, USD2014*, pages 1–14.

[Capiez-Lernout et al., 2012] Capiez-Lernout, E., Soize, C., and Mignolet, M. (2012). Computational stochastic statics of an uncertain curved structure with geometrical nonlinearity in three-dimensional elasticity. *Computational Mechanics*, 49(1):87–97.

[Carassale and Solari, 2002] Carassale, L. and Solari, G. (2002). Wind modes for structural dynamics: a continuous approach. *Probabilistic Engineering Mechanics*, 17(2):157–166.

[Cardarelli, 2000] Cardarelli, F. (2000). *Materials handbook*. Springer.

[Caughey, 1960] Caughey, T. (1960). Classical normal modes in damped linear dynamic systems. *Journal of Applied Mechanics*, 27(2):269–271.

[Chan and Keller, 1982] Chan, T. F. and Keller, H. (1982). Arc-length continuation and multigrid techniques for nonlinear elliptic eigenvalue problems. *SIAM Journal on Scientific and Statistical Computing*, 3(2):173–194.

[Chang, 2008] Chang, S.-Y. (2008). Performance of the hht-α method for the solution of nonlinear systems. *International Journal of Structural Stability and Dynamics*, 8(02):321–337.

[Chapman et al., 2017] Chapman, T., Avery, P., Collins, P., and Farhat, C. (2017). Accelerated mesh sampling for the hyper reduction of nonlinear computational models. *International Journal for Numerical Methods in Engineering*, 109(12):1623–1654.

[Chaturantabut and Sorensen, 2010] Chaturantabut, S. and Sorensen, D. C. (2010). Nonlinear model reduction via discrete empirical interpolation. *SIAM Journal on Scientific Computing*, 32(5):2737–2764.

[Chau et al., 2003] Chau, O., Fernández, J., Han, W., and Sofonea, M. (2003). Variational and numerical analysis of a dynamic frictionless contact problem with adhesion. *Journal of computational and applied mathematics*, 156(1):127–157.

[Chinesta et al., 2010] Chinesta, F., Ammar, A., and Cueto, E. (2010). Recent advances and new challenges in the use of the proper generalized decomposition for solving multidimensional models. *Archives of Computational methods in Engineering*, 17(4):327–350.

[Chinesta et al., 2011] Chinesta, F., Ladeveze, P., and Cueto, E. (2011). A short review on model order reduction based on proper generalized decomposition. *Archives of Computational Methods in Engineering*, 18(4):395.

[Couplet et al., 2005] Couplet, M., Basdevant, C., and Sagaut, P. (2005). Calibrated reduced-order pod-galerkin system for fluid flow modelling. *Journal of Computational Physics*, 207(1):192–220.

[Craig and Bampton, 1968] Craig, R. and Bampton, M. (1968). Coupling of substructures for dynamic analyses. *AIAA journal*, 6(7):1313–1319.

[Craig Jr, 1985] Craig Jr, R. R. (1985). A review of time-domain and frequency-domain component mode synthesis method.

[da Silva and Hodges, 1986] da Silva, M. C. and Hodges, D. (1986). Nonlinear flexure and torsion of rotating beams, with application to helicopter rotor blades - ii. response to stability results. *Vertica*, 10(2):171–186.

[Dahl, 1968] Dahl, P. R. (1968). A solid friction model. Technical report, Aerospace Corp El Segundo Ca.

[Desceliers, 2001] Desceliers, C. (2001). *Dynamique non linéaire en déplacements finis des structures tridimensionnelles viscoélastiques en rotation.* PhD thesis, Châtenay-Malabry, École centrale Paris.

[Drozdowski et al., 2016] Drozdowski, R., Völker, L., Häfele, M., and Vogt, D. M. (2016). Numerical and experimental analysis of low-pressure steam turbine blades coupled with lacing wire. *Proceedings of the Institution of Mechanical Engineers, Part A: Journal of Power and Energy*, 230(3):332–342.

[Du et al., 1994] Du, H., Lim, M., and Liew, K. (1994). A power series solution for vibration of a rotating timoshenko beam. *Journal of Sound and Vibration*, 175(4):505–523.

[Duvaut and Lions, 1972] Duvaut, G. and Lions, J. L. (1972). *Les inéquations en mécanique et en physique.* Dunod.

[D'Ambrosio et al., 2005] D'Ambrosio, F., Chatelet, E., and Jacquet, G. (2005). Influence of contact states on the dynamic behavior of rubbing structures. In *ASME Turbo Expo 2005: Power for Land, Sea, and Air*, pages 429–440. American Society of Mechanical Engineers.

[EDF, 1989] EDF (1989). Finite element *code_aster*, analysis of structures and thermomechanics for studies and research. Open source on www.code-aster.org.

[Engblom and Chang, 1991] Engblom, J. and Chang, C. (1991). Nonlinear dynamical response of impulsively loaded structures-a reduced basis approach. *AIAA journal*, 29(4):613–618.

[Erlicher et al., 2002] Erlicher, S., Bonaventura, L., and Bursi, O. S. (2002). The analysis of the generalized-α method for non-linear dynamic problems. *Computational Mechanics*, 28(2):83–104.

[Farhat et al., 2015] Farhat, C., Chapman, T., and Avery, P. (2015). Structure-preserving, stability, and accuracy properties of the energy-conserving sampling and weighting method for the hyper reduction of nonlinear finite element dynamic models. *International Journal for Numerical Methods in Engineering*, 102(5):1077–1110.

[Farvaque et al., 1984] Farvaque, M., Gantenbien, F., Gibert, R., and Guilbaud, D. (1984). Formalisme du programme d'analyse dynamique par sous-structuration oscar développé dans le cadre du système castem 2000. *Rapport technique, CEA*.

[Fichera, 1964] Fichera, G. (1964). *Problemi elastostatici con vincoli unilaterali: il problema di Signorini con ambigue condizioni al contorno*. Accademia nazionale dei Lincei.

[Firrone et al., 2011] Firrone, C. M., Zucca, S., and Gola, M. M. (2011). The effect of underplatform dampers on the forced response of bladed disks by a coupled static/dynamic harmonic balance method. *International Journal of Non-Linear Mechanics*, 46(2):363–375.

[Gastaldi et al., 2017] Gastaldi, C., Grossi, E., Berruti, T., et al. (2017). On the choice of contact parameters for the forced response calculation of a bladed disk with underplatform dampers. In *Global Power and Propulsion Forum (GPPF), Zurich, Switzerland, Jan*, pages 16–18.

[Genta and Silvagni, 2014] Genta, G. and Silvagni, M. (2014). On centrifugal softening in finite element method rotordynamics. *Journal of Applied Mechanics*, 81(1):011001.

[Genta et al., 2013] Genta, G., Silvagni, M., and Qingwen, C. (2013). Dynamic analysis of rotors: Comparison between the simplified one-dimensional results and those obtained through 3-d modeling.

[Géradin and Rixen, 2014] Géradin, M. and Rixen, D. J. (2014). *Mechanical vibrations: theory and application to structural dynamics*. John Wiley & Sons.

[Griffin, 1989] Griffin, J. (1989). An alternating frequency/time domain method for calculating the steady-state response of nonlinear dynamic systems. *Journal of applied mechanics*, 56:149.

[Grolet and Thouverez, 2010] Grolet, A. and Thouverez, F. (2010). Vibration analysis of a nonlinear system with cyclic symmetry. *Journal of Engineering for Gas Turbines and Power*, 133(2):022502.

[Guskov et al., 2008] Guskov, M., Sinou, J.-J., and Thouverez, F. (2008). Multi-dimensional harmonic balance applied to rotor dynamics. *Mechanics Research Communications*, 35(8):537–545.

[Hager et al., 1968] Hager, R. D., Lewis, G. W., and Wagner, J. M. (1968). Use of wire lacing to reduce blade vibration in an axial-flow compressor rotor. Technical report, NASA.

[Han and Feeny, 2003] Han, S. and Feeny, B. (2003). Application of proper orthogonal decomposition to structural vibration analysis. *Mechanical Systems and Signal Processing*, 17(5):989–1001.

[Hansen, 1990] Hansen, P. (1990). Truncated singular value decomposition solutions to discrete ill-posed problems with ill-determined numerical rank. *SIAM Journal on Scientific and Statistical Computing*, 11(3):503–518.

[Henry, 1981] Henry, R. (1981). *Contribution à l'étude dynamique des machines tournantes*. PhD thesis, INSA Lyon, France.

[Hestenes, 1969] Hestenes, M. R. (1969). Multiplier and gradient methods. *Journal of optimization theory and applications*, 4(5):303–320.

[Hilber et al., 1977] Hilber, H. M., Hughes, T. J., and Taylor, R. L. (1977). Improved numerical dissipation for time integration algorithms in structural dynamics. *Earthquake Engineering & Structural Dynamics*, 5(3):283–292.

[Hodges et al., 1996] Hodges, D. H., Shang, X., and Cesnik, C. E. (1996). Finite element solution of nonlinear intrinsic equations for curved composite beams. *Journal of the American helicopter society*, 41(4):313–321.

[Hollkamp and Gordon, 2008] Hollkamp, J. J. and Gordon, R. W. (2008). Reduced-order models for nonlinear response prediction: Implicit condensation and expansion. *Journal of Sound and Vibration*, 318(4):1139–1153.

[Hong et al., 2011] Hong, S.-K., Epureanu, B. I., Castanier, M. P., and Gorsich, D. J. (2011). Parametric reduced-order models for predicting the vibration response of complex structures with component damage and uncertainties. *Journal of sound and vibration*, 330(6):1091–1110.

[Hosen et al., 2012] Hosen, M. A., Rahman, M. S., Alam, M. S., and Amin, M. R. (2012). An analytical technique for solving a class of strongly nonlinear conservative systems. *Applied Mathematics and Computation*, 218(9):5474–5486.

[Huang and Han, 2010] Huang, H. and Han, Q. (2010). Research on nonlinear postbuckling of functionally graded cylindrical shells under radial loads. *Composite Structures*, 92(6):1352–1357.

[Hulbert, 1993] Hulbert, G. (1993). A time integration algorithm for structural dynamics with improved numerical dissipation: The generalized-en? method. *Ann Arbor*, 1050:48109–2125.

[Hurty, 1960] Hurty, W. C. (1960). Vibrations of structural systems by component mode synthesis. *Journal of the Engineering Mechanics Division*, 86(4):51–70.

[Hurty, 1965] Hurty, W. C. (1965). Dynamic analysis of structural systems using component modes. *AIAA journal*, 3(4):678–685.

[Idelsohn and Cardona, 1985] Idelsohn, S. R. and Cardona, A. (1985). A load-dependent basis for reduced nonlinear structural dynamics. *Computers & Structures*, 20(1-3):203–210.

[Ismail et al., 2009] Ismail, M., Ikhouane, F., and Rodellar, J. (2009). The hysteresis bouc-wen model, a survey. *Archives of Computational Methods in Engineering*, 16(2):161–188.

[Iwan, 1966] Iwan, W. D. (1966). A distributed-element model for hysteresis and its steady-state dynamic response. *Journal of Applied Mechanics*, 33(4):893–900.

[Jezequel and Lamarque, 1991] Jezequel, L. and Lamarque, C.-H. (1991). Analysis of non-linear dynamical systems by the normal form theory. *Journal of sound and vibration*, 149(3):429–459.

[Jiang et al., 2005] Jiang, D., Pierre, C., and Shaw, S. (2005). The construction of non-linear normal modes for systems with internal resonance. *International Journal of Non-Linear Mechanics*, 40(5):729–746.

[Jiazhe et al., 2018] Jiazhe, Z., Yanrong, W., Yanbin, L., and Xiaojie, Z. (2018). A vibration damping analysis method of turbine blade shroud dampers based on a given eigen-mode. In *ASME 2018 International Design Engineering Technical Conferences and Computers and Information in Engineering Conference*, pages V008T10A014–V008T10A014. American Society of Mechanical Engineers.

[Kalmár-Nagy and Balachandran, 2011] Kalmár-Nagy, T. and Balachandran, B. (2011). Forced harmonic vibration of a duffing oscillator with linear viscous damping. *The Duffing Equation: Nonlinear Oscillators and Their Behaviour, Wiley, New York*, pages 139–173.

[Kapania and Byun, 1993] Kapania, R. and Byun, C. (1993). Reduction methods based on eigenvectors and ritz vectors for nonlinear transient analysis. *Computational mechanics*, 11(1):65–82.

[Kikuchi and Oden, 1988] Kikuchi, N. and Oden, J. T. (1988). *Contact problems in elasticity: a study of variational inequalities and finite element methods*, volume 8. siam.

[Kirby et al., 1990] Kirby, M., Boris, J., and Sirovich, L. (1990). A proper orthogonal decomposition of a simulated supersonic shear layer. *International journal for numerical methods in fluids*, 10(4):411–428.

[Klarmann and Wagner, 2015] Klarmann, S. and Wagner, W. (2015). Enhanced studies on a composite time integration scheme in linear and nonlinear dynamics. *Computational Mechanics*, 55(3):455–468.

[Konyukhov and Schweizerhof, 2012] Konyukhov, A. and Schweizerhof, K. (2012). *Computational Contact Mechanics: geometrically exact theory for arbitrary shaped bodies*, volume 67. Springer Science & Business Media.

[Kovacic and Brennan, 2011] Kovacic, I. and Brennan, M. J. (2011). *The Duffing equation: nonlinear oscillators and their behaviour*. John Wiley & Sons.

[Krack et al., 2017] Krack, M., Salles, L., and Thouverez, F. (2017). Vibration prediction of bladed disks coupled by friction joints. *Archives of Computational Methods in Engineering*, 24(3):589–636.

[Krenk, 2009] Krenk, S. (2009). *Non-linear modeling and analysis of solids and structures*. Cambridge University Press.

[Kuhl and Ramm, 1996] Kuhl, D. and Ramm, E. (1996). Constraint energy momentum algorithm and its application to non-linear dynamics of shells. *Computer methods in applied mechanics and engineering*, 136(3-4):293–315.

[Kumar et al., 2015] Kumar, S., Mitra, A., and Roy, H. (2015). Geometrically nonlinear free vibration analysis of axially functionally graded taper beams. *Engineering Science and Technology, an International Journal*, 18(4):579–593.

[Kunisch and Volkwein, 2002] Kunisch, K. and Volkwein, S. (2002). Galerkin proper orthogonal decomposition methods for a general equation in fluid dynamics. *SIAM Journal on Numerical analysis*, 40(2):492–515.

[Kurstak et al., 2018] Kurstak, E., Wilber, R., and D'Souza, K. (2018). Parametric reduced order models for bladed disks with mistuning and varying operational speed. *Journal of Engineering for Gas Turbines and Power*.

[Lanczos, 1950] Lanczos, C. (1950). *An iteration method for the solution of the eigenvalue problem of linear differential and integral operators*. United States Governm. Press Office Los Angeles, CA.

[Laursen, 2002] Laursen, T. (2002). Computational contact and impact mechanics. 2002.

[Legrand et al., 2008] Legrand, M., Pierre, C., and Cartraud, P. (2008). Full 3d strategies for rotor-stator contact interaction in turbomachinery. In *12th*

International Symposium on Transport Phenomena and Dynamics of Rotating Machinery.

[Lenaerts et al., 2003] Lenaerts, V., Kerschen, G., and Golinval, J.-C. (2003). Identification of a continuous structure with a geometrical non-linearity. part ii: Proper orthogonal decomposition. *Journal of Sound and vibration*, 262(4):907–919.

[Li et al., 2019] Li, D., Xu, C., Liu, T., Gola, M. M., and Wen, L. (2019). A modified iwan model for micro-slip in the context of dampers for turbine blade dynamics. *Mechanical Systems and Signal Processing*, 121:14–30.

[Lim and Lai, 2006] Lim, C. and Lai, S. (2006). Accurate higher-order analytical approximate solutions to nonconservative nonlinear oscillators and application to van der pol damped oscillators. *International journal of mechanical sciences*, 48(5):483–492.

[Lions and Stampacchia, 1967] Lions, J.-L. and Stampacchia, G. (1967). Variational inequalities. *Communications on pure and applied mathematics*, 20(3):493–519.

[Luco and Lanzi, 2017] Luco, J. E. and Lanzi, A. (2017). Optimal caughey series representation of classical damping matrices. *Soil Dynamics and Earthquake Engineering*, 92:253–265.

[Lülf, 2013] Lülf, F. A. (2013). *An integrated method for the transient solution of reduced order models of geometrically nonlinear structural dynamic systems*. PhD thesis, CNAM, Paris, France.

[Luongo et al., 2009] Luongo, C., Masson, P., Nam, T., Mavris, D., D. Kim, H., V. Brown, G., Waters, M., and Hall, D. (2009). Next generation more-electric aircraft: A potential application for hts superconductors. *Applied Superconductivity, IEEE Transactions on*, 19:1055 – 1068.

[MacNeal, 1971] MacNeal, R. H. (1971). A hybrid method of component mode synthesis. *Computers & Structures*, 1(4):581–601.

[Martin and Thouverez, 2019] Martin, A. and Thouverez, F. (2019). Dynamic analysis and reduction of a cyclic symmetric system subjected to geometric nonlinearities. *Journal of Engineering for Gas Turbines and Power*, 141(4):041027.

[Martinez et al., 1985] Martinez, D. R., Miller, A. K., and Carne, T. G. (1985). Combined experimental/analytical modeling of shell/payload structures. Technical report, Sandia National Labs., Albuquerque, NM (USA).

[Maschho and Sorensen, 1996] Maschho, K. J. and Sorensen, D. (1996). A portable implementation of arpack for distributed memory parallel architectures. In *Proceedings of the Copper Mountain Conference on Iterative Methods*, volume 1.

[McNally, 1977] McNally, W. D. (1977). Review of experimental work on transonic flow in turbomachinery.

[Menq, 1985] Menq, C. (1985). Vibratory response of frictionally constrained gas turbine blades. *Ph. D. Thesis, Carnegie-Mellon University*.

[Menq and Yang, 1998] Menq, C. and Yang, B. (1998). Non-linear spring resistance and friction damping of frictional constraint having two-dimensional motion. *Journal of Sound and Vibration*, 217(1):127–143.

[Menq et al., 1986] Menq, C.-H., Bielak, J., and Griffin, J. (1986). The influence of microslip on vibratory response, part i: a new microslip model. *Journal of Sound and Vibration*, 107(2):279–293.

[Metropolis and Ulam, 1949] Metropolis, N. and Ulam, S. (1949). The monte carlo method. *Journal of the American statistical association*, 44(247):335–341.

[Mickens, 1984] Mickens, R. (1984). Comments on the method of harmonic balance. *Journal of Sound and Vibration*.

[Mickens, 1996] Mickens, R. E. (1996). *Oscillations in planar dynamic systems*, volume 37. World Scientific.

[Mignolet et al., 2013] Mignolet, M. P., Przekop, A., Rizzi, S. A., and Spottswood, S. M. (2013). A review of indirect/non-intrusive reduced order modeling of nonlinear geometric structures. *Journal of Sound and Vibration*, 332(10):2437–2460.

[Mindlin, 1949] Mindlin, R. (1949). Compliance of elastic bodies in contact. *J. Appl. Mech., ASME*, 16:259–268.

[Muravyov and Rizzi, 2003] Muravyov, A. A. and Rizzi, S. A. (2003). Determination of nonlinear stiffness with application to random vibration of geometrically nonlinear structures. *Computers & Structures*, 81(15):1513–1523.

[Nayfeh and Sanchez, 1989] Nayfeh, A. H. and Sanchez, N. E. (1989). Bifurcations in a forced softening duffing oscillator. *International Journal of Non-Linear Mechanics*, 24(6):483–497.

[Newmark, 1959] Newmark, N. M. (1959). A method of computation for structural dynamics. *Journal of the engineering mechanics division*, 85(3):67–94.

[Padova et al., 2007] Padova, C., Barton, J., Dunn, M. G., and Manwaring, S. (2007). Experimental results from controlled blade tip/shroud rubs at engine speed. *Journal of turbomachinery*, 129(4):713–723.

[Peletan, 2012] Peletan, L. (2012). *Stratégie de modélisation simplifiée et de résolution accélérée en dynamique non linéaire des machines tournantes: Application au contact rotor-stator*. PhD thesis, INSA de Lyon, France.

[Peletan et al., 2014] Peletan, L., Baguet, S., Torkhani, M., and Jacquet-Richardet, G. (2014). Quasi-periodic harmonic balance method for rubbing self-induced vibrations in rotor–stator dynamics. *Nonlinear Dynamics*, 78(4):2501–2515.

[Perez et al., 2014] Perez, R., Wang, X., and Mignolet, M. P. (2014). Nonintrusive structural dynamic reduced order modeling for large deformations: enhancements for complex structures. *Journal of Computational and Nonlinear Dynamics*, 9(3):031008.

[Pesheck et al., 2001] Pesheck, E., Pierre, C., and Shaw, S. (2001). Accurate reduced-order models for a simple rotor blade model using nonlinear normal modes. *Mathematical and Computer Modelling*, 33(10-11):1085–1097.

[Pesheck et al., 2002] Pesheck, E., Pierre, C., and Shaw, S. W. (2002). Modal reduction of a nonlinear rotating beam through nonlinear normal modes. *Journal of vibration and Acoustics*, 124(2):229–236.

[Petrov and Ewins, 2002] Petrov, E. and Ewins, D. (2002). Analytical formulation of friction interface elements for analysis of nonlinear multi-harmonic vibrations of bladed discs. In *ASME Turbo Expo 2002: Power for Land, Sea, and Air*, pages 899–908. American Society of Mechanical Engineers.

[Petrov and Ewins, 2006] Petrov, E. and Ewins, D. (2006). Effects of damping and varying contact area at blade-disk joints in forced response analysis of bladed disk assemblies. *Journal of turbomachinery*, 128(2):403–410.

[Petrov and Ewins, 2007] Petrov, E. and Ewins, D. (2007). Advanced modeling of underplatform friction dampers for analysis of bladed disk vibration. *Journal of Turbomachinery*, 129(1):143–150.

[Placzek, 2009] Placzek, A. (2009). *Construction de modèles d'ordre réduit non-linéaires basés sur la décomposition orthogonale propre pour l'aéroélasticité*. PhD thesis, Conservatoire national des arts et metiers-CNAM.

[Pnueli, 1972] Pnueli, D. (1972). Natural bending frequency comparable to rotational frequency in rotating cantilever beam. *Journal of Applied Mechanics*, 39(2):602–604.

[Powell, 1969] Powell, M. J. (1969). A method for nonlinear constraints in minimization problems. *Optimization*, pages 283–298.

[Radu et al., 2004] Radu, A., Yang, B., Kim, K., and Mignolet, M. (2004). Prediction of the dynamic response and fatigue life of panels subjected to thermo-acoustic loading. In *Proceedings of the 45th Structures, Structural Dynamics, and Materials Conference*, pages 19–22.

[Rizzi and Muravyov, 2001] Rizzi, S. A. and Muravyov, A. A. (2001). Improved equivalent linearization implementations using nonlinear stiffness evaluation. *NASA/TM-2001-210838, L-18068, NAS 1.15:210838*.

[Rook, 2002] Rook, T. (2002). An alternate method to the alternating time-frequency method. *Nonlinear Dynamics*, 27(4):327–339.

[Rosenberg, 1962] Rosenberg, R. (1962). The normal modes of nonlinear n-degree-of-freedom systems.

[Rubin, 1975] Rubin, S. (1975). Improved component-mode representation for structural dynamic analysis. *AIAA journal*, 13(8):995–1006.

[Ryckelynck, 2005] Ryckelynck, D. (2005). A priori hyperreduction method: an adaptive approach. *Journal of computational physics*, 202(1):346–366.

[Sampaio and Soize, 2007] Sampaio, R. and Soize, C. (2007). Remarks on the efficiency of POD for model reduction in non-linear dynamics of continuous elastic systems. *International Journal for numerical methods in Engineering*, 72(1):22–45.

[Sanliturk and Ewins, 1996] Sanliturk, K. and Ewins, D. (1996). Modelling two-dimensional friction contact and its application using harmonic balance method. *Journal of sound and vibration*, 193(2):511–523.

[Sanliturk et al., 2001] Sanliturk, K. Y., Ewins, D. J., and Stanbridge, A. B. (2001). Underplatform dampers for turbine blades: theoretical modeling, analysis, and comparison with experimental data. *Journal of Engineering for Gas Turbines and Power*, 123(4):919–929.

[Sayed, 2011] Sayed, B. A. (2011). *Comportement dynamique des ensembles tournants de turbomachines: Maîtrise des effets des dispositifs de liaisonnement amortisseurs*. PhD thesis, Lyon, INSA.

[Schotte, 2001] Schotte, J.-S. (2001). *Influence de la gravité sur les vibrations linéaires d'une structure élastique partiellement remplie par un liquide incompressible*. PhD thesis, Conservatoire national des arts et metiers-CNAM.

[Schotté and Ohayon, 2009] Schotté, J.-S. and Ohayon, R. (2009). Various modelling levels to represent internal liquid behaviour in the vibration analysis of complex structures. *Computer Methods in Applied Mechanics and Engineering*, 198(21-26):1913–1925.

[Sénéchal et al., 2009] Sénéchal, A., Thomas, O., Deu, J.-F., and Jean, P. (2009). Atténuation des vibrations de structures complexes par shunt piézoélectrique-application à un modèle simplifié d'aube de turbomachine. In *9e Colloque national en calcul des structures*.

[Shaw and Pierre, 1992] Shaw, S. W. and Pierre, C. (1992). On nonlinear normal modes. In *Winter Annual Meeting of the American Society of Mechanical Engineers*, pages 1–5. Publ by ASME.

[Sirovich, 1987] Sirovich, L. (1987). Turbulence and the dynamics of coherent structures. i-iii. coherent structures. *Quarterly of applied mathematics*, 45(3):561–571.

[Slaats et al., 1995] Slaats, P., De Jongh, J., and Sauren, A. (1995). Model reduction tools for nonlinear structural dynamics. *Computers & structures*, 54(6):1155–1171.

[Stafford and Giurgiutiu, 1975] Stafford, R. and Giurgiutiu, V. (1975). Semi-analytic methods for rotating timoshenko beams. *International Journal of Mechanical Sciences*, 17(11-12):719–727.

[Sternchüss, 2009] Sternchüss, A. (2009). *Multi-level parametric reduced models of rotating bladed disk assemblies*. PhD thesis, Ecole Centrale Paris, France.

[Strang, 1980] Strang, G. (1980). Linear algebra and its applications.

[Strutt and Rayleigh, 1945] Strutt, J. W. and Rayleigh, B. (1945). *The theory of sound*. Dover.

[Sundararajan and Noah, 1997] Sundararajan, P. and Noah, S. (1997). Dynamics of forced nonlinear systems using shooting/arc-length continuation method—application to rotor systems. *Journal of vibration and acoustics*, 119(1):9–20.

[Tang and Dowell, 1996] Tang, D. and Dowell, E. (1996). Nonlinear response of a non-rotating rotor blade to a periodic gust. *Journal of Fluids and Structures*, 10(7):721–742.

[Thomas et al., 2016] Thomas, O., Sénéchal, A., and Deü, J.-F. (2016). Hardening/softening behavior and reduced order modeling of nonlinear vibrations of rotating cantilever beams. *Nonlinear Dynamics*, 86(2):1293–1318.

[Touzé and Amabili, 2006] Touzé, C. and Amabili, M. (2006). Nonlinear normal modes for damped geometrically nonlinear systems: Application to reduced-order modelling of harmonically forced structures. *Journal of sound and vibration*, 298(4-5):958–981.

[Tran, 1992] Tran, D.-M. (1992). Méthodes de synthèse modale mixtes. *Révue Européenne des Eléments finis*.

[Tran, 1993] Tran, D.-M. (1993). Hybrid methods of component mode synthesis. In *Actes du Forum International Aéroélasticité et Dynamique des Structures, AAAF, Strasbourg*.

[Tran, 2009a] Tran, D.-M. (2009a). Component mode synthesis method using partial interface modes: Application to tuned and mistuned bladed disk with local non-linearity. In *ASME 2009 International Design Engineering Technical Conferences and Computers and Information in Engineering Conference*, pages 889–898. American Society of Mechanical Engineers.

[Tran, 2009b] Tran, D.-M. (2009b). Component mode synthesis methods using partial interface modes: Application to tuned and mistuned structures with cyclic symmetry. *Computers & Structures*, 87(17-18):1141–1153.

[Vakakis, 1992] Vakakis, A. (1992). Dynamics of a nonlinear periodic structure with cyclic symmetry. *Acta Mechanica*, 95(1):197–226.

[van Rossum, 1995] van Rossum, G. (1995). Python tutorial. Technical Report CS-R9526, Centrum voor Wiskunde en Informatica (CWI), Amsterdam.

[Von Groll and Ewins, 2000] Von Groll, G. and Ewins, D. J. (2000). On the dynamics of windmilling in aero-engines. In *IMechE Conference Transactions*, volume 6, pages 721–730. Professional Engineering Publishing; 1998.

[Wang and Chen, 1992] Wang, J.-H. and Chen, W. (1992). Investigation of the vibration of a blade with friction damper by hbm. In *ASME 1992 International Gas Turbine and Aeroengine Congress and Exposition*, pages V005T14A003–V005T14A003. American Society of Mechanical Engineers.

[Wiart et al., 2016] Wiart, L., Atinault, O., Boniface, J.-C., and Barrier, R. (2016). Aeropropulsive performance analysis of the NOVA configurations. *30th Congress of the International Council of the Aerodynamical Sciences*.

[Wiart et al., 2015] Wiart, L., Atinault, O., Grenon, R., Paluch, B., and Hue, D. (2015). Development of nova aircraft configurations for large engine integration studies. In *33rd AIAA Applied Aerodynamics Conference*, page 2254.

[Wilson and Penzien, 1972] Wilson, E. and Penzien, J. (1972). Evaluation of orthogonal damping matrices. *International Journal for numerical methods in engineering*, 4(1):5–10.

[Wood et al., 1980] Wood, W., Bossak, M., and Zienkiewicz, O. (1980). An alpha modification of newmark's method. *International Journal for Numerical Methods in Engineering*, 15(10):1562–1566.

[Wriggers and Nackenhorst, 2006] Wriggers, P. and Nackenhorst, U. (2006). *Analysis and simulation of contact problems*, volume 1. Springer.

[Wriggers and Zavarise, 2004] Wriggers, P. and Zavarise, G. (2004). Computational contact mechanics. *Encyclopedia of computational mechanics*.

[Wu et al., 2006] Wu, B., Sun, W., and Lim, C. (2006). An analytical approximate technique for a class of strongly non-linear oscillators. *International Journal of Non-Linear Mechanics*, 41(6):766–774.

[Yajie et al., 2006] Yajie, S., Jie, H., Yingchun, S., and Zigen, Z. (2006). Forced response analysis of shrouded blades by an alternating frequency/time domain method. In *ASME Turbo Expo 2006: Power for Land, Sea, and Air*, pages 865–872. American Society of Mechanical Engineers.

[Yastrebov, 2011] Yastrebov, V. (2011). *Computational contact mechanics: geometry, detection and numerical techniques*. PhD thesis, École Nationale Supérieure des Mines de Paris.

[Yuan and Jiang, 2017] Yuan, J.-W. and Jiang, Y.-L. (2017). A parameterized model order reduction method for parametric systems based on laguerre polynomials. *International Journal of Control*, pages 1–17.

[Zhang et al., 2014] Zhang, J., Guo, L., Wu, H., Zhou, A., Hu, D., and Ren, J. (2014). The influence of wind shear on vibration of geometrically nonlinear wind turbine blade under fluid–structure interaction. *Ocean engineering*, 84:14–19.

[Zienkiewicz et al., 1977] Zienkiewicz, O. C., Taylor, R. L., Nithiarasu, P., and Zhu, J. (1977). *The finite element method*, volume 3. McGraw-hill London.

Appendix A

Polynomial approximation of nonlinear forces in the frequency domain

Due to the polynomial form of the purely nonlinear forces in the time domain (see the equation (2.40)), an analytical expression in the frequency domain can be obtained. The generalized coordinates are approximated by truncated Fourier series of N harmonics:

$$q_s = a_0^s + \sum_{k=1}^{N} a_k^s \cos(k\omega t) + b_k^s \sin(k\omega t) \qquad s = i, j, m \ , \tag{3.11}$$

where N is the number of harmonics, a_0^s, a_k^s and b_k^s are respectively the constant, odd and even Fourier coefficients of the generalized coordinates for $s = i, j, m$.

$$a_0^s = \frac{1}{T}\int_0^T q_s(\omega, t)\mathrm{d}t \ , \tag{3.12}$$

$$a_k^s = \frac{2}{T}\int_0^T q_s(\omega, t)\cos(k\omega t)\mathrm{d}t \ , \tag{3.13}$$

$$b_k^s = \frac{2}{T}\int_0^T q_s(\omega, t)\sin(k\omega t)\mathrm{d}t \ . \tag{3.14}$$

To perform the Galerkin procedure (equation (2.133)), the integration of multiple products of trigonometric functions with different indices is necessary[1].

$$\frac{2}{T}\int_0^T \cos(n\omega t)\cos(m\omega t)\mathrm{d}t = \delta_{nm} \ , \tag{3.15}$$

$$\frac{2}{T}\int_0^T \cos(n\omega t)\sin(m\omega t)\mathrm{d}t = 0 \ , \tag{3.16}$$

$$\frac{2}{T}\int_0^T \sin(n\omega t)\sin(m\omega t)\mathrm{d}t = \delta_{nm} \ . \tag{3.17}$$

[1] The integral over a period T of an odd periodic function is equal to zero, $\int_0^T$ odd function $\mathrm{d}t = 0$.

In order to simplify the mathematical expression of the purely nonlinear force in the frequency domain, the ζ functions family is introduced.

$$\zeta_{Number\ of\ cosines,\{cosine\ index\ group\},\{sine\ index\ group\}} \begin{cases} 3\ term\ product : \zeta_{Cnml} \\ 4\ term\ product : \zeta_{Cnmlr} \end{cases}$$

where, C is the number of cosines inside the integral, n, m, l and r are the index of the multiplicative constants of the excitation frequency (i.e. see the equations (3.18) and (3.19)).

$$\zeta_{1nmlr} = \frac{2}{T}\int_0^T \cos(n\omega t)\sin(m\omega t)\sin(l\omega t)\sin(r\omega t)\mathrm{d}t\ , \tag{3.18}$$

$$\zeta_{3nmlr} = \frac{2}{T}\int_0^T \cos(n\omega t)\cos(m\omega t)\cos(l\omega t)\sin(r\omega t)\mathrm{d}t\ . \tag{3.19}$$

Thus, ζ functions family is defined as follows where δ_{nm} is the Kronecker delta defined in the equation (2.74):

$$\zeta \begin{cases} \zeta_{Cnml} \begin{cases} \zeta_{0nml} = 0 \\ \zeta_{1nml} = \frac{1}{2}\left(-\delta_{n,m+l} + \delta_{m,n+l} + \delta_{l,n+m}\right) \\ \zeta_{2nml} = 0 \\ \zeta_{3nml} = \frac{1}{2}\left(\delta_{n,m+l} + \delta_{m,n+l} + \delta_{l,n+m}\right) \end{cases} \\ \zeta_{Cnmlr} \begin{cases} \zeta_{0nmlr} = \frac{1}{4}\left(-\delta_{n,m+l+r} - \delta_{m,n+l+r} - \delta_{l,n+m+r} - \delta_{r,n+m+l}\right. \\ \qquad \left. +\delta_{n+m,l+r} + \delta_{n+l,m+r} + \delta_{n+r,m+l}\right) \\ \zeta_{1nmlr} = 0 \\ \zeta_{2nmlr} = \frac{1}{4}\left(-\delta_{n,m+l+r} - \delta_{m,n+l+r} + \delta_{l,n+m+r} + \delta_{r,n+m+l}\right. \\ \qquad \left. -\delta_{n+m,l+r} + \delta_{n+l,m+r} + \delta_{n+r,m+l}\right) \\ \zeta_{3nmlr} = 0 \\ \zeta_{4nmlr} = \frac{1}{4}\left(\delta_{n,m+l+r}\right. \\ \qquad +\delta_{m,n+l+r} + \delta_{l,n+m+r} + \delta_{r,n+m+l} + \delta_{n+m,l+r} \\ \qquad \left. +\delta_{n+l,m+r} + \delta_{n+r,m+l}\right) \end{cases} \end{cases}$$

The nonlinear force $\tilde{\mathbf{f}}_e(\mathrm{X}, t)$ is obtained by substituting the equation (3.11) in the expression of the nonlinear force defined in the equation (2.40), then, the harmonic balance procedure is performed in order to erase the time dependence.

The nonlinear forces constant, odd and even coefficients related to each generalized coordinate $p = 1, ..., r$ of the polynomial approximation in the

frequency domain are:

$$G_0^p(X) = \sum_{i=1}^{r}\sum_{j=i}^{r}\frac{A_{ij}^p}{2}\left(2a_0^ia_0^j + \sum_{k=1}^{N}\left(a_k^ia_k^j + b_k^ib_k^j\right)\right) + \sum_{i=1}^{r}\sum_{j=i}^{r}\sum_{m=j}^{r}\frac{B_{ijm}^p}{2}\Bigg[2a_0^ia_0^ja_0^m + a_0^i\sum_{s=1}^{N}\left(a_s^ja_s^m + b_s^jb_s^m\right) + a_0^j\sum_{k=1}^{N}\left(a_k^ia_k^m + b_k^ib_k^m\right) + a_0^m\sum_{k=1}^{N}\left(a_k^ia_k^j + b_k^ib_k^j\right) + \sum_{k=1}^{N}\sum_{s=1}^{N}\sum_{p=1}^{N}\left(a_k^ia_s^ja_p^m\zeta_{3ksp} + a_k^ib_s^jb_p^m\zeta_{1ksp} + b_k^ia_s^jb_p^m\zeta_{1skp} + b_k^ib_s^ja_p^m\zeta_{1pks}\right)\Bigg], \tag{3.20}$$

$$G_{a_l}^p(X) = \sum_{i=1}^{r}\sum_{j=i}^{r}A_{ij}^p\left(a_0^ia_l^j + a_l^ia_0^j + \sum_{k=1}^{N}\sum_{s=1}^{N}\left(a_k^ia_s^j\zeta_{3ksl} + b_k^ib_s^j\zeta_{1lksl}\right)\right) + \sum_{i=1}^{r}\sum_{j=i}^{r}\sum_{m=j}^{r}B_{ijm}^p\Bigg[a_0^ia_0^ja_l^m + a_0^ia_l^ja_0^m + a_l^ia_0^ja_0^m + a_0^i\sum_{s=1}^{N}\sum_{p=1}^{N}\left(a_s^ja_p^m\zeta_{3spl} + b_s^jb_p^m\zeta_{1lsp}\right) + a_0^j\sum_{k=1}^{N}\sum_{p=1}^{N}\left(a_k^ia_p^m\zeta_{3kpl} + b_k^ib_p^m\zeta_{1lkp}\right) + a_0^m\sum_{k=1}^{N}\sum_{s=1}^{N}\left(a_k^ia_s^j\zeta_{3ksl} + b_k^ib_s^j\zeta_{1lks}\right) + \sum_{k=1}^{N}\sum_{s=1}^{N}\sum_{p=1}^{N}\left(a_k^ia_s^ja_p^m\zeta_{4kspl} + a_k^ib_s^jb_p^m\zeta_{2klsp} + b_k^ia_s^jb_p^m\zeta_{2slkp} + b_k^ib_s^ja_p^m\zeta_{2plks}\right)\Bigg], \tag{3.21}$$

and

$$G_{b_l}^p(X) = \sum_{i=1}^{r}\sum_{j=i}^{r}A_{ij}^p\left(a_0^ib_l^j + b_l^ia_0^j + \sum_{k=1}^{N}\sum_{s=1}^{N}\left(a_k^ib_s^j\zeta_{1ksl} + b_k^ia_s^j\zeta_{1skl}\right)\right) + \sum_{i=1}^{r}\sum_{j=i}^{r}\sum_{m=j}^{r}B_{ijm}^p\Bigg[a_0^ia_0^jb_l^m + a_0^ib_l^ja_0^m + b_l^ia_0^ja_0^m + a_0^i\sum_{s=1}^{N}\sum_{p=1}^{N}\left(a_s^jb_p^m\zeta_{1spl} + b_s^ja_p^m\zeta_{1psl}\right) + a_0^j\sum_{k=1}^{N}\sum_{p=1}^{N}\left(a_k^ib_p^m\zeta_{1kpl} + b_k^ia_p^m\zeta_{1pkl}\right) + a_0^m\sum_{k=1}^{N}\sum_{s=1}^{N}\left(a_k^ib_s^j\zeta_{1ksl} + b_k^ia_s^j\zeta_{1skl}\right) + \sum_{k=1}^{N}\sum_{s=1}^{N}\sum_{p=1}^{N}\left(a_k^ia_s^jb_p^m\zeta_{2kspl} + a_k^ib_s^ja_p^m\zeta_{2kpsl} + b_k^ia_s^ja_p^m\zeta_{2spkl} + b_k^ib_s^jb_p^m\zeta_{0kspl}\right)\Bigg]. \tag{3.22}$$

To solve the equation system (2.134) with the Newton-Raphson method, the Jacobian ("tangent matrix") of the nonlinear equation system should be computed first. The nonlinearity of the problem imposes the need to calculate the nonlinear part of the Jacobian at every iteration increasing the global computational time.

$$\mathbf{J} = \frac{\partial \mathrm{R}(\omega, \mathrm{X})}{\partial \mathrm{X}} = \mathbf{J}_l(\omega) + \mathbf{J}_{nl}(\mathrm{X}) = \mathbf{Z}(\omega) + \frac{\partial \mathrm{G_{nl}}(\mathrm{X})}{\partial \mathrm{X}} \ . \tag{3.23}$$

The nonlinear part of the Jacobian is written hereunder.

$$\mathbf{J}_{nl}(\mathrm{X}) = \begin{bmatrix} \frac{\partial \mathrm{G}_0}{\partial a_0} & \frac{\partial \mathrm{G}_0}{\partial a_1} & \frac{\partial \mathrm{G}_0}{\partial b_1} & \cdots & \frac{\partial \mathrm{G}_0}{\partial a_N} & \frac{\partial \mathrm{G}_0}{\partial b_N} \\ \frac{\partial \mathrm{G}_{a_1}}{\partial a_0} & \frac{\partial \mathrm{G}_{a_1}}{\partial a_1} & \frac{\partial \mathrm{G}_{a_1}}{\partial b_1} & \cdots & \frac{\partial \mathrm{G}_{a_1}}{\partial a_N} & \frac{\partial \mathrm{G}_{a_1}}{\partial b_N} \\ \frac{\partial \mathrm{G}_{b_1}}{\partial a_0} & \frac{\partial \mathrm{G}_{b_1}}{\partial a_1} & \frac{\partial \mathrm{G}_{b_1}}{\partial b_1} & \cdots & \frac{\partial \mathrm{G}_{b_1}}{\partial a_N} & \frac{\partial \mathrm{G}_{b_1}}{\partial b_N} \\ \vdots & \vdots & \vdots & \ddots & \vdots & \vdots \\ \frac{\partial \mathrm{G}_{a_N}}{\partial a_0} & \frac{\partial \mathrm{G}_{a_N}}{\partial a_1} & \frac{\partial \mathrm{G}_{a_N}}{\partial b_1} & \cdots & \frac{\partial \mathrm{G}_{a_N}}{\partial a_N} & \frac{\partial \mathrm{G}_{a_N}}{\partial b_N} \\ \frac{\partial \mathrm{G}_{b_N}}{\partial a_0} & \frac{\partial \mathrm{G}_{b_N}}{\partial a_1} & \frac{\partial \mathrm{G}_{b_N}}{\partial b_1} & \cdots & \frac{\partial \mathrm{G}_{b_N}}{\partial a_N} & \frac{\partial \mathrm{G}_{b_N}}{\partial b_N} \end{bmatrix}_{r(2N+1)\times r(2N+1)} \ . \tag{3.24}$$

Each block in the Jacobian $\mathbf{J}_{nl}(\mathrm{X})$ is a $r \times r$ submatrix. For instance, the (p, r) term of $\frac{\partial \mathrm{G}_0}{\partial a_0}$, for $p = 1, \ldots, r$ and $z = 1, \ldots, r$ is:

$$\frac{\partial \mathrm{G}_0}{\partial a_0} = \begin{bmatrix} \frac{\partial \mathrm{G}_0^1}{\partial a_0^1} & \cdots & \frac{\partial \mathrm{G}_0^1}{\partial a_0^r} \\ \vdots & \ddots & \vdots \\ \frac{\partial \mathrm{G}_0^r}{\partial a_0^1} & \cdots & \frac{\partial \mathrm{G}_0^r}{\partial a_0^r} \end{bmatrix}_{r\times r} = \left[\frac{\partial \mathrm{G}_0^p}{\partial a_0^z},\ p = 1, \ldots,\ r,\ z = 1, \ldots,\ r \right] \ . \tag{3.25}$$

The derivatives of the purely nonlinear force's constant coefficients in the frequency domain for $p = 1, \ldots, r$, $v = 1, \ldots, N$ and $z = 1, \ldots, r$ are defined as follows:

$$\begin{aligned} \frac{G_0^p}{a_0^z} = & \sum_{i=1}^{r} \sum_{j=i}^{r} A_{ij}^p \left(\delta_{iz} a_0^j + a_0^i \delta_{jz} \right) + \sum_{i=1}^{r} \sum_{j=i}^{r} \sum_{m=j}^{r} \frac{B_{ijm}^p}{2} \Bigg[2 \left(\delta_{iz} a_0^j a_0^m + a_0^i \delta_{jz} a_0^m \right. \\ & \left. + \delta_{mz} a_0^i a_0^j \right) + \delta_{iz} \sum_{s=1}^{N} \left(a_s^j a_s^m + b_s^j b_s^m \right) + \delta_{jz} \sum_{k=1}^{N} \left(a_k^i a_k^m + b_k^i b_k^m \right) \\ & + \delta_{mz} \sum_{k=1}^{N} \left(a_k^i a_k^j + b_k^i b_k^j \right) \Bigg] \ , \end{aligned} \tag{3.26}$$

$$\frac{G_0^p}{a_v^z} = \sum_{i=1}^{r}\sum_{j=i}^{r} \frac{A_{ij}^p}{2}\left(\delta_{iz}a_v^j + a_v^i\delta_{jz}\right) + \sum_{i=1}^{r}\sum_{j=i}^{r}\sum_{m=j}^{r} \frac{B_{ijm}^p}{2}\Bigg[a_0^i\left(\delta_{jz}a_v^m + a_v^j\delta_{mz}\right) + a_0^j\left(\delta_{iz}a_v^m + a_v^i\delta_{mz}\right) + a_0^m\left(\delta_{iz}a_v^j + a_v^i\delta_{jz}\right) + \sum_{k=1}^{N}\sum_{s=1}^{N}\sum_{p=1}^{N}\Big(\zeta_{3ksp}\left(\delta_{iz}\delta_{kv}a_s^j a_p^m + a_k^i\delta_{jz}\delta_{sv}a_p^m + a_k^i a_s^j\delta_{mz}\delta_{pv}\right) + \delta_{iz}\delta_{kv}b_s^j b_p^m\zeta_{1ksp} + b_k^i\delta_{jz}\delta_{sv}b_p^m\zeta_{1skp} + b_k^i b_s^j\delta_{mz}\delta_{pv}\zeta_{1pks}\Big)\Bigg], \tag{3.27}$$

and

$$\frac{G_0^p}{b_v^z} = \sum_{i=1}^{r}\sum_{j=i}^{r} \frac{A_{ij}^p}{2}\left(\delta_{iz}b_v^j + b_v^i\delta_{jz}\right) + \sum_{i=1}^{r}\sum_{j=i}^{r}\sum_{m=j}^{r} \frac{B_{ijm}^p}{2}\Bigg[a_0^i\left(\delta_{jz}b_v^m + b_v^j\delta_{mz}\right) + a_0^j\left(\delta_{iz}b_v^m + b_v^i\delta_{mz}\right) + a_0^m\left(\delta_{iz}b_v^j + b_v^i\delta_{jz}\right) + \sum_{k=1}^{N}\sum_{s=1}^{N}\sum_{p=1}^{N}\Big(\zeta_{1ksp}a_k^i\left(\delta_{jz}\delta_{sv}b_p^m + b_s^j\delta_{mz}\delta_{pv}\right) + \zeta_{1skp}a_s^j\left(\delta_{iz}\delta_{kv}b_p^m + b_k^i\delta_{mz}\delta_{pv}\right) + \zeta_{1pks}a_p^m\left(\delta_{iz}\delta_{kv}b_s^j + b_k^i\delta_{jz}\delta_{sv}\right)\Big)\Bigg]. \tag{3.28}$$

The derivatives of the purely nonlinear force's odd Fourier coefficients in the frequency domain for $p = 1,\ldots,r$, $v = 1,\ldots,N$ and $z = 1,\ldots,r$ are defined hereunder:

$$\frac{\partial G_{a_l}^p(X)}{\partial a_0^z} = \sum_{i=1}^{r}\sum_{j=i}^{r} A_{ij}^p\left(\delta_{iz}a_l^j + \delta_{jz}a_l^i\right) + \sum_{i=1}^{r}\sum_{j=i}^{r}\sum_{m=j}^{r} B_{ijm}^p\Bigg[a_l^i\left(\delta_{jz}a_0^m + \delta_{mz}a_0^j\right) + a_l^j\left(\delta_{iz}a_0^m + \delta_{mz}a_0^i\right) + a_l^m\left(\delta_{iz}a_0^j + \delta_{jz}a_0^i\right) + \delta_{iz}\sum_{s=1}^{N}\sum_{p=1}^{N}\left(a_s^j a_p^m\zeta_{3spl} + b_s^j b_p^m\zeta_{1lsp}\right) + \delta_{jz}\sum_{k=1}^{N}\sum_{p=1}^{N}\left(a_k^i a_p^m\zeta_{3kpl} + b_k^i b_p^m\zeta_{1lkp}\right) + \delta_{mz}\sum_{k=1}^{N}\sum_{s=1}^{N}\left(a_k^i a_s^j\zeta_{3ksl} + b_k^i b_s^j\zeta_{1lks}\right)\Bigg], \tag{3.29}$$

$$\frac{\partial G^p_{a_l}(X)}{\partial a^z_v} = \sum_{i=1}^{r}\sum_{j=i}^{r} A^p_{ij}\left(a^i_0\delta_{jz}\delta_{vl} + \delta_{iz}\delta_{vl}a^j_0 + \sum_{k=1}^{N}\sum_{s=1}^{N}\zeta_{3ksl}\left(a^k_i\delta_{jz}\delta_{sv} + \delta_{iz}\delta_{kv}a^j_s\right)\right)$$
$$+ \sum_{i=1}^{r}\sum_{j=i}^{r}\sum_{m=j}^{r} B^p_{ijm}\Bigg[\delta_{lv}\left(a^i_0a^j_0\delta_{mz} + a^i_0\delta_{jz}a^m_0 + \delta_{iz}a^j_0a^m_0\right)$$
$$+ a^i_0\sum_{s=1}^{N}\sum_{p=1}^{N}\zeta_{3spl}\left(a^j_s\delta_{mz}\delta_{pv} + \delta_{jz}\delta_{sv}a^m_p\right) + a^j_0\sum_{k=1}^{N}\sum_{p=1}^{N}\zeta_{3kpl}\left(a^i_k\delta_{mz}\delta_{pv}\right.$$
$$\left.\delta_{iz}\delta_{kv}a^m_p\right) + a^m_0\sum_{k=1}^{N}\sum_{s=1}^{N}\zeta_{3ksl}\left(a^i_k\delta_{jz}\delta_{sv} + \delta_{iz}\delta_{kv}a^j_s\right) + \sum_{k=1}^{N}\sum_{s=1}^{N}\sum_{p=1}^{N}\Big(\big(\delta_{iz}\delta_{kv}a^j_sa^m_p$$
$$+\ a^i_k\delta_{jz}\delta_{sv}a^m_p + a^i_ka^j_s\delta_{mz}\delta_{pv}\big)\zeta_{4kspl} + \delta_{iz}\delta_{kv}b^j_sb^m_p\zeta_{2klsp} + b^i_k\delta_{jz}\delta_{sv}b^m_p\zeta_{2slkp}$$
$$+ b^i_kb^j_s\delta_{mz}\delta_{pv}\zeta_{2plks}\Big)\Bigg], \tag{3.30}$$

and

$$\frac{\partial G^p_{a_l}(X)}{\partial b^z_v} = \sum_{i=1}^{r}\sum_{j=i}^{r} A^p_{ij}\left(\sum_{k=1}^{N}\sum_{s=1}^{N}\zeta_{1lks}\left(b^k_i\delta_{jz}\delta_{sv} + \delta_{iz}\delta_{kv}b^j_s\right)\right)$$
$$+ \sum_{i=1}^{r}\sum_{j=i}^{r}\sum_{m=j}^{r} B^p_{ijm}\Bigg[a^i_0\sum_{s=1}^{N}\sum_{p=1}^{N}\zeta_{1lsp}\left(b^j_s\delta_{mz}\delta_{pv} + \delta_{jz}\delta_{sv}b^m_p\right)$$
$$+ a^j_0\sum_{k=1}^{N}\sum_{p=1}^{N}\zeta_{1lkp}\left(b^i_k\delta_{mz}\delta_{pv} + \delta_{iz}\delta_{kv}a^m_p\right) + a^m_0\sum_{k=1}^{N}\sum_{s=1}^{N}\zeta_{1lks}\left(b^i_k\delta_{jz}\delta_{sv} + \delta_{iz}\delta_{kv}b^j_s\right)$$
$$+ \sum_{k=1}^{N}\sum_{s=1}^{N}\sum_{p=1}^{N}\left(a^i_k\zeta_{2klsp}\left(\delta_{jz}\delta_{sv}b^m_p + b^j_s\delta_{mz}\delta_{pv}\right) + a^j_s\zeta_{2slkp}\left(\delta_{iz}\delta_{kv}b^m_p + b^i_k\delta_{mz}\delta_{pv}\right)\right.$$
$$\left.+ a^m_p\zeta_{2plks}\left(\delta_{iz}\delta_{kv}b^j_s + b^i_k\delta_{jz}\delta_{sv}\right)\right)\Bigg]. \tag{3.31}$$

Hereunder, the derivatives of the purely nonlinear force's even coefficients in the frequency domain for $p = 1, \ldots, r$, $v = 1, \ldots, N$ and $z = 1, \ldots, r$ are

defined:

$$\frac{\partial G^p_{b_l}(X)}{\partial a^z_0} = \sum_{i=1}^{r}\sum_{j=i}^{r} A^p_{ij}\left(\delta_{iz}b^j_l + \delta_{jz}b^i_l\right) + \sum_{i=1}^{r}\sum_{j=i}^{r}\sum_{m=j}^{r} B^p_{ijm}\Bigg[a^i_l\left(\delta_{jz}a^m_0 + \delta_{mz}a^j_0\right) + b^j_l\left(\delta_{iz}a^m_0 + \delta_{mz}a^i_0\right) + b^m_l\left(\delta_{iz}a^j_0 + \delta_{jz}a^i_0\right) + \delta_{iz}\sum_{s=1}^{N}\sum_{p=1}^{N}\left(a^j_s b^m_p \zeta_{1spl} + b^j_s a^m_p \zeta_{1psl}\right) + \delta_{jz}\sum_{k=1}^{N}\sum_{p=1}^{N}\left(a^i_k b^m_p \zeta_{1kpl} + b^i_k a^m_p \zeta_{1pkl}\right) + \delta_{mz}\sum_{k=1}^{N}\sum_{s=1}^{N}\left(a^i_k b^j_s \zeta_{1ksl} + b^i_k a^j_s \zeta_{1skl}\right)\Bigg], \tag{3.32}$$

$$\begin{aligned}\frac{\partial G^p_{b_l}(X)}{\partial a^z_v} = {} & \sum_{i=1}^{r}\sum_{j=i}^{r} A^p_{ij}\left(\sum_{k=1}^{N}\sum_{s=1}^{N}\left(b^k_i\delta_{jz}\delta_{sv}\zeta_{1skl} + \delta_{iz}\delta_{kv}b^j_s\zeta_{1ksl}\right)\right) \\ & + \sum_{i=1}^{r}\sum_{j=i}^{r}\sum_{m=j}^{r} B^p_{ijm}\Bigg[\delta_{iz}\delta_{lv}a^j_0 a^m_0 + a^i_0\sum_{s=1}^{N}\sum_{p=1}^{N}\left(b^j_s\delta_{mz}\delta_{pv}\zeta_{1psl} + \delta_{jz}\delta_{sv}b^m_p\zeta_{1spl}\right) \\ & + a^j_0\sum_{k=1}^{N}\sum_{p=1}^{N}\left(b^i_k\delta_{mz}\delta_{pv}\zeta_{1pkl} + \delta_{iz}\delta_{kv}b^m_p\zeta_{1kpl}\right) + a^m_0\sum_{k=1}^{N}\sum_{s=1}^{N}\left(b^i_k\delta_{jz}\delta_{sv}\zeta_{1skl}\right. \\ & \left. + \delta_{iz}\delta_{kv}b^j_s\zeta_{1ksl}\right) + \sum_{k=1}^{N}\sum_{s=1}^{N}\sum_{p=1}^{N}\left(\left(\delta_{jz}\delta_{sv}a^m_p + a^j_s\delta_{mz}\delta_{pv}\right)b^i_k\zeta_{2spkl} + \left(\delta_{iz}\delta_{kv}a^m_p\right.\right. \\ & \left.\left. + a^i_k\delta_{mz}\delta_{pv}\right)b^j_s\zeta_{2kpsl} + \left(\delta_{iz}\delta_{kv}a^j_s + a^i_k\delta_{jz}\delta_{sv}\right)b^m_p\zeta_{2kspl}\right)\Bigg],\end{aligned} \tag{3.33}$$

and

$$\begin{aligned}\frac{\partial G^p_{b_l}(X)}{\partial b^z_v} = &\sum_{i=1}^{r}\sum_{j=i}^{r} A^p_{ij}\left(a^i_0\delta_{jz}\delta_{lv} + \delta_{iz}\delta_{lv}a^j_0 + \sum_{k=1}^{N}\sum_{s=1}^{N}\left(a^k_i\delta_{jz}\delta_{sv}\zeta_{1ksl} + \delta_{iz}\delta_{kv}a^j_s\zeta_{1skl}\right)\right)\\
&+ \sum_{i=1}^{r}\sum_{j=i}^{r}\sum_{m=j}^{r} B^p_{ijm}\Bigg[\delta_{lv}\left(a^i_0\delta_{jz}a^m_0 + a^i_0a^j_0\delta_{mz} + a^j_0a^m_0\delta_{iz}\right)\\
&+ a^i_0\sum_{s=1}^{N}\sum_{p=1}^{N}\left(a^j_s\delta_{mz}\delta_{pv}\zeta_{1spl} + \delta_{jz}\delta_{sv}a^m_p\zeta_{1psl}\right) + a^j_0\sum_{k=1}^{N}\sum_{p=1}^{N}\left(a^i_k\delta_{mz}\delta_{pv}\zeta_{1kpl}\right.\\
&\left.+ \delta_{iz}\delta_{kv}a^m_p\zeta_{1pkl}\right) + a^m_0\sum_{k=1}^{N}\sum_{s=1}^{N}\left(a^i_k\delta_{jz}\delta_{sv}\zeta_{1ksl} + \delta_{iz}\delta_{kv}a^j_s\zeta_{1skl}\right)\\
&+ \sum_{k=1}^{N}\sum_{s=1}^{N}\sum_{p=1}^{N}\left(a^i_ka^j_s\delta_{mz}\delta_{pv}\zeta_{2kspl} + a^i_k\delta_{jz}\delta_{sv}a^m_p\zeta_{2kpsl} + \delta_{iz}\delta_{kv}a^j_s\zeta_{2spkl}a^m_p\right.\\
&\left.+ \left(\delta_{iz}\delta_{kv}b^j_sb^m_p + b^i_k\delta_{jz}\delta_{sv}b^m_p + b^i_kb^j_s\delta_{mz}\delta_{pv}\right)\zeta_{0kspl}\right)\Bigg]\ .\end{aligned} \tag{3.34}$$

However, the time to compute the Jacobian increases with the number of harmonics taken into consideration.

Resumé du mémoire (français)

Introduction

Les structures tournantes sont largement utilisées dans des applications industrielles telles que les turbomachines, les pales d'hélicoptères et les éoliennes. La tendance à la conception des composants structuraux plus minces, plus souples et plus légers sous des excitations d'intensité plus élevée augmente le comportement non linéaire de ces composants. Ainsi, la nécessité de prédire avec précision la réponse dynamique des structures géométriquement non linéaires devient essentielle pour le concepteur.

Pour réduire le coût de calcul des modèles non linéaires d'éléments finis de grande précision, certains chercheurs ont développé la construction de modèles non linéaires d'ordre réduit (ROM). Cependant, sans techniques spéciales pour créer des modèles réduits efficaces et capables d'évaluer les matrices du système de façon autonome lorsque la structure se déforme, le coût de calcul devient équivalent au temps nécessaire pour effectuer l'analyse d'éléments finis de grande taille, ce qui diminue les avantages de la réduction de modèles. Une approche efficace de l'analyse structurale non linéaire réalisée dans [Muravyov and Rizzi, 2003] permet de représenter les forces internes par une formulation polynomiale du troisième ordre en fonction des déplacements. Cette méthode est connue sous le nom de "Stiffness Evaluation Procedure" (STEP). Les coefficients de la représentation polynomiale sont obtenus par une série de calculs statiques obtenus avec le modèle éléments finis complet. Comme une extension de la méthode STEP, les modèles d'ordre réduit "non intrusifs" ont été examinés par [Mignolet et al., 2013] et validés pour la prédiction de la fatigue, les calculs stochastiques non linéaires, les analyses de flambement et les structures complexes. La procédure d'évaluation de la rigidité des éléments (E-STEP) généralise la procédure STEP aux problèmes d'optimisation permettant la paramétrisation de la procédure d'évaluation de la raideur. L'hyper-réduction et la linéarisation par morceaux [Ryckelynck, 2005, Farhat et al., 2015] sont des techniques alternatives pour faciliter les problèmes de calcul des matrices du système.

Dans le cadre des structures tournantes les vibrations des poutres linéaires

ont été largement étudiées, étendues à l'étude de modèles de poutres géométriquement non linéaires encastrées et adaptées aux structures tournantes. L'effet de la rotation crée un couplage entre les mouvements axiaux et transversaux. Basé sur une formulation de von Karman, un modèle réduit pour une poutre en rotation est effectué grâce aux modes non linéaires et des variétés invariantes [Jiang et al., 2005]. Une étude de comparaison entre plusieurs modèles d'une poutre tournant en termes de précision et de validité est présentée par [Thomas et al., 2016]. Ces modèles sont principalement utilisés dans l'étude des pales d'hélicoptères, de turbomachines [Grolet and Thouverez, 2010], des modélisations de poutres minces, de coques minces et des interactions fluide-structure. Une formulation par éléments finis des structures tournantes est présentée dans [Sternchüss, 2009]. La nécessité de développer des modèles éléments finis 3D pour l'étude dynamique de structures tournantes est mis en évidence dans [Genta et al., 2013].

Les travaux présents dans la litterature ont permis le développement du cadre théorique continu pour modéliser le comportement dynamique des structures tournantes avec grands déplacements et mettre en œuvre des simulations des problèmes de contact. De plus, le développement de modèles autonomes d'ordre réduit, indépendants du FOM, a augmenté les performances de la phase ONline. Le paramétrage de la base réduite par rapport à la vitesse de rotation a élargi l'application des modèles linéaires d'ordre réduit pour une gamme de vitesses de rotation. De plus, les techniques de synthèse modale fournissent un outil capable de réduire la dimension du problème tout en gardant dans les coordonnées généralisées les degrés de liberté physiques de l'interface. Néanmoins, ces modèles d'ordre réduit ne sont pas capables de traiter la dynamique des structures tournantes avec des déplacements importants et des non-linéarités de contact par friction. Enfin, les vibrations autour de l'état d'équilibre précontraint induit par la rotation sont considérées comme linéaires.

C'est ce qui justifie cette étude, qui consiste à développer des modèles non linéaires d'ordre réduit indépendants du FOM (autonome) pour l'étude de la dynamique des structures tournantes avec des non-linéarités à grands déplacements et avec des non-linéarités de contact frottant.

Quatre contributions principales sont présentées dans cette thèse: i) les déplacements autour de l'équilibre précontraint sont considérés comme non linéaires. Ainsi, l'identification des coefficients de rigidité non linéaires de la méthode STEP sont adaptés afin d'étudier les vibrations géométriquement non linéaires. ii) Les forces non linéaires à l'intérieur de la structure sont corrigées avec une base POD de forces non linéaires (avant que la projection ne soit effectuée) afin d'éliminer les artefacts parasites observés dans les ROM sans

correction. iii) Le ROM non linéaire est paramétré par rapport à la vitesse de rotation de la structure et il est construit de manière à être valide pour une plage donnée de vitesses de rotation. iv) La non-linéarité géométrique est combinée avec la non-linéarité de contact frottant en utilisant une base réduite de type Craig-Bampton qui est capable de conserver certains des degrés de liberté physiques dans les déplacements généralisés.

Dans le présent travail, le logiciel par éléments finis Code_Aster [EDF, 1989] et les langages de programmation Python [van Rossum, 1995] et Fortran ont été utilisés. Code _Aster est capable d'exécuter du code Python fournissant un environnement intégré pour le FOM et la ROM. Le modèle d'ordre réduit est entièrement implémenté en Python/Fortran, ce qui conduit à une programmation très flexible. Le code_Aster est capable de fournir les informations nécessaires pour effectuer la construction OFFline des ROMs et pour effectuer les solutions FOM utilisées comme référence.

Chapitre 1: Équations du mouvement de structures nonlinéaires en rotation

Ce premier chapitre fournit les bases théoriques pour résoudre la dynamique de structures tournantes avec non linéarités de grand déplacement et contact frottant qui est le problème physique pour lequel les modèles d'ordre réduit (ROM) sont développés et étudiés dans les chapitres suivants. Premièrement, la forme "l'intégrale" ou "faible" du problème physique, proprice à la discrétisation, est obtenue à partir de sa "forme différentielle" ou "forte". Ensuite, avec la méthode des éléments finis (FEM) la formulation continue est discrétisée et le modèle d'haute fidelité (FOM) de la structure est défini. Le mouvement de la structure est représenté comme la somme d'un déplacement statique induit par la rotation et d'une vibration non linéaire autour de l'état statique. Le FOM défini dans ce chapitre fournira la solution de référence des modèles d'ordre réduit (ROM) développés plus tard.

Dynamique du modèle éléments finis haute fidélité

L'équation de la dynamique discretisée par éléments finis dans le repère tournant [Sternchüss, 2009] avec non linéarités de type géométrique et de contact frottant s'écrit,

$$\mathbf{M}\ddot{\mathbf{u}}_p + [\mathbf{C} + \mathbf{G}(\Omega)]\,\dot{\mathbf{u}}_p + \mathbf{K}_c(\Omega)\mathbf{u}_p + \mathbf{g}(\mathbf{u}_p) = \mathbf{f}_e(t) + \mathbf{f}_{ei}(\Omega) + \mathbf{f}_c(\mathbf{u}_p, \dot{\mathbf{u}}_p)\ ,$$

en fonction de la vitesse de rotation, Ω. Les vecteurs $\mathbf{u}_p$, $\dot{\mathbf{u}}_p$ et $\ddot{\mathbf{u}}_p$ représentent les déplacements, vitesses et accélérations physiques des nœuds de la structure.

Ces derniers ont une dimension égale au nombre de degrés de liberté (d.d.l.) du modèle élément finis de grande taille (FOM). Les matrices $\mathbf{M}$, $\mathbf{C}$, $\mathbf{G}(\Omega)$ et $\mathbf{K}_c(\Omega)$ sont les matrices de masse, d'amortissement visqueux, de couplage gyroscopique et d'assouplissement centrifuge. Les forces non linéaires internes (dont la non linéarité géométrique) sont représentées par le vecteur $\mathbf{g}(\mathbf{u}_p)$. $\mathbf{f}_e(\mathrm{t})$ est le vecteur des forces externes appliquées sur la structure, $\mathbf{f}_{ei}(\Omega)$ est le vecteur des efforts inertiels et $\mathbf{f}_c(\mathbf{u}_p\ ,\ \dot{\mathbf{u}}_p)$ est le vecteur des forces de contact frottant.

Dans un premier temps, l'état statique $\mathbf{u}_s$ de la structure sous l'effet de la rotation seule est obtenu en tenant compte des non linéarités géométriques, ce qui permet d'obtenir la matrice de raideur tangente $\mathbf{K}_s(\mathbf{u}_s)$ composée de la raideur élastique $\mathbf{K}_e$ et la raideur géométrique de précontrainte $\mathbf{K}_g(\mathbf{u}_s)$.

On considère les déplacements relatifs $\mathbf{u}$ de la structure autour de l'état statique $\mathbf{u}_s$, $\mathbf{u}_p = \mathbf{u}_s + \mathbf{u}$.

Les forces non linéaires autour de la position d'équilibre (1.86) sont développées comme la somme d'une partie linéaire et d'une partie purement non linéaire.

$$\mathbf{g}(\mathbf{u}_\mathrm{s} + \mathbf{u}) = \mathbf{g}(\mathbf{u}_\mathrm{s}) + \left.\frac{\partial \mathbf{g}(\mathbf{u}_\mathrm{p})}{\partial \mathbf{u}_p}\right|_{\mathbf{u}_p = \mathbf{u}_s} \mathbf{u} + \mathbf{g}_{nl}\left(\mathbf{u}\right) = \mathbf{g}(\mathbf{u}_\mathrm{s}) + \mathbf{K}_s\mathbf{u} + \mathbf{g}_{nl}\left(\mathbf{u}\right)\ .$$

L'équation de mouvement de la structure en rotation en fonction des déplacements relatifs s'écrit,

$$\mathbf{M}\ddot{\mathbf{u}} + \left[\mathbf{C} + \mathbf{G}(\Omega)\right]\dot{\mathbf{u}} + \mathbf{K}(\Omega)\mathbf{u} + \mathbf{g}_{nl}(\mathbf{u}) = \mathbf{f}_e(t) + \mathbf{f}_c(\mathbf{u}_s + \mathbf{u}, \dot{\mathbf{u}})\ ,$$

avec $\mathbf{K}(\Omega) = \mathbf{K}_c(\Omega) + \mathbf{K}_s(\mathbf{u}_s) + \mathbf{K}_e$ la matrice de rigidité totale. $\mathbf{g}_{nl}(\mathbf{u})$ est le vecteur d'efforts de type géométrique purement non linéaires et $\ddot{\mathbf{u}}$, $\dot{\mathbf{u}}$ et $\mathbf{u}$ sont les vecteurs d'accélération, de vitesse et de déplacement aux nœuds autour de la position d'équilibre statique.

La résolution répétitive des équations du système haute fidélité conduit à des temps de calculs prohibitifs pour des configurations industrielles complexes avec beaucoup de d.d.l. C'est pour cela que l'utilisation de modèles réduits s'avère intéressant.

Chapitre 2: Construction et résolution du modèle d'ordre réduit

Dans ce deuxième chapitre la construction de modèles d'ordre réduit qui représentent le modèle haute fidelité non linéaire discrétisé (FOM) des struc-

tures tournantes, défini dans le chapitre précédent, est développée. Premièrement, la technique de l'ordre réduit est introduite et certaines des bases réduites classiques sont présentées. Deuxièmement, avec projection de Galeking le modèle d'ordre réduit (ROM) est construit. Troisièmement, les méthodes d'inflation (classique) et STEP (polynomiale) utilisées pour évaluer les forces généralisées non linéaires sont présentées et une correction originale basée sur la POD est proposée afin de résoudre l'inexactitude de ces méthodes classiques pour l'étude de la réponse forcée des structures élancés non linéaires. Quatrièmement, les ROM proposées sont paramétrées afin de réduire le coût de calcul hors ligne du modèle d'ordre réduit. Enfin, les méthodes de résolution utilisées pour évaluer la réponse temporelle des modèles d'ordre réduit proposés sont présentées.

Techniques de réduction des modèles

Dans la plupart des techniques de réduction, les déplacements nodaux du FOM sont approximés par un produit linéaire entre une base d'approximation, $\mathbf{Q}_{app.}$ et le vecteur de déplacements généralisés, $\mathbf{q}$,

$$\mathbf{u} = \mathbf{Q}_{app.}\mathbf{q} \, .$$

La construction du modèle d'ordre réduit est réalisée dans une phase *OFFline* où des calculs FOM coûteux en temps sont effectués. Ensuite, une fois le modèle d'ordre réduit est défini, la solution du problème est obtenue pendant la phase *ONline* avec un coût de calcul minimal.

Pour certaines techniques, la phase OFFline est plus coûteuse qu'un seul calcul FOM, cependant, sur un nombre donné de calculs, la combinaison de la consommation de temps entre les phases OFFline et ONline du modèle d'ordre réduit est plus rapide que les calculs FOM comme il est illustré ci-dessous.

Ci-dessous, certaines des approches les plus courantes pour la base d'approximation et pour les techniques de réduction sont présentées. La base d'approximation, $\mathbf{Q}_{app.}$, également appelée *base réduite* et représentée par $\mathbf{\Phi}$.

Modes linéaires de la structure (LNM)

Les modes linéaires sont obtenus en évaluant les valeurs propres et les vecteurs propres du système linéarisé sous-jacent,

$$\mathbf{K\Phi} = \mathbf{M\Phi\omega}^2 \, ,$$

où $\mathbf{K}$ est la matrice de rigidité à la configuration d'équilibre.

La construction de la base LNM est très simple et largement mise en œuvre dans les codes par éléments finis industriels (Nastran, Code_Aster, ...). Pour

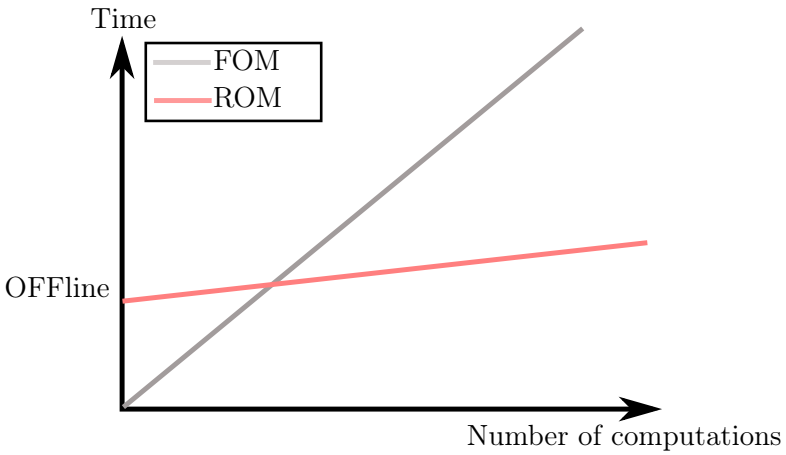

Temps de calcul du FOM par rapport au ROM.

un très grand nombre de degrés de liberté, le temps de calcul du problème des valeurs propres est optimisé par des méthodes itératives telles que la méthode de Sorensen [Maschho and Sorensen, 1996] capable de calculer directement les premières valeurs propres et vecteurs propres r.

Méthodes à interface fixes

Les déplacements physiques pour la méthode à interface fixe Craig-Bampton sont divisés en ddl intérieur, $\mathbf{u}_i$, et l'interface limite ddl, $\mathbf{u}_b$. Avec cette méthode, les matrices de rigidité et de masse sont partitionnées par rapport aux valeurs internes et limites d.o.f.,

$$\mathbf{K}(\Omega) = \begin{bmatrix} \mathbf{K}_{ii} & \mathbf{K}_{ib} \\ \mathbf{K}_{bi} & \mathbf{K}_{bb} \end{bmatrix} \quad , \quad \mathbf{M} = \begin{bmatrix} \mathbf{M}_{ii} & \mathbf{M}_{ib} \\ \mathbf{M}_{bi} & \mathbf{M}_{bb} \end{bmatrix} .$$

La même partition est applicable à tous les éléments de l'équation de mouvement de la structure, Eqn. (1.74).

Ensuite, comme pour tout modèle d'ordre réduit basé sur une base de réduction, les déplacements physiques relatifs du FOM sont approximés comme une combinaison linéaire entre la base de réduction et les déplacements généralisés comme,

$$\mathbf{u} = \mathbf{Q}\mathbf{q} = \Phi_{CB} \begin{Bmatrix} \mathbf{q}_i \\ \mathbf{u}_b \end{Bmatrix} = [\Phi_c \ \Psi_c] \begin{Bmatrix} \mathbf{q}_i \\ \mathbf{u}_b \end{Bmatrix} .$$

Dans la méthode Craig-Bampton, la base réduite, $\mathbf{Q} = \Phi_{CB}$, est composée de r_c modes normaux linéaires d'interface fixe Φ_c et les modes de contrainte r_b Ψ_c, tandis que les coordonnées généralisées, $\mathbf{q}$, sont composées des coordonnées modales $\mathbf{q}_i$ et du ddl de l'interface frontière, $\mathbf{u}_b$. Le nombre de vecteurs dans la base réduite, $\mathbf{Q}$, est $r = r_c + r_b$.

Modèles d'ordre réduits par projection

Dans cette section, les modèles d'ordre réduits par *projection de base* sont introduits. Les déplacements physiques du FOM sont approximés par le produit linéaire entre une base d'approximation, $\mathbf{Q}_{app.}$, et les déplacements généralisés de la structure, $\mathbf{q}$. Le nombre d'équations, r, à résoudre dans le modèle d'ordre réduit est considérablement plus petit que le nombre de degrés de liberté (égal au nombre d'équations) dans le FOM, $r \ll n$. Ensuite, introduisant cette dernière approximation dans l'équation. (1.88), l'équation du mouvement est réécrite comme suit,

$$\mathbf{M}\mathbf{Q}_{app.}\ddot{\mathbf{q}} + \mathbf{C}\mathbf{Q}_{app.}\dot{\mathbf{q}} + \mathbf{K}(\Omega)\mathbf{Q}_{app.}\mathbf{q} + \mathbf{g}_{nl}(\mathbf{Q}_{app.}\mathbf{q}) = \mathbf{f}_e(\mathrm{t}) + \mathbf{f}_c(\mathbf{Q}_{app.}\mathbf{q} + \mathbf{u}_s,\, \mathbf{Q}_{app.}\dot{\mathbf{q}}) \ .$$

Cependant, afin de réduire le nombre d'équations à résoudre, cette dernière expression est pré-multipliée par une base de projection, $\mathbf{Q}_{proj.}$, et l'équation de mouvement d'ordre réduit est définie comme suit,

$$\tilde{\mathbf{M}}\ \ddot{\mathbf{q}} + \tilde{\mathbf{C}}\ \dot{\mathbf{q}} + \tilde{\mathbf{K}}(\Omega)\mathbf{q} + \tilde{\mathbf{g}}_{nl}(\mathbf{q}) = \tilde{\mathbf{f}}_e(t) + \tilde{\mathbf{f}}_c(\mathbf{q}, \dot{\mathbf{q}}) \ ,$$

où $\tilde{\mathbf{M}} = \mathbf{Q}_{proj.}^T\mathbf{M}\mathbf{Q}_{app.}$, $\tilde{\mathbf{C}} = \mathbf{Q}_{proj.}^T\mathbf{C}\mathbf{Q}_{app.}$ et $\tilde{\mathbf{K}}(\Omega) = \mathbf{Q}_{proj.}^T\mathbf{K}(\Omega)\mathbf{Q}_{app.}$ sont les matrices de masse, d'amortissement et de rigidité généralisées, $\tilde{\mathbf{f}}_e(t)$ est le vecteur de force externe généralisé, $\tilde{\mathbf{g}}_{nl}(\mathbf{q})$ est le vecteur de force purement non linéaire généralisé et $\tilde{\mathbf{f}}_c(\mathbf{q}, \dot{\mathbf{q}})$ est le vecteur généralisé des forces de contact. D'une part, lorsque la base de projection est la même que la base d'approximation, $\mathbf{Q}_{proj.} = \mathbf{Q}_{app.}$, la procédure de projection est appelée une *projection Galerkin*. En revanche, lorsque les deux bases sont différentes, $\mathbf{Q}_{proj.} \neq \mathbf{Q}_{app.}$, la projection prend le nom d'un *projection Petrov-Galerkin*. Ci-après, les modèles d'ordre réduit proposés sont obtenus par une *projection de Galerkin*.

Correction des forces géométriques non linéaires

L'utilisation des méthodes d'inflation et STEP pour des structures élancées

Les bases considérées ne sont pas a priori capables de représenter les déplacements non linéaires d'une structure élancée comme les poutres en porte-à-faux ou les aubes de turbine avec un nombre de modes réduit (par exemple pour le couplage aéroélastique). Les forces non linéaires de la structure ne sont pas bien représentées dans l'espace réduit, les amplitudes des réponses de déplacement sont considérablement réduites et, dans certains cas, la réponse présente des oscillations parasites (composantes harmoniques élevées) comme indiqué dans [Grolet and Thouverez, 2010, Andersen and Poulsen, 2014]. De plus, la méthode STEP n'est pas adaptée aux applications avec des structures élancées telles que les poutres en porte-à-faux [Rizzi and Muravyov, 2001]. Cependant, la simplicité des bases étudiées et les performances temporelles du STEP combinés ensemble, fournissent une ROM simple à construire en utilisant n'importe

quel logiciel commercial d'éléments finis. Certains auteurs résolvent ce problème en prenant en considération les termes de dérivée seconde du LNM, Eqn. (2.6), $\frac{\partial \mathbf{\Phi}_i}{\partial q_i}$ [Grolet and Thouverez, 2010, Martin and Thouverez, 2019]. Les modes doubles [Mignolet et al., 2013, Radu et al., 2004, Capiez-Lernout et al., 2012] améliorent la représentativité de la base réduite en effectuant des calculs statiques non linéaires et en extrayant le vecteur de déplacements purement non linéaires. Ce dernier est utilisé pour améliorer la base réduite. Ces méthodes ont été validées pour les éléments finis de type poutre, cependant, si la complexité en torsion ou géométrique de ces structures doit être prise en compte, des éléments finis 3D sont nécessaires. D'autres techniques prometteuses d'ordre réduit pour étudier les structures géométriques non linéaires sont les modes normaux non linéaires (NNM) [Rosenberg, 1962, Shaw and Pierre, 1992, Jezequel and Lamarque, 1991, Touzé and Amabili, 2006]. Ces techniques sont encore en développement pour des structures complexes à plusieurs degrés de liberté. Des techniques de réduction telles que l'hyper-réduction [Ryckelynck, 2005] ou la méthode d'interpolation empirique discrète (DEIM) [Chaturantabut and Sorensen, 2010] fournissent des résultats précis pour évaluer les forces non linéaires dans l'espace réduit au moyen d'une base de force préalablement calculée, $\mathbf{\Phi}_f$, et l'évaluation des forces non linéaires FOM sur un petit ensemble de nœuds choisis de la structure. Cependant, ces techniques ne fournissent pas de ROM entièrement autonomes car pour chaque pas de temps les forces non linéaires sont réévaluées à certains nœuds choisis du FOM.

Correction basée sur POD pour les forces non linéaires

Pour améliorer la précision de la réponse et éviter la réduction d'amplitude, avant de projeter les forces non linéaires du FOM sur la base réduite, ces dernières forces sont approximées au moyen d'une base POD des forces non linéaires, $\mathbf{\Phi}_f$, calculée précédemment.

Le concept de la méthode proposée est de *filtrer la force non linéaire pour la restreindre à un sous-espace plus représentatif déduit des forces non linéaires FOM.*

La correction proposée est valable à la fois pour les méthodes STEP et d'inflation car la correction est effectuée avant la projection des forces non linéaires. Cette procédure est divisée en deux phases: a) une phase OFFline où la base des forces non linéaires est construite et b) une phase ONline où les forces non linéaires sont calculées. La phase ONline telle que présentée ci-dessous correspond à la correction de la méthode d'inflation présentée précé-demment. La correction du STEP est effectuée lors de l'identification du coefficient de rigidité en phase OFFline. Ci-après, les ROM associées à une correction des forces non linéaires sont respectivement appelées ROM InflationC ou ROM StepC (C représentant la correction, c'est-à-dire STEP avec

correction ≡ StepC).

Phase hors ligne: construction de la base des forces non linéaires

La base non linéaire utilisée pour approximer les forces non linéaires FOM, $\mathbf{\Phi}_f$, est calculée par une procédure POD dont la base est calculée par une SVD. Comme indiqué dans l'Eqn. (2.75), les forces non linéaires sont collectées pour un nombre donné de snapshots qui représentent un ensemble de déplacements caractéristiques dans la réponse. Ensuite, pour chaque instant, les forces non linéaires associées sont évaluées,

$$\mathbf{A} = [\mathbf{g}_{nl}(\mathbf{u}_1), \cdots, \mathbf{g}_{nl}(\mathbf{u}_m)] \ .$$

L'ensemble des instantanés peut être obtenu à partir de données expérimentales ou par d'autres moyens (par exemple avec ensemble de forces non linéaires liées à un espace de déplacement formé par une combinaison linéaire de modes ...).

Ensuite, une décomposition de valeur singulière tronquée (SVD) [Hansen, 1990] est implémentée comme dans Eqn. (2.16) et la *base des forces non linéaires* est formée par une troncature ou en choisissant explicitement un nombre, r_f, de vecteurs de base non linéaires,

$$\mathbf{A} = \mathbf{U}\Sigma\mathbf{V}^T \approx \mathbf{U}_{r_f}\Sigma_{r_f}\mathbf{V}_{r_f}^T \ .$$

La base non linéaire consiste à tronquer les modes r_f dans les vecteurs singuliers gauches résultants de la base SVD, $\mathbf{\Phi}_f = \mathbf{U}_{r_f}$ vérifiant $\mathbf{\Phi}_f^T\mathbf{\Phi}_f = \mathbf{I}$.

Phase ONline (Inflation): Calcul des forces non linéaires

Une fois la base des forces non linéaires construite, comme défini dans l'Eqn. (2.77), les forces non linéaires dans le FOM sont approximées comme une combinaison linéaire entre la base des forces non linéaires et les coordonnées des forces approximées (similaire au concept de réduction de base, Eqn. (2.1)).

$$\mathbf{g}_{nl}(\mathbf{u}) \approx \mathbf{\Phi}_f\mathbf{q}_{nl}^f = \mathbf{g}_{nl}^f(\mathbf{u}) \, ,$$

où les coordonnées de force sont calculées par une approche des moindres carrés. L'approximation des forces non linéaires FOM dans l'espace FOM est calculée par,

$$\mathbf{g}_{nl}^f(\mathbf{u}) = \mathbf{\Phi}_f \left(\mathbf{\Phi}_f^T\mathbf{\Phi}_f\right)^{-1}\mathbf{\Phi}_f^T\mathbf{g}_{nl}(\mathbf{u}) = \mathbf{\Phi}_f\mathbf{\Phi}_f^T\mathbf{g}_{nl}(\mathbf{u}) \ .$$

Ensuite, les forces généralisées dans l'espace ROM sont calculées comme,

$$\tilde{\mathbf{g}}_{nl}(\mathbf{q}) = \mathbf{\Phi}^T\mathbf{g}_{nl}^f(\mathbf{u}) = \mathbf{\Phi}^T\mathbf{\Phi}_f\mathbf{\Phi}_f^T\mathbf{g}_{nl}(\mathbf{u}) = \mathbf{B}^T\mathbf{g}_{nl}(\mathbf{u}) \ .$$

où $B^T = \mathbf{\Phi}^T \mathbf{\Phi}_f \mathbf{\Phi}_f^T$ est la matrice de correction (filtrage).

La correction proposée pour les forces non linéaires est une technique non intrusive car elle n'a lieu que dans la projection des forces non linéaires dans l'espace ROM et ne nécessite pas de calculs FOM supplémentaires une fois qu'elle est construite. Cette dernière correction pourrait être comprise comme un filtre pour les directions et l'amplitude des forces non linéaires FOM tout en effectuant la projection dans l'espace réduit. La précision de la réponse dépend de la qualité de la base des forces non linéaires, $\mathbf{\Phi}_f$, et de la base de l'ordre réduit, $\mathbf{\Phi}$.

STEP avec correction (StepC)

Combinant la méthode STEP et la correction POD proposée, la ROM StepC est construite avec les coeff A_{ij} et B_{ijm} identifiés à partir des forces statiques **filtrées** $\mathbf{B}^T\mathbf{g}_{nl}(\mathbf{u})$ correspondant à Eqn. (2.79) au lieu des forces statiques d'origine $\mathbf{g}_{nl}(\mathbf{u})$, dans la phase OFFline. En ce qui concerne la méthode STEP classique, l'identification des coefficients non linéaires est, $\mathbf{B}_p^T$ étant la p -ème ligne de $\mathbf{B}^T$,

$$
\begin{aligned}
A^p_{ii} &= \frac{1}{2q_i^2}\left[\mathbf{B}_p^T\mathbf{g}_{nl}\left(\mathbf{u}_1\right) + \mathbf{B}_p^T\mathbf{g}_{nl}\left(\mathbf{u}_2\right)\right] \ , \\
A^p_{ij} &= \frac{1}{2q_iq_j}\left[\mathbf{B}_p^T\mathbf{g}_{nl}\left(\mathbf{u}_3\right) + \mathbf{B}_p^T\mathbf{g}_{nl}\left(\mathbf{u}_4\right) - 2A^p_{ii}q_i^2 - 2A^p_{jj}q_j^2\right] \ , \\
B^p_{iii} &= \frac{1}{2q_i^3}\left[\mathbf{B}_p^T\mathbf{g}_{nl}\left(\mathbf{u}_1\right) - \mathbf{B}_p^T\mathbf{g}_{nl}\left(\mathbf{u}_2\right)\right] \ , \\
B^p_{ijj} &= \frac{1}{2q_iq_j^2}\left[\mathbf{B}_p^T\mathbf{g}_{nl}\left(\mathbf{u}_3\right) + \mathbf{B}_p^T\mathbf{g}_{nl}\left(\mathbf{u}_5\right) - 2A^p_{ii}q_i^2 - 2A^p_{jj}q_j^2 - 2B^p_{iii}q_i^3\right] , \\
B^p_{iij} &= \frac{1}{2q_i^2q_j}\left[-\mathbf{B}_p^T\mathbf{g}_{nl}\left(\mathbf{u}_4\right) - \mathbf{B}_p^T\mathbf{g}_{nl}\left(\mathbf{u}_5\right) + 2A^p_{ii}q_i^2 + 2A^p_{jj}q_j^2 - 2B^p_{jjj}q_j^3\right] , \\
B^p_{ijm} &= \frac{1}{q_iq_jq_m}\left[\mathbf{B}_p^T\mathbf{g}_{nl}(\mathbf{u}_6) - A^p_{ii}q_i^2 - A^p_{ij}q_iq_j - A^p_{im}q_iq_m - A^p_{jj}q_j^2\right. \\
&\quad -A^p_{jm}q_jq_m - A^p_{mm}q_m^2 - B^p_{iii}q_i^3 - B^p_{iij}q_i^2q_j - B^p_{iim}q_i^2q_m \\
&\quad -B^p_{ijj}q_iq_j^2 - B^p_{imm}q_iq_m^2 - B^p_{jjj}q_j^3 - B^p_{jjm}q_j^2q_m \\
&\quad \left.-B^p_{jmm}q_jq_m^2 - B^p_{mmm}q_m^3\right] \ .
\end{aligned}
$$

Ensuite, les forces non linéaires sont calculées dans la phase ONline par Eqn. (2.40). La figure ci-dessous représente l'organigramme pour identifier les coefficients de rigidité corrigés, A_{ij} et B_{ijk}.

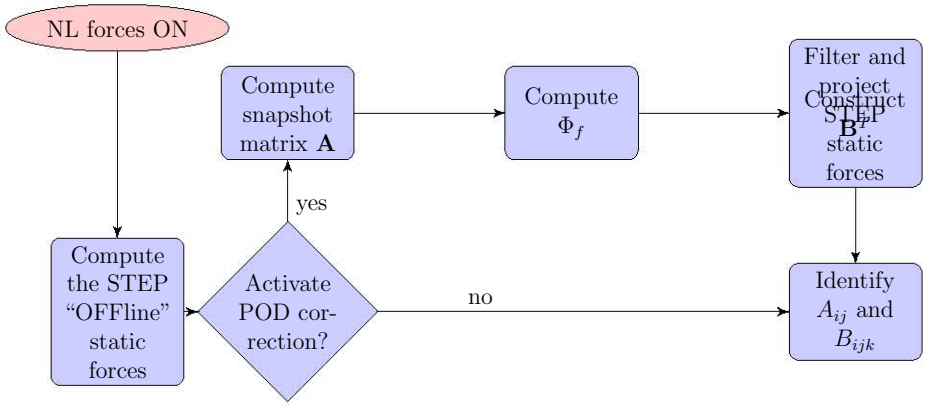

Flow chart of the identification process of the nonlinear stiffness force coefficients by STEP and StepC POD correction methods.

Résumé des ROM linéaires, STEP et StepC

La suivante figure présente l'organigramme pour construire la ROM StepC qui est utilisée dans la phase ONline. Pendant la phase OFFline, la matrice de correction, $\mathbf{B}^T$, est construite et les bases de réduction peuvent être optimisées. Les deux sont introduits dans la méthode STEP pour obtenir les forces non linéaires généralisées, $\tilde{\mathbf{g}}_{nl}(\mathbf{q})$. Ce dernier combiné avec la base réduite permet de créer la ROM StepC qui correspond à l'Eqn. (2.37).

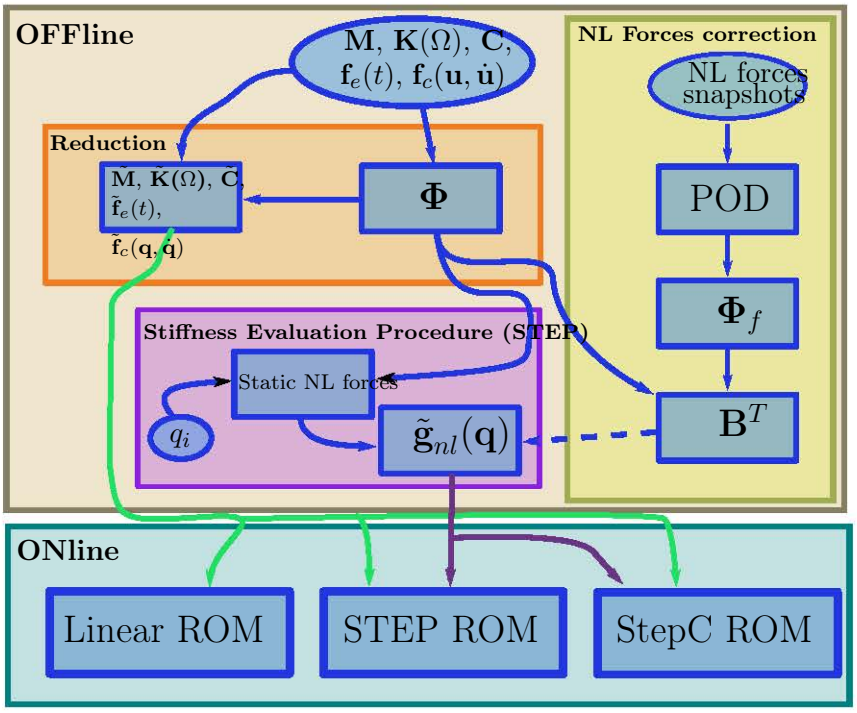

Synthèse de la construction des ROM étudiées.

Chapitre 3: Applications numériques

Les modèles d'ordre réduit développés dans le chapitre précédent sont maintenant évalués pour trois structures différentes. La première structure est un faisceau en porte-à-faux épais qui est utilisé pour mettre en évidence la nécessité de la correction basée sur POD associée à la ROM StepC. La deuxième structure est une poutre en porte-à-faux mince où son comportement non linéaire est significatif. Dans cette application, la construction de la ROM StepC est analysée en termes d'influence de la base réduite et de la base des forces non linéaires sur la solution. De plus, la ROM StepC est validée pour un boîtier résonnant dynamique. La non-linéarité de contact est également implémentée pour un cas simple. La troisième structure, est une étude de cas complexe représentant une pale de ventilateur développée à l'ONERA. De plus, la ROM est paramétrée par rapport à la vitesse de rotation afin de réduire le temps de construction.

Dans le cadre de ce resumé, seulement la dernière application est prise en compte afin de surligner l'intérêt du modèle proposé sur une application d'intérêt industriel.

Première mode de résonance linéarisé

Dans ce qui suit, on considère que les effets non linéaires sont significatifs lorsque la différence entre la ROM linéarisée et les solutions périodiques FOM non linéaires diffère de plus de 10 %. Dans ces cas, le coût de développement de ROM non linéaires est justifié.

Ci-dessous la solution périodique de l'aube à 2000 tr/min et 4043 tr/min. Le facteur de charge α_f est choisi pour être 0.5 N pour la première vitesse de rotation et 1.5 pour la seconde afin d'obtenir une différence significative entre les solutions FOM linéarisées et non linéaires.

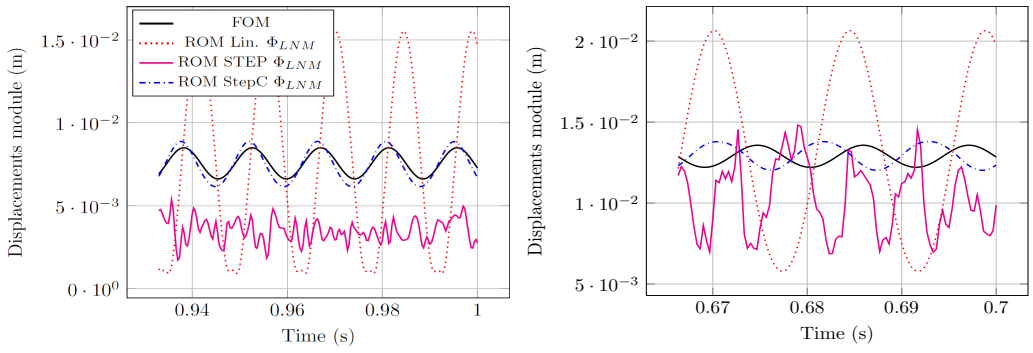

(a) $\Omega = 2000$ rpm, $\alpha_f = 0.5$.

(b) $\Omega = 4043$ rpm, $\alpha_f = 1.5$.

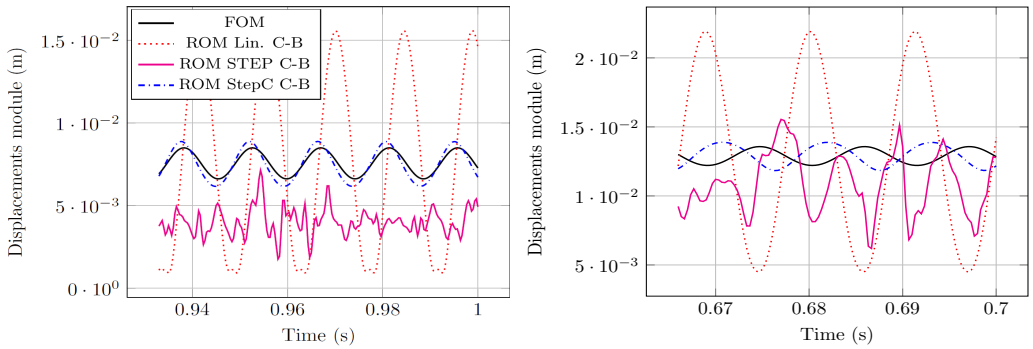

(c) $\Omega = 2000$ rpm, $\alpha_f = 0.5$. (d) $\Omega = 4043$ rpm, $\alpha_f = 1.5$.

Periodic response for a first mode resonant harmonic excitation.

Les modèles non linéaires StepC fournissent des résultats plus précis que la ROM linéarisée et la ROM STEP pour les deux bases réduites. On observe que les solutions ont un décalage dans le temps. Cet effet est mis en évidence lorsque Ω diffère de la vitesse de rotation pour laquelle la base de force non linéaire est construite. L'objectif est de prédire avec précision la fréquence et l'amplitude de la réponse, cet effet reste donc hors de la portée de l'étude. Cependant, pour les études de couplage aéroélastique où le déphasage influerait sur la précision de la solution, la base des forces non linéaires devrait être calculée de telle sorte que la phase entre le FOM et le ROM StepC reste la même.

La suivante figure présente les déplacements globaux de la structure aux déplacements maximaux instantanés amplifiés par un facteur 5 à $\Omega = 4043$ rpm. La ROM linéaire présente des déplacements plus importants que la solution FOM de référence, cependant, le mouvement de flexion est bien capturé. Les déplacements de la ROM STEP ont des amplitudes plus petites que la ROM linéaire, donc, ils fournissent une erreur plus petite, cependant, la réponse ne représente pas la flexion de la structure (les déplacements montrés sur la figure ne sont pas entièrement représentatifs) et ne sont pas périodiques à l'heure. La ROM StepC fournit des résultats précis et les déplacements obtenus sont du même ordre de grandeur que le FOM pris comme référence. De plus, le comportement en flexion est correctement représenté.

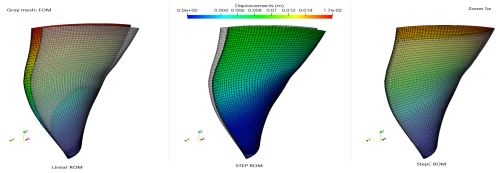

Displacements of the ROMs for $\Omega = 4043$ rpm and $\alpha_f = 1.5$.

Performances en temps de calcul

Les performances temporelles de l'étape ONline entre les ROM et le FOM sont évaluées ici et présentées dans la table suivante. Le temps de calcul des ROM est similaire quelle que soit la base réduite choisie. Ainsi, seules les performances temporelles du LNM avec $\Omega = 2000$ tr/min et 3000 pas de temps sont présentées. ROM STEP et ROM StepC ont tous deux besoin du même temps de calcul en ligne pour être résolus. La ROM linéaire est le modèle le plus rapide avec un facteur 1,28 par rapport aux ROM non linéaires, cependant, le modèle n'est pas assez précis. Ensuite, la ROM StepC proposée offre le meilleur compromis entre précision et consommation de temps avec un gain de temps de 16 523 fois plus rapide en ligne que le FOM. Notez que la consommation de temps du FOM correspond à un seul temps séquentiel CPU, le vrai *temps d'horloge* du FOM correspond à une valeur inférieure (environ 5h) si les calculs sont effectués avec 25 cœurs en parallèle. Cependant, même si des calculs multicœurs sont implémentés, la ROM StepC est environ 1500 fois plus rapide que le FOM parallélisé.

En ce qui concerne la construction des ROM, en plus du calcul de base réduit, l'étape OFFline comprend l'évaluation des coefficients polynomiaux (≈ 540 de temps CPU). De plus, pour construire la base de force non linéaire des ROM non linéaires StepC, un calcul FOM supplémentaire est effectué pour 60 périodes d'excitation et 2000 pas de temps (≈ 64 h temps CPU).

Temps de calcul des ROMs.

Model	Time	t_{FOM} / t_{ROM}
FOM	90 h 52 min 48 s	
ROM Lin. Φ_{LNM}	15.2s	21 524
ROM STEP Φ_{LNM}	19.6s	16 692
ROM StepC Φ_{LNM}	19.8s	16 523

Conclusions

Les structures tournantes dans l'industrie telles que les pales de ventilateur ou de compresseur, les pales d'hélicoptère ou les pales d'éoliennes, entre autres, sont soumises à de grandes non-linéarités de déplacement au cours de leur cycle de vie. Ce dernier est particulièrement vrai dans le contexte réel où la tendance de conception est de créer des structures élancées plus flexibles et plus grandes conduisant à une amplification des effets non linéaires dus à des

déplacements plus importants. Ces effets créent une dépendance du comportement de la structure par rapport à son état de déplacement. En outre, des non-linéarités de contact de frottement supplémentaires doivent être prises en compte lors de l'étude de l'interaction entre le disque et le pied de lame ou entre la lame et le système de caoutchouc. Ces interactions ont un impact sur le comportement de la structure car elles conduisent à une dissipation d'énergie ainsi qu'à d'éventuels effets de surface tels que l'usure ou les vibrations induites.

Quatre contributions principales ont été présentées dans ce travail: i) les déplacements autour de l'équilibre précontraint ont été considérés comme non linéaires. Ainsi, l'identification des coefficients de rigidité non linéaires de la méthode STEP a été adaptée afin d'étudier les vibrations géométriquement non linéaires. ii) Les forces non linéaires à l'intérieur de la structure ont été corrigées au moyen d'une base POD de forces non linéaires (avant la projection) afin de supprimer les artefacts parasites observés dans les ROM sans correction. iii) La ROM non linéaire a été paramétrée par rapport à la vitesse de rotation de la structure et a été construite afin d'être valide pour une gamme donnée de vitesses de rotation. iv) La non-linéarité géométrique a été combinée avec la non-linéarité de contact de frottement au moyen d'une base réduite de Craig-Bampton qui était capable de conserver certains des degrés de liberté physiques comme déplacements généralisés.

Des modèles d'ordre réduit basés sur la projection ont été développés afin d'étudier l'analyse dynamique non linéaire des structures tournantes. Pour construire les modèles d'ordre réduit, quatre bases de réduction différentes ont été considérées: a) les modes normaux linéaires (LNM), b) la décomposition orthogonale correcte (POD), c) le LNM obtenu avec une procédure MAC par rapport aux modes POD de la structure, et d) la base réduite de Craig-Bampton. Les LNM sont faciles à calculer, cependant, le comportement de couplage non linéaire n'est pas capturé. Une méthode pour améliorer la représentativité des ROM est de choisir judicieusement les LNM qui représentent le mieux le comportement de la structure. Pour ce faire, une base POD a été construite et les LNM ont été comparés à la base POD au moyen du numéro MAC. La base POD est capable de fournir des résultats précis, mais elle peut conduire à des constructions très coûteuses du modèle.

Les forces non linéaires généralisées ont été obtenues au moyen de la procédure STEP qui est une approximation polynomiale du troisième ordre. Les coefficients de rigidité non linéaires ont été évalués avec un ensemble de calculs statiques FOM non linéaires. Cependant, la procédure STEP classique combinée à la base réduite considérée ne fournit généralement pas de résultats précis pour les structures élancées. Afin d'améliorer la ROM STEP, une correction originale des forces non linéaires basée sur POD a été proposée au moyen d'une base de forces non linéaires, $\mathbf{\Phi}_f$. Pour les structures étudiées, la

meilleure façon d'évaluer $\mathbf{\Phi}_f$ est de réaliser un calcul statique FOM avec une charge externe appliquée dans le sens du chargement dynamique jusqu'à ce que l'amplitude de déflexion attendue soit atteinte. On obtient alors un POD des vecteurs de forces non linéaires au moyen d'une décomposition en valeurs singulières (SVD). La base des forces non linéaires est ensuite construite avec le premier vecteur. Dans certains cas, deux vecteurs peuvent être nécessaires. Cependant, dans la plupart des cas, un seul vecteur était valide.

Trois modèles d'ordre réduit sont étudiés pour chaque base de réduction. La ROM linéaire correspond au modèle linéarisé classique où la précontrainte est considérée comme non linéaire mais les vibrations sont supposées linéaires, la ROM STEP correspond à la procédure STEP classique sans correction et la ROM StepC (STEP avec correction) est la ROM d'origine proposé dans cet ouvrage. Ces dernières ROM sont évaluées pour trois structures rotatives différentes:

1. La première structure correspond à une poutre en porte-à-faux épaisse. Dans ce cas d'étude, l'intérêt de la correction des forces non linéaires basée sur le POD est mis en évidence.

2. La deuxième structure est une poutre en porte-à-faux mince où le comportement non linéaire de la structure diffère considérablement du comportement linéaire. Dans cette application, la représentativité du couplage entre les déplacements verticaux et longitudinaux est bien saisie avec la ROM StepC fournissant des résultats plus précis qu'avec les ROM classiques étudiées. Le choix de la base réduite a une grande influence sur la précision de la ROM qui est considérablement améliorée lorsque la base réduite représente avec précision le comportement de la structure. De plus, la qualité de la base des forces non linéaires est améliorée lorsque les instantanés sont obtenus à partir de calculs statiques. Ils peuvent également être obtenus à partir de la solution dynamique FOM, mais l'identification des vecteurs qui, à partir des forces non linéaires, est plus complexe dans les cas étudiés.

3. La troisième application numérique correspond à une structure complexe représentant une pale de ventilateur. Le paramétrage des ROM est implémenté et la réponse dynamique de la ROM StepC fournit des résultats nettement plus précis que les ROM linéaires ou STEP. La réponse temporelle à la résonance du premier mode fournit des résultats précis en termes d'amplitude et de fréquence de la solution. De plus, la réponse forcée de la structure est bien représentée et le temps de calcul des ROM est environ 15 500 fois plus rapide qu'un seul calcul FOM.

Deux méthodes de résolution sont implémentées dans ce travail: la méthode HHT - α qui est une méthode d'intégration temporelle de la famille de méthodes Newmark et la méthode Harmonic Balance (HBM) qui calcule la solution dans le domaine fréquentiel. La correction de la base des forces non linéaires impliquée dans la ROM StepC n'a besoin que d'une modification mineure de ces méthodes. La solution temporelle est généralement effectuée avec la méthode HHT-α qui fournit la solution transitoire contrairement au HBM qui ne calcule que l'état périodique convergé.

À l'avenir, la ROM STEP pourrait être corrigée au moyen d'une correction pondérée en fonction de la rigidité en projetant l'équation FOM par $\mathbf{\Phi}^T\mathbf{K}(\Omega)$ (semblable à une projection de Petrov-Galerkin). Cela conduirait à une régularisation de la solution qui pourrait réduire les artefacts parasites observés avec la ROM STEP. Néanmoins, une identification des coefficients de rigidité sans considérer les termes quadratiques, pourrait conduire à une amélioration de la solution en cas de comportement non linéaire où les termes quadratiques n'ont aucune influence. Cela pourrait réduire l'erreur numérique induite par ces termes.

En ce qui concerne la construction de la base des forces non linéaires, de nouvelles méthodes pourraient être mises en œuvre: i) en utilisant les forces non linéaires calculées par la solution STEP comme matrice d'instantanés, ii) en calculant des charges de calcul alternées pour obtenir une réponse symétrique. iii) Combiner les vecteurs de forces non linéaires POD obtenus à partir de calculs FOM statiques et dynamiques. iv) Une base générale des forces non linéaires, paramétrée par rapport à la fréquence d'excitation ou par rapport au mode excité à la résonance.

La ROM StepC pourrait être également mise en œuvre pour des cas d'étude plus complexes tels que l'étude dynamique d'un disque à lame au moyen de propriétés de symétrie cyclique. De plus, pour les applications de turbomachines, le comportement géométriquement non linéaire du disque à aubes pour les cas accordés et mal accordés pourrait être étudié. De plus, la charge externe imposée pourrait être obtenue à partir d'un couplage aéroélastique en projetant les forces aérodynamiques sur la structure. Si des non-linéarités de contact sont également prises en compte, l'étude d'un stade industriel de turbomachines pourrait être mise en œuvre.

FOLIO ADMINISTRATIF

THESE DE L'UNIVERSITE DE LYON OPEREE AU SEIN DE L'INSA LYON

NOM : BALMASEDA AGUIRRE DATE de SOUTENANCE : 19/09/2019

Prénom: Mikel

TITRE: Reduced Order Models for Nonlinear Dynamic Analysis of Rotating Structures: Application to Turbomachinery Blades

NATURE : Doctorat Numéro d'ordre : 2019LYSEI067

Ecole doctorale : Mécanique - Energétique - Génie civil - Acoustique (MEGA)

Spécialité : Mécanique – Génie Mécanique

RESUME :
Dans le présent travail, des modèles d'ordre réduits (ROM) indépendants des modèles éléments finis haute fidelité (FOM) ont été développés pour l'étude de la dynamique non linéaire des structures en rotation. Les vibrations de la structure autour de l'équilibre précontraint induit par la rotation sont considérées comme non linéaires, élargissant l'approche linéarisée classique.
Les forces généralisées non linéaires sont approximées par un polynôme d'ordre trois obtenu avec la procédure Stiffness Evaluation Procédure (STEP). Ici, une approche originale est proposée pour corriger les forces non linéaires à l'aide d'une base de forces non linéaires obtenue avec une décomposition orthogonale propre (POD). Ce modèle est nommé STEP avec Correction (StepC ROM). Différents types de bases réduites sont présentés et testés. Certaines de ces bases sont paramétrées en fonction de la vitesse de rotation, ce qui réduit considérablement le temps de construction du modèle réduit.
Les modèles réduits avec correction (StepC ROM) sont capables de reproduire le couplage en déplacement entre les degrés de liberté de la structure. De plus, les résultats obtenus avec ce modèle sont plus précis que ceux obtenus avec le ROM linéarisées classiques ou le modèle STEP ROM sans correction. Le modèle StepC ROM proposé offre donc le meilleur compromis entre précision et temps de construction du ROM.

MOTS-CLÉS : Modèle d'ordre réduit, Structure tournante, Dynamique non linéaire, non linéarité géométrique, STiffness Evaluation Procedure (STEP), Proper Orthogonal Decomposition (POD), non linéarité de contact frottant.

Laboratoire (s) de recherche : LaMCoS/UMR CNRS 5259/ INSA Lyon
27bis Av. Jean Capelle
F-69621, Villeurbanne CEDEX

ONERA
29 Av. de la Division Leclerc
F-92322, Châtillon CEDEX

Directeur de thèse: M. Georges JACQUET-RICHARDET

Président de jury : M. Gaël CHEVALLIER

Composition du jury :

J.-F Deü	CNAM	**C. Touzé**	ENSTA Paris
T. Berruti	Politecnico di Torino	**E. Capiez-Lernout**	Université Paris-Est Marne-la-Vallée
G . Chevallier	Université Franche Comté	**G. Jacquet-Richardet**	INSA-Lyon/LaMCoS
D.-M. Tran	ONERA	**A. Placzek**	ONERA